Grant Agreement
No. 101015442

SILVARSTAR

Soil Vibration and Auralisation Software Tools for Application in Railways

H2020 Collaborative Projects
Research and Innovation Action
S2R-OC-CCA-01-2020: Noise and Vibration

Deliverable D1.1

STATE-OF-THE-ART AND

CONCEPT OF THE VIBRATION PREDICTION TOOL

Project coordinator:
Pascal Bouvet
Vibratec
pascal.bouvet@vibratec.fr

Grant Agreement
No. 101015442

Domain	WP1, Tasks T1.1 and T1.2
Leader	Geert Degrande[1]
Deliverable	D1.1
Title	State-of-the-art and concept of the vibration prediction tool
Authors	Geert Degrande[1], Geert Lombaert[1], Evangelos Ntotsios[2], David Thompson[2], Brice Nélain[3], Pascal Bouvet[3], Silke Grabau[4], Janosch Blaul[4] and Andreas Nuber[4]
Partners	[1]KU Leuven, [2]University of Southampton, [3]Vibratec, and [4]Wölfel
Document Code	20210525_D1.1_V1.0_KULeuven
Due date	30 April 2021
Submission date	28 May 2021

This project has received funding from the Shift2Rail Joint Undertaking under the European Union's Horizon 2020 Research and Innovation Programme under Grant Agreement 101015442

Document history		
Revision	Date	Description
V0.1	09 April 2021	First draft
V0.2	22 April 2021	Second draft
V0.3	15 May 2021	Third draft
V0.4	21 May 2021	Fourth draft
V1.0	25 May 2021	Final version

Dissemination level		
PU	Public	X
CO	Confidential, restricted under conditions set out in Model Grant Agreement	
CI	Classified, information as referred to in Commission Decision 2001/844/EC	

TABLE OF CONTENTS

LIST OF FIGURES

LIST OF TABLES

LIST OF ABBREVIATIONS

2D	Two-dimensional
2.5D	Two-and-a-half-dimensional
3D	Three-dimensional
BE	Boundary element
BEM	Boundary element method
BS	British Standards
DB	Deutsche Bahn
DOF	Degree of freedom
DIN	Deutsche Institut für Normung
EU	European Union
eVDV	Estimated vibration dose value
FE	Finite element
FEM	Finite element method
FP7	Seventh Framework Programme
FRA	Federal Railroad Administration
FTA	Federal Transit Administration
GIS	Geographical Information System
GUI	Graphical User Interface
HSL	High speed line
HST	High speed train
IC	Intercity
ICE	Intercity Experimental
ISO	International Organization for Standardization
MTVV	Maximum transient vibration value
NS	Standard Norge
OSM	Open Street Map
PML	Perfectly matched layer
PSD	Power spectral density
RMS	Root mean square
RSMV	Rolling Stiffness Measurement Vehicle
SASW	Spectral Analysis of Surface Waves
SBB	Swiss Federal Railways
SCPT	Seismic Cone Penetration Test
SPL	Sound pressure level
SS	Svensk Standard
TA Lärm	Technische Anleitung zum Schutz gegen Lärm
UIC	International Union of Railways
UNI	Ente Nazionale Italiano di Unificazione
VDI	Verein Deutscher Ingenieure
VDV	Vibration dose value
WP	Work Package

EXECUTIVE SUMMARY

This report represents Deliverable D1.1 "State-of-the-art and concept of the vibration prediction tool" of the Collaborative Project SILVARSTAR that is funded under the European Union's Horizon 2020 Research and Innovation Programme under the open call S2R-OC-CCA-01-2020 as part of the Cross Cutting Activities of the Shift2Rail Joint Undertaking.

Part I of this report presents the state-of-the-art of prediction models for railway induced vibration, corresponding to Task T1.1 in the Description of Work, and differentiating between numerical, empirical and hybrid models. Main excitation mechanisms defining quasi-static and dynamic axle loads are discussed, followed by a general formulation to compute the response of 3D media under moving axle loads. Efficient numerical methods are presented to compute dynamic axle loads, to solve the train-track interaction problem, and to compute the response of the track and the free field. The focus is on models that exploit the longitudinal invariance of track and soil. This is followed by a review of empirical models with particular emphasis on the general framework recommended in ISO 14837-1:2005, as well as the empirical procedure for Detailed Vibration Assessment pro-posed by the Federal Railroad Administration and the Federal Transit Administration of the U.S. Department of Transportation. These offer the opportunity to develop hybrid models that combine experimental data with numerical prediction.

Part II of this report presents the concept and framework of the hybrid vibration prediction tool that will be developed in SILVARSTAR, corresponding to Task T1.2 in the Description of Work. A hybrid prediction methodology is proposed, based on the general framework recommended in ISO 14837-1:2005, the state-of-the-art numerical models developed by the partners in the project, and the empirical procedures recommended in the FRA/FTA guidelines. Particular attention is paid to compatibility with international standards and guidelines, as well as with external GIS software through the IMMI software. It is also explained how the proposed hybrid methodology is expected to be used for vibration prediction in a wide range of practical situations.

1. INTRODUCTION

Ground-borne noise and vibration studies are performed all around the world [22] to assess the environmental impact of new railway lines or the extension of existing lines on the surrounding inhabitants (figure 1). However, analysis is performed by simulation engineers, measurement specialists, and academic researchers, using a wide range of models with different degrees of complexity and precision. Depending on the background and experience of a project team, a combination of in-house software or tools developed at universities and research institutes may be used. A lack of uniformity and interfaces is observed, which does not facilitate the comparison of results obtained with different prediction models. Moreover, the quality of the predictions and the associated uncertainty strongly depend on the available data and the experience of the noise and vibration consultants involved. Existing models are not well integrated in the railway project development process. There is a general lack of user-friendly software incorporating widely accepted solution methods.

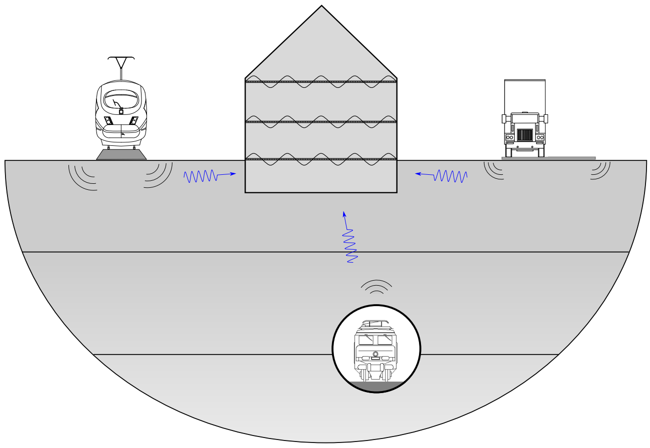

Figure 1: Railway induced vibration in the built environment.

The first overall objective of SILVARSTAR is to provide the railway community with a commonly accepted, practical and validated methodology and a user-friendly prediction tool for ground vibration impact studies. This tool will be used for environmental impact assessment of new or upgraded railways on a system level. It will provide access to ground vibration predictions to a wider range of suitably qualified engineers and will facilitate project planning and implementation by improved simulation processes.

A frequency-based hybrid prediction tool for ground vibration will be developed, that combines results computed with state-of-the-art numerical models and site-specific field measurements. The reason for using a hybrid approach, combining experimental data with numerical predictions, is that a purely experimental approach is constrained to the cases that have been measured, whereas a purely numerical approach, such as finite element and boundary element modelling, generally involves excessive computation times. The SILVARSTAR hybrid approach is much more flexible and practical.

The proposed method follows the general framework recommended in ISO 14837-1:2005 [88], where the vibration level in a point in the free field or in a building is written as the product of a source, a propagation, and a receiver term; each of these terms is frequency-dependent and can be represented by numerical prediction or by experimental data. At every stage of the propagation path (source, propagation, receiver), the user will have the option to use computed or measured data:

- The vibration source is the train-track interaction. The proposed method will allow the properties of the vehicles, the track, and the underlying ground to be fully taken into account, as well as excitation in terms of the track and wheel surface unevenness.
- The propagation path is highly complex, depending on the local soil properties. The use of measured transfer functions can directly take account of on-site complexity, but cannot allow for situations that do not yet exist. In this way, numerical approaches are also useful.
- At the receiver, noise and vibration levels depend on the building structure and its foundation type. The large variety of structures is generally addressed with statistical transfer functions that depend on overall building type and use. This approach will be adopted and coupled to the previous terms.

The SILVARSTAR partners have experience with the development and validation of hybrid models for ground vibration of trains running at grade, as well as the know-how to extend and validate such models for trains running in tunnels [192, 117, 111, 110, 134].

ISVR and KU Leuven developed a range of complementary semi-analytical numerical prediction tools, MOTIV [163, 140, 141] and TRAFFIC [121, 116, 119, 120, 115], for trains running on a track at grade or in tunnels, supported by or embedded in a layered ground. These tools will be used as the basis of further development in SILVARSTAR. As will be explained in section 4, more detailed numerical models have also been developed using 2.5D, periodic and 3D coupled Finite Element (FE) and Boundary Element (BE) methods which allow more complex situations to be modelled [167, 36, 33, 67, 57, 56, 90]. However, the versatility of such modelling comes at a high computational cost.

Based on its wide experience in engineering consulting, Vibratec uses hybrid methods that combine a numerical computation of the dynamic axle loads with experimental transfer functions to predict free field vibration levels. This approach is implemented in the software package GroundVIB [134], and will also serve as a basis for further development in SILVARSTAR.

The model will finally be implemented in an existing noise mapping software IMMI, developed by Wölfel. This will include a user-friendly Graphical User Interface (GUI) similar to that already used for noise mapping. It will also allow interface to Geographical Information systems (GIS) including Open Street Map (OSM), information on the terrain, the location of buildings as well as geological data. Train types, track types, traffic information, and other relevant data will share a common database with that used for noise mapping. Outputs will include descriptors that are compatible with international vibration standards and guidelines. The result will be an operational and flexible prediction tool, based on the latest scientific developments. It should allow assessment of vibration levels for large scale studies (project wide), as well as studies of specific situations in more detail.

This report is divided into two main parts.

Part I of this report presents the state-of-the-art of prediction models for railway induced vibration, corresponding to Task T1.1 in the Description of Work. Part I comprises sections 2-6.

- Section 2 discusses the main excitation mechanisms for railway induced vibration, differentiating between quasi-static and dynamic axle loads; track unevenness and parametric excitation are discussed in more detail.

- Section 3 presents a general formulation to compute the response of a 3D medium, characterized by its transfer function, under moving axle loads. Particular attention is paid to the case of translationally invariant media, for which an efficient formulation is possible in the wavenumber-frequency domain.
- Section 4 subsequently presents efficient numerical methods to compute the transfer function of the coupled track-soil system, to solve the train-track interaction problem (resulting in the dynamic axle loads), as well as to compute the response of the track and the free field under the action of moving loads. A case history of a ballasted track is considered, and numerical results obtained with the MOTIV and GroundVIB software are used for illustration.
- Section 5 presents empirical models with particular emphasis on the general framework recommended in ISO 14837-1:2005 [88], as well as the empirical procedure for Detailed Vibration Assessment proposed by the Federal Railroad Administration (FRA) and the Federal Transit Administration (FTA) of the U.S. Department of Transportation [71, 72, 70, 152]. The latter is illustrated by means of in situ vibration measurements along the high speed line L2 Brussels-Köln in Lincent and in a three-storey reinforced concrete building located at about 40 m from the railway line L1390 Leuven-Ottignies.
- Section 6 discusses possiblilites to develop hybrid models, combining results computed with state-of-the-art numerical models and site-specific field measurements. This is also illustrated considering the Lincent case history, as well as the GroundVIB software.

Part II of this report presents the concept and framework of the hybrid vibration prediction tool that will be developed in SILVARSTAR, corresponding to Task T1.2 in the Description of Work. Part II builds upon the state-of-the-art outlined in Part I and comprises sections 7-8.

- Section 7 presents the proposed hybrid methodology, which is based on the work presented in section 6, following the general framework recommended in ISO 14837-1:2005 (section 5) and using the state-of-the-art numerical models presented in section 4. Particular attention is paid to compatibility with international standards and guidelines and external GIS software. SILVARSTAR will also ensure that the developed methodology is compatible with the requirements defined by the complementary project FINE-2.
- Section 8 explains how the proposed hybrid methodology is expected to be very useful for making vibration prediction in a wide range of practical situations.

Part I

STATE-OF-THE-ART

2. EXCITATION MECHANISMS

2.1 Introduction

This section is based on the keynote paper of Lombaert et al. [117] presented at IWRN11.

The loads applied to the track by a running train can be decomposed into a static and dynamic component. The static axle load follows from the distribution of the weight of each carriage. The dynamic axle loads are due to several mechanisms such as wheel and rail unevenness, impact excitation due to rail joints and wheel flats, switches and crossings, and parametric excitation due to sleeper periodicity [176].

The time history $g_{kj}(t)$ of each axle load k in the direction $\mathbf{e}_j$ can be decomposed into a static component $g_{\mathrm{s}kj}$ and a dynamic component $g_{\mathrm{d}kj}(t)$:

$$g_{kj}(t) \quad = \quad g_{\mathrm{s}kj} + g_{\mathrm{d}kj}(t) \tag{1}$$

Assuming a linear behaviour of the track and the supporting soil, the resulting ground vibration $u_j(t)$ can be decomposed into the quasi-static contribution $u_{\mathrm{s}j}(t)$ and the dynamic contribution $u_{\mathrm{d}j}(t)$:

$$u_j(t) \quad = \quad u_{\mathrm{s}j}(t) + u_{\mathrm{d}j}(t) \tag{2}$$

2.2 Quasi-static excitation

The static component $g_{\mathrm{s}kj}$ of the vertical axle loads follows from the distribution of the weight of each carriage over the axles and is equal to $w_k\delta_{zj}$, where w_k is the weight carried by axle k and δ_{zj} is the Kronecker delta that equals 1 when j refers to the z-coordinate and 0 when j refers to the x- or y-coordinate.

In section 3, the response of a 3D and a translationally invariant medium due to quasi-static axle loads moving at a speed v will be derived in detail.

When the train speed is situated in the sub-critical range, i.e. well below the wave speeds in the track-ground system, the quasi-static response of the soil resembles a sequence of bowl shaped deflections that travel with the train. The time variation of the response at a fixed point is therefore due to successive rising and falling of the response at the passage of each axle. The repeated passage of axles leads to the characteristic peaks and troughs in the narrow-band frequency spectrum of the response that are determined by the axle and bogie passage frequencies [34, 7, 8]. This can be understood by writing the quasi-static response as a superposition of the contributions of different train axles:

$$u_{\mathrm{s}j}(t) \quad = \quad \sum_{k=1}^{n_{\mathrm{a}}} w_k u_{\mathrm{s}0j}\left(t - \frac{y_{k0}}{v}\right) \tag{3}$$

where n_{a} is the number of axles of the train, w_k is the weight carried by axle k, $u_{\mathrm{s}0j}(t)$ is the response due to a moving load with a unit magnitude, y_{k0} is the position of the axle on the track at a reference time

$t = 0$, and v is the train speed. In the frequency domain, this expression becomes:

$$\hat{u}_{sj}(\omega) = \hat{u}_{s0j}(\omega)\left[\sum_{k=1}^{n_a} w_k \exp\left(+i\omega\frac{y_{k0}}{v}\right)\right] \quad (4)$$

where the bracketed term depends on the distribution of the weight over the axles and the train speed v and gives rise to the characteristic shape of the narrow band response spectrum [34, 7, 8].

Example 2.1: Quasi-static sleeper response.

The effect of quasi-static excitation is now illustrated for the computed response of the sleeper due to the passage of an InterCity train at the site of Lincent next to the high speed line L2 Brussels-Köln. For more details regarding the model and input parameters, the reader is referred to Lombaert and Degrande [115].

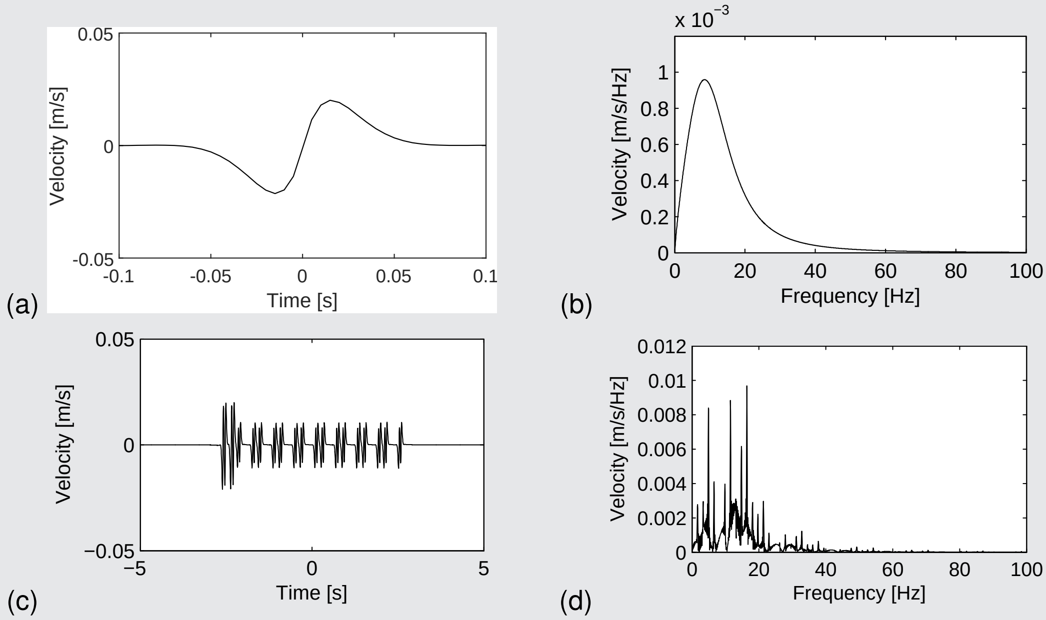

Figure 2: Quasi-static contribution to the sleeper response due to the passage of an InterCity train at a speed of 156 km/h: (a) time history and (b) narrow-band spectrum of the velocity during the passage of the first axle of the locomotive and (c) time history and (d) narrow-band spectrum of the velocity during the passage of the entire train.

Figures 2a and 2b show the time history and narrow-band spectrum of the sleeper velocity due to the passage of the first axle of an InterCity train at a speed of 156 km/h, which is well below the lower limit of the Rayleigh wave velocities in the soil. Due to the short duration of the quasi-static sleeper response for a single axle (figure 2a), the passages of individual axles do not overlap in time and are still observed in the time history response for the entire train (figure 2c). The InterCity train is in "pull mode" where the axles of the locomotive that carry the largest weight come first. Comparison of the narrow-band spectra for a single axle (figure 2b) and the full train (figure 2d) shows how the characteristic peaks and troughs appear by multiplication with the bracketed term in equation (4).

In the range of sub-critical train speeds, the narrow-band spectrum of the quasi-static contribution to the free field response becomes increasingly concentrated at low frequencies with increasing distance from the track. This is due to the characteristic bowl shape of the deflection field for each axle. At a larger distance from the track, the arrival of a single axle is detected earlier and its passage lasts for a longer time. The time scale over which the response rises and falls therefore increases with the distance from the track, implying that its representation in the frequency domain gets more concentrated at lower frequencies. This is fundamentally different from the reduction in the frequency at which the peak value of the transfer functions is found, as the latter is due to energy dissipation characterized by the material damping ratio. Furthermore, as the distance from the track increases, contributions from different axles and bogies coalesce and can no longer be identified in the time history of the vibration response.

2.3 Dynamic excitation

The dynamic load component is determined by train-track interaction resulting from several excitation mechanisms, such as wheel and track unevenness, impact excitation due to rail joints and wheel flats, switches and crossings, and parametric excitation due to the spatial variation of support stiffness, e.g. due to the discrete nature of sleeper support [176, 73, 101, 137]. In the following, wheel and track unevenness, including impact excitation due to localized defects, are discussed first, as these excitation mechanisms are at present the best understood and quantified. Parametric excitation, which has received less attention in the context of ground-borne vibration, is considered next.

The following subsections describe the important excitation mechanisms, while a more detailed (mathematical) description and numerical implementation will be discussed in section 4.

2.3.1 Wheel and track unevenness

In order to understand how parameters of the vehicle, track, and supporting soil affect the dynamic loads, it is instructive to consider how these loads are computed from the combined wheel and track unevenness [119, 7, 166].

In section 4, it will be derived how, in the particular case of a longitudinally invariant track and assuming perfect contact between the train and the track, the dynamic axle loads $\hat{\mathbf{g}}_{\mathrm{d}}(\omega)$ can be computed in the frequency domain as follows:

$$\left[\hat{\mathbf{C}}^{\mathrm{t}}(\omega) + \hat{\mathbf{C}}^{\mathrm{v}}(\omega)\right] \hat{\mathbf{g}}_{\mathrm{d}}(\omega) \quad = \quad -\hat{\mathbf{u}}_{\mathrm{w/r}}(\omega) \tag{5}$$

where $\hat{\mathbf{g}}_{\mathrm{d}}(\omega)$ and $\hat{\mathbf{u}}_{\mathrm{w/r}}(\omega)$ are vectors that collect the dynamic axle loads and the unevenness experienced at all axles. $\hat{\mathbf{C}}^{\mathrm{t}}(\omega)$ is the track compliance matrix, evaluated in the frame of reference that moves with the train, while $\hat{\mathbf{C}}^{\mathrm{v}}(\omega)$ is the vehicle compliance matrix.

The geometrical irregularities considered here include broad-band unevenness of a random nature, typically modelled as a stationary random process characterized by its power spectral density (PSD) [143], but can also represent localized irregularities such as rail joints giving rise to impact excitation. It will be demonstrated in section 4 that, in the absence of wheel unevenness, all axles experience the same excitation apart from a shift in time accounted for by a phase shift $\exp\left(\mathrm{i}\omega y_{k0}/v\right)$. When all train carriages have similar characteristics and track unevenness is the dominant source of excitation, the resulting dynamic loads will also be similar and the narrow-band spectrum of the dynamic response contribution will have a similar shape to that of the quasi-static response contribution.

Excitation at a frequency $f = \omega/(2\pi)$ is due to unevenness characterized by a wavenumber $k_y = 2\pi f/v$ or wavelength $\lambda_y = v/f$. The spectral content of the unevenness $\tilde{u}_{\mathrm{rz}}(k_y)$ in the wavenumber domain is related as follows to the excitation $\hat{u}_{\mathrm{w/r}}(\omega)$ experienced by the k-th axle in the frequency domain:

$$\hat{u}_{\mathrm{w/r}}(\omega) = \frac{1}{v}\tilde{u}_{\mathrm{r}z}\left(-\frac{\omega}{v}\right)\exp\left(+\mathrm{i}\omega\frac{y_{k0}}{v}\right) \tag{6}$$

Table 1 shows that the relevant range of wavelengths for ground-borne vibration and noise extends from several centimetres up to a hundred metres, depending on the train speed and the specific problem at hand. The measurement bandwidth of track recording cars is usually restricted, however, to wavelengths between a few metres and 20 to 30 m [48] and these data therefore need to be supplemented by data obtained from other measurement devices such as trolleys. This is not trivial, as the unevenness measured by a track recording car is the one experienced by the car that includes a load dependent contribution from parametric excitation, and is therefore not a pure representation of imperfect track geometry.

Table 1: Relevant range of wavelengths λ_y for ground-borne vibration and noise as a function of the train speed v.

	Ground-borne vibration		Ground-borne noise	
Train speed/frequency	1 Hz	80 Hz	16 Hz	250 Hz
$v = 72\,\mathrm{km/h}$	20 m	0.25 m	1.25 m	0.08 m
$v = 360\,\mathrm{km/h}$	100 m	1.25 m	6.25 m	0.40 m

For wheel unevenness, a similar range of wavelengths is important, although the largest wavelength present in the wheel roughness is equal to the wheel circumference. Recent measurements along the conventional line Paris-Bordeaux have shown that the time history of the ground vibration velocity during the passage of a freight train has a significantly more irregular character than for high speed trains and passenger trains [118]. This suggests that wheel unevenness is more important in the case of freight traffic, which in Europe has historically been characterised by cast-iron brake blocks.

Note that equation (5) does not allow account to be taken of large deflections or loss of contact, e.g. in the presence of wheel flats [205]; this would require a non-linear model. Furthermore, it has been implicity assumed that the track dynamic properties are translationally invariant in the longitudinal direction of the track. This assumption is also acceptable for discretely supported ballasted tracks as the rail receptance at a sleeper and in between two sleepers are similar in the low frequency range of interest for ground-borne vibration [101, 205]. Equation (5) therefore provides a reasonable basis for investigating how vehicle-track interaction affects the dynamic train loads.

Example 2.2: Dynamic response in the free field.

In order to illustrate the importance of the dynamic excitation due to track unevenness, the total calculated response in the free field is now considered for the same passage of an InterCity train at the site in Lincent. The dynamic response has been calculated considering the track unevenness measured by a track recording car [115]. Figure 3a shows the time history of the free field velocity at 16 m from the track.

In contrast to what was observed for the quasi-static contribution to the sleeper response in figure 2c, the passage of individual axles can no longer be identified. Even when the dynamic response contribution was not accounted for, this would be the case as at a larger distance from the track, the quasi-static response contributions from different axles and bogies coalesce.

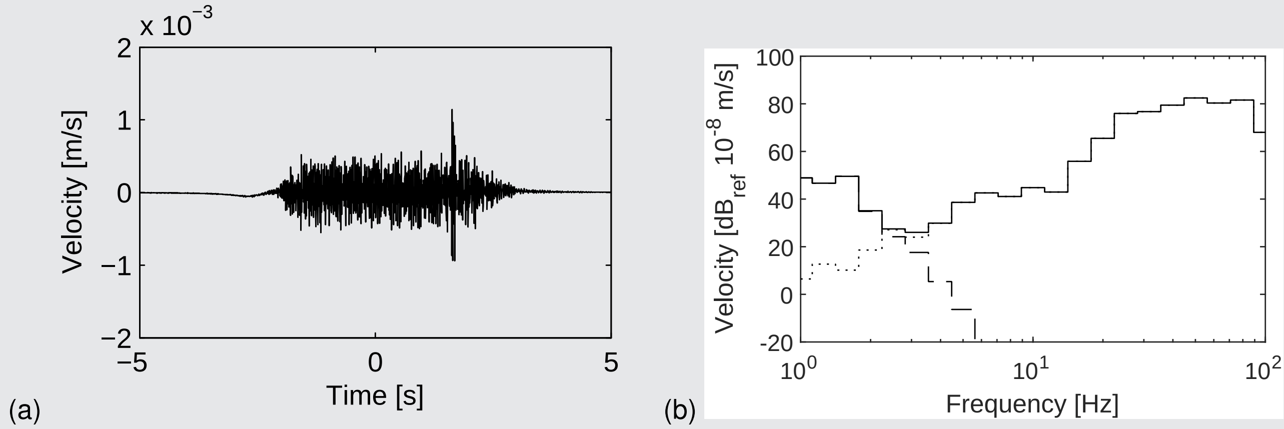

Figure 3: Free field response at 16 m from the track due to the passage of an InterCity train at a speed of 156 km/h: (a) time history and (b) one-third octave band spectra of the total response (solid line), quasi-static (dashed line) and dynamic (dotted line) response contribution.

Figure 3b shows the one-third octave band spectra of the free field velocity at 16 m from the track. The one-third octave band spectra are computed according to the German standard DIN 45672-2 [37] for a reference period T_2 which is here considered as the duration of the stationary part of the response. Comparing the one-third octave band spectra of the total response, and the quasi-static and dynamic response contributions in figure 3b shows that the latter dominates the total response. A significant contribution of the quasi-static excitation to the total response is in this case only found in the frequency range below 3 Hz.

The quasi-static contribution to the response generally remains important, however, in the immediate vicinity of the track. No attempt can therefore be made to use an equation as $\hat{u}(r,\omega) = \hat{H}(r,\omega)\hat{f}(r,\omega)$ for estimating the dynamic loads $\hat{f}(r,\omega)$ applied to the track from the response $\hat{u}(r,\omega)$ measured close to the track and transfer functions $\hat{H}(r,\omega)$ between the track and the free field [181]. Furthermore, this also implies that the estimation of insertion loss values from field tests requires measurements at a sufficiently large distance from the track. The relative importance of quasi-static and dynamic excitation depends on the train speed, the ratio of the static and dynamic axle loads, and the dynamic characteristics of the track and the soil as indicated by Sheng et al. [166, 165], Auersch [8], Lombaert and Degrande [115], and Triepaischajonsak et al. [181, 180].

2.3.2 Parametric excitation

Parametric excitation is another source of excitation that relates to the spatial variation of the support stiffness. A first obvious source is the spatial variation of the dynamic track stiffness of a conventional ballasted track within one sleeper bay. A wheel running over the rail experiences the relatively small spatial variation in stiffness and is excited at the sleeper-passing frequency v/d, with d the sleeper spacing [7, 205, 180]. For conventional railway traffic, the sleeper-passing frequency is generally situated within the relevant range for ground-borne vibration, whereas for high speed trains it is in the range for ground-borne noise. For example at 80 km/h and a sleeper spacing of 0.6 m the sleeper-passing frequency occurs at 37 Hz whereas at 300 km/h it occurs at 139 Hz.

A second source of parametric excitation occurs at transition zones where the change in stiffness, e.g. resulting from a transition from one type of track to another, will also excite the vehicle [58, 183]. The length and suddenness of the transition zone will determine the frequency range of excitation.

Parametric excitation may also be caused by other less obvious variations in the stiffness of the track and the subsoil. Experimental investigations have shown significant scatter in the sleeper support stiffness [144] and the Young's modulus and thickness of the ballast and subgrade layers [154]. Variations in support stiffness from one sleeper to another and support stiffness variations on a larger spatial scale can also lead to excitation of the vehicle and ground-borne vibration.

At present, the importance of this source of excitation is not fully understood, as track stiffness measurements are not routinely performed by infrastructure managers and require specially designed measurement cars such as the Rolling Stiffness Measurement Vehicle (RSMV) [11, 202]. One could argue that the distinction between geometric imperfections and support stiffness variations is unimportant to some extent as both sources contribute to the unevenness measured by track recording cars. Using these data for a similar type of carriage should therefore allow the dynamic vehicle loads to be predicted and the resulting ground-borne vibration to be assessed. The distinction between geometric unevenness and parametric excitation is very important, however, for determining the effectiveness of mitigation measures at the track, e.g. resilient rail support systems [79], or track maintenance measures.

3. RESPONSE TO MOVING LOADS

3.1 Introduction

This section explains how the displacement time history $u_i(\mathbf{x}', t)$ of a 3D medium due to a set of n_a time varying axle loads $g_{kj}(t)$ can be computed from these axle loads and the transfer functions (or impulse response functions) $h_{ij}(\mathbf{x}', \mathbf{x}, t - \tau)$. Corresponding expressions in the frequency domain are also derived using a forward Fourier transformation.

It is also explained how particular expressions can be derived for translationally invariant media (or 2.5D media) with homogeneous geometry and material properties in the direction $\mathbf{e}_y$ of the moving load (figure 4). This is accomplished by a complementary forward Fourier transformation of the longitudinal coordinate y to the horizontal wavenumber k_y, resulting in a solution in the wavenumber-frequency domain. Inverse Fourier transformation allow closed-form expressions to be recovered in the spatial-frequency and spatial-time domains. Very efficient semi-analytical and numerical models can be formulated in the wavenumber-frequency domain, as will be discussed further in section 4; these include 2.5D finite element (FE) formulations in combination with perfectly matched layers (PML) and 2.5D finite element - boundary element (FE-BE) formulations.

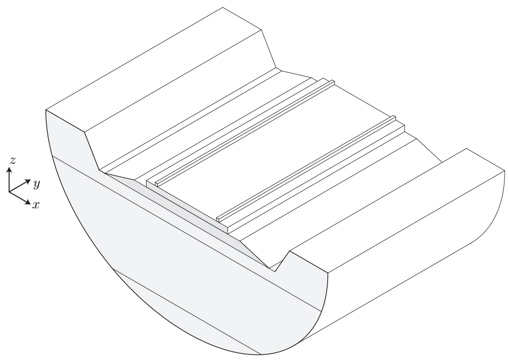

Figure 4: A longitudinally invariant track-soil domain.

In subsection 3.2, we derive the response of a 3D medium with arbitrary geometry and material properties, characterised by 3D transfer functions, to a sequence of axle loads moving at constant speed. The response in both the spatial-time and the spatial-frequency domain is presented. In subsection 3.3, we subsequently explain how these expressions can be simplified if it is assumed that the geometry and material properties of the track and soil do not vary in the longitudinal direction along the track. The response due to moving loads is presented in the spatial-time, wavenumber-frequency and spatial-frequency domain. These expressions are used in subsection 3.4 to derive the response of a 2.5D medium in the spatial-frequency domain due to static and dynamic axle loads. In subsection 3.5, the response in the spatial-frequency domain is derived in a frame of reference that moves with the train, which will serve in section 4 to derive the compliance of the track.

Although essential for a thorough understanding of how the response of 3D and 2.5D media, characterised by their transfer functions, due to moving static and dynamic axle loads is efficiently computed, a reader may wish to skip these mathematical derivations upon first reading, and continue with section 4 and the following, before having a more detailed read of this section.

3.2 Response of 3D media to moving axle loads

3.2.1 Response in the spatial-time domain

The response of a coupled track-soil system due to multiple moving axle loads is calculated by means of a transfer function (impulse response function) $h_{ij}(\mathbf{x}', \mathbf{x}, t)$, that represents the response at a point $\mathbf{x}$ in the direction $\mathbf{e}_j$ at a time t due to an impulse load at a point $\mathbf{x}'$ in the direction $\mathbf{e}_i$ at the time $t = 0$. The displacement $u_i(\mathbf{x}', t)$ due to an arbitary body load $\rho b_j(\mathbf{x}, t)$ is calculated by means of the dynamic reciprocity theorem:

$$u_i(\mathbf{x}', t) \quad = \quad \int_{-\infty}^{t} \int_{\Omega} h_{ij}(\mathbf{x}', \mathbf{x}, t - \tau) \rho b_j(\mathbf{x}, \tau) \, \mathrm{d}\mathbf{x} \, \mathrm{d}\tau \tag{7}$$

where Ω is the domain of the coupled track-soil system. Furthermore, it is assumed that the body load $\rho b_j(\mathbf{x}, t)$ may act along three directions, so summation on the repeated index j is understood. In the following, dynamic reciprocity is used to replace $h_{ij}(\mathbf{x}', \mathbf{x}, t - \tau)$ by $h_{ji}(\mathbf{x}, \mathbf{x}', t - \tau)$.

For n_a axle loads moving at a constant speed v in the direction $\mathbf{e}_y$, the body load $\rho b_j(\mathbf{x}, t)$ is equal to:

$$\rho b_j(\mathbf{x}, t) \quad = \quad \sum_{k=1}^{n_\mathrm{a}} \delta(\mathbf{x} - \mathbf{x}_k(t)) g_{kj}(t) \tag{8}$$

where $\mathbf{x}_k(t) = \mathbf{x}_{k0} + vt\mathbf{e}_y$ is the time-dependent position of the k-th load, $\mathbf{x}_{k0}$ is the position at the time $t = 0$ and $g_{kj}(t)$ represents the time history of the j-th component of the k-th axle load. Axle loads are assumed to be positive when their action on the track is in the positive coordinate direction (figure 4).

Introducing the moving axle loads (8) into equation (7), and taking into consideration the Dirac functions as well as the dynamic reciprocity of the transfer function ($h_{ij}(\mathbf{x}', \mathbf{x}, t - \tau) = h_{ji}(\mathbf{x}, \mathbf{x}', t - \tau)$), the response due to the moving axle loads is calculated as follows:

$$u_i(\mathbf{x}, t) \quad = \quad \sum_{k=1}^{n_\mathrm{a}} \int_{-\infty}^{t} h_{ji}(\mathbf{x}_k(\tau), \mathbf{x}, t - \tau) g_{kj}(\tau) \mathrm{d}\tau \tag{9}$$

where the prime on the receiver coordinate $\mathbf{x}$ is omitted. This expression is generally applicable, independent of the complexity of the track-soil system. The coupling between the position $\mathbf{x}_k(\tau)$ of the k-th axle and the time history of the load $g_{kj}(\tau)$ through the time τ gives rise to the Doppler effect.

3.2.2 Response in the spatial-frequency domain

The response $\hat{u}_i(\mathbf{x}, \omega)$ in the frequency domain is calculated as the forward Fourier transform of the time t to the circular frequency ω:

$$\hat{u}_i(\mathbf{x}, \omega) \quad = \quad \int_{-\infty}^{+\infty} u_i(\mathbf{x}, t) \exp(-\mathrm{i}\omega t) \, \mathrm{d}t \tag{10}$$

where the displacement $u_i(\mathbf{x},t)$ is equal to expression (9):

$$\hat{u}_i(\mathbf{x},\omega) \quad = \quad \int_{-\infty}^{+\infty} \sum_{k=1}^{n_\mathrm{a}} \int_{-\infty}^{t} h_{ji}(\mathbf{x}_k(\tau),\mathbf{x},t-\tau) g_{kj}(\tau)\,\mathrm{d}\tau \exp\left(-\mathrm{i}\omega t\right) \mathrm{d}t \tag{11}$$

The exponential term on the right hand side of this equation is replaced by $\exp\left[-\mathrm{i}\omega(t-\tau)\right]\exp\left(-\mathrm{i}\omega\tau\right)$, while the order of integration is changed:

$$\hat{u}_i(\mathbf{x},\omega) \quad = \quad \sum_{k=1}^{n_\mathrm{a}} \int_{-\infty}^{t} \left[\int_{-\infty}^{+\infty} h_{zj}(\mathbf{x}_k(\tau),\mathbf{x},t-\tau) \exp\left[-\mathrm{i}\omega(t-\tau)\right] \mathrm{d}t\right] g_{kj}(\tau) \exp\left(-\mathrm{i}\omega\tau\right) \mathrm{d}\tau \tag{12}$$

The bracketed term represents the Fourier transform $\hat{h}_{ji}(\mathbf{x}_k(\tau),\mathbf{x},\omega)$ of the transfer function, so that the Fourier transform $\hat{u}_i(\mathbf{x},\omega)$ of the response finally becomes:

$$\hat{u}_i(\mathbf{x},\omega) \quad = \quad \sum_{k=1}^{n_\mathrm{a}} \int_{-\infty}^{t} \hat{h}_{ji}(\mathbf{x}_k(\tau),\mathbf{x},\omega) g_{kj}(\tau) \exp\left(-\mathrm{i}\omega\tau\right) \mathrm{d}\tau \tag{13}$$

In this expression, a general dependence of the axle loads $g_{kj}(\tau)$ on the time τ is accounted for.

Due to the Doppler effect, this expression cannot be written in a simple form as $\hat{u}_i(\mathbf{x},\omega) = \hat{h}_{ji}(\mathbf{x},\omega)\hat{g}_{kj}(\omega)$ unless the train is assumed to be at a fixed position, i.e. $\mathbf{x}_k(\tau) \approx \mathbf{x}_{k0}$, as for calculating the stationary part of the vibration response [192].

Equations (9) and (13) are generally valid to compute the response of 3D media due to moving loads. In the following subsection, we will further elaborate these equations for the particular case when the geometry and material properties of the track-soil system are invariant in the direction $\mathbf{e}_y$, resulting in efficient computation of the transfer function, the dynamic axle loads and the free field response. Similar developments are possible for periodic media; however, the computational effort is generally higher than required for invariant media. For the development of a vibration prediction model that is fast to run, we will therefore prefer an invariant or 2.5D formulation.

3.3 Response of invariant media due to moving axle loads

3.3.1 Response in the spatial-time domain

In the particular case where the domain Ω is invariant with respect to the longitudinal direction $\mathbf{e}_y$ (figure 4), the transfer function only depends on the difference $y - y_{k0} - v\tau$ of the receiver and source coordinates, and equation (9) simplifies to:

$$u_i(\mathbf{x},t) \quad = \quad \sum_{k=1}^{n_\mathrm{a}} \int_{-\infty}^{t} h_{ji}(x_{k0},z_{k0},x,y-y_{k0}-v\tau,z,t-\tau) g_{kj}(\tau)\,\mathrm{d}\tau \tag{14}$$

In the following, the dependence of the displacement $u_i(\mathbf{x},t)$ on the receiver coordinates x and z and the dependence of the transfer function $h_{ji}(x_{k0},z_{k0},x,y-y_{k0}-v\tau,z,t-\tau)$ on the source coordinates x_{k0}

and z_{k0} and the receiver coordinates x and z will be omitted for brevity, so that equation (14) simplifies to:

$$u_i(y,t) \quad = \quad \sum_{k=1}^{n_\mathrm{a}} \int_{-\infty}^{t} h_{ji}(y - y_{k0} - v\tau, t-\tau) g_{kj}(\tau)\,\mathrm{d}\tau \tag{15}$$

This solution procedure has been originally proposed by Aubry et al. [6] and Clouteau et al. [21] to study the interaction of an infinite beam with a horizontally layered elastic halfspace in the wavenumber–frequency domain.

3.3.2 Response in the wavenumber-frequency domain

Analogously to the derivation of equation (13), the frequency content $\hat{u}_i(y,\omega)$ of the response is calculated as the forward Fourier transform of the time t to the circular frequency ω:

$$\hat{u}_i(y,\omega) \quad = \quad \sum_{k=1}^{n_\mathrm{a}} \int_{-\infty}^{t} \hat{h}_{ji}(y - y_{k0} - v\tau, \omega) g_{kj}(\tau) \exp\left(-\mathrm{i}\omega\tau\right) \mathrm{d}\tau \tag{16}$$

The response $\tilde{u}_i(k_y,\omega)$ in the wavenumber-frequency domain is obtained as the forward Fourier transform of the coordinate y to the longitudinal wavenumber k_y:

$$\tilde{u}_i(k_y,\omega) \quad = \quad \int_{-\infty}^{+\infty} \hat{u}_i(y,\omega) \exp\left(+\mathrm{i}k_y y\right) \mathrm{d}y \tag{17}$$

where the displacement is equal to equation (16):

$$\tilde{u}_i(k_y,\omega) \quad = \quad \int_{-\infty}^{+\infty} \sum_{k=1}^{n_\mathrm{a}} \int_{-\infty}^{t} \hat{h}_{ji}(y - y_{k0} - v\tau, \omega) g_{kj}(\tau) \exp\left(-\mathrm{i}\omega\tau\right) \mathrm{d}\tau \exp\left(+\mathrm{i}k_y y\right) \mathrm{d}y \tag{18}$$

Elaboration results in the following expression in the wavenumber-frequency domain:

$$\tilde{u}_i(k_y,\omega) \quad = \quad \sum_{k=1}^{n_\mathrm{a}} \tilde{h}_{ji}(k_y,\omega) \hat{g}_{kj}(\omega - k_y v) \exp\left(+\mathrm{i}k_y y_{k0}\right) \tag{19}$$

This result shows that the response in the wavenumber-frequency domain is the product of the transfer function and the frequency content of the load, provided that the latter is shifted by $k_y v$. Müller and Huber [130] were among the first to propose such a formulation to compute the response of a layered elastic halfspace due to a moving load.

3.3.3 Response in the spatial-frequency domain

The response $\hat{u}_i(y,\omega)$ in the frequency domain is obtained after evaluation of an inverse wavenumber transform:

$$\hat{u}_i(y,\omega) \quad = \quad \sum_{k=1}^{n_\mathrm{a}} \frac{1}{2\pi} \int_{-\infty}^{+\infty} \tilde{h}_{ji}(k_y,\omega) \hat{g}_{kj}(\omega - k_y v) \exp\left[-\mathrm{i}k_y (y - y_{k0})\right] \mathrm{d}k_y \tag{20}$$

This expression is particularly useful when the transfer function is available in the wavenumber-frequency domain. An efficient evaluation of the inverse wavenumber transform is proposed by Lieb [113] and Grundmann et al. [65] based on an additional wavelet transform of the response in the wavenumber-frequency domain. A change of variables according to $k_y = (\omega - \tilde{\omega})/v$ moves the frequency shift from the frequency content of the moving load to the wavenumber content of the transfer function:

$$\hat{u}_i(y,\omega) = \sum_{k=1}^{n_\mathrm{a}} \frac{1}{2\pi v} \int_{-\infty}^{+\infty} \tilde{h}_{ji}\left(\frac{\omega-\tilde{\omega}}{v},\omega\right) \hat{g}_{kj}(\tilde{\omega}) \exp\left[-\mathrm{i}\frac{\omega-\tilde{\omega}}{v}(y-y_{k0})\right] \mathrm{d}\tilde{\omega} \quad (21)$$

The transfer function is evaluated at a wavenumber $k_y = (\omega - \tilde{\omega})/v$ that couples the frequency $\tilde{\omega}$ emitted by the moving source to the frequency ω observed at the receiver. Due to the Doppler effect, a source at a fixed frequency $\tilde{\omega}$ contributes to the response in a frequency range $[\tilde{\omega}/(1+v/C), \tilde{\omega}/(1-v/C)]$, determined by the smallest phase velocity C of interest.

A single harmonic vertical point load with a time history $g_{1j}(t) = P_1 \exp(+i\Omega t)\delta_{zj}$ and initial position y_{10}, moving with a speed v is now considered. The Fourier transformation of the time history $g_{1j}(t)$ is equal to $\hat{g}_{1j}(\omega) = 2\pi P_1 \delta(\omega - \Omega)\delta_{zj}$. The displacement $\hat{u}_i(y,\omega)$ in the frequency domain is equal to:

$$\hat{u}_i(y,\omega) = \frac{1}{2\pi v} \int_{-\infty}^{+\infty} \tilde{h}_{ji}\left(\frac{\omega-\tilde{\omega}}{v},\omega\right) 2\pi P_1 \delta(\tilde{\omega}-\Omega)\delta_{zj} \exp\left[-\mathrm{i}\frac{\omega-\tilde{\omega}}{v}(y-y_{10})\right] \mathrm{d}\tilde{\omega} \quad (22)$$

As the integrand includes the Dirac function $\delta(\tilde{\omega} - \Omega)$, this expression reduces to:

$$\hat{u}_i(y,\omega) = \frac{P_1}{v} \tilde{h}_{zi}\left(\frac{\omega-\Omega}{v},\omega\right) \exp\left[-\mathrm{i}\frac{\omega-\Omega}{v}(y-y_{10})\right] \quad (23)$$

Equation (23) demonstrates that the displacement $\hat{u}_i(y,\omega)$ in the frequency domain due to a moving harmonic load oscillating at a frequency Ω is easily found by evaluating the transfer function at a wavenumber $k_y = (\omega - \Omega)/v$, which is a straight line in the wavenumber-frequency domain, and a frequency ω.

3.4 Response to a train passage

In the following, the response of the coupled track-soil system due to a train passage is calculated. A distinction is made between the quasi-static and dynamic contribution to the response, based on a decomposition of the time history $g_{kj}(t)$ of each axle load into a static component $g_{\mathrm{s}kj}$ and a dynamic component $g_{\mathrm{d}kj}(t)$:

$$g_{kj}(t) = g_{\mathrm{s}kj} + g_{\mathrm{d}kj}(t) \quad (24)$$

3.4.1 Response to static axle loads

The static axle loads $g_{\mathrm{s}kj}$ follow from the distribution of the weight of each carriage over the axles and dominates the track response as well as the free field response in the immediate vicinity of the track. The static component $g_{\mathrm{s}kj}$ of the vertical axle loads is equal to $w_k\delta_{zj}$, where w_k is the weight carried by axle k.

Introducing the Fourier transform $\hat{g}_{\mathrm{s}kj} = 2\pi w_k \delta(\omega)\delta_{zj}$ in equation (21) gives the quasi-static response:

$$\hat{u}_i(y,\omega) = \left[\frac{1}{v}\tilde{h}_{zi}\left(\frac{\omega}{v},\omega\right)\exp\left(-\mathrm{i}\frac{\omega}{v}y\right)\right]\left[\sum_{k=1}^{n_{\mathrm{a}}} w_k \exp\left(+\mathrm{i}\frac{\omega}{v}y_{k0}\right)\right] \tag{25}$$

The first bracketed term on the right hand side is the response due to a moving unit axle load; the transfer function is evaluated at a wavenumber $k_y = \omega/v$, which is a straight line in the wavenumber-frequency domain, and a frequency ω. The second bracketed term represents a modulation of the response, determined by the distribution of the weight over the axles and by the train speed v [34, 7, 8]. This expression is rewritten as follows:

$$\hat{\mathbf{u}}(y,\omega) = \left[\frac{w_l}{v}\tilde{h}_{zi}\left(\frac{\omega}{v},\omega\right)\exp\left(-\mathrm{i}\frac{\omega}{v}(y-y_{l0})\right)\right]\left[\sum_{k=1}^{n_{\mathrm{a}}} \frac{w_k}{w_l}\exp\left(+\mathrm{i}\frac{\omega}{v}(y_{k0}-y_{l0})\right)\right] \tag{26}$$

where the first bracketed term on the right hand side now represents the response due to an (arbitrary) axle l with weight w_l and initial position y_{l0}.

3.4.2 Response to dynamic axle loads

The dynamic axle loads $g_{\mathrm{d}kj}(t)$ are determined by dynamic train-track interaction, resulting from a large number of excitation mechanisms, such as the spatial variation of the support stiffness, the combined wheel and track unevenness, impact excitation due to rail joints, wheel flats, switches and crossings, and parametric excitation due to sleeper periodicity [176]. The dynamic axle loads are computed by means of a compliance formulation in a moving frame of reference [21], as will be demonstrated in subsection 3.5. The dynamic contribution to the track and free field response is found by introducing the Fourier transform $\hat{g}_{\mathrm{d}kj}(\omega)$ of the dynamic axle loads $g_{\mathrm{d}kj}(t)$ in equation (20):

$$\hat{u}_i(y,\omega) = \sum_{k=1}^{n_{\mathrm{a}}} \frac{1}{2\pi}\int_{-\infty}^{+\infty} \tilde{h}_{ji}(k_y,\omega)\hat{g}_{\mathrm{d}kj}(\omega-k_y v)\exp\left[-\mathrm{i}k_y(y-y_{k0})\right]\mathrm{d}k_y \tag{27}$$

According to equation (21), this can be reformulated as:

$$\hat{u}_i(y,\omega) = \sum_{k=1}^{n_{\mathrm{a}}} \frac{1}{2\pi v}\int_{-\infty}^{+\infty} \tilde{h}_{ji}\left(\frac{\omega-\tilde{\omega}}{v},\omega\right)\hat{g}_{\mathrm{d}kj}(\tilde{\omega})\exp\left[-\mathrm{i}\frac{\omega-\tilde{\omega}}{v}(y-y_{k0})\right]\mathrm{d}\tilde{\omega} \tag{28}$$

3.5 Response in a moving frame of reference

As will be demonstrated in the following section, the dynamic component $g_{\mathrm{d}kj}(t)$ of the axle loads is determined by dynamic train-track interaction and computed by means of a compliance formulation in a moving frame of reference [21]. This requires the calculation of the track response in a coordinate system $\hat{\mathbf{x}} = \{x, \hat{y}, z\}^{\mathrm{T}}$ with $\hat{y} = y - vt$. The latter is derived from equation (20) by an additional inverse Fourier transform with respect to ω and by replacing y by $\hat{y} + vt$ on the right hand side:

$$u_i(\hat{y},t) = \sum_{k=1}^{n_{\mathrm{a}}} \frac{1}{2\pi}\int_{-\infty}^{+\infty}\frac{1}{2\pi}\int_{-\infty}^{+\infty} \tilde{h}_{ji}(k_y,\omega)g_{\mathrm{d}kj}(\omega-k_y v)\exp\left[-\mathrm{i}k_y(\hat{y}+vt-y_{k0})\right]\mathrm{d}k_y\exp(\mathrm{i}\omega t)\,\mathrm{d}\omega \tag{29}$$

A change of variables $\omega = \tilde{\omega} + k_y v$ leads to the following expression:

$$u_i(\hat{y}, t) = \frac{1}{2\pi} \int_{-\infty}^{+\infty} \sum_{k=1}^{n_\mathrm{a}} \left[\frac{1}{2\pi} \int_{-\infty}^{+\infty} \tilde{h}_{ji}(k_y, \tilde{\omega} + k_y v) \exp\left[-\mathrm{i}k_y(\hat{y} - y_{k0})\right] \, \mathrm{d}k_y \right] \hat{g}_{\mathrm{d}kj}(\tilde{\omega}) \exp(\mathrm{i}\tilde{\omega}t) \, \mathrm{d}\tilde{\omega} \quad (30)$$

For each axle k, the response is obtained as the inverse Fourier transform with respect to $\tilde{\omega}$ of the product of the bracketed term and the frequency content $\hat{g}_{\mathrm{d}kj}(\tilde{\omega})$ of the moving load. Each column of the bracketed term represents the response in a moving frame of reference due to an impulsive moving load located at y_{k0} at the time $t = 0$.

3.6 Conclusion

In the previous subsections, we derived general expressions in the spatial-time and spatial-frequency domain for the response of a 3D and 2.5D medium, that is characterized by its transfer function, to a sequence of (static or dynamic) axle loads moving at constant speed. In the case of a 2.5D medium, a complementary transformation to the wavenumber-frequency domain is made. In the following section, we will detail how the transfer function of a track-soil system can be computed by means of semi-analytical or numerical methods. Furthermore, it will be shown how the dynamic axle loads can be derived from the vehicle and track compliance and the track unevenness.

4. NUMERICAL MODELS

4.1 Introduction

This section is based on the keynote paper of Lombaert et al. [117] presented at IWRN11, the TRAFFIC User's Guide, [121], and journal papers by Lombaert and Degrande [115], Ntotsios et al. [140, 141] and Thompson et al. [179].

During the past decades, a lot of effort was spent to the development of numerical models to predict vibration in buildings due to trains running at grade and in tunnels, as well as to assess the performance of vibration mitigation measures at the track, in the propagation path and at the buildings.

As explained in section 2, railway induced vibration is generated by quasi-static and dynamic axle loads. The latter are due to wheel and rail unevenness, impacts due to rail joints and wheel flats, and parametric excitation due to sleeper periodicity [176]. When moving axle loads are applied to the track, elastic waves propagate in the soil and excite nearby buildings, resulting in vibration and re-radiated noise [162, 210, 3].

The prediction of ground-borne vibration in buildings is usually performed in a two-step procedure, where the free field response due to a running train is calculated first and subsequently used for computing the building response. The wavelength in the soil is usually assumed to be short compared to the track-building distance, so that the dynamic axle loads are not affected by the presence of nearby buildings [29].

If the incident wave field in the soil is available, the response of a building can be computed using methods that were developed for seismic analysis of structures. Dynamic soil-structure interaction can, for example, be accounted for by means of a 3D coupled finite element - boundary element (FE-BE) model [151, 55, 197], taking into consideration the effect of the structure on the incoming wave field. When dynamic soil-structure interaction is disregarded, classical structural dynamic analysis methods can be employed to compute the response of a building due to imposed base motion [19]. Re-radiated noise in the building can finally be evaluated by solving Helmholtz' equation with imposed structural velocities along the boundaries, assuming weak coupling between structural vibration and structure-borne noise [50, 51].

In the following, we will assume that the aforementioned methods to evaluate the building response are available, so that our focus can be on the prediction of the free field response (or the incident wave field). Furthermore, the discussion is limited to models that take into account dynamic excitation, as this is of main interest for problems involving ground-borne vibration.

Numerical prediction models for railway induced ground vibration are generally obtained by coupling sub-models for the train, the track, and the soil. The dynamic behaviour of the train is usually represented by a relatively simple multi-body vehicle model whereas a much larger modelling and computational effort is required for capturing the dynamic behaviour of the track and the soil. In order to obtain accurate numerical prediction of ground-borne vibration, detailed information is needed regarding the parameters that characterize the dynamic behaviour of these components as well as the excitation. Of particular importance are the dynamic soil characteristics that must be derived indirectly from in situ geophysical tests [119, 92]. Given the small amplitude of deformations in the soil, linear elastic behaviour is assumed.

The prediction of the incident wave field usually also consists of two steps. First, the train-track-soil interaction problem is solved in order to compute the dynamic axle loads. For example, this can be done by means of equation (5) when assuming translational invariance of the problem geometry and a perfect contact between the train and the track. Second, the dynamic axle loads are applied to the track and the free field response is computed. When a set of transfer functions or impulse response functions $\mathbf{H}(\mathbf{x}, \mathbf{x}', t)$ is available that relates the response at a point $\mathbf{x}'$ to the load at a point $\mathbf{x}$ on the track, this can be formally written according to equation (9), which is repeated here for convenience (using vector-matrix notation in stead of index notation):

$$\mathbf{u}(\mathbf{x}, t) = \sum_{k=1}^{n_a} \int_{-\infty}^{t} \mathbf{H}(\mathbf{x}_k(\tau), \mathbf{x}, t-\tau) \mathbf{g}_k(\tau) \, \mathrm{d}\tau \tag{31}$$

The transfer function $\mathbf{H}(\mathbf{x}, \mathbf{x}', t)$ between the track and the free field determines how the load applied at a position $\mathbf{x}$ on the track is transferred to the soil, to provide response at a point $\mathbf{x}'$. The transfer is determined by track-soil interaction, which will give rise to waves of the coupled system that propagate along the track. The resulting load transfer could be compared with a combined filtering in the time and space domain. Generally, a distribution of the load over a larger area, determined by the load spreading across the track width and in the direction along the track, will result in a reduction in the high frequency vibration transmitted to the free field. This is due to destructive interference of waves transmitted by different parts of the contact area. An accurate prediction of the stress distribution at the track-soil interface is therefore essential for predicting ground-borne vibration due to railway traffic, in particular when the wavelength in the soil is comparable or smaller than the characteristic dimension of the stress distribution area [172].

Numerical models with different degrees of complexity have been developed for the prediction of vibration due to trains running at grade and in tunnels; they range from (semi-)analytical models to 3D coupled finite element-boundary element models (FE-BE), taking into consideration dynamic soil-structure interaction at the source and receiver, as well as geometrical characteristics of the problem (e.g. 2.5D and periodic models versus 3D models).

General purpose 3D finite element (FE) methods offer the largest flexibility in modelling, but require appropriate absorbing boundary conditions to avoid spurious reflections at the boundaries of the finite volume of soil accounted for in the analysis [46, 45]. Local absorbing boundary conditions, infinite elements [208], integral transform methods [131], and perfectly matched layers [56] have been used to account for Sommerfeld's radiation conditions. Alternatively, 3D coupled FE-BE methods can be used [58, 142]. The versatility of 3D FE and 3D FE-BE models comes at a very high computational cost, however. Dedicated models have therefore been developed that exploit the (assumed) regularity of the track and the underlying soil.

When the track and the soil are regarded as translationally invariant, a Fourier transformation from the longitudinal coordinate y along the track to the wavenumber k_y leads to an efficient solution in the wavenumber-frequency domain [6, 57], as explained in detail in subsection 3.3. In this so-called 2.5D methodology, a problem with 2D geometry is solved for each wavenumber k_y and frequency ω to compute $\tilde{u}_i(x, k_y, z, \omega)$ according to equation (19). The 3D solution $\hat{u}_i(x, y, z, \omega)$ is recovered by evaluation of an inverse Fourier transformation of the wavenumber k_y to the longitudinal coordinate y, according to equations (20) or (21). Because of their high computational efficiency and relatively modest modelling effort, 2.5D methods have been applied by a large number of researchers to study ground-borne vibration due to railway traffic at grade, for example the research groups at ISVR [163, 164, 168, 169], TU Delft [127], NGI [124], NTU [208], BAM [7], FEUP [24, 23], Chalmers University [97], and KU Leuven [119, 115], as well as for underground railway traffic, for example at the University of Cambridge [54, 53, 83], NTU [209], TU Munich [131], ISVR [167, 4, 140, 90, 141], and KU Leuven [57, 56, 81].

Due to the assumed invariance in the longitudinal direction along the track, 2.5D models do not allow account to be taken of periodicity as occurring e.g. in a ballasted track where the rails are discretely supported by sleepers. Therefore, the stress distribution under the sleepers is not entirely correctly predicted, which is important at high frequencies when wavelengths in the track and soil are of the same order of magnitude as the sleeper dimensions. For the same reason, 2.5D models cannot account for parametric excitation, unless represented by an equivalent geometric unevenness [7], nor for segmented tunnel structures. In order to take into account the periodicity of the track or tunnel structure, a similar methodology may be used which is based on the Floquet instead of the Fourier transform [20, 36, 33]. In this case, the 3D solution is obtained based on the discretization of a single periodic cell. Periodic FE-PML and FE-BE models [67, 18] are more demanding from a computational point of view, however, and will therefore not be used within the frame of SILVARSTAR.

Applications of invariant and periodic models include the design of mitigation measures at the source (rail and under-sleeper pads, floating slab tracks) [82], in the transmission path (wave barriers, heavy masses next to the track) [25, 178], and at the receiver (base isolation, tuned mass dampers) [175]. 2.5D coupled FE-BE models were used by ISVR and KU Leuven in the FP7 project RIVAS to assess the efficiency of vibration mitigation measures in the transmission path, such as jet grouting walls [28, 25, 177], sheet pile walls [42], open trenches and soft-filled barriers [178], and heavy masses on the surface [41].

Still other types of model are required for the analysis of vibration generated by trains crossing transition zones, switches and crossings [58, 148]. Limitations arising from the use of a linear translationally invariant or periodic model for the track can be partially circumvented [92] by using a more detailed model for the train and the track with a suitably chosen soil stiffness [137, 180, 139, 91] in the first step where the dynamic vehicle loads are considered. The use of time domain FE analysis allows for the consideration of non-linear components, e.g. rail pad behaviour, as well as loss of contact between the wheel and the rail [139].

Numerical models have undoubtedly contributed to a better understanding of physical mechanisms in the generation of ground-borne vibration, providing insight into results of field measurements and vibration problems encountered in practice. In design, numerical models are particularly useful in situations where a new building is to be built close to an existing track or tunnel or where a new railway line is to be constructed close to existing buildings. They can be used to assess the environmental impact of new railway lines or to develop and design mitigation measures aimed at reducing vibration nuisance to an acceptable level.

There are also, however, important limitations in the use of numerical models which can be attributed to model and parameter uncertainty. First, the simplifications introduced for modelling may be too restrictive for the model to be useful. The geometry of the track and the soil may not be translationally invariant or periodic, e.g. due to the presence of transition zones in the track, inclined soil layers or heterogeneities in the soil. Hunt and his co-workers have recently assessed a number of simplifying assumptions in the prediction of ground-borne vibration due to underground railway traffic. Deviations of up to $10\,\mathrm{dB}$ have been found at particular locations and frequencies, when assuming horizontal soil stratification and disregarding the slightly inclined nature of soil layers [93], disregarding voids at the tunnel–soil interface [94] or leaving out of consideration a neighbouring tunnel [108]. Second, even when situations are adequately represented by simple model geometries, the model parameters are also subject to significant uncertainty. For new-build situations, estimations will have to be made based on prior experience or engineering judgement. In existing situations, measurements of track unevenness [115] or in situ tests for identification of track and soil properties will not allow all model parameter uncertainty to be eliminated. Schevenels et al. [160] have quantified the uncertainty in the prediction of ground vibration transmission that arises from the limited resolution of a Spectral Analysis of Surface Waves test. Hunt and Hussein [80] have shown that deviations due to model parameter uncertainty are expected to be of the same order of magnitude as those arising from model uncertainty. Although the importance of prediction uncertainty is generally recognized, its quantification in the numerical prediction of ground-borne vibrations has seldom been addressed. This is essential, however, in order to arrive at robust predictions as needed in engineering practice.

It can be concluded that, during the past decades, great advances have been made regarding the development of numerical models for railway induced vibration due to trains running at grade and in tunnels. For industrial applications, 2.5D models are particularly attractive as they offer realistic predictions at a reasonable computational cost. Examples of such software tools developed at universities and research centres are MOTIV (ISVR) [140, 141], TRAFFIC (KU Leuven) [121, 116, 119, 120, 115, 57], the Pipe-in-Pipe model (University of Cambridge) [83, 84, 81, 85], and MEFISSTO (CSTB) [155, 197].

In the following, we will therefore explain in more detail the key components of 2.5D models: the computation of the transfer functions of the track-soil system, the estimation of the dynamic axle loads (based on vehicle and track compliance, as well as track unevenness), and the computation of the free field response. These will be essential components of the proposed vibration prediction tool in SILVARSTAR. Throughout this section, we will illustrate the results using a case study based on the dynamic response of a ballasted track analysed with the software tools MOTIV (ISVR) and GroundVIB (Vibratec).

4.2 Transfer functions of the coupled track-soil system

4.2.1 General formulation

The equations of motion of the coupled track-soil system are formulated in the wavenumber–frequency domain by assembling the dynamic stiffness matrices (also called impedance matrices) of the track and the layered subsoil. In a first step, these equations are solved for a vertical unit load at a fixed track position, resulting in the response of the track and the interface between the track and the soil. In a second step, the latter is used to compute the transfer functions from the excitation point on the track to a receiver in the free field.

The track is assumed to be located at the surface of a horizontally layered halfspace, with a geometry that is invariant in the longitudinal direction $\mathbf{e}_y$. This allows to perform a Fourier transformation of the coordinate y to the wavenumber k_y, resulting in the following equations of motion of the coupled track-soil system in the wavenumber-frequency domain:

$$\left[\tilde{\mathbf{K}}^{\mathrm{tr}} + \tilde{\mathbf{K}}^{\mathrm{s}}\right] \tilde{\mathbf{u}}_{\mathrm{tr}} = \tilde{\mathbf{f}}_{\mathrm{tr}} \tag{32}$$

where $\tilde{\mathbf{K}}^{\mathrm{tr}}$ and $\tilde{\mathbf{K}}^{\mathrm{s}}$ represent the dynamic stiffness matrices of the track and the soil, respectively, while $\tilde{\mathbf{u}}_{\mathrm{tr}}$ is the track displacement vector and $\tilde{\mathbf{f}}_{\mathrm{tr}}$ is the force vector applied to the track. As introduced in section 3, a tilde above a variable denotes its representation in the wavenumber-frequency domain, so that the arguments k_y and ω can be omitted for all variables.

It is convenient to distinguish between the n_{t} degrees of freedom of the track, collected in the displacement vector $\tilde{\mathbf{u}}_{\mathrm{t}}$, and the n_{s} degrees of freedom on the track-soil interface, collected in the displacement vector $\tilde{\mathbf{u}}_{\mathrm{s}}$, and to split the dynamic stiffness matrices of the track and the soil in equation (32) accordingly:

$$\begin{bmatrix} \tilde{\mathbf{K}}^{\mathrm{tr}}_{\mathrm{tt}} & \tilde{\mathbf{K}}^{\mathrm{tr}}_{\mathrm{ts}} \\ \tilde{\mathbf{K}}^{\mathrm{tr}}_{\mathrm{st}} & \tilde{\mathbf{K}}^{\mathrm{tr}}_{\mathrm{ss}} + \tilde{\mathbf{K}}^{\mathrm{s}}_{\mathrm{ss}} \end{bmatrix} \begin{Bmatrix} \tilde{\mathbf{u}}_{\mathrm{t}} \\ \tilde{\mathbf{u}}_{\mathrm{s}} \end{Bmatrix} = \begin{Bmatrix} \tilde{\mathbf{f}}_{\mathrm{t}} \\ \mathbf{0} \end{Bmatrix} \tag{33}$$

where the loading is only applied to degrees of freedom related to the track (super-)structure.

The solution procedure can be applied to continuously supported tracks, as well as to discretely supported tracks, provided that equivalent characteristics of the discrete track are calculated. Knothe and Grassie [101] have investigated the track receptance of a discretely supported track and show how the rail receptance at a sleeper and between sleepers has a similar behaviour up to about 500 Hz. Knothe and Wu [102] have compared the track receptance for a discretely supported track and a continuously supported track and found similar results up to 600 Hz. Equivalent continuous track models therefore provide a reliable prediction of the track receptance, but do not account for parametric excitation as the small spatial variation of the support stiffness of the discretely supported track is disregarded.

In the following, we will first elaborate an expression for the track impedance matrix $\tilde{\mathbf{K}}^{\rm tr}$, restricting the discussion to the case of a ballast track. A very similar procedure can be followed to formulate the impedance matrix of a (floating) slab track [114, 121]. This is followed by the derivation of the soil impedance matrix $\tilde{\mathbf{K}}^{\rm s}_{\rm ss}$ by means of a boundary element or (equivalent) collocation formulation.

Particular attention is paid to formulations as implemented in the TRAFFIC toolbox (KU Leuven) [119] and in the MOTIV software (ISVR) [163, 140, 141], since these are the state-of-the-art prediction models that will be used in SILVARSTAR.

4.2.2 Track impedance matrix

The ballast track under consideration is represented by an equivalent continuous model (figure 5). The origin of the Cartesian frame of reference is at the centre of the track-soil interface Σ, with the $x-$axis pointing to the right and the $z-$axis pointing upwards. Analytical expressions are derived for the elements of the track impedance matrix $\tilde{\mathbf{K}}^{\rm tr}$.

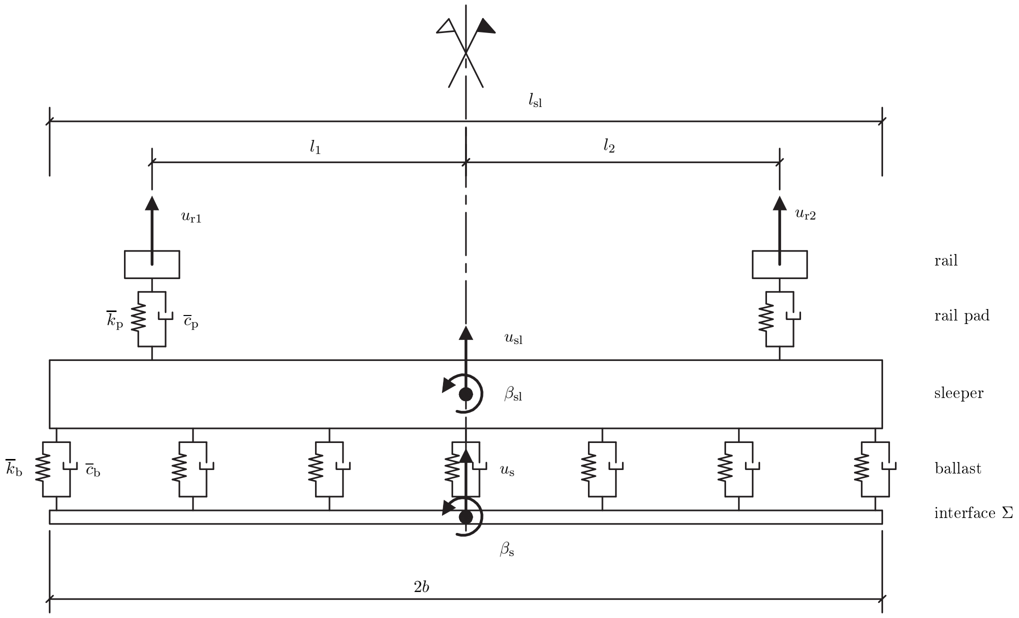

Figure 5: Cross section of a ballasted track model.

The rails are modelled as Euler-Bernoulli beams with a bending stiffness $E_\mathrm{r}I_\mathrm{r}$ and a mass $\rho_\mathrm{r}A_\mathrm{r}$ per unit length. The rail displacements are denoted as $u_{\mathrm{r}1}(y,t)$ and $u_{\mathrm{r}2}(y,t)$. The positions of the rail are determined by l_1 and l_2.

The rail pads are modelled as continuous spring–damper connections. The stiffness k_rp and damping coefficient c_rp of a single rail pad are used to calculate an equivalent stiffness per unit length $\overline{k}_\mathrm{rp} = k_\mathrm{rp}/d$ and damping coefficient $\overline{c}_\mathrm{rp} = c_\mathrm{rp}/d$ in the continuous model, where d is the sleeper distance.

The sleepers are assumed to be rigid in the plane of the track cross-section, so that the vertical sleeper displacements along the track are determined by the vertical displacement $u_\mathrm{sl}(y,t)$ at the centre of mass of the sleeper and the rotation $\beta_\mathrm{sl}(y,t)$ about this centre. The sleepers are assumed not to contribute to the longitudinal stiffness of the track, and are modelled as a uniformly distributed mass $\overline{m}_\mathrm{sl} = m_\mathrm{sl}/d$ per unit length along the track, where m_sl is the mass of an individual sleeper. The width $2b$ of the track-soil interface is often taken equal to the sleeper length l_sl.

If the ballast bed is assumed to act as a set of distributed, independent linear springs and dampers, each sleeper is only supported by that part of the ballast that is in contact with the sleeper. For reasons of stability, the sleeper is usually only supported under the rails, so that the vertical spring stiffness k_b per sleeper [N/m] is calculated from the effective support length e_sl per rail, the sleeper width b_sl and the ballast stiffness K_b [N/m^3] as $2e_\mathrm{sl}b_\mathrm{sl}K_\mathrm{b}$. The smeared ballast stiffness $\overline{k}_\mathrm{b}$ [N/m^2] is equal to k_b/d. When viscous damping in the ballast bed is accounted for, the ballast impedance equals $\overline{k}_\mathrm{b} + \mathrm{i}\omega\overline{c}_\mathrm{b}$. In a similar way, the discrete support of the sleepers and the effective width determine the part of the ballast mass that is coupled to the sleepers and the soil.

The software packages TRAFFIC and MOTIV use a similar model for the ballast track, but differ with respect to the assumed kinematic conditions on the track-soil interface Σ in the track's cross-section.

Implementation in the TRAFFIC toolbox. In the TRAFFIC software, rigid body kinematics are assumed on the track-soil interface Σ in the plane of the track cross section, limiting the number of degrees of freedom on the track-soil interface to $n_\mathrm{s} = 2$. The vertical displacement $u_{\mathrm{s}z}(x,y,t)$ at the track-soil interface is determined by the vertical displacement $u_\mathrm{s}(y,t)$ at the centre of the track-soil interface and the rotation $\beta_\mathrm{s}(y,t)$ about this centre:

$$u_{\mathrm{s}z}(x,y,t) \;=\; u_\mathrm{s}(y,t) + \beta_\mathrm{s}(y,t)x = \boldsymbol{\phi}_\mathrm{t}(x)\mathbf{u}_\mathrm{s}(y,t) \qquad \text{on}\,\Sigma \tag{34}$$

where $\boldsymbol{\phi}_\mathrm{t}(x)$ is the vector $\{1, x\}$ that contains the rigid body displacement modes of track-soil interface, while the vector $\mathbf{u}_\mathrm{s}(y,t)$ contains the vertical displacement $u_\mathrm{s}(y,t)$ and the rotation $\beta_\mathrm{s}(y,t)$, which can be interpreted as generalized degrees of freedom.

In the wavenumber-frequency domain, and for the ballast track under consideration, the displacement vector of the track (super-structure) $\tilde{\mathbf{u}}_\mathrm{t} = \{\tilde{u}_{\mathrm{r}1}, \tilde{u}_{\mathrm{r}2}, \tilde{u}_\mathrm{sl}, \tilde{\beta}_\mathrm{sl}\}^\mathrm{T}$ has $n_\mathrm{t} = 4$ degrees of freedom, while the displacement vector of the track-soil interface $\tilde{\mathbf{u}}_\mathrm{s} = \{\tilde{u}_\mathrm{s}, \tilde{\beta}_\mathrm{s}\}^\mathrm{T}$ has $n_\mathrm{s} = 2$ degrees of freedom. The vector $\tilde{\mathbf{f}}_\mathrm{t}$ contains the forces applied on both rails and is equal to $\{\tilde{f}_{\mathrm{r}1}, \tilde{f}_{\mathrm{r}2}, 0, 0\}^\mathrm{T}$.

Consequently, the track impedance matrix $\tilde{\mathbf{K}}^{\mathrm{tr}}$ is of dimension $(n_{\mathrm{t}}+n_{\mathrm{s}}) \times (n_{\mathrm{t}}+n_{\mathrm{s}})$ and detailed as:

$$\tilde{\mathbf{K}}^{\mathrm{tr}} = \begin{bmatrix} \tilde{K}_{\mathrm{r}}+\tilde{K}_{\mathrm{rp}} & 0 & -\tilde{K}_{\mathrm{rp}} & -\tilde{K}_{\mathrm{rp}}x_1 & 0 & 0 \\ 0 & \tilde{K}_{\mathrm{r}}+\tilde{K}_{\mathrm{rp}} & -\tilde{K}_{\mathrm{rp}} & -\tilde{K}_{\mathrm{rp}}x_2 & 0 & 0 \\ -\tilde{K}_{\mathrm{rp}} & -\tilde{K}_{\mathrm{rp}} & 2\tilde{K}_{\mathrm{rp}}+\tilde{K}_{\mathrm{sl,b}}+\tilde{K}_{\mathrm{b}}-\frac{\overline{m}_{\mathrm{b}}}{3}\omega^2 & \tilde{K}_{\mathrm{rp}}(x_1+x_2) & -\tilde{K}_{\mathrm{b}}-\frac{\overline{m}_{\mathrm{b}}}{6}\omega^2 & 0 \\ -\tilde{K}_{\mathrm{rp}}x_1 & -\tilde{K}_{\mathrm{rp}}x_2 & \tilde{K}_{\mathrm{rp}}(x_1+x_2) & \begin{array}{c}\tilde{K}_{\mathrm{sl,t}}+\tilde{K}_{\mathrm{rp}}\left(x_1^2+x_2^2\right) \\ +\frac{b^2}{3}\left(\tilde{K}_{\mathrm{b}}-\frac{\overline{m}_{\mathrm{b}}}{3}\omega^2\right)\end{array} & 0 & -\frac{b^2}{3}\left(\tilde{K}_{\mathrm{b}}+\frac{\overline{m}_{\mathrm{b}}}{6}\omega^2\right) \\ 0 & 0 & -\tilde{K}_{\mathrm{b}}-\frac{\overline{m}_{\mathrm{b}}}{6}\omega^2 & 0 & \tilde{K}_{\mathrm{b}}-\frac{\overline{m}_{\mathrm{b}}}{3}\omega^2 & 0 \\ 0 & 0 & 0 & -\frac{b^2}{3}\left(\tilde{K}_{\mathrm{b}}+\frac{\overline{m}_{\mathrm{b}}}{6}\omega^2\right) & 0 & +\frac{b^2}{3}\left(\tilde{K}_{\mathrm{b}}-\frac{\overline{m}_{\mathrm{b}}}{3}\omega^2\right) \end{bmatrix} \quad (35)$$

where x_1 and x_2 are the coordinates of the rails, $\tilde{K}_{\mathrm{r}} = E_{\mathrm{r}}I_{\mathrm{r}}k_y^4 - \rho_{\mathrm{r}}A_{\mathrm{r}}\omega^2$ denotes the rail impedance in the wavenumber–frequency domain and $\tilde{K}_{\mathrm{rp}} = \overline{k}_{\mathrm{rp}} + \mathrm{i}\omega\overline{c}_{\mathrm{rp}}$ is the dynamic stiffness of the rail pads. The sleeper's translational inertia term $\tilde{K}_{\mathrm{sl,b}}$ and rotational inertia term $\tilde{K}_{\mathrm{sl,t}}$ are calculated from the mass per unit length $\overline{m}_{\mathrm{sl}}$ as $-\overline{m}_{\mathrm{sl}}\omega^2$ and $-b^2\overline{m}_{\mathrm{sl}}\omega^2/3$, respectively. The dynamic stiffness $\tilde{K}_{\mathrm{b}}$ of the ballast in the vertical direction is equal to $\overline{k}_{\mathrm{b}} + \mathrm{i}\omega\overline{c}_{\mathrm{b}}$. The rotational impedance equals $b^2\tilde{K}_{\mathrm{b}}/3$, assuming a uniform support of the ballast along the width $2b$ of the interface.

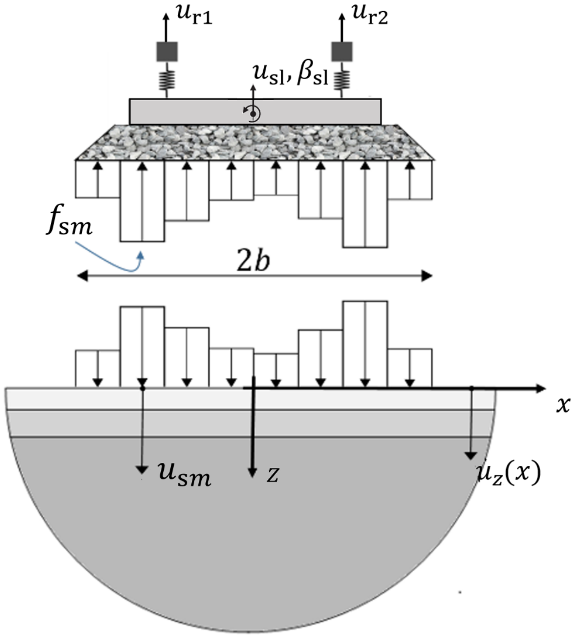

Figure 6: Discretization of the stress field across the track-soil interface in MOTIV [140].

Implementation in the MOTIV software. The MOTIV software follows a similar approach where it is assumed that the track exerts a vertical distributed load on the track-soil interface Σ in the plane of the track's cross-section (so relaxed boundary conditions are assumed). However, in order to allow for an arbitrary distribution of displacements and tractions across the width of the track, the interface conditions are discretised (figure 6). The discretisation introduces a finite sum of the normal tractions at the track-soil interface Σ, which is divided in $n_{\mathrm{s}} = 2b/\Delta$ strips of equal width Δ. Across the interface, discrete values $x_m = -b + \Delta(2m-1)/2$ of the x-coordinate are selected, positioned at the middle of each strip m, where $1 \leq m \leq n_\mathrm{s}$. Within each strip m the stresses are assumed to be constant, while displacement compatibility is required along the lines $x = x_m$.

In the wavenumber-frequency domain, and for the ballast track under consideration, the displacement vector of the track (super-structure) $\tilde{\mathbf{u}}_\mathrm{t} = \{\tilde{u}_\mathrm{r1}, \tilde{u}_\mathrm{r2}, \tilde{u}_\mathrm{sl}, \tilde{\beta}_\mathrm{sl}\}^\mathrm{T}$ has $n_\mathrm{t} = 4$ degrees of freedom. The displacement vector of the track-soil interface is equal to $\tilde{\mathbf{u}}_\mathrm{s} = \{\tilde{u}_\mathrm{s1}, \ldots, \tilde{u}_{\mathrm{s}n_\mathrm{s}}\}^\mathrm{T}$ and contains n_s vertical degrees of freedom on the track-soil interface at positions $x = x_m$. The track impedance matrix $\tilde{\mathbf{K}}^\mathrm{tr}$ is of dimension $(n_\mathrm{t} + n_\mathrm{s}) \times (n_\mathrm{t} + n_\mathrm{s})$ and equal to:

$$\tilde{\mathbf{K}}^\mathrm{tr} = \begin{bmatrix} \tilde{K}_\mathrm{r}+\tilde{K}_\mathrm{rp} & 0 & -\tilde{K}_\mathrm{rp} & -\tilde{K}_\mathrm{rp}x_1 & \mathbf{0}_{n_\mathrm{s}}^\mathrm{T} \\ 0 & \tilde{K}_\mathrm{r}+\tilde{K}_\mathrm{rp} & -\tilde{K}_\mathrm{rp} & -\tilde{K}_\mathrm{rp}x_2 & \mathbf{0}_{n_\mathrm{s}}^\mathrm{T} \\ -\tilde{K}_\mathrm{rp} & -\tilde{K}_\mathrm{rp} & 2\tilde{K}_\mathrm{rp}+\tilde{K}_\mathrm{sl,b}+\tilde{K}_\mathrm{b}-\frac{\overline{m}_\mathrm{b}}{3}\omega^2 & \tilde{K}_\mathrm{rp}(x_1+x_2) & -\frac{1}{n_\mathrm{s}}\left(\tilde{K}_\mathrm{b}+\frac{\overline{m}_\mathrm{b}}{6}\omega^2\right)\mathbf{1}_{n_\mathrm{s}}^\mathrm{T} \\ -\tilde{K}_\mathrm{rp}x_1 & -\tilde{K}_\mathrm{rp}x_2 & \tilde{K}_\mathrm{rp}(x_1+x_2) & \tilde{K}_\mathrm{sl,t}+\tilde{K}_\mathrm{rp}\left(x_1^2+x_2^2\right)-\frac{1}{n_\mathrm{s}}\sum_{m=1}^{n_\mathrm{s}}\tilde{K}_\mathrm{b}x_m|x_m| & \frac{1}{n_\mathrm{s}}\left(\tilde{K}_\mathrm{b}-\frac{\overline{m}_\mathrm{b}}{6}\omega^2\right)\mathbf{x}_{n_\mathrm{s}}^\mathrm{T} \\ \mathbf{0}_{n_\mathrm{s}} & \mathbf{0}_{n_\mathrm{s}} & -\frac{1}{n_\mathrm{s}}\left(\tilde{K}_\mathrm{b}+\frac{\overline{m}_\mathrm{b}}{6}\omega^2\right)\mathbf{1}_{n_\mathrm{s}} & \frac{1}{n_\mathrm{s}}\left(\tilde{K}_\mathrm{b}-\frac{\overline{m}_\mathrm{b}}{6}\omega^2\right)\mathbf{x}_{n_\mathrm{s}} & \frac{1}{n_\mathrm{s}}\left(\tilde{K}_\mathrm{b}-\frac{\overline{m}_\mathrm{b}}{3}\omega^2\right)\mathbf{I}_{n_\mathrm{s}} \end{bmatrix} \quad (36)$$

where x_1 and x_2 are the coordinates of the rails and $\mathbf{x}_{n_\mathrm{s}} = \{x_1, \ldots, x_{n_\mathrm{s}}\}^\mathrm{T}$ is the vector that collects the n_s lateral discrete coordinates x_m of each strip; $\mathbf{0}_{n_\mathrm{s}}$ and $\mathbf{1}_{n_\mathrm{s}}$ are vectors of n_s elements formed of zeros and ones, respectively, and $\mathbf{I}_{n_\mathrm{s}}$ is the identity matrix of size $n_\mathrm{s} \times n_\mathrm{s}$.

4.2.3 Soil impedance matrix

As natural soil deposits are often horizontally layered, it will be assumed that the soil can be represented by a horizontally layered halfspace. Each layer is characterized by its thickness d, and five material properties: the shear wave velocity C_s (or S-wave, secondary wave, rotational wave), the dilatational wave velocity C_p (or P-wave, primary wave, compression wave), the hysteretic material damping ratio in shear and dilatational deformation D_s and D_p, and the density ρ. The shear and dilatational wave velocity are equal to:

$$C_\mathrm{s} = \sqrt{\frac{\mu}{\rho}} \quad ; \quad C_\mathrm{p} = \sqrt{\frac{\lambda + 2\mu}{\rho}} \quad (37)$$

where the Lamé coefficients μ and λ are defined as follows in terms of Young's modulus E and Poisson's ratio ν:

$$\mu = \frac{E}{2(1+\nu)} \quad ; \quad \lambda = \frac{E\nu}{(1+\nu)(1-2\nu)} \quad (38)$$

Relative motion and friction between grains in the solid skeleton or presence of moisture in the pores results in energy dissipation or material damping. This can be accounted for in the frequency domain by means of the correspondence principle where both Lamé coefficients are replaced by the following complex moduli:

$$\mu^\star = \mu(1 + 2D_\mathrm{s}\mathrm{i}) \quad ; \quad (\lambda + 2\mu)^\star = (\lambda + 2\mu)(1 + 2D_\mathrm{p}\mathrm{i}) \quad (39)$$

where i is the imaginary unit. These complex Lamé coefficients in turn result in complex wave velocities $C_\mathrm{s}^\star$ and $C_\mathrm{p}^\star$.

In order to compute the impedance of the soil below the track, a boundary element or (equivalent) collocation method can be used. The Green's functions or fundamental solutions used in a boundary element formulation represent the displacement and traction tensors in the structure (here a layered halfspace) at a receiver $\mathbf{x}^{\mathrm{R}}$ in a direction $\mathbf{e}_j$ due to an impulsive load $\delta(t)$ applied at a source $\mathbf{x}^{\mathrm{S}}$ in a direction $\mathbf{e}_j$. In the frequency domain, these Green's functions will be denoted as $\hat{u}_{ij}^{\mathrm{G}}(\mathbf{x}^{\mathrm{S}}, \mathbf{x}^{\mathrm{R}}, \omega)$ and $\hat{t}_{ij}^{\mathrm{G}}(\mathbf{x}^{\mathrm{S}}, \mathbf{x}^{\mathrm{R}}, \omega)$. The Green's functions of a horizontally layered halfspace can be computed with a direct stiffness method or a thin layer method, as developed by Kausel and Roësset [100, 99] and implemented, for example, in the Elastodynamics Toolbox (EDT) [157] developed at KU Leuven.

Implementation in the TRAFFIC toolbox. In the TRAFFIC software, rigid body kinematics are assumed on the track-soil interface Σ. A weak formulation of the vertical equilibrium at the track-soil interface Σ is elaborated to calculate the elements of the 2×2 soil impedance matrix $\tilde{\mathbf{K}}_{\mathrm{ss}}^{\mathrm{s}}$:

$$\tilde{\mathbf{K}}_{\mathrm{ss}}^{\mathrm{s}} = \begin{bmatrix} \tilde{K}_{\mathrm{ss}11}^{\mathrm{s}} & 0 \\ 0 & \tilde{K}_{\mathrm{ss}22}^{\mathrm{s}} \end{bmatrix} \tag{40}$$

with

$$\tilde{K}_{\mathrm{ss}ij}^{\mathrm{s}}(k_y, \omega) = \int_{\Sigma} \phi_{\mathrm{t}i} \tilde{t}_{\mathrm{s}z}(\tilde{\mathbf{u}}_{\mathrm{sc}}(\phi_{\mathrm{t}j}))\, \mathrm{d}\Gamma \tag{41}$$

where $\tilde{\mathbf{u}}_{\mathrm{sc}}(\phi_{\mathrm{t}j})$ is the scattered wave field in the soil due to an imposed displacement $\phi_{\mathrm{t}j}$ at the track-soil interface Σ in the wavenumber–frequency domain. $\tilde{t}_{\mathrm{s}z}(\tilde{\mathbf{u}}_{\mathrm{sc}}(\phi_{\mathrm{t}j}))$ is the vertical component of the soil traction vector $\tilde{\mathbf{t}}_{\mathrm{s}} = \tilde{\boldsymbol{\sigma}}_{\mathrm{s}}\mathbf{n}$ on a boundary with unit outward normal $\mathbf{n}$ due to this scattered wave field $\tilde{\mathbf{u}}_{\mathrm{sc}}(\phi_{\mathrm{t}j})$.

A boundary element method is used to calculate the soil tractions $\tilde{t}_{\mathrm{s}z}(\tilde{\mathbf{u}}_{\mathrm{sc}}(\phi_{\mathrm{t}j}))$ at the track-soil interface Σ, assuming that the track is located at the soil's surface [116, 6]. The boundary element formulation is based on the boundary integral equations in the wavenumber-frequency domain, using the Green's functions of a horizontally layered soil [122, 32, 100, 99].

Implementation in the MOTIV software. An alternative but equivalent approach is applied in the MOTIV software, where the vector $\tilde{\mathbf{u}}_{\mathrm{s}} = \{\tilde{u}_{\mathrm{s}1}, \ldots, \tilde{u}_{\mathrm{s}n_{\mathrm{s}}}\}^{\mathrm{T}}$ collects the vertical displacements on the track-soil interface Σ along the lines $x = x_m$ $(m = 1, \ldots, n_{\mathrm{s}})$. The vertical displacement $\tilde{u}_{\mathrm{s}m}(x_m, k_y, \omega)$ of a point on the ground at position x_m can be calculated as the superposition of the displacements due to the excitation $\tilde{f}_{\mathrm{s}j}(x_j, k_y, \omega)$ at each strip with centre at $x = x_j$ $(j = 1, \ldots, n_{\mathrm{s}})$:

$$\tilde{u}_{\mathrm{s}}(x_m, k_y, \omega) = \sum_{j=1}^{n_{\mathrm{s}}} \tilde{h}_{\mathrm{ss}}(x_{jm}, k_y, \omega) \tilde{f}_{\mathrm{s}j}(x_j, k_y, \omega) \tag{42}$$

where $\tilde{h}_{\mathrm{ss}}(x_{jm}, k_y, \omega)$ is the response at line m with coordinate x_m, due to an impulse load $\delta(t)$ at a strip j with centre at $x = x_j$ and width Δ, where $x_{jm} = x_j - x_m$.

The transfer function of the ground surface ($z = 0$) due to a strip load of width Δ and constant amplitude $1/\Delta$, distributed symmetrically about $x = 0$, can be calculated by weighting the displacement Green's function $\tilde{\tilde{u}}_{zz}^{\mathrm{G}}(k_x, k_y, z, \omega)$ of the (layered) soil by the factor $\frac{\sin(k_x \Delta)}{\Delta/2}$ corresponding to the transformation of the uniform strip load to the wavenumber domain. For the m-th strip, due to symmetry in the k_x domain, the transfer function is given by:

$$\tilde{h}_{\mathrm{ss}}(x_{jm}, k_y, \omega) = \frac{1}{2\pi} \int_0^{\infty} \tilde{\tilde{u}}_{zz}^{\mathrm{G}}(k_x, k_y, 0, \omega) \frac{\sin(k_x \Delta)}{\Delta/2} \cos(k_x x_{jm}) \mathrm{d}k_x. \tag{43}$$

The Green's function $\tilde{\tilde{u}}^{\mathrm{G}}_{zz}(k_x, k_y, z, \omega)$ is the representation in the (double) wavenumber–frequency domain of the displacement Green's function $u^{\mathrm{G}}_{zz}(x, y, z, t)$ of the soil. The latter represents the displacement in the vertical direction $\mathbf{e}_z$ at a time t at a point $\{x, y, z\}^{\mathrm{T}}$ due to an impulse load $\delta(t)$ in the vertical direction $\mathbf{e}_z$ at the origin of the frame of reference.

The resulting system of equations for all strips can be written in matrix form as:

$$\tilde{\mathbf{u}}_{\mathrm{s}} = \tilde{\mathbf{H}}_{\mathrm{ss}}\tilde{\mathbf{f}}_{\mathrm{s}} \tag{44}$$

where $\tilde{\mathbf{f}}_{\mathrm{s}}$ contains the forces (tractions) at the track-soil interface Σ and is equal to $\{\tilde{f}_{\mathrm{s}1}, \ldots, \tilde{f}_{\mathrm{s}n_{\mathrm{s}}}\}^{\mathrm{T}}$ and $\tilde{\mathbf{H}}_{\mathrm{ss}}$ is an $n_{\mathrm{s}} \times n_{\mathrm{s}}$ compliance matrix, detailed as:

$$\tilde{\mathbf{H}}_{\mathrm{ss}} = \begin{bmatrix} \tilde{h}_{\mathrm{ss}}(0, k_y, \omega) & \tilde{h}_{\mathrm{ss}}(\Delta, k_y, \omega) & \ldots & \tilde{h}_{\mathrm{ss}}((n_{\mathrm{s}}-1)\Delta, k_y, \omega) \\ \tilde{h}_{\mathrm{ss}}(\Delta, k_y, \omega) & \tilde{h}_{\mathrm{ss}}(0, k_y, \omega) & \ldots & \tilde{h}_{\mathrm{ss}}((n_{\mathrm{s}}-2)\Delta, k_y, \omega) \\ \vdots & \vdots & \ddots & \vdots \\ \tilde{h}_{\mathrm{ss}}((n_{\mathrm{s}}-1)\Delta, k_y, \omega) & \tilde{h}_{\mathrm{ss}}((n_{\mathrm{s}}-2)\Delta, k_y, \omega) & \ldots & \tilde{h}_{\mathrm{ss}}(0, k_y, \omega) \end{bmatrix}. \tag{45}$$

The equilibrium equation of the track-soil system is now written as:

$$\begin{bmatrix} \tilde{\mathbf{K}}^{\mathrm{tr}}_{\mathrm{tt}} & \tilde{\mathbf{K}}^{\mathrm{tr}}_{\mathrm{ts}} \\ \tilde{\mathbf{K}}^{\mathrm{tr}}_{\mathrm{st}} & \tilde{\mathbf{K}}^{\mathrm{tr}}_{\mathrm{ss}} \end{bmatrix} \begin{Bmatrix} \tilde{\mathbf{u}}_{\mathrm{t}} \\ \tilde{\mathbf{u}}_{\mathrm{s}} \end{Bmatrix} = \begin{Bmatrix} \tilde{\mathbf{f}}_{\mathrm{t}} \\ -\tilde{\mathbf{f}}_{\mathrm{s}} \end{Bmatrix} \tag{46}$$

with $-\tilde{\mathbf{f}}_{\mathrm{s}}$ the (unknown) reaction forces on the track along the track-soil interface Σ.

Equation (46) can be solved in two ways. Introduction of equation (44) into the equilibrium equation (46) results in:

$$\begin{bmatrix} \tilde{\mathbf{K}}^{\mathrm{tr}}_{\mathrm{tt}} & \tilde{\mathbf{K}}^{\mathrm{tr}}_{\mathrm{ts}} \\ \tilde{\mathbf{K}}^{\mathrm{tr}}_{\mathrm{st}} & \tilde{\mathbf{K}}^{\mathrm{tr}}_{\mathrm{ss}} \end{bmatrix} \begin{Bmatrix} \tilde{\mathbf{u}}_{\mathrm{t}} \\ \tilde{\mathbf{H}}_{\mathrm{ss}}\tilde{\mathbf{f}}_{\mathrm{s}} \end{Bmatrix} = \begin{Bmatrix} \tilde{\mathbf{f}}_{\mathrm{t}} \\ -\tilde{\mathbf{f}}_{\mathrm{s}} \end{Bmatrix} \tag{47}$$

This equation can be re-arranged as follows:

$$\left(\begin{bmatrix} \tilde{\mathbf{K}}^{\mathrm{tr}}_{\mathrm{tt}} & \tilde{\mathbf{K}}^{\mathrm{tr}}_{\mathrm{ts}} \\ \tilde{\mathbf{K}}^{\mathrm{tr}}_{\mathrm{st}} & \tilde{\mathbf{K}}^{\mathrm{tr}}_{\mathrm{ss}} \end{bmatrix} \begin{bmatrix} \mathbf{I}_{\mathrm{tt}} & \mathbf{0} \\ \mathbf{0} & \tilde{\mathbf{H}}_{\mathrm{ss}} \end{bmatrix} + \begin{bmatrix} \mathbf{0} & \mathbf{0} \\ \mathbf{0} & \mathbf{I}_{\mathrm{ss}} \end{bmatrix} \right) \begin{Bmatrix} \tilde{\mathbf{u}}_{\mathrm{t}} \\ \tilde{\mathbf{f}}_{\mathrm{s}} \end{Bmatrix} = \begin{Bmatrix} \tilde{\mathbf{f}}_{\mathrm{t}} \\ \mathbf{0} \end{Bmatrix} \tag{48}$$

where $\mathbf{I}_{\mathrm{tt}}$ and $\mathbf{I}_{\mathrm{ss}}$ are identity matrices of order n_{t} and n_{s}, respectively, and $\mathbf{0}$ represents a square or rectangular zero matrix (or vector) of appropriate dimensions.

An alternative way to solve equation (46) would be to rewrite equation (44) as:

$$\tilde{\mathbf{f}}_{\mathrm{s}} = \tilde{\mathbf{H}}^{-1}_{\mathrm{ss}}\tilde{\mathbf{u}}_{\mathrm{s}} = \tilde{\mathbf{K}}^{\mathrm{s}}_{\mathrm{ss}}\tilde{\mathbf{u}}_{\mathrm{s}} \tag{49}$$

where $\tilde{\mathbf{K}}^{\mathrm{s}}_{\mathrm{ss}}$ is the soil impedance matrix. Introduction of equation (49) into equation (46) then results in an equilibrium equation of the same form as equation (33).

4.2.4 Track-soil transfer functions

The dynamic reciprocity theorem is finally used for the calculation of the transfer function $\tilde{h}_{zi}(x, k_y, z, \omega)$ between the track and the soil:

$$\tilde{h}_{zi}(x, k_y, z, \omega) = \int_{\Sigma} \tilde{u}^{\mathrm{G}}_{zi}(x - x', k_y, z, \omega) \tilde{t}_{\mathrm{s}z}(x', k_y, z' = 0, \omega) \, \mathrm{d}\Gamma \tag{50}$$

The transfer function $\tilde{h}_{zi}(x, k_y, z, \omega)$ is the representation in the wavenumber–frequency domain of the transfer function $h_{zi}(x, y, z, t)$, which gives the displacement at a point $\{x, y, z\}^{\mathrm{T}}$ in the free field in the direction $\mathbf{e}_i$, due to an impulse load $\delta(t)$ applied on the track in the vertical direction $\mathbf{e}_z$. The Green's function $\tilde{u}^{\mathrm{G}}_{zi}(x, k_y, z, \omega)$ in equation (50) is the representation in the wavenumber–frequency domain of the displacement Green's function $u^{\mathrm{G}}_{zi}(x, y, z, t)$ or fundamental solution of the layered soil. The latter represents the displacement in the direction $\mathbf{e}_i$ at a time t in a point $\{x, y, z\}^{\mathrm{T}}$ due to an impulse load $\delta(t)$ in the vertical direction $\mathbf{e}_z$ at the origin of the frame of reference. Note that the traction Green's function does not appear in the present application of the representation theorem (50) since the track is located at the surface of the layered halfspace where tractions are zero.

Implementation in the TRAFFIC software. The solution of the track-soil interaction equation (32) provides the soil displacements $\tilde{\mathbf{u}}_{\mathrm{s}} = \{\tilde{u}_{\mathrm{s}}, \tilde{\beta}_{\mathrm{s}}\}^{\mathrm{T}}$ at the track-soil interface Σ, which allows the soil tractions $\tilde{t}_{sz}(x, k_y, z = 0, \omega)$ to be computed at this interface:

$$\tilde{t}_{\mathrm{s}z}(x, k_y, z = 0, \omega) = \tilde{\mathbf{t}}_{\mathrm{s}z}(\mathbf{u}_{\mathrm{sc}}(\boldsymbol{\phi}_{\mathrm{t}}))\tilde{\mathbf{u}}_{\mathrm{s}} \tag{51}$$

where $\tilde{\mathbf{t}}_{\mathrm{s}z}(\mathbf{u}_{\mathrm{sc}}(\boldsymbol{\phi}_{\mathrm{t}}))$ contains the vertical component of the soil tractions due to the scattered wave fields in the soil. The tractions $\tilde{t}_{sz}(x, k_y, z = 0, \omega)$ are subsequently used to evaluate the transfer functions between the track and the soil according to equation (50).

Implementation in the MOTIV software. The solution of the system of equations (48) gives the tractions at the track-soil interface Σ, which are subsequently used in equation (50) to evaluate the transfer functions between the track and the soil.

Example 4.1: Track receptance and transfer functions in the free field for a ballasted track

In this example, the track receptance and the transfer functions between the track and the free field are illustrated for the case of a typical ballasted track on top of a homogeneous ground. The properties of the ballasted track model are listed in table 9 of Appendix A.1. The elastic halfspace model used to represent the soil is defined in terms of its shear and dilatational wave velocity, together with its density and hysteretic material damping ratios in shear and dilatational deformation, as described in Section 4.2.3. The values used in the current example are given in table 10 of Appendix A.1 for the case of stiff soil. The calculations are performed with the MOTIV and the GroundVIB models and the results are compared. A second track case with softer rail pads is also included for the simulations in this example. For that, the rail pad stiffness k_{rp} is assumed equal to 30 MN/m with a damping loss factor $\eta_{\mathrm{rp}} = 0.25$.

In the GroundVib model, a weak coupling approach between the track and the soil is used. The track-soil interaction forces are first estimated using a track model on a rigid base. The rails are modelled as Timoshenko beams and supported by a two-layer spring-mass system, representing the rail pads, sleepers, under sleeper pads and/or ballast. The soil transfer functions are subsequently calculated with a 2.5D soil model. The latter are then used together with the interaction forces to compute the free field response. Hence, there are two approximations compared to MOTIV: the track receptance is computed without taking into consideration the flexibility of the soil and the coupling between the track and the soil is performed in the spatial rather than the wavenumber domain. More detailed information on the GroundVIB model is given in subsection 6.7.

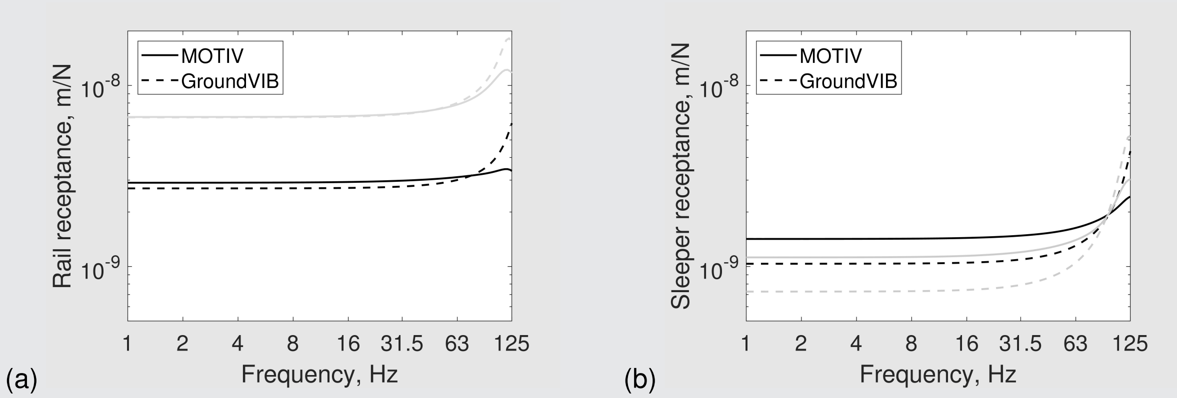

Figure 7: Track receptances for the ballasted track with grooved rail pads (black lines) and with soft pads (grey lines): (a) rail driving point receptance and (b) sleeper receptance.

Figure 7 shows the modulus of the track receptance for the rail and the sleeper, where it is understood that sleeper receptance here refers to the displacement of the sleeper due to a unit force applied on the rails (0.5 N on each rail). It can be seen that for the rail receptances, the results obtained from the implementation using the MOTIV model and those from the GroundVIB model are in good agreement for frequencies below about 80 Hz. For frequencies above 80 Hz, the receptances calculated with the GroundVIB model show higher magnitude than those from the MOTIV model; this is due to the rigid ground assumption used in the GroundVIB model. For the same reason, for frequencies below about 80 Hz, the sleeper transfer receptance magnitudes calculated using the MOTIV model are higher than those calculated with the GroundVIB model.

Figure 8 shows the modulus of the ground transfer function at different distances from the track centre line. Comparing the results from the two models, a good agreement is achieved for frequencies below about 50 Hz. In GroundVIB, the rigid ground assumption in the track model results in higher forces transmitted from the track to the soil; this results in higher response in the soil. The dip in the transfer receptances for the MOTIV system around 105 Hz is caused by the width of the track load applied by the track on the ground, that is $2b = 3.6$ m for this track. At this frequency, this distance corresponds to the Rayleigh wavelength for this type of ground.

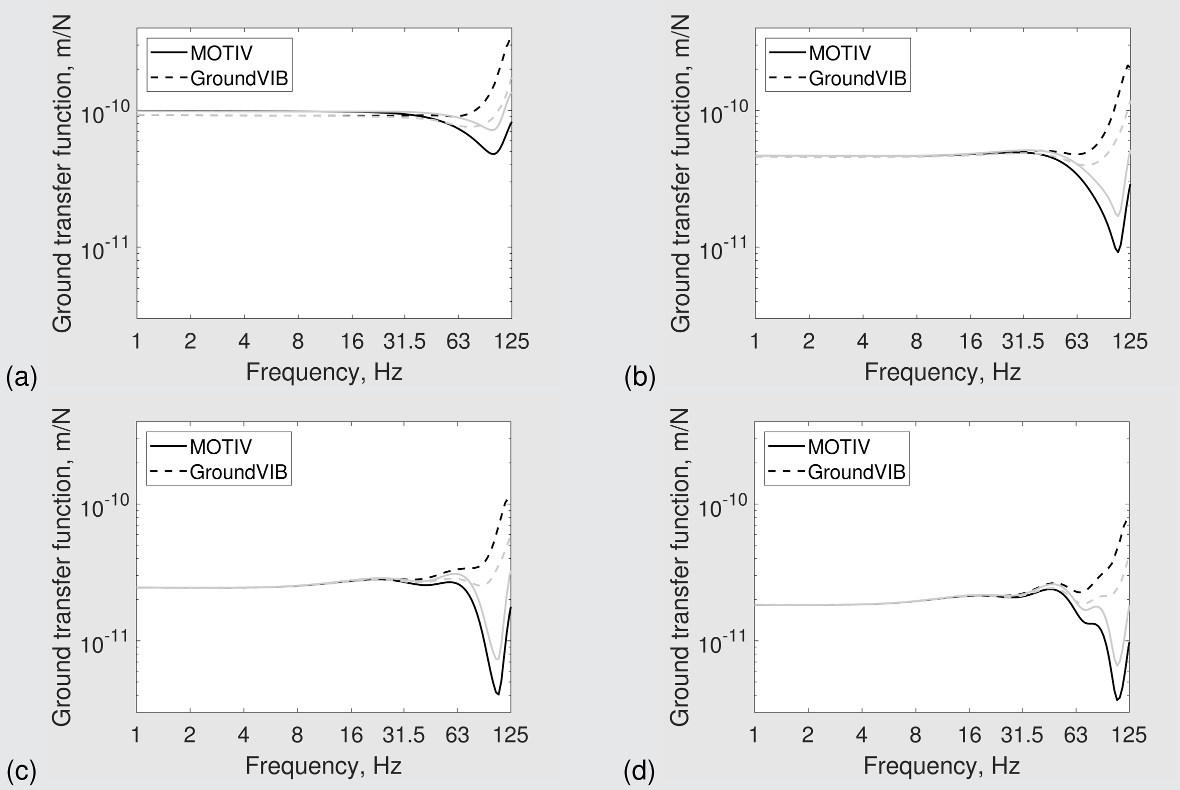

Figure 8: Ground transfer functions for the ballasted track with grooved rail pads (black lines) and with soft pads (grey lines): (a) 4 m, (b) 8 m, (c) 15 m, and (d) 20 m from the track centre line.

4.2.5 Alternative formulations

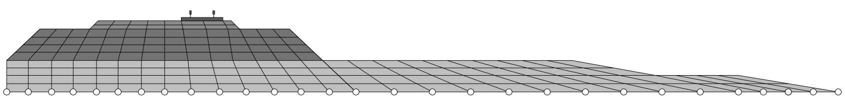

Figure 9: 2.5D FE-BE model of a ballast track on an embankment [61].

In an alternative approach, instead of an analytical track model, a 2.5D FE-BE or a 2.5D FE-PML model of the track and the soil can be used. This is accomplished using a 2D FE mesh for the track cross section, with the third dimension along the track represented by a wavenumber spectrum using a Fourier transform. This technique is particularly useful for cases where the track is located on a high embankment [168, 58, 57, 61] or in a cutting [61, 62], and for trains in tunnels [169, 90] where the track-embankment, cutting, or track-tunnel structure can be modelled in detail with finite elements. As an example, figure 9 shows a 2.5D model where a ballast track on an embankment is modelled with finite elements and coupled to a 2.5D boundary element mesh along the interface with a layered soil [61]; the nodes of the BE mesh are indicated with circles. Figure 10 shows a 2.5 FE-BE model of a ballast track with subgrade

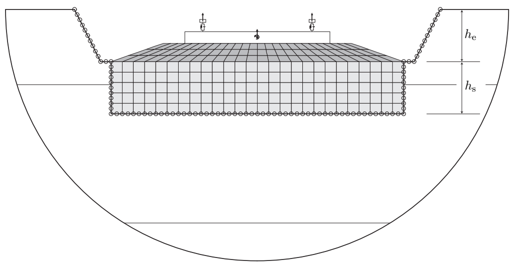

Figure 10: 2.5D FE-BE model of a ballast track with subgrade stiffening in a cutting [62].

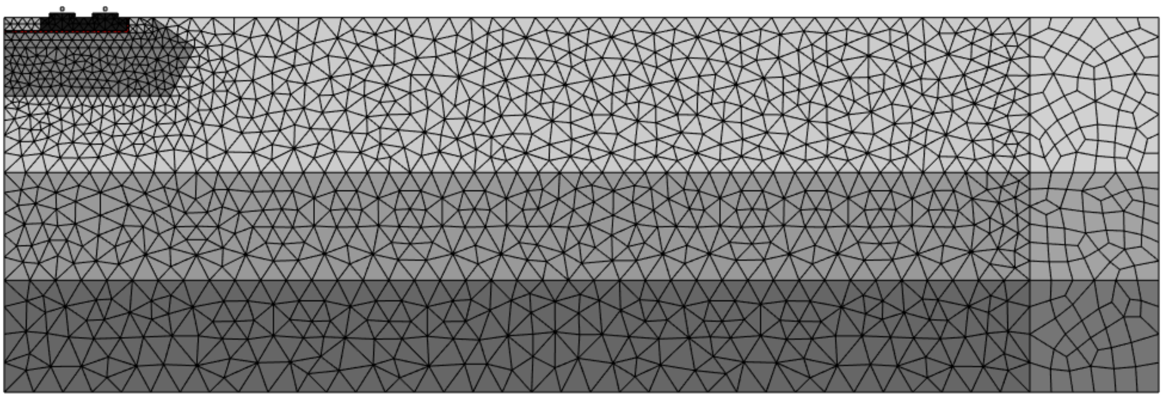

Figure 11: 2.5D FE-PML model of a floating slab track on a layer of gravel and crushed rock, embedded in a layered soil on bedrock [153]. The left boundary is an axis of symmetry, while Perfectly Matched Layers are included on the right hand side.

stiffening in a cutting [62], embedded in a layered halfspace; the 2.5D BE mesh is no longer located on the surface, necessitating the computation of displacement and traction Green's functions for source-receiver combinations at different depths. Finally figure 11 shows a 2.5D FE-PML model of a floating slab track on a layer of gravel and crushed rock, embedded in a layered soil supported by bedrock [153]. In this case, finite elements are used to discretize the cross section, while Perfectly Matched Layers are introduced along the right-hand boundary to allow for wave propagation without spurious reflection. In all of these examples, the versatility of modelling comes at a higher computational cost due to the computational effort needed to set up and solve the 2.5D FE-BE or 2.5D FE-PML equations.

4.3 The train-track interaction problem

4.3.1 Dynamic axle loads

In this subsection, we will explain how the dynamic axle loads are computed from the combined wheel and track unevenness [119, 7, 166]. This will reveal how the parameters of the vehicle, track, and supporting soil affect the dynamic loads.

The calculation of the dynamic component $\mathbf{g}_{\mathrm{d}k}(t)$ of the axle loads is based on the assumption of a perfect contact between the train and the track. For each wheelset k, this requires the continuity of displacements at the contact point between the wheelset and the track:

$$\mathbf{u}_{\mathrm{c}k}(t) \quad = \quad \mathbf{u}_{\mathrm{t}k}(t) + \mathbf{u}_{\mathrm{w/r}k}(t) \tag{52}$$

where $\mathbf{u}_{\mathrm{c}k}(t)$ is the displacement of axle k and $\mathbf{u}_{\mathrm{t}k}(t)$ is the track displacement at the moving contact point between the k-th wheelset and the rail. An irregular wheel or track geometry is accounted for in the term $\mathbf{u}_{\mathrm{w/r}k}(t)$ that represents the combined wheel and rail unevenness perceived by axle k. Here, the deflection of the contact spring is included within the wheelset displacement.

When it is assumed that the wheels are perfectly smooth and only vertical track unevenness $u_{\mathrm{r}z}(y)$ is accounted for, $\mathbf{u}_{\mathrm{w/r}k}(t)$ becomes:

$$\mathbf{u}_{\mathrm{w/r}k}(t) \quad = \quad u_{\mathrm{r}z}(y_{k0} + vt)\mathbf{e}_z \tag{53}$$

and all axles experience the same excitation, apart from a time delay.

Equation (52) is now formulated in the frequency domain as follows:

$$\hat{\mathbf{u}}_{\mathrm{c}k}(\omega) \quad = \quad \hat{\mathbf{u}}_{\mathrm{t}k}(\omega) + \hat{\mathbf{u}}_{\mathrm{w/r}k}(\omega) \tag{54}$$

The displacement $\hat{\mathbf{u}}_{\mathrm{c}k}(\omega)$ of axle k and the track displacement $\hat{\mathbf{u}}_{\mathrm{t}k}(\omega)$ are written in terms of the dynamic axle loads $\hat{\mathbf{g}}_{\mathrm{d}k}(\omega)$.

In subsection 4.3.2, it will be shown how, in the particular case of a longitudinally invariant track, the track displacements at the contact points can be computed as follows from the dynamic axle loads:

$$\hat{\mathbf{u}}_{\mathrm{t}}(\omega) \quad = \quad \hat{\mathbf{C}}^{\mathrm{t}}(\omega)\hat{\mathbf{g}}_{\mathrm{d}}(\omega) \tag{55}$$

where $\hat{\mathbf{u}}_{\mathrm{t}}(\omega)$ and $\hat{\mathbf{g}}_{\mathrm{d}}(\omega)$ are $3n_{\mathrm{a}} \times 1$ vectors that collect the track displacements at all axles and the dynamic axle loads, while $\hat{\mathbf{C}}^{\mathrm{t}}(\omega)$ is the $3n_{\mathrm{a}} \times 3n_{\mathrm{a}}$ track compliance matrix (which is equal to the inverse of the dynamic stiffness matrix).

A mechanical model of the train is used to calculate the vehicle compliance matrix $\hat{\mathbf{C}}^{\mathrm{v}}(\omega)$:

$$\hat{\mathbf{u}}_{\mathrm{c}}(\omega) \quad = \quad -\hat{\mathbf{C}}^{\mathrm{v}}(\omega)\hat{\mathbf{g}}_{\mathrm{d}}(\omega) \tag{56}$$

where $\hat{\mathbf{u}}_{\mathrm{c}}(\omega)$ is a $3n_{\mathrm{a}} \times 1$ vector that collects the displacements of the contact points between the wheels and the rails. The signs in equations (55) and (56) are different due to the convention that axle loads are positive when their action on the track is in the positive coordinate direction and on the wheelset in the negative coordinate direction. Expressions for the vehicle compliance matrix will be given in subsection 4.3.3.

Introducing equations (55) and (56) in equation (54) leads to the following system of equations for the dynamic axle loads $\hat{\mathbf{g}}_{\mathrm{d}}(\omega)$:

$$\left[\hat{\mathbf{C}}^{\mathrm{t}}(\omega) + \hat{\mathbf{C}}^{\mathrm{v}}(\omega)\right]\hat{\mathbf{g}}_{\mathrm{d}}(\omega) \quad = \quad -\hat{\mathbf{u}}_{\mathrm{w/r}}(\omega) \tag{57}$$

where $\hat{\mathbf{u}}_{\mathrm{w/r}}(\omega)$ is $3n_{\mathrm{a}} \times 1$ vector that collects the unevenness $\hat{\mathbf{u}}_{\mathrm{w/r}k}(\omega)$ at all axles. The representation of the track unevenness will be discussed in more detail in subsection 4.3.4. The inverse $[\hat{\mathbf{C}}^{\mathrm{t}}(\omega) + \hat{\mathbf{C}}^{\mathrm{v}}(\omega)]^{-1}$

of the combined track and vehicle compliance matrix can be considered as the dynamic stiffness matrix of the coupled vehicle-track system.

Disregarding wheel unevenness for the moment and assuming that vertical rail unevenness dominates, the term $\hat{\mathbf{u}}_{\mathrm{w/r}}(\omega)$ on the right hand side of equation (57) can be further elaborated as:

$$\hat{\mathbf{u}}_{\mathrm{w/r}}(\omega) \quad = \quad \frac{1}{v}\tilde{u}_{\mathrm{rz}}\left(-\frac{\omega}{v}\right)\hat{\mathbf{T}}(\omega) \tag{58}$$

where $\tilde{u}_{\mathrm{rz}}(k_y)$ is the wavenumber transform of the rail unevenness $u_{\mathrm{rz}}(y)$ and $\hat{\mathbf{T}}(\omega)$ is a $3n_{\mathrm{a}} \times 1$ vector that collects the phase shift for each axle:

$$\hat{\mathbf{T}}(\omega) \quad = \quad \left\{\ldots, 0, \exp\left(+\mathrm{i}\omega\frac{y_{k0}}{v}\right), 0, \ldots\right\}^{\mathrm{T}} \tag{59}$$

where y_{k0} is the initial position of axle k and v is the train speed.

Similar expressions as equation (57) are given by Sheng et al. [166] and Auersch [7], who couples a finite element model for a finite part of the track to a boundary element model for the soil. Grundmann and Lenz [64] present an alternative solution that allows for the coupling of a non-linear single degree of freedom system to the track.

In the following subsections, each of these terms in equation (57) will be elaborated in more detail.

4.3.2 Track compliance matrix

In order to determine the elements of the track compliance matrix $\hat{\mathbf{C}}^{\mathrm{t}}(\omega)$, we reconsider equation (30) to write the track displacement $\hat{\mathbf{u}}_{\mathrm{t}l}(\omega)$ at the contact point between the $l-$th axle and the rail in the frame of reference that moves with the train speed v:

$$\hat{\mathbf{u}}_{\mathrm{t}l}(\omega) \quad = \quad \sum_{k=1}^{n_{\mathrm{a}}}\left[\frac{1}{2\pi}\int_{-\infty}^{+\infty}\tilde{\mathbf{H}}^{\mathrm{T}}(k_y, \omega + k_y v)\exp\left[-\mathrm{i}k_y(y_{l0} - y_{k0})\right]\,\mathrm{d}k_y\right]\hat{\mathbf{g}}_{\mathrm{d}k}(\omega) \tag{60}$$

The bracketed term is the 3×3 matrix $\hat{\mathbf{C}}^{\mathrm{t}}_{lk}(\omega)$ that relates the track displacement at axle l to the dynamic load at axle k. These matrices are collected into the $3n_{\mathrm{a}} \times 3n_{\mathrm{a}}$ track compliance matrix $\hat{\mathbf{C}}^{\mathrm{t}}(\omega)$ that links the vector $\hat{\mathbf{u}}_{\mathrm{t}}(\omega)$ with the track displacements at all axles to the vector $\hat{\mathbf{g}}_{\mathrm{d}}(\omega)$ with dynamic loads:

$$\hat{\mathbf{u}}_{\mathrm{t}}(\omega) \quad = \quad +\hat{\mathbf{C}}^{\mathrm{t}}(\omega)\hat{\mathbf{g}}_{\mathrm{d}}(\omega) \tag{61}$$

Implementation in the TRAFFIC software. In the TRAFFIC software, the compliance matrix $\hat{\mathbf{C}}^{\mathrm{t}}(\omega)$ of the track is computed following the procedure outlined in the previous paragraph.

Implementation in the MOTIV software. In the MOTIV software, only the vertical interaction forces are considered and only the vertical dynamics of the track are included. Thus, the compliance matrix $\hat{\mathbf{C}}^{\mathrm{t}}(\omega)$ of the track is of size $n_{\mathrm{a}} \times n_{\mathrm{a}}$ when the dynamic loads on the two rails are considered symmetrical and of size $2n_{\mathrm{a}} \times 2n_{\mathrm{a}}$ when the two rails experience different dynamic loading. The elements of the track compliance matrix $\hat{\mathbf{C}}^{\mathrm{t}}(\omega)$ are calculated from the solution of equation (48) considering a loading vector $\tilde{\mathbf{f}}_{\mathrm{s}}$ that comprises only a unit axle load on the rails and is solved in the moving frame of reference at frequencies $\omega + k_y v$.

Example 4.2: Compliance of a ballasted track

The vertical track compliance of a ballasted track in a moving frame of reference is calculated in this example using the MOTIV model. The track is the same ballasted track used in example 4.1 with properties given in table 9 of Appendix A.1. The results are given for different soil types (table 10 of Appendix A.1) and for different load speeds, 150 km/h and 300 km/h.

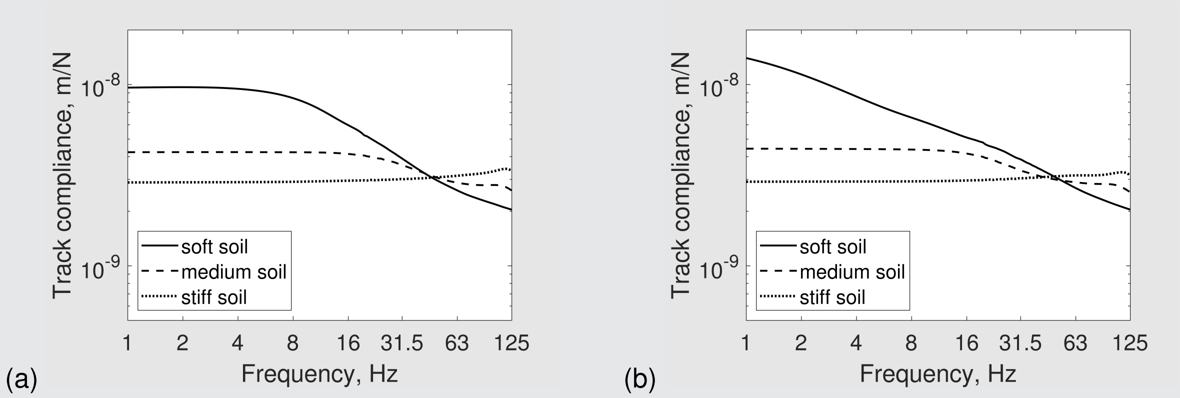

Figure 12: Track compliance for the ballasted track supported by soft, medium and stiff soil in the moving frame of reference at (a) 150 km/h and (b) 300 km/h.

Figure 12 shows the modulus of the rail compliance in the frequency range from 1 Hz to 125 Hz. For the medium and stiff soil cases, there is almost no difference between the results for the two load speeds. Also, by comparing the rail compliance in the moving frame of reference for the stiff soil with the rail receptance calculated in example 4.1 and shown in figure 7, no differences can be seen. From this it can be understood that for these soil types the current load speeds do not affect the response of the rail.

For the soft soil, however, the increase of the speed from 150 km/h to 300 km/h results in a higher rail compliance at the very low frequencies. This is due to the fact that the load speed of 300 km/h (83.3 m/s) is relatively close to the critical wave speed for the specific soil case (about 92 m/s), resulting in high levels of track and soil vibration.

4.3.3 Vehicle compliance matrix

For the estimation of the dynamic axle loads, the vehicle is usually modelled as a multi-degree of freedom system, where the vehicles' car body, bogies and wheelsets are considered as rigid parts (characterized by their mass and mass moment of inertia), while the vehicle's primary and secondary suspensions are represented by spring and damper elements.

Figure 13 shows an example of a two-dimensional 10-DOF vehicle model consisting of the vehicle body, two bogies, four axles, as well as primary and secondary suspensions. The degrees of freedom of this

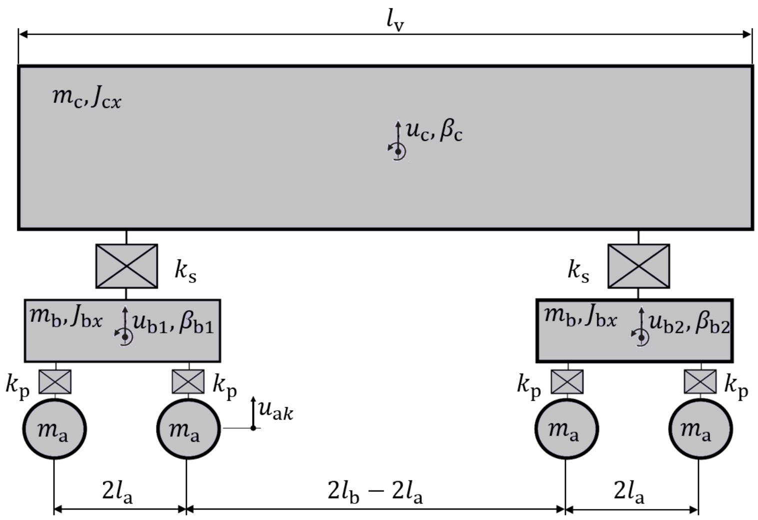

Figure 13: A 10-DOF vehicle model with primary and secondary suspensions.

model are the vertical displacement u_c and rotation β_c of the car body, the vertical displacements u_{b1} and u_{b2} and rotations β_{b1} and β_{b2} of the bogies, and the vertical displacements u_{ak} $(k = 1, \ldots, 4)$ of the four axles. The model is characterized by the mass m_c and the pitching moment of inertia J_{cx} of the car body, the mass m_b and the pitching moment of inertia J_{bx} of the bogies (assumed equal here), the mass m_a of the wheelset, the stiffness k_p and viscous damping c_p of the primary suspension and the stiffness k_s and viscous damping c_s of the secondary suspension.

Depending on the application, this model can be further simplified to a 4-DOF model, a 2-DOF model with an unsprung and sprung wheel mass, or even a single-degree-of-freedom (1-DOF) model consisting only of an unsprung wheel mass, as shown in figure 14.

Alternatively, more complex vehicle models, such as a 16-DOF model that incorporates rolling around the longitudinal axis, can be developed so that different wheel loads can be applied on the left and right rail. Flexible bodies could also be included. Such more complicated models will not be used in SILVARSTAR, however.

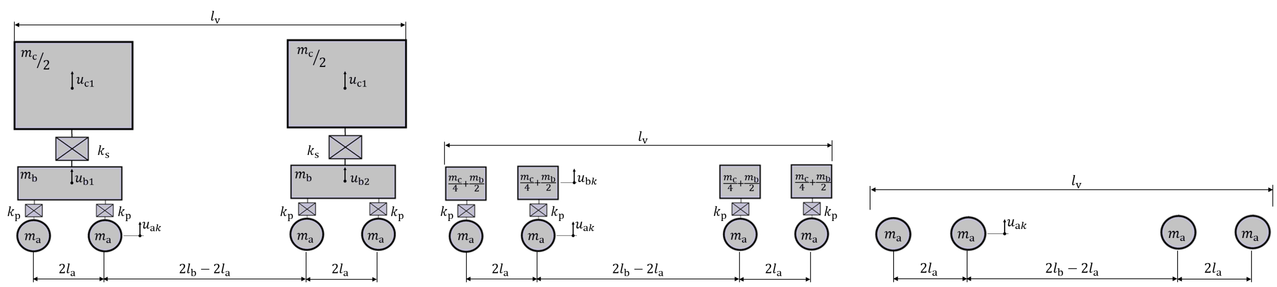

Figure 14: (a) 4-DOF vehicle model with primary and secondary suspensions; (b) 2-DOF vehicle model with primary suspensions; (c) 1-DOF vehicle model (unsprung mass).

The vehicle's equation of motion can be written in the following general form in the frame of reference that moves with the train, distinguishing between the displacements $\hat{\mathbf{u}}_b$ of the car body and the bogies, $\hat{\mathbf{u}}_a$ of the axles and $\hat{\mathbf{u}}_{\mathrm{c}}$ at the vehicle-track contact points:

$$\begin{bmatrix} \mathbf{S}_{\mathrm{bb}} & \mathbf{S}_{\mathrm{ba}} & \mathbf{0} \\ \mathbf{S}_{\mathrm{ab}} & \mathbf{S}_{\mathrm{aa}} + \mathbf{S}^{\mathrm{H}}_{\mathrm{aa}} & -\mathbf{S}^{\mathrm{H}}_{\mathrm{aa}} \\ \mathbf{0} & -\mathbf{S}^{\mathrm{H}}_{\mathrm{aa}} & +\mathbf{S}^{\mathrm{H}}_{\mathrm{aa}} \end{bmatrix} \left\{ \begin{array}{c} \hat{\mathbf{u}}_{\mathrm{b}} \\ \hat{\mathbf{u}}_{\mathrm{a}} \\ \hat{\mathbf{u}}_{\mathrm{c}} \end{array} \right\} = \left\{ \begin{array}{c} \mathbf{0} \\ \mathbf{0} \\ -\hat{\mathbf{g}}_{\mathrm{d}} \end{array} \right\} \tag{62}$$

where $\mathbf{S}$ represents a dynamic stiffness matrix, represented here as a block matrix differentiating between the degrees of freedom a and b. $\mathbf{S}^{\mathrm{H}}_{\mathrm{aa}}$ is the dynamic stiffness matrix that corresponds to the Hertzian contact springs between the wheels and the rails [165]. In the frequency range of interest for ground-borne vibration, the contact stiffness is relatively high compared to the track and vehicle stiffness, so that the corresponding flexibility can generally be disregarded.

The solution of these equations of motion allows the vehicle's compliance matrix $\hat{\mathbf{C}}^{\mathrm{v}}(\omega)$, that relates the contact displacements $\hat{\mathbf{u}}_{\mathrm{c}}(\omega)$ to the vehicle-track interaction forces $\hat{\mathbf{g}}_{\mathrm{d}}(\omega)$, to be computed as follows:

$$\hat{\mathbf{u}}_{\mathrm{c}}(\omega) = -\hat{\mathbf{C}}^{\mathrm{v}}(\omega)\hat{\mathbf{g}}_{\mathrm{d}}(\omega) \tag{63}$$

Each element $\hat{C}^{\mathrm{v}}_{kl}(\omega)$ of the vehicle's compliance matrix represents the displacements at the contact point k due to a unit harmonic load at the contact point l. As the equations of motion have been derived in the frame of reference that moves with the train, these elements obviously do not depend on the train speed.

The reader is referred to the literature for detailed expressions of the vehicle's compliance matrix in each of these cases [60].

Example 4.3: Vehicle compliance

The vehicle compliance of three vehicle models is presented in this example. The vehicle models under consideration are the 10-DOF model shown in figure 13 and the 4-DOF and 1-DOF model shown in figures 14(a) and 14(c), respectively. The vehicle properties are given in table 8 of Appendix A.1.

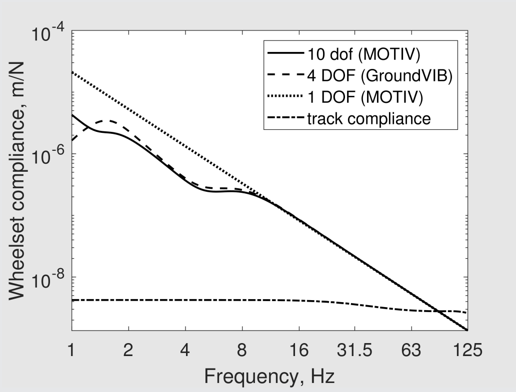

Figure 15: Wheelset compliance for the 10-DOF, 4-DOF and 1-DOF vehicles and compliance of the ballasted track on medium soil in a moving frame of reference at 150 km/h.

Figure 15 shows the amplitude of the wheelset compliance for the three vehicle models. For frequencies above about 10 Hz, only the unsprung mass of the vehicle affects the dynamic response of the wheelsets, and the wheelset compliance of the three vehicle models is identical. Below 10 Hz, the differences found in the wheelset compliance are due to the different levels of modelling detail of the car, bogies and vehicle suspensions.

In figure 15, the track compliance in a moving frame of reference at 150 km/h is also shown for the case of the medium soil (cf. figure 12). The wheelset and track compliance magnitudes are equal at around 87 Hz, which is identified as the P2 resonance where the combined wheelset and rail mass is bouncing on the track stiffness.

Example 4.4: Dynamic axle loads for an unsprung mass model

Simplifying equation (57) for a single axle allows effects from vehicle-track interaction to be highlighted. If the train speed is relatively low, the corresponding track compliance in a moving frame of reference is approximately equal to the track receptance, and can roughly be represented as the inverse $1/k_{\mathrm{t}}$ of the track stiffness when its imaginary part and frequency dependence are disregarded (cf. example 4.2 and figure 12). At frequencies of more than a few Hertz [101], the vehicle's primary and secondary suspension isolate the body and the bogie from the wheelset. At sufficiently high frequencies (above approximately 10 Hz), the vehicle's unsprung mass M_{u} is therefore the only component that affects the vertical dynamic loads and can be represented as a rigid body [101]. In this case, the compliance of a single axle becomes $-1/(M_{\mathrm{u}}\omega^2)$. Introducing both expressions in equation (57) leads to the following expression for the dynamic load k:

$$\hat{g}_{\mathrm{d}}(\omega) \quad = \quad -\left[\frac{k_{\mathrm{t}} M_{\mathrm{u}}\omega^2}{k_{\mathrm{t}} - M_{\mathrm{u}}\omega^2}\right] \hat{u}^{k}_{\mathrm{w/r}}(\omega) \tag{64}$$

The denominator on the right hand side of equation (64) becomes zero at the frequency $\omega = \sqrt{k_{\mathrm{t}}/M_{\mathrm{u}}}$ where "resonance" of the unsprung mass on the track stiffness (sometimes denoted as the P2 resonance) occurs. At this frequency, the narrow-band spectrum of the dynamic axle load $\hat{g}_{\mathrm{d}}(\omega)$ displays a resonance peak. The peak is strongly damped in reality as the track stiffness has a significant imaginary part which is mainly due to radiation damping.

4.3.4 Track unevenness

Random track unevenness $u_{\mathrm{r}z}(y)$ is modelled as a stationary Gaussian random process characterized by its one-sided power spectral density (PSD) function $\tilde{S}_{\mathrm{r}zz}(k_y)$ $[\mathrm{m}^2/(\mathrm{rad/m})]$ [143]. The spectral representation theorem [171, 170] is used to generate samples $u_{\mathrm{r}z}(y)$ of track unevenness as a superposition of harmonic functions with random phase angles:

$$u_{\mathrm{r}z}(y) \quad = \quad \sum_{m=1}^{n} \sqrt{2\tilde{S}_{\mathrm{r}zz}(k_{ym})\Delta k_y} \cos(k_{ym} y - \theta_m) \tag{65}$$

where $k_{ym} = m\Delta k_y$ is the wavenumber sampling, Δk_y the wavenumber spacing and θ_m are independent random phase angles uniformly distributed in the interval $[0, 2\pi]$. Each harmonic in equation (65) is independent, which is justified by the hypothesis that unevenness of different wavenumbers is due to different causes [166]. The correctness of this assumption can be questioned, however, when the wavenumber spacing Δk_y becomes very small. The samples have a period $Y = 2\pi/\Delta k_y$ and are asymptotically Gaussian as n tends to infinity and Δk_y tends to zero for a fixed value of $k_y^{\max} = n\Delta k_y$. The second term on the right-hand side of equation (58) becomes:

$$\frac{1}{v}\tilde{u}_{\mathrm{rz}}\left(-\frac{\omega}{v}\right) = \sum_{m=1}^{n} \frac{-1}{\sqrt{v}}\sqrt{2\tilde{S}_{\mathrm{rz}z}\left(\frac{|\omega_m|}{v}\right)\Delta\omega_m}\left[\pi\delta(\omega-\omega_m)e^{+\mathrm{i}\theta_m} + \pi\delta(\omega+\omega_m)e^{-\mathrm{i}\theta_m}\right] \tag{66}$$

where $\Delta\omega_m = v\Delta k_y$ and $\omega_m = -vk_{ym}$. For different samples of unevenness, the harmonic functions have the same modulus, but a different random phase.

The influence of the train speed v on the modulus of the perceived unevenness can easily be quantified when the PSD $\tilde{S}_{\mathrm{rz}z}(k_y)$ is proportional to k_y^{-n} in the relevant range of wavelengths. For trains running at speeds between 150 km/h and 330 km/h and a frequency range between 1 Hz and 150 Hz, this range of wavelengths is situated between 0.3 m and 100 m. When the PSD $\tilde{S}_{\mathrm{rz}z}(k_y)$ is proportional to k_y^{-n} with $n > 1$, $\tilde{S}_{\mathrm{rz}z}(|\omega_m|/v)$ increases with the speed v as v^n for a fixed sampling in the frequency domain. The modulus of the perceived unevenness in equation (66) therefore increases as $v^{0.5(n-1)}$. In many cases, however, the dependence of the PSD on the wavenumber is more complex and the influence of the vehicle speed is less straightforward.

Formulation in the TRAFFIC software. The system of equations (57) is further elaborated by means of equations (58), (59) and (66):

$$\begin{aligned}\hat{\mathbf{g}}_{\mathrm{d}}(\omega) &= -\left[\hat{\mathbf{C}}^{\mathrm{t}}(\omega) + \hat{\mathbf{C}}^{\mathrm{v}}(\omega)\right]^{-1}\hat{\mathbf{T}}(\omega)\sum_{m=1}^{n}\frac{-1}{\sqrt{v}}\sqrt{2\tilde{S}_{\mathrm{rz}z}\left(\frac{|\omega_m|}{v}\right)\Delta\omega_m} \\ &\quad \times\left[\pi\delta(\omega-\omega_m)e^{+\mathrm{i}\theta_m} + \pi\delta(\omega+\omega_m)e^{-\mathrm{i}\theta_m}\right]\end{aligned} \tag{67}$$

An inverse Fourier transform of this equation shows that the time history of each axle load is a superposition of harmonic functions. For different realisations of the track unevenness according to equation (66), different values are obtained for the random phase angles θ_m, while the amplitude of the harmonic functions remains the same.

Formulation in the MOTIV software. In an alternative but equivalent approach, the influence of the characterized track unevenness can be postponed until after calculating the response due to dynamic excitation (see section 4.4.2). In MOTIV, the system of equations in (57) is solved considering unit amplitude track unevenness $\hat{\mathbf{u}}_{\mathrm{w/r}}(\omega)$ for each harmonic excitation frequency ω_m. In practice, the dynamic axle loads $\hat{\mathbf{g}}_{\mathrm{d}}(\omega_m)$ due to unit track unevenness are calculated by omitting the summation term on the right hand side of equation (67).

Example 4.5: PSD functions for track unevenness

The FRA defined the following PSD $\tilde{S}_{\mathrm{rz}z}(k_y)$ $[\mathrm{m}^2/(\mathrm{rad/m})]$ based on the database of Hamid and Yang [69]:

$$\tilde{S}_{\mathrm{rz}z}(k_y) = \frac{1}{2\pi}A\frac{n_{y2}^2(n_y^2+n_{y2}^2)}{n_y^4(n_y^2+n_{y1}^2)} \tag{68}$$

where $n_y = k_y/2\pi$ and the constants $n_{y1} = 0.0233\,\mathrm{m}^{-1}$ and $n_{y2} = 0.13\,\mathrm{m}^{-1}$ are determined based on the database. The parameter A depends on the track quality class, labelled from 1 to 6, where 1 represents the poorest and 6 the best track quality [69, 60]. Table 2 gives the value of A for each class, while figure 16 shows the PSD of the unevenness for several FRA track quality classes. Based on the PSD, an unevenness profile $\hat{u}_{\mathrm{rz}}(\omega)$ is generated according to equations (58) and (66).

Table 2: Track quality parameters according to the FRA database [69].

Class	1	2	3	4	5	6
$A\,[10^{-7}\,\mathrm{m}]$	16.72	9.53	5.29	2.96	1.67	0.96

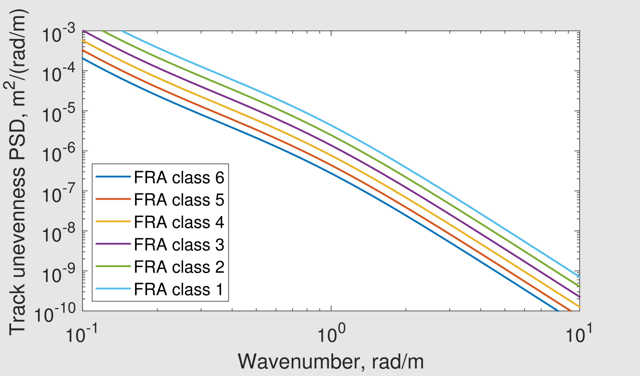

Figure 16: PSD of the track unevenness for different FRA track quality classes.

Example 4.6: Track unevenness and dynamic axle loads

In this example, the dynamic train-track interaction problem is solved for a given track unevenness and the dynamic axle loads are calculated. Following the formulation presented in the previous subsections and the calculations in examples 4.2 and 4.3, results are presented here for the case of a train passage at 150 km/h on the ballasted track on top of the medium soil with the properties listed in Appendix A.1. As in example 4.1, the case of soft rail pads (30 MN/m) is also considered here additionally.

Figure 17 shows the modulus of the wheel-rail contact force calculated for unit amplitude track unevenness, as it is implemented in MOTIV and GroundVIB. Results obtained with the MOTIV model are shown for a 10-DOF vehicle model. GroundVIB uses a 4-DOF vehicle model for each wheelset with no coupling through the track structure. The two models show good agreement with most of the differences around the P2 resonance where the GroundVIB model calculates higher dynamic axle loads for the case of standard grooved rail pads (150 MN/m), which is due to the rigid ground assumption.

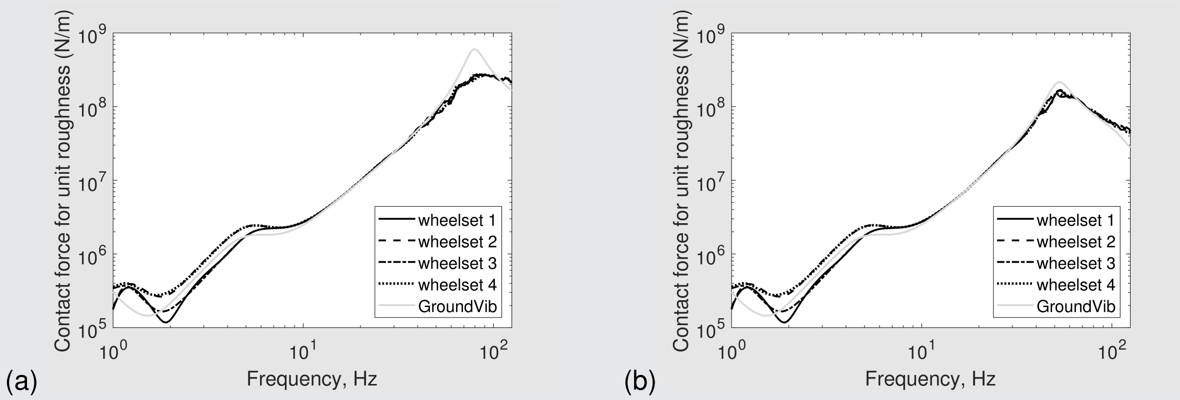

Figure 17: Dynamic axle load per rail for unit amplitude unevenness for the ballasted track on medium soil with (a) grooved rail pads (150 MN/m) and (b) soft rail pads (30 MN/m).

Next, the actual track unevenness is applied to the dynamic axle loads that were calculated for unit amplitude track unevenness. In this example, the track unevenness selected is an extrapolation for long wavelengths of the ISO:3095-2013 [89] acoustic rail roughness, as shown in figure 18 in one-third octave wavelength bands. For comparison, the FRA class 6 and class 1 unevenness are also shown in figure 18.

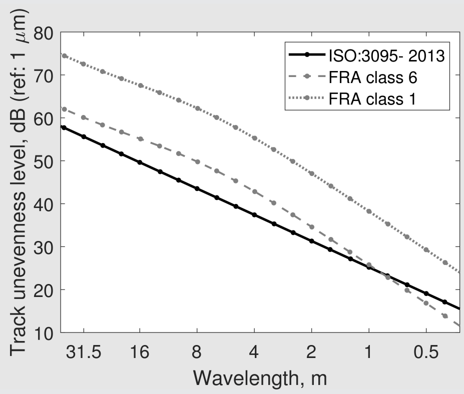

Figure 18: One-third octave wavelength band spectra of the used track unevenness (ISO:3095-2013) and the FRA class 6 and class 1 unevenness.

Figure 19 shows the contact forces in one-third octave bands calculated with MOTIV and GroundVIB. The results are given for both rail pads and for different vehicle models. For the 10-DOF model used in MOTIV, only the contact force of the first axle is shown. As expected from results discussed in example 4.3, the dynamic axle load computed with the 1-DOF vehicle model only differs from the dynamic axle load obtained with a 10-DOF model for frequencies below 10 Hz. The 4-DOF model used in GroundVIB model gives higher contact forces close to the P2 resonance in the case of grooved rail pads, due to the rigid ground assumption.

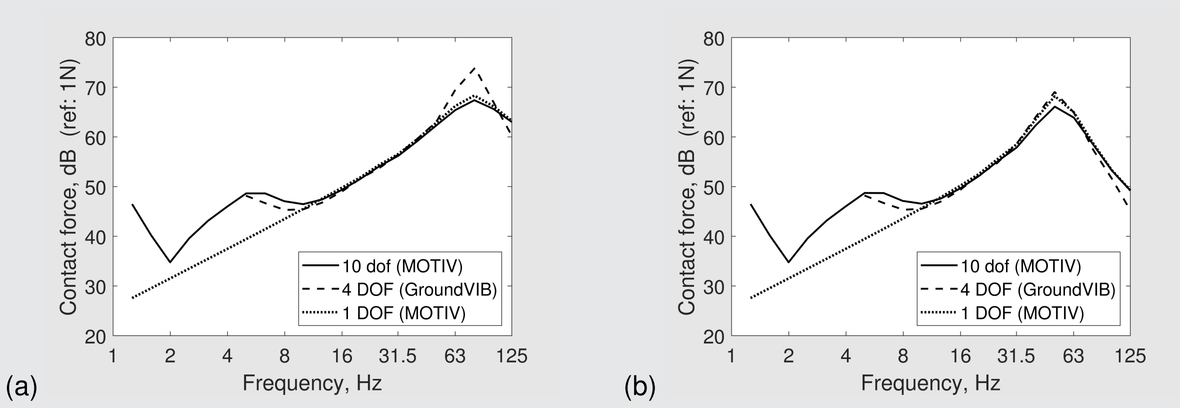

Figure 19: One-third octave frequency band spectra of the contact force for the ballasted track on medium soil with (a) grooved rail pads (150 MN/m) and (b) soft rail pads (30 MN/m), computed with different vehicle models.

Figure 20 finally compares the one-third octave band contact forces for the soft, medium and stiff soil. The results shown are computed with the MOTIV model for the 10-DOF vehicle and shown for the first axle. No significant differences are observed below 31.5 Hz, while some differences appear around the P2 resonance.

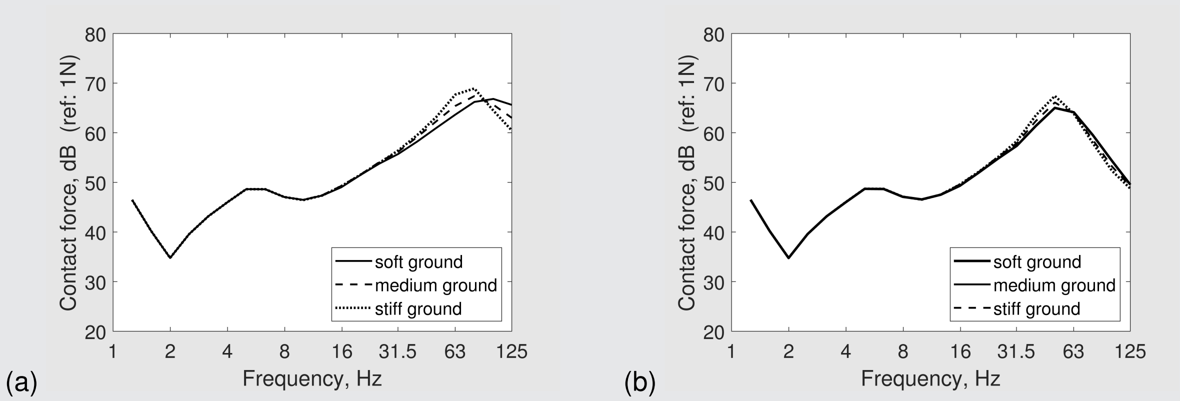

Figure 20: One-third octave frequency band spectra of the contact force for the ballasted track on soft, medium and stiff soil with (a) grooved rail pads (150 MN/m) and (b) soft rail pads (30 MN/m).

4.3.5 Parametric excitation

As discussed in section 2, parametric excitation occurs due to the variation of track stiffness along the track. In practice, the effect of the parametric excitation is not always observed at the ground surface. It is rarely observed for urban rolling stock (tramway, metro) with slab tracks, but trains running on ballasted tracks can show a peak at the sleeper-passing frequency. Measurements performed in Switzerland during the RIVAS project [138], showed a clear peak, sometimes with a similar amplitude to the P2 resonance (around 80 Hz). These investigations also showed that the peak was not always distinguishable, depending on the site (with similar ballasted tracks, but different soil conditions). The peak amplitude of the parametric excitation depends on the train load [132].

Thompson [176] derived analytical equations for parametric excitation expressed as an equivalent unevenness. The equivalent unevenness $\hat{\mathbf{u}}_{\mathrm{w}}(\omega)$ for excitation of the wheel is:

$$\hat{\mathbf{u}}_{\mathrm{w}}(\omega) = -\frac{\Delta k_{\mathrm{t}}(\omega)}{k_{\mathrm{t}}(\omega)} \frac{P_0}{k_{\mathrm{t}}(\omega)} \tag{69}$$

while the equivalent unevenness $\hat{\mathbf{u}}_{\mathrm{r}}(\omega)$ for excitation of the rail is:

$$\hat{\mathbf{u}}_{\mathrm{r}}(\omega) = \frac{\Delta k_{\mathrm{t}}(\omega)}{k_{\mathrm{t}}(\omega)} \frac{P_0}{M_{\mathrm{w}}\omega^2} \tag{70}$$

where $k_{\mathrm{t}}(\omega)$ is the track stiffness, $\Delta k_{\mathrm{t}}(\omega)$ the variation of the track stiffness, P_0 the static axle load, and M_{w} the unsprung wheel mass. These two expressions are equal at the P2 resonance frequency.

Auersch [7] performed an in-depth numerical analysis, with comparison to experimental results, demonstrating that the peak amplitude of the parametric excitation depends on the train speed. He also derived an analytical formulation to express the parametric excitation as an equivalent roughness, which corresponds to the equivalent unevenness from the wheel as expressed in equation (69).

Nélain and Vincent [133] combined the same approximation to track and soil models to obtain the ground vibration response due to parametric excitation. The track receptance and the stiffness variation were computed using a finite element model. The model included random variation of rail support stiffness, resulting in a broad-band excitation in addition to the sleeper periodicity. As a result, the stiffness variation can be expressed in the form of a spectrum, which in turn gives the equivalent unevenness spectrum:

$$\hat{\mathbf{u}}_{\mathrm{w}}(\omega) = \frac{\Delta k_{\mathrm{t}}(\omega) P_0}{k_{\mathrm{t}}^2} \tag{71}$$

which is equivalent to equation (69), where the track stiffness $k_{\mathrm{t}}(\omega)$ is replaced by the mean static track stiffness k_{t}.

This equivalent unevenness spectrum was subsequently used as input in a 2.5D train-track-soil interaction model to compute the ground vibration level. These investigations show the dependency of the parametric excitation on the static wheel load, the mean track stiffness, and the train speed. It was also demonstrated that the unevenness excitation is generally higher than the unevenness due to the parametric excitation, unless the track stiffness variation and the static axle load are sufficiently important.

The following example illustrates how equation (71) can be used to calculate the order of magnitude of the wheel equivalent unevenness.

Example 4.7: Equivalent unevenness for parametric excitation

In this example, we compute the equivalent unevenness to account for parametric excitation for a UIC60 rail that is discretely supported by a flexible support every 0.6 m, using equation (71) and a finite element model of the rail.

The rail is modelled with beam elements supported on discrete springs every 0.6 m (figure 21a). The model is sufficiently long to avoid any influence of wave reflection on the boundaries. The discrete supports represent the stiffness of the rail pads and the components below (sleeper, ballast, subgrade,...). Several models are made for different support stiffness k_s, as described in table 3.

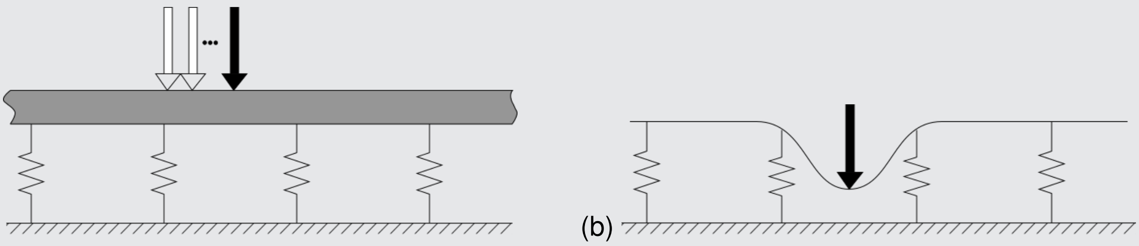

Figure 21: (a) Discretely supported rail and (b) vertical displacement due to a unit vertical load applied above a sleeper.

A unit load is applied at different positions along the rail to obtain the vertical displacement. Figure 21b shows the vertical displacement of the rail for a unit load above a sleeper. The inverse of the displacement at the load point gives the static track stiffness $k_\mathrm{t}(y)$ for this load position y. This computation is repeated for several positions of the load; the resulting static track stiffness is shown in figure 22 for tracks with different support stiffness. The mean static track stiffness k_t is obtained as the average over one sleeper bay. The peak stiffness variation Δk_t is obtained as the difference between the maximum track stiffness $k_\mathrm{t}^\mathrm{max}$ (above a sleeper) and the minimum track stiffness $k_\mathrm{t}^\mathrm{min}$ (between two sleepers). This peak stiffness peak variation Δk_t is an approximation of the peak stiffness peak variation $\Delta k_\mathrm{t}(\omega_\mathrm{s})$ at the sleeper passege frequency $\omega_\mathrm{s} = 2\pi v/d$.

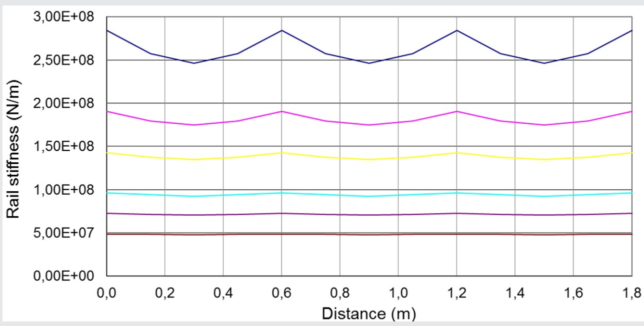

Figure 22: Static track stiffness as a function of the distance along the track.

The results are presented in table 3. The equivalent unevenness $\hat{\mathbf{u}}_\mathrm{w}(\omega_\mathrm{s})$ for an axle load $P_0 = 100\,\mathrm{kN}$ is obtained from equation (71) as a first order approximation of the equivalent unevenness amplitude (peak to peak) at the sleeper passage frequency. The Root Mean Square (RMS) value is obtained by dividing by $2\sqrt{2}$ and can be combined with an unevenness spectrum by quadratic summation of both terms at the sleeper passage frequency.

The present example gives a fast way to obtain an equivalent unevenness approximation at the sleeper passage frequency from a simple FE model of the track. More complex models and approaches can be used. In particular, Zhang et. al. [212] showed that the value obtained is an over-estimation of the amplitude at the sleeper passage frequency, because the variation is not harmonic, as can be seen in figure 22.

Table 3: Equivalent unevenness for parametric excitation (axle load 100 kN, UIC60 rail, sleeper distance 0.6 m).

	Track grade	Stiffness per discrete support k_s [MN/m]	Mean track stiffness k_t [MN/m]	Stiffness variation $\Delta k_\mathrm{t}(\omega_\mathrm{s})$ [MN/m]	Equivalent unevenness $\hat{\mathbf{u}}_\mathrm{w}(\omega_\mathrm{s})$ [μm peak to peak]
1	Very stiff	165	260	38	45
2	Stiff	100	180	15	38
3	Medium	65	140	8	33
4	Medium soft	40	95	3.6	32
5	Soft	30	75	1.5	24
6	Very soft	15	50	0.7	22

4.4 Response to moving loads

In this subsection, we briefly recapitulate the equations derived in subsection 3.4 explaining how the track and free field response can be computed from the transfer function and the quasi-static and dynamic axle loads.

4.4.1 Response to quasi-static excitation

Due to the motion of the train, the response due to the static axle loads is time-dependent. For high-speed tracks on soft soils, the train speed can be close to or even larger than the critical phase velocity of the coupled track-soil system, in which case the quasi-static excitation leads to large amplitudes of vibration and track displacement, affecting track stability and safety [2, 128].

The quasi-static contribution to the response is found from the static component $\mathbf{g}_{\mathrm{s}k}$ of the axle loads, which is equal to $w_k\mathbf{e}_z$, where w_k is the weight carried by axle k. Accounting for the Fourier transform $\hat{\mathbf{g}}_{\mathrm{s}k} = w_k\mathbf{e}_z 2\pi\delta(\omega)$ of the quasi-static axle load, the quasi-static response is equal to:

$$\hat{\mathbf{u}}(y,\omega) \quad = \quad \left[\frac{1}{v}\tilde{\mathbf{H}}^\mathrm{T}\left(\frac{\omega}{v},\omega\right)\mathbf{e}_z \exp\left(-\mathrm{i}\frac{\omega}{v}y\right)\right]\left[\sum_{k=1}^{n_\mathrm{a}} w_k \exp\left(\mathrm{i}\frac{\omega}{v}y_{k0}\right)\right] \tag{72}$$

The first bracketed term on the right-hand side is the response due to a unit axle load, while the second bracketed term represents a modulation of the response, determined by the distribution of the static axle loads over the track and the train speed v [7, 8, 34].

4.4.2 Response to dynamic excitation

The dynamic axle loads $\hat{\mathbf{g}}_{\mathrm{d}k}(\omega)$ are now introduced in equation (20):

$$\hat{\mathbf{u}}(y,\omega) \;=\; \sum_{k=1}^{n_{\mathrm{a}}} \frac{1}{2\pi} \int_{-\infty}^{+\infty} \tilde{\mathbf{H}}^{\mathrm{T}}(k_y,\omega)\hat{\mathbf{g}}_{\mathrm{d}k}(\omega - k_y v) \exp\left[-\mathrm{i}k_y(y-y_{k0})\right] \mathrm{d}k_y \tag{73}$$

A change of variables according to $k_y = (\omega - \tilde{\omega})/v$ moves the frequency shift from the frequency content of the moving load to the wavenumber content of the transfer function:

$$\hat{\mathbf{u}}(y,\omega) \;=\; \sum_{k=1}^{n_{\mathrm{a}}} \frac{1}{2\pi v} \int_{-\infty}^{+\infty} \tilde{\mathbf{H}}^{\mathrm{T}}\left(\frac{\omega-\tilde{\omega}}{v},\omega\right) \hat{\mathbf{g}}_{\mathrm{d}k}(\tilde{\omega}) \exp\left[-\mathrm{i}\left(\frac{\omega-\tilde{\omega}}{v}\right)(y-y_{k0})\right] \mathrm{d}\tilde{\omega} \tag{74}$$

The transfer function is evaluated at a wavenumber $k_y = (\omega - \tilde{\omega})/v$ that couples the frequency $\tilde{\omega}$ emitted by the moving source to the frequency ω observed at the receiver. Due to the Doppler effect, a dynamic axle load $\hat{\mathbf{g}}_{\mathrm{d}k}(\tilde{\omega})$ with a source frequency $\tilde{\omega}$ moving at a speed v, results in a response at a fixed receiver in a frequency range $[\tilde{\omega}/(1+v/C), \tilde{\omega}/(1-v/C)]$, determined by the smallest phase velocity C of interest.

When the train speed v is low with respect to this smallest phase velocity C, the dependence of the dynamic axle load $\hat{\mathbf{g}}_{\mathrm{d}k}(\omega - k_y v)$ on v in equation (73) can be omitted, so that the response is simplified to:

$$\hat{\mathbf{u}}(y,\omega) \;=\; \sum_{k=1}^{n_{\mathrm{a}}} \hat{\mathbf{g}}_{\mathrm{d}k}(\omega) \left[\frac{1}{2\pi} \int_{-\infty}^{+\infty} \tilde{\mathbf{H}}^{\mathrm{T}}(k_y,\omega) \exp\left[-\mathrm{i}k_y(y-y_{k0})\right] \mathrm{d}k_y\right] \tag{75}$$

The response is now obtained as the superposition of each dynamic axle load, that is multiplied with a transfer function that is obtained after evaluation of an inverse wavenumber transformation:

$$\hat{\mathbf{u}}(y,\omega) \;=\; \sum_{k=1}^{n_{\mathrm{a}}} \hat{\mathbf{g}}_{\mathrm{d}k}(\omega)\, \hat{\mathbf{H}}^{\mathrm{T}}(y-y_{k0},\omega) \tag{76}$$

This low speed approximation will be used in SILVARSTAR whenever possible.

Example 4.8: Free field response due to moving loads

In this example, the free field response is calculated by applying the dynamic axle loads calculated in example 4.6 on the ballasted track and soil. The calculations are performed using the MOTIV and GroundVIB models for the passage of a single vehicle at 150 km/h.

Figure 23 shows the narrow band spectra of the quasi-static and dynamic components of the PSD of the vertical velocity at 4 m and 20 m from the track centre line. The results are computed with the MOTIV model for the case of medium soil (see table 10 in Appendix A.1). The results are the average vibration during the passage of the train, including the full pass-by but normalised to the pass-by duration corresponding to the train length.

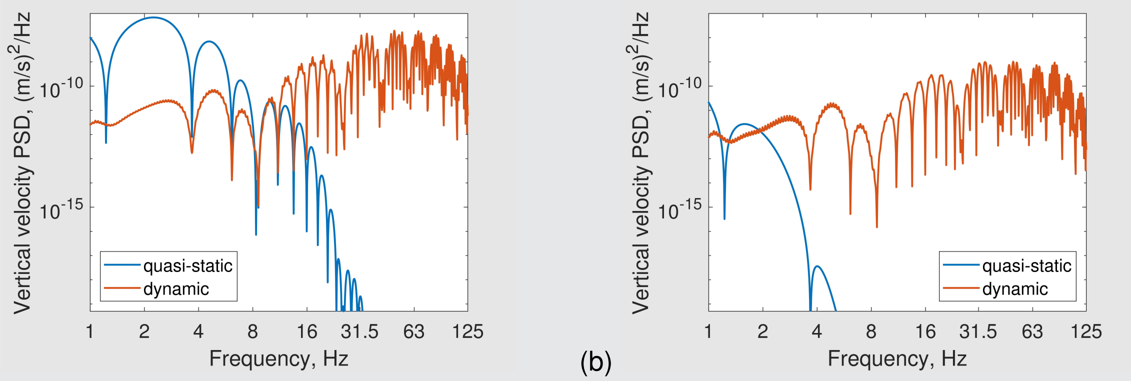

Figure 23: Narrow band spectra of the quasi-static and dynamic components of the PSD of the vertical velocity of the ground response at (a) 4 m and (b) 20 m from the track centre line.

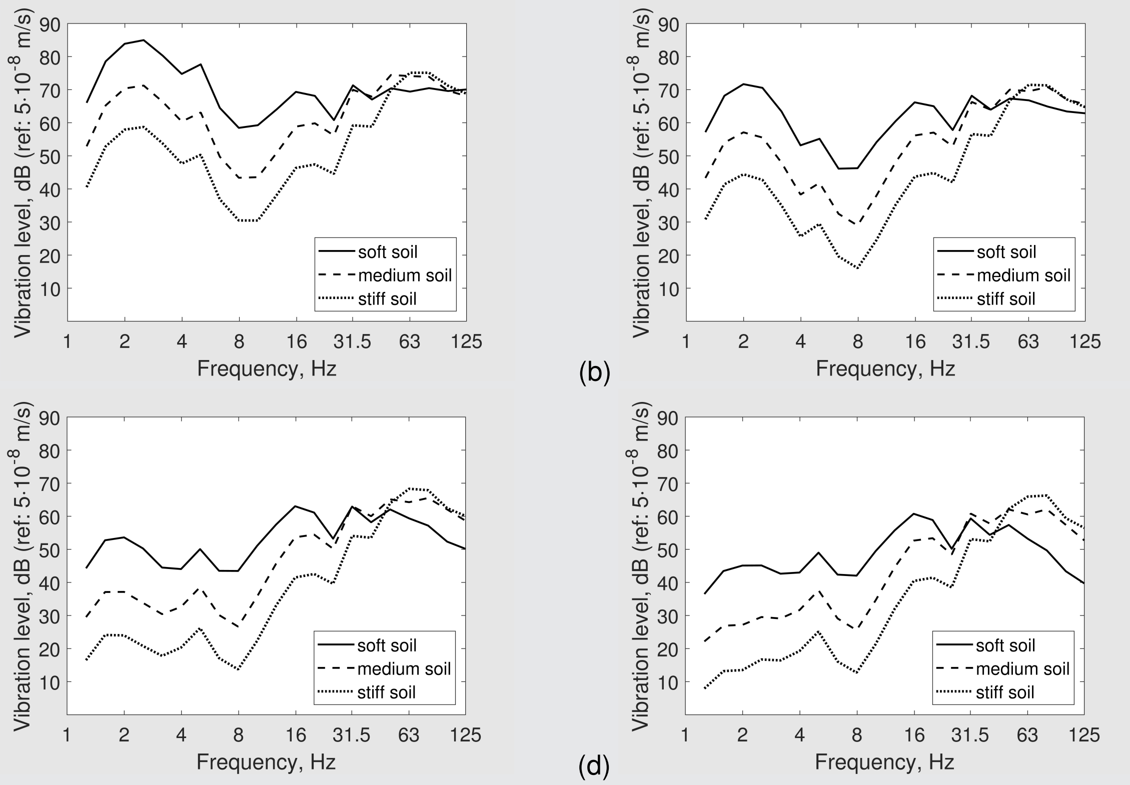

Figure 24: Free field vertical vibration levels in one-third octave bands at (a) 4 m, (b) 8 m, (c) 15 m, and (d) 20 m from the track centre line.

Comparing the vibration spectra at both distances, it can be noticed that the response decays significantly with distance, especially the quasi-static component. Close to the track (figure 23a) the quasi-static contribution to the total response is significant at low frequencies below about 10 Hz. Further away from the track (figure 23b), the response is dominated by the dynamic component.

Figure 24 shows the vertical velocity level at the ground surface due to the passage of the train for the three ground types. The results are computed with MOTIV at 4 m, 8 m, 15 m and 20 m from the track and are expressed as average one-third octave band spectra during the train passage; they incorporate the effect of the moving quasi-static and dynamic axle loads. It can be noticed that the response decays significantly with distance. Larger differences are found in the lower frequencies (below 10 Hz at 4 m and 8 m and below 4 Hz at 15 m and 20 m), where the quasi-static component is important. Comparing the different ground types, for frequencies below about 20 Hz, the soil stiffness has a significant effect on the free field response; the level of vibration increases by about 10 dB when the soil stiffness reduces from the stiff to the medium soil or from the medium to the soft. Above 20 Hz, these differences reduce and at about 50 Hz, the free field response is similar for all soil types. Above 50 Hz, the free field vibration levels increase with the soil stiffness especially for larger distances (15 m and 20 m) from the track, which is mainly due to material damping in the soil.

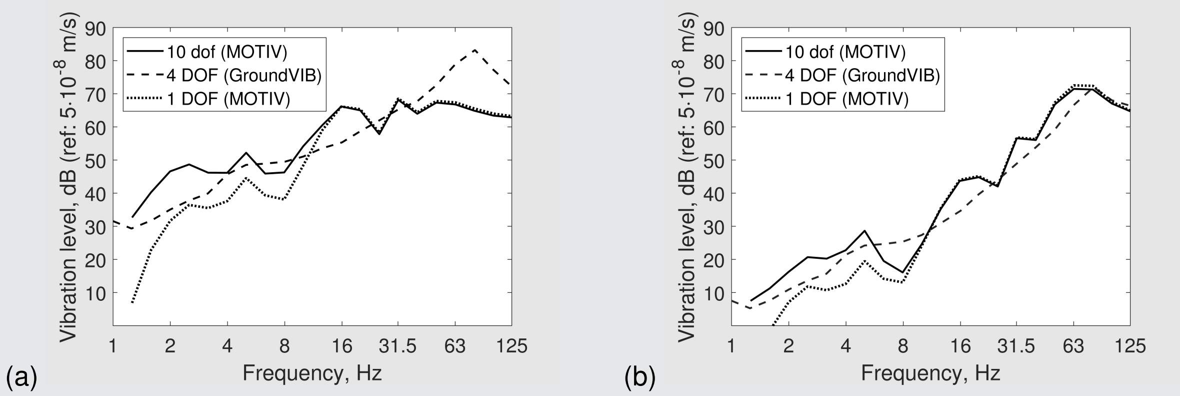

Figure 25: One-third octave band dynamic component of the free field vertical vibration levels at 8 m from the track centre line for the (a) soft and (b) stiff soil.

Figure 25 shows the dynamic component of the free field velocity at 8 m from the track for the different vehicle models; the 10-DOF and 1-DOF vehicle models are used in MOTIV, while the 4-DOF model is used in GroundVIB. Results are presented for soft and stiff soil. Compared with the 10-DOF model, the 1-DOF model underestimates the dynamic response at low frequencies (below 10 Hz for the soft soil and below 8 Hz for the stiff soil). However, in the total free field response these differences are not expected to be prominent, as the quasi-static component dominates the response at low frequencies. Predictions with the 4-DOF model in GroundVIB show the same trends as with the 10-DOF model in MOTIV for both ground types, although lacking some of the spectral detail. This is because in the GroundVIB model there is no correlation between the applied axle loads through the vehicle and the track structures. For the case of the soft soil (figure 25a), the GroundVIB model overestimates the free field response for frequencies above about 63 Hz due to the rigid ground assumption in the calculation of the contact forces (cf. example 4.6).

4.5 Conclusion

In this section, we explained how railway induced vibration (on track and in the free field) can be computed by means of the track-soil transfer functions and the quasi-static and dynamic axle loads, with particular emphasis to 2.5D semi-analytical and numerical models as implemented in the MOTIV and TRAFFIC software, since these are efficient models that will be used in SILVARSTAR.

We will employ these models in a hybrid vibration prediction model, that is inspired by experimental procedures outlined in the ISO 14837-1:2005 standard and the FRA/FTA manuals. We will combine experimental procedures with numerical prediction, based on track impedance and track-soil transfer functions that are pre-computed for a selected range of track and soil conditions, hence facilitating quick vibration assessment in an early design phase. Alternatively, these functions can also be computed in real-time if sufficient computational resources are available.

In the following sections, we will review these experimental procedures in more detail and explain how they can serve as a basis for a hybrid vibration prediction tool.

5. EMPIRICAL MODELS

5.1 Introduction

Notwithstanding the large progress in the development of numerical models for railway induced vibration, they are still mainly used for research. In contrast, engineering practice mostly still makes use of empirical methods. The ISO 14837-1:2005 standard [88] provides general guidance on ground-borne noise and vibration arising from rail systems. This standard indicates that requirements for absolute predictions change during the various stages of development and distinguishes between scoping models (earliest stage), environmental assessment models (planning process) and detailed design models (part of construction and design). This categorization is seen in many of the empirical models in use but, of course, also applies to numerical models.

Examples of empirical methods include the procedures developed by the Federal Railroad Administration (FRA) and the Federal Transit Administration (FTA) of the U.S. Department of Transportation [71, 72, 70, 152], the method developed by the Swiss Federal Railways (SBB) [112], the method of Madshus et al. [123] which is based on measurements in Norway and Sweden, and the method of Hood et al. [76] which was developed within the frame of the Channel Tunnel Rail Link project in the UK. The procedures developed by FRA and FTA distinguish between the three different levels of assessment of the ISO 14837-1 standard [88]. The Detailed Vibration Assessment is based on a prediction technique developed by Bovey [14] and Nelson and Saurenman [136] and presents a more elaborate method for the prediction of ground-borne vibration and re-radiated noise in buildings. The method developed by SBB [112] distinguishes between two prediction models, VIBRA-1 and VIBRA-2, where the latter is more detailed and considers, for example, frequency-dependent attenuation models. The empirical methods by Madshus et al. [123] and Hood et al. [76] follow a similar structure as the one by SBB, and additionally consider the issue of prediction uncertainty.

In this section, we will focus on the general framework for vibration analysis recommended in the ISO 14837-1:2005 standard [88], together with the empirical procedure for Detailed Vibration Assessment proposed by FRA and FTA [71, 72, 70, 152]. Within the SILVARSTAR project, these procedures will serve as a basis to develop a frequency-based hybrid vibration prediction tool, combining experiments with numerical prediction, as will be explained in sections 6 and 7.

This section is based on the aforementioned ISO 14837-1:2005 standard [88], the reports published by FRA and FTA [71, 72, 70, 152], the keynote paper of Lombaert et al. [117] presented at IWRN11, the PhD thesis of Verbraken [187], and journal papers by Verbraken et al. [192, 193] and Kuo et al. [111, 110].

5.2 General framework recommended by ISO 14837-1:2005

The aforementioned empirical methods aim at predicting the magnitude of the quasi-stationary vibration level $A(f)$ in a building during a train passage and can be cast in the following general form of the ISO

14837-1:2005 standard [88] as a product of three terms:

$$A(f) = S(f)P(f)R(f) \tag{77}$$

where the vibration level $A(f)$ typically is a root mean square value (of velocity or acceleration) in one-third octave bands, $S(f)$ represents the source strength, $P(f)$ accounts for the propagation path, and $R(f)$ characterizes the receiver. ISO 14837-1:2005 [88] stipulates that each of these terms should be further divided into relevant components, which interact and can only be assumed uncoupled in some situations for simplified models.

To obtain the vibration level $A(f)$ at a given frequency f, each of the three terms in equation (77) is calculated at the same frequency f, which is strictly speaking not valid for moving sources due to the Doppler effect [187]. As a result, the source magnitude $S(f)$ will also depend on the distance r. Equation (77) is expected to provide a reasonable estimate for the quasi-stationary response, however, when the train speed is relatively low compared with the wave velocities in the soil [192].

The source term $S(f)$ forms the basis of the prediction and, according to ISO 14837-1:2005, it "may be a forcing function at the wheel/rail interface or, alternatively, may be a vibration response (velocity or acceleration) at a defined location (e.g. tunnel invert, tunnel wall or in the ground to the side of the tunnel, or to the side of the track at grade)." The first approach, where $S(f)$ represents the force at the wheel/rail interface, follows the approach of Nelson and Saurenman (1987) who proposed a method based on an equivalent force density, that was later adopted in the empirical procedure procedure. In the second approach, $S(f)$ could be the vibration spectrum on the ground close to the track, for example at 8 m or at 25 m.

Within SILVARSTAR, we will generally prefer the first approach where $S(f)$ represents the force at the wheel/rail interface. The second approach will also be accommodated with an appropriate formulation of each term. Furthermore, we will preferentially express the vibration level $A(f)$ as a velocity, understanding that a conversion to acceleration can easily be made.

Empirical prediction methods have shown their value in practice by providing reasonable estimates of vibration velocity levels. Crucial for the prediction quality is the availability of a suitable source characterization, either in terms of a force density or a reference vibration level. Equation (57) that relates the dynamic train loads to the wheel and track unevenness shows that this requires a match in the type and level of excitation, train characteristics, as well as characteristics of the track and the soil. This implies that empirical models based on in situ vibration measurements can only be applied for prediction at sites where the conditions (rolling stock, track, soil) are very similar to those at the sites where the data were collected; they can, in general, not be used in situations where new train or track types are implemented or at sites with deviating soil conditions. A study of prediction errors arising from a mismatch in soil conditions for the Detailed Vibration Assessment of the U.S. Department of Transportation was presented by Verbraken et al. [191]. Example 4.6 suggests that, although the soil conditions affect the track receptance, they have much less influence on the dynamic axle loads, especially at low frequencies where the vehicle receptances are much higher than the track receptance.

5.3 The FRA/FTA procedure

The empirical procedure for Detailed Vibration Assessment proposed by the FRA and FTA [71, 72, 70, 152] is a popular approach, based on a prediction technique developed by Bovey [14] and Nelson and

Saurenman [136]. The procedure conforms to the general framework recommended in ISO 14837-1:2005 [88] using division of source, propagation, and receiver terms and will be used in SILVARSTAR as a basis for the development of a hybrid vibration prediction tool. The term characterizing the propagation path $P(f)$ is determined from field measurements by adding contributions from incoherent point sources at different positions along the track, leading to the so-called line source transfer mobility. The source strength $S(f)$, which is termed the force density, is determined indirectly from the measured response and the experimental line source transfer mobility. A database with source strengths obtained at different sites can then be used to predict ground vibration levels at sites where the line source transfer mobility has been determined. The advantage of this method when compared with numerical models is that it inherently takes into account characteristics of the vibration transmission at a given site by the direct use of measured transfer functions. In this way, simplifying assumptions, such as the horizontal nature of the soil stratification, and identification of the dynamic soil characteristics from in situ geophysical tests are avoided.

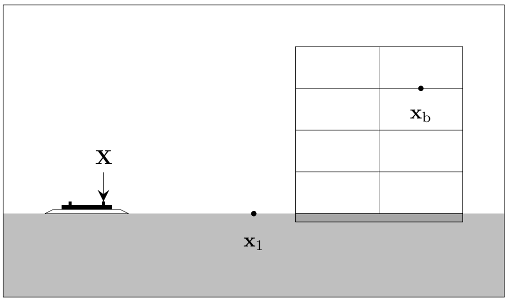

Figure 26: Position of the source and receiver points for the FRA procedure when the railway is present.

The detailed vibration assessment predicts the vibration velocity level $\mathrm{L_v}(\mathbf{x}_\mathrm{b})$ at a receiver $\mathbf{x}_\mathrm{b}$ in the building (figure 26) as the root mean square (RMS) value v_RMS of the velocity during the stationary part of a train passage. It is measured in decibels (e.g. $\mathrm{dB\ ref\ } 1 \times 10^{-8}\,\mathrm{m/s}$) in one-third octave bands, resulting in a summation of the source, propagation, and receiver terms, rather than a product as per equation (77):

$$\mathrm{L_v}(\mathbf{x}_\mathrm{b}) \quad = \quad \mathrm{L_F}(\mathbf{X}, \mathbf{x}_1) + \mathrm{TM_L}(\mathbf{X}, \mathbf{x}_1) + \mathrm{C_b}(\mathbf{x}_1, \mathbf{x}_\mathrm{b}) \tag{78}$$

The first term $\mathrm{L_F}(\mathbf{X}, \mathbf{x}_1)$ is the equivalent force density level $[\mathrm{dB\,ref\,1N}/\sqrt{\mathrm{m}}]$ and is a measure for the power per unit length radiated by the source. The vector $\mathbf{X}$ collects all of the source points, located on the rail heads, while the receiver points $\mathbf{x}_1$ are located on the ground surface; it will be explained further why the force density $\mathrm{L_F}(\mathbf{X}, \mathbf{x}_1)$ may depend on $\mathbf{x}_1$. The second term $\mathrm{TM_L}(\mathbf{X}, \mathbf{x}_1)$ is the line source transfer mobility $[\mathrm{dB\,ref\,}10^{-8}\frac{\mathrm{m/s}}{\mathrm{N}/\sqrt{\mathrm{m}}}]$ and is a measure for the vibration energy that is transmitted through the soil relative to the power per unit length radiated by the source. The third term $\mathrm{C_b}(\mathbf{X}, \mathbf{x}_\mathrm{b})$ is the receiver term or the building's coupling loss; it is computed as a combination of adjustment factors to account for soil-structure interaction at foundation level and attenuation and amplification within the building.

A reference value of $1 \times 10^{-8}\,\mathrm{m/s}$ was used in the PhD thesis of Verbraken [187] and in the cited journal papers of Verbraken et al. [192, 193] and Kuo et al. [111, 110] to compute the vibration velocity level $\mathrm{L_v}(\mathbf{x}_\mathrm{b})$. It must be noted that, in the reports published by FRA and FTA [71, 72, 70, 152], a reference value of $1 \times 10^{-6}\,\mathrm{in/s}$ is used, while FINE-2 partners propose a reference value of $5 \times 10^{-8}\,\mathrm{m/s}$ [173].

In the following, we will discuss and illustrate how each of the these terms can be measured, as elaborated in more detail in the PhD thesis of Verbraken [187].

5.3.1 Line source transfer mobility

The vibration propagation from the track, through the soil to the receiver $\mathbf{x}_1$ on the soil surface is contained within the line source transfer mobility term $\mathrm{TM_L}(\mathbf{X}, \mathbf{x}_1)$. This involves the superposition of point source transfer mobility levels $\mathrm{TM_P}(\mathbf{X}_k, \mathbf{x}_1)$ for a series of n equidistant source points $\mathbf{X}_k$ with spacing h:

$$\mathrm{TM_L}(\mathbf{X}, \mathbf{x}_1) \quad = \quad 10 \log_{10} \left[h \sum_{k=1}^{n} 10^{\frac{\mathrm{TM_P}(\mathbf{X}_k, \mathbf{x}_1)}{10}} \right] \tag{79}$$

Figure 27a shows a measurement setup for vibration propagation tests with a track at grade. Impacts are given at equally spaced points $\mathbf{X}$ along the track and the resulting vibration velocity is measured along a line of receivers $\mathbf{x}_1$ perpendicular to the track. The transfer function between the applied force at a single impact point $\mathbf{X}_k$ and the velocity at a receiver $\mathbf{x}_1$ is called the point source transfer mobility $\mathrm{TM}_{\mathrm{P}_k}$ and is determined in one-third octave bands. For the case of a new railway that has not yet been built, source points $\mathbf{X}$ at the rail heads are not available, so alternative impact locations $\mathbf{X}_1$ on the soil's surface close to the future track position are used (figure 27b).

A similar procedure is applied for a track in a tunnel, where impacts are given on the rail head or in a borehole if a tunnel has not yet been built.

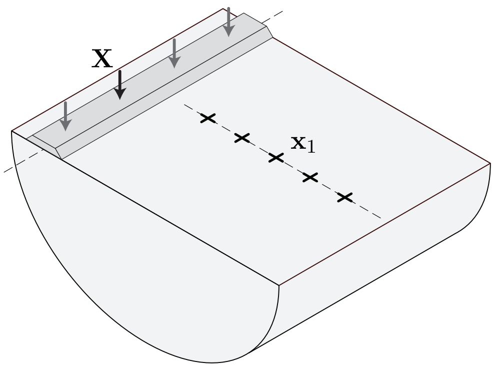

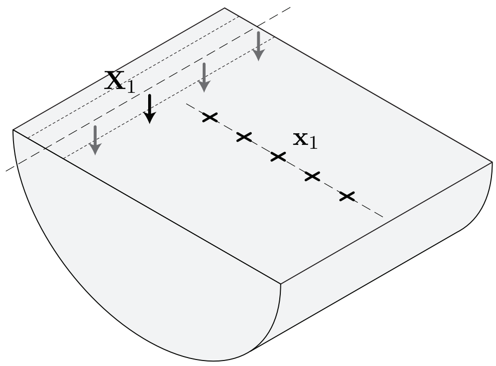

Figure 27: Setup for vibration propagation tests for a track at grade with impact locations (a) on the track and (b) adjacent to a future track.

Based on an analytical derivation (assuming fixed and incoherent axle loads), the following alternative formulation can be found for the line source transfer mobility [187]:

$$\mathrm{TM_L}(\mathbf{X}, \mathbf{x}_1) \quad = \quad 10 \log_{10} \left[\frac{L_\mathrm{t}}{n_\mathrm{a}} \sum_{k=1}^{n_\mathrm{a}} 10^{\frac{\mathrm{TM_P}(\mathbf{X}_k, \mathbf{x}_1)}{10}} \right] \tag{80}$$

where L_t is the length of the train, n_a is the number of axles, and impact loads are now applied at axle positions $\mathbf{X}_k$ (figure 28a). The ratio between the sum and the number of axles n_a on the right hand side of equation (80) is the average value of the transmitted vibration energy for all axles, each represented by an impact at position $\mathbf{X}_k$. The vibration transfer due to a line source is obtained by multiplying this average vibration transfer with the train length L_t.

Instead of considering n_a sources at axle positions, $n_\mathrm{b} = n_\mathrm{a}/2$ sources at the centre of each bogie can be considered (figure 28a). The vibration due to a single source point is affected by its exact position. It can be expected, however, that the average vibration for a long train is relatively insensitive to the exact positions of the axles, so that it can also be represented by n_a equidistant source points [187].

As the average value of the transmitted vibration energy is not strongly affected by the number n_a of source points, an arbitrarily chosen number n of source locations with spacing h can be used to represent the line source with length L_t, provided that the sampling of the line source is sufficiently dense (figures 28c and 28d). When the spacing $h = L_\mathrm{t}/n$ is introduced in equation (80), expression (79) is indeed obtained [187].

An alternative approach is proposed in the FRA procedure [71], where two edge points are considered and a different spacing $h' = n/(n-1)h$ is used (figure 28e), resulting in a slightly different expression for the line source transfer mobility, that does not give different results [187].

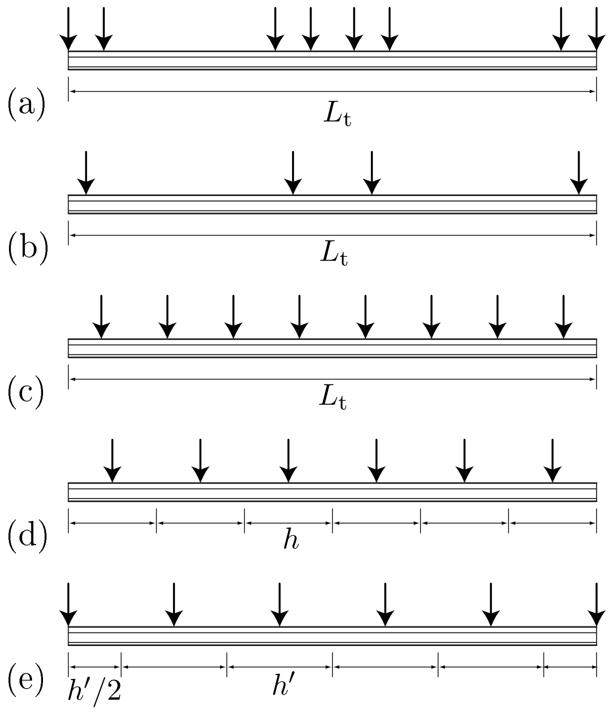

Figure 28: Location of the source points for the determination of the line source transfer mobility level with (a) n_a source points corresponding to the axle locations, (b) n_b source points corresponding to the bogie locations, (c) n_a equidistant source points, (d) n equidistant source points with spacing h, and (e) n equidistant source points with spacing h' including two edge points [187].

The consideration of n impact points along the track, where repeated impacts need to be given, may result in a time-consuming measurement campaign. Assuming lateral homogeneity of the soil, one may also consider to measure point transfer mobilities with a single impact point and several receivers on a measurement line perpendicular to the track up to sufficiently long distance. The line source transfer mobility can be reconstructed by superposition of point transfer mobilities at measured (or interpolated) source-receiver distances. The appropriateness of such simplified procedure still needs to be verified, however.

Example 5.1: Line source transfer mobility

Vibration measurements were performed on a site in Lincent (Belgium) next to the HST line L2 Brussels-Köln [188, 189, 187]. Vibration was recorded on 5 parallel measurement lines (separated by 10.2 m and 9.6 m, respectively) on the flange of the rail, on the edge of the sleeper and in the free field at 8 locations on line C and 2 locations on lines A, B, D, and E (figure 29).

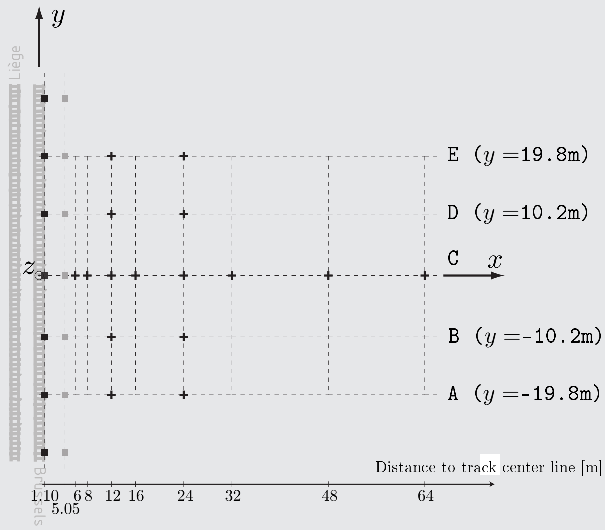

Figure 29: Measurement setup on the track and in the free field at the site in Lincent, indicating the receiver points (✚) and the source points at the track (■) and at the soil's surface adjacent to the track (■).

Vibration was measured during the passage of InterCity and high speed (Thalys and ICE) trains. Furthermore, transfer functions between the track and the free field were measured using an instrumented impact hammer. Impacts were given on the edge of the sleeper at 21 locations equally distributed over a distance of 200 m. Additionally, impacts were also given on a square aluminium foundation that was located at 5.05 m from the track at 17 positions equally distributed over a distance of 160 m. For each position, the number of impacts was $N = 100$ in order to improve the signal-to-noise ratio (the standard deviation on the transfer function is inversely proportional to $\sqrt{N}$).

Several complementary measurement campaigns were performed on this site to determine dynamic soil characteristics by means of geophysical prospection methods (SASW, SCPT, seismic refraction) and laboratory tests (bender element tests) and to measure transfer functions as well as vibration during train passages. The resulting data sets have been used (1) to validate numerical models [119, 115], (2) to apply and verify empirical methods [193], and (3) to support the development of hybrid models [111]. In the examples of section 5, we focus on the application of empirical methods.

As transfer functions from the track to the free field were measured with 21 impact locations separated by 10 m over a distance of 200 m, while 100 impacts were given, these experimental results can be used to assess the influence of the spacing between impact points and the length of the source length on the prediction of the line source transfer mobility. This is illustrated in figures 30 and 31, respectively, which demonstrate that the source length can be reduced to 100 m without affecting too much the accuracy of the line source transfer mobility at 12 m and 48 m from the track. These results were confirmed by a numerical parametric study considering the effect of the source length, sampling of the line source, and the position of the impact points (equally distributed on both rails, at the centre or edge of the sleeper, at the centre of a future track, or adjacent to the track) [187].

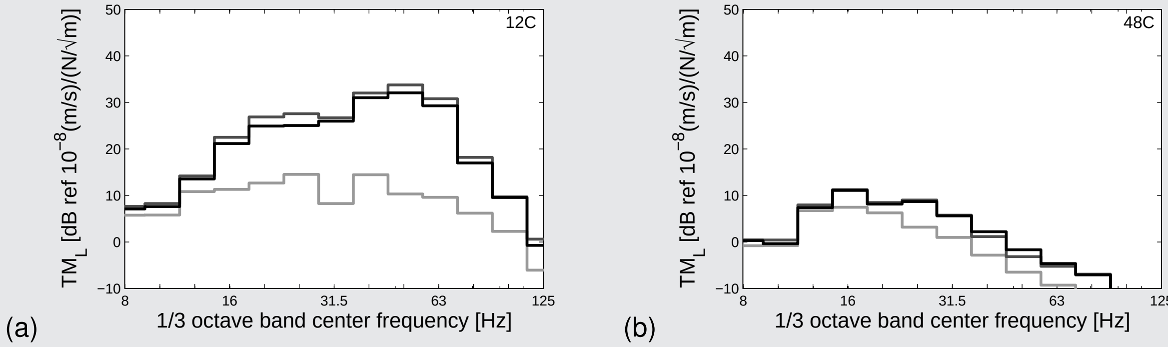

Figure 30: Measured line source transfer mobility at (a) $12\,\mathrm{m}$ and (b) $48\,\mathrm{m}$ determined with source points $\mathbf{X}_{\mathrm{SE}}$ at the edge of the sleeper for a source length of $200\,\mathrm{m}$ and a source point spacing of $40\,\mathrm{m}$, $20\,\mathrm{m}$, and $10\,\mathrm{m}$ (grey to black lines).

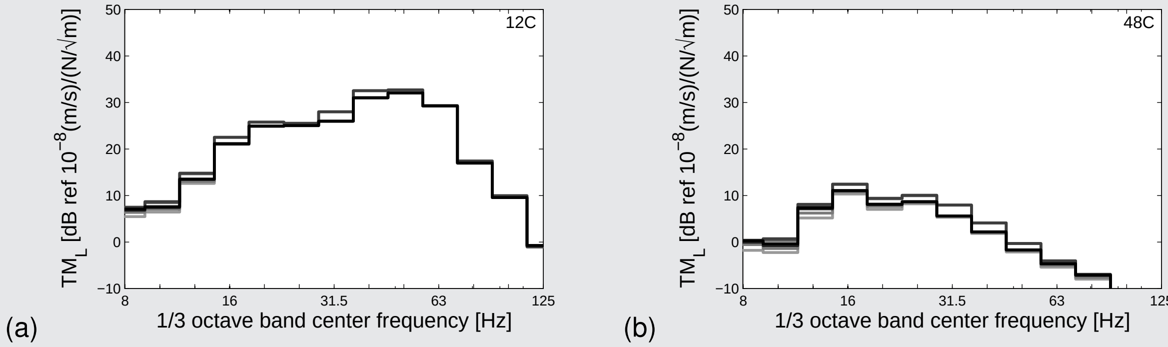

Figure 31: Measured line source transfer mobility at (a) $12\,\mathrm{m}$ and (b) $48\,\mathrm{m}$ determined with source points $\mathbf{X}_{\mathrm{SE}}$ at the edge of the sleeper for a source length of $100\,\mathrm{m}$, $120\,\mathrm{m}$, $140\,\mathrm{m}$, $160\,\mathrm{m}$, $180\,\mathrm{m}$, and $200\,\mathrm{m}$ (grey to black lines) and a source point spacing of $10\,\mathrm{m}$.

5.3.2 Equivalent force density

The omission of the building's coupling loss term from equation (78) gives the expression for the vibration velocity level at a receiver $\mathbf{x}_1$ located in the free field, however (possibly) still in presence of the building:

$$\mathrm{L_v}(\mathbf{x}_1) \quad = \quad \mathrm{L_F}(\mathbf{X}, \mathbf{x}_1) + \mathrm{TM_L}(\mathbf{X}, \mathbf{x}_1) \tag{81}$$

Depending on the location of the receiver $\mathbf{x}_1$ with respect to the building, this may include the effect of soil-structure interaction.

Rearranging equation (81) gives a method of determining indirectly the excitation force, represented by the equivalent force density level $\mathrm{L_F}(\mathbf{X}, \mathbf{x}_1)$:

$$\mathrm{L_F}(\mathbf{X}, \mathbf{x}_1) \quad = \quad \mathrm{L_v}(\mathbf{x}_1) - \mathrm{TM_L}(\mathbf{X}, \mathbf{x}_1) \tag{82}$$

This excitation force term represents the equivalent fixed line source that results in the same vibration velocity level as the train passage. The force density level depends on both the actual force generated at the wheel/rail interface and the dynamic characteristics of the transit structure, including the track, subgrade and soil.

The equivalent force density due to a train passage is determined using equation (82) as follows. The vibration velocity level $\mathrm{L_v}(\mathbf{x}_1)$ due to the train passage is measured at a point $\mathbf{x}_1$. Also, the line source transfer mobility $\mathrm{TM_L}(\mathbf{X}, \mathbf{x}_1)$ is determined at the same point $\mathbf{x}_1$ using the previously described experimental procedure. Equation (82) reveals that the equivalent force density level $\mathrm{L_F}(\mathbf{X}, \mathbf{x}_1)$ indeed is influenced by the position $\mathbf{X}$ of the source points used for the determination of the line source transfer mobility as well as by the position of the receiver $\mathbf{x}_1$ where the difference between the vibration velocity level $\mathrm{L_v}(\mathbf{x}_1)$ and line source transfer mobility $\mathrm{TM_L}(\mathbf{X}, \mathbf{x}_1)$ is made. This is the consequence of the approximations embeddded in the FRA formulation, e.g. the fact that it does not account for the Doppler effect.

Verbraken [187] assessed the influence of the position of the source and receiver on the force density level by means of numerical calculations and experimental data collected at the site in Lincent. In the numerical assessment, the reference distance, the position of the source point on the track and the location of the receiver were considered. One important conclusion is that, as the response close to the track is dominated by quasi-static axle loads, the receiver point $\mathbf{x}_1$ should be located outside the influence zone of the moving static axle loads, at a sufficiently large distance from the track (which was estimated as larger than 6 m). In the following example, we focus on the analysis based on experimental data.

Example 5.2: Equivalent force density

Figure 32 shows the vibration velocity level at 12 m and 48 m from the track during the passage of 17 IC trains with speeds around 200 km/h.

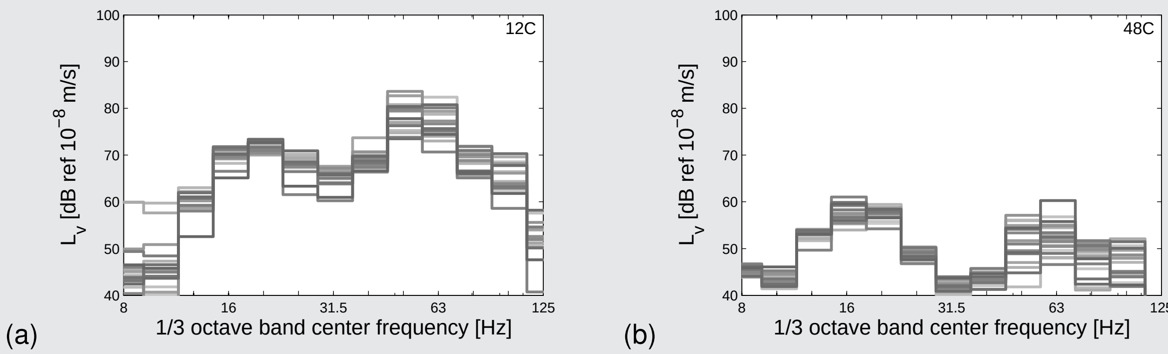

Figure 32: One-third octave band RMS level of the measured vertical free field velocity at line C ($y = 0\,\mathrm{m}$) at (a) $12\,\mathrm{m}$ and (b) $48\,\mathrm{m}$ from the track centre line during the passage of 17 IC trains ($193 - 203\,\mathrm{km/h}$).

The equivalent force density due to 12 IC train passages in the same speed range is now determined using equation (82) and subtracting the line source transfer mobility $\mathrm{TM_L}(\mathbf{X}, \mathbf{x}_1)$ (determined for a source length of 200 m and a source point spacing of 10 m, as shown in figure 30) from the vibration velocity level $\mathrm{L_v}(\mathbf{x}_1)$ at the same point $\mathbf{x}_1$. Figure 33 demonstrates that indeed the force density determined in this way depends on the output location and also reveals substantial variation in certain frequency bands depending on the train.

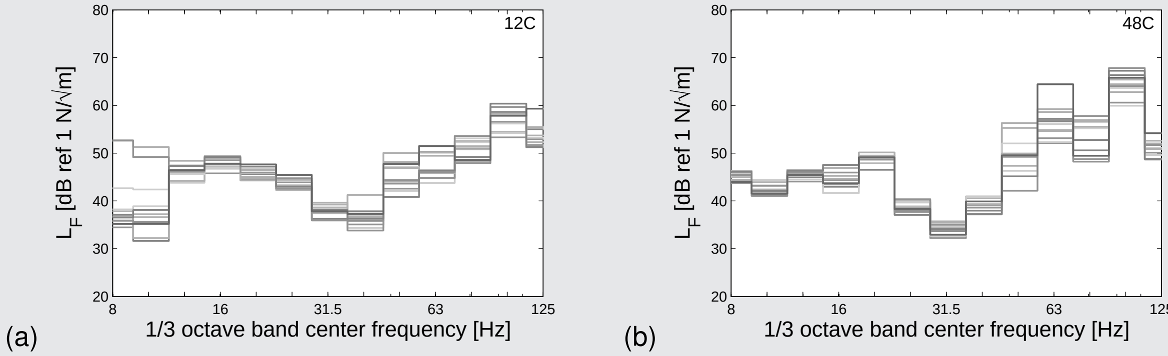

Figure 33: Measured force density level based on the response at (a) $12\,\mathrm{m}$ and (b) $48\,\mathrm{m}$ for 12 IC trains $(192 - 200\,\mathrm{km/h})$ (grey to black lines).

Figure 34 compares the force density for a single passage of an IC train at 198 km/h when the line source transfer mobility has been measured with impacts on the edge of the sleeper or, alternatively, at the soil's surface adjacent to the track. The observed difference is due to the combined effect of asymmetric loading of the track, the track filtering and the modified track-receiver distance; the difference is relatively small, though, at larger distances, demonstrating that the force density determined with source points at the soil's surface adjacent to the track could be used as an approximation for the force density determined with source points at the edge of the sleeper.

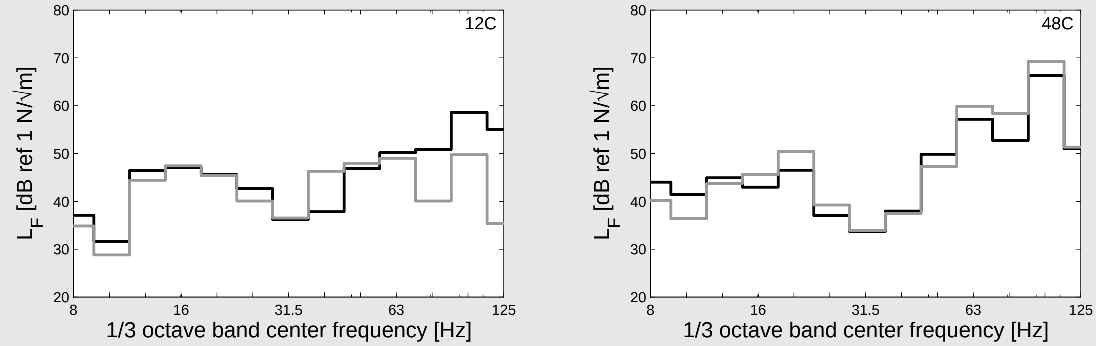

Figure 34: Measured force density level based on the response at (a) $12\,\mathrm{m}$ and (b) $48\,\mathrm{m}$ for an IC train $(198\,\mathrm{km/h})$ determined with source points $\mathbf{X}_{\mathrm{SE}}$ at the edge of the sleeper (black line) and $\mathbf{X}_{\mathtt{FA}}$ at the soil's surface adjacent to the track (grey line).

Figure 35 finally illustrates the dependency of the estimated force density on the location of the receiver point determined with source points on the edge of the sleeper and at the soil's surface adjacent to the track. Figure 35a shows lower variation in the mid frequency band; in the higher frequency range, the force density decreases when based on the response at increasing distance from the track, which is partly due to the asymmetric loading of the track as also observed in numerical predictions. Much larger variation with distance is observed when the force is applied at the soil's surface adjacent of the track (figure 35b), which must be taken into consideration when applying this procedure for predictions.

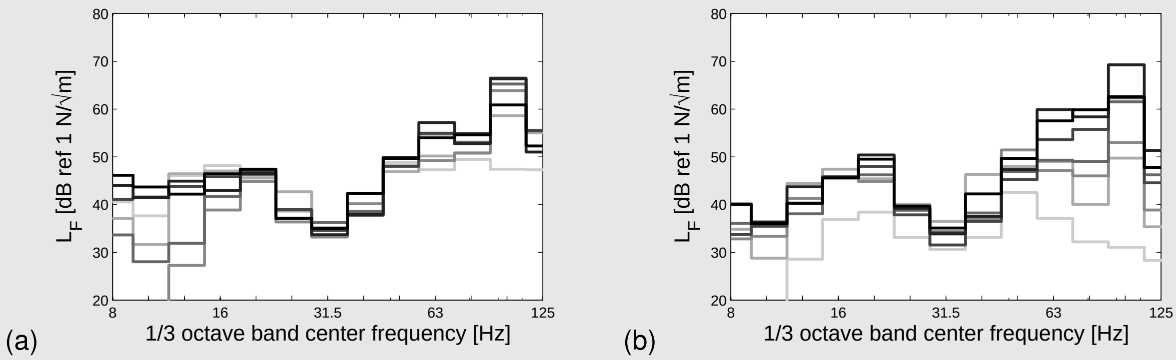

Figure 35: Measured force density level based on the response at $6\,\mathrm{m}$ to $64\,\mathrm{m}$ (grey to black lines) for an IC train ($198\,\mathrm{km/h}$) determined with source points (a) $\mathbf{X}_{\mathtt{SE}}$ at the edge of the sleeper and (b) $\mathbf{X}_{\mathtt{FA}}$ at the soil's surface adjacent to the track.

5.3.3 Receiver term or building's coupling loss

The receiver term $\mathrm{C_b}(\mathbf{x}_1, \mathbf{x}_\mathrm{b})$ represents the building's coupling loss. The FRA approach [72] computes this term as a combination of three dimensionless frequency-dependent adjustment factors that are applied to the free field vibration velocity level: (a) those that represent the change in the incident ground-surface vibration due to the presence of the building foundation, (b) the attenuation of vibration as it travels from foundation to the upper floors, assumed at a rate of 1 to 2 dB per floor, and (c) amplification of approximately 6 dB in the frequency range of the fundamental floor resonances (15-20 Hz for wood-frame, 20-30 Hz for reinforced concrete slabs). For (a), zero correction is applied when estimating basement floor vibration or vibration of at-grade slabs, and frequency dependent attenuation ranging from 0-15 dB is prescribed for masonry buildings on piles and spread footings. The reader is referred to the FRA reports [72] for a detailed overview of these adjustment factors.

According to equation (78), these adjustment factors $\mathrm{C_b}(\mathbf{x}_1, \mathbf{x}_\mathrm{b})$ are added to the ground-surface vibration levels at location $\mathbf{x}_1$ near the building, to estimate the vibration level $\mathrm{L_v}(\mathbf{x}_\mathrm{b})$ inside the building at location $\mathbf{x}_\mathrm{b}$.

When both a railway and building are present, if follows immediately from equations (78) and (81) that the receiver term $\mathrm{C_b}(\mathbf{x}_1, \mathbf{x}_\mathrm{b})$ can be quantified as a difference in vibration velocity level $\mathrm{L_v}(\mathbf{x}_\mathrm{b})$ at some point $\mathbf{x}_\mathrm{b}$ in the building, and $\mathrm{L_v}(\mathbf{x}_1)$ at some point $\mathbf{x}_1$ on the ground surface with the building present. This is illustrated in figure 26 and expressed as:

$$\mathrm{C_b}(\mathbf{x}_1, \mathbf{x}_\mathrm{b}) = \mathrm{L_v}(\mathbf{x}_\mathrm{b}) - \mathrm{L_v}(\mathbf{x}_1) \tag{83}$$

This definition of the building's coupling loss is regarded as the reference expression for the receiver term. The vibration velocity levels can either be determined using field measurements of the vibrations produced during a train passage, or they can be calculated numerically using a train-track-soil-building model.

The coupling loss value will depend on the positions of $\mathbf{x}_1$ and $\mathbf{x}_\mathrm{b}$ relative to the track; the closer $\mathbf{x}_1$ is to the building, the more the vibration level $\mathrm{L_v}(\mathbf{x}_1)$ will be influenced by the presence of the building. Moreover, locating the receiver point $\mathbf{x}_1$ far from the building will result in a coupling loss that includes a greater contribution (proportionally) from the propagation path. The position $\mathbf{x}_\mathrm{b}$ can also vary within the building; the location $\mathbf{x}_\mathrm{b}$ will determine whether the receiver term incorporates effects such as floor-to-floor attenuation and floor resonances.

The reference definition of the building's coupling loss can be further elaborated by expressing the two vibration velocity levels as the sum of excitation force and propagation path terms. For example, writing:

$$\mathrm{L_v}(\mathbf{x}_\mathrm{b}) = \mathrm{L_F}(\mathbf{X}, \mathbf{x}_\mathrm{b}) + \mathrm{TM_L}(\mathbf{X}, \mathbf{x}_\mathrm{b}) \tag{84}$$

and incorporating the expression for $\mathrm{L_v}(\mathbf{x}_1)$ in equation (81), results in:

$$\mathrm{C_b}(\mathbf{x}_1, \mathbf{x}_\mathrm{b}) = \mathrm{TM_L}(\mathbf{X}, \mathbf{x}_\mathrm{b}) - \mathrm{TM_L}(\mathbf{X}, \mathbf{x}_1) + \mathrm{L_F}(\mathbf{X}, \mathbf{x}_\mathrm{b}) - \mathrm{L_F}(\mathbf{X}, \mathbf{x}_1) \tag{85}$$

By assuming the two force density terms to be equal, the building coupling loss is alternatively written as:

$$\mathrm{C_b^*}(\mathbf{x}_1, \mathbf{x}_\mathrm{b}) = \mathrm{TM_L}(\mathbf{X}, \mathbf{x}_\mathrm{b}) - \mathrm{TM_L}(\mathbf{X}, \mathbf{x}_1) \tag{86}$$

where $\mathrm{TM_L}(\mathbf{X}, \mathbf{x}_\mathrm{b})$ and $\mathrm{TM_L}(\mathbf{X}, \mathbf{x}_1)$ are the line source transfer mobilities measured at some point $\mathbf{x}_\mathrm{b}$ in the building and at some point $\mathbf{x}_1$ on the ground surface in the presence of the building, respectively. The asterisk in equation (86) indicates that this is an approximate expression based on the assumption that the force densities are equivalent. The source points used to determine the line source transfer mobilities are collected in the vector $\mathbf{X}$ and are located at the rail heads, thus this calculation of the building's coupling loss does not require the passage of a train. This makes it a useful means of measuring the coupling loss in the field, provided the excitation applied at $\mathbf{X}$ is sufficiently large to produce a measurable building response. It also simplifies a numerical computation of the building response by removing the need for a vehicle model and characterisation of the wheel-rail unevenness.

Within the FP7 project RIVAS, building receiver terms were also computed [196]. These functions were integrated in the GroundVIB software, as will be explained in section 6.

Example 5.3: Receiver term

Extensive vibration measurements were performed in a three-storey reinforced concrete building, located in Heverlee, Belgium, at about 40 m from the railway line L1390 Leuven-Ottignies [110, 146], as will also be discussed in subsection 7.3. Synchrous vibration measurements were performed on the rail and sleepers, on three parallel measurement lines in the free field (figure 36) and at 4 locations on each of the 4 stories of the building (figure 37), resulting in 84 measurement directions.

Transfer functions were measured between track, free field and building, applying multiple impacts with an instrumented hammer on 17 sleepers spaced 12 m over a total distance of 192 m along the track [125, 107]. Continuous monitoring during one week resulted in a database of over 500 freight and passenger train passages, including track, free field and building response.

In this example, we demonstrate how these measurements were used to determine building coupling loss factors according to the FRA procedure. The reader is referred to reference [110] for an in-depth discussion.

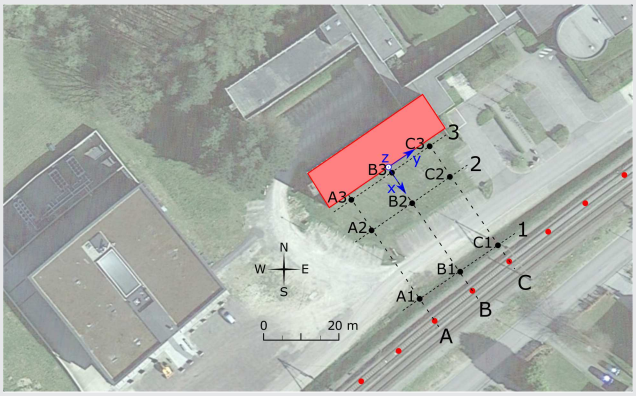

Figure 36: Free field measurement locations (black dots). Measurement lines A, B, and C are located at $y = -12$ m, $y = 0$ m and $y = 12$ m. Measurement lines 1, 2, and 3 correspond to $x = 32$ m, $x = 12$ m, and $x = 1$ m. Eight of the seventeen hammer impact locations are also shown (red dots).

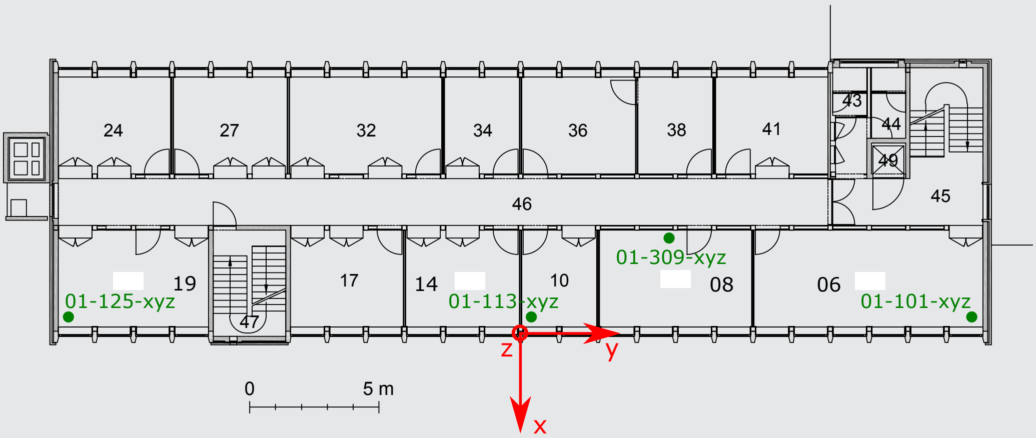

Figure 37: Measurement locations at the first floor of Blok D.

Figure 38 shows the average vertical vibration velocity level at various distances from the track and at various floors in the building for 117 passages of three-carriage passenger trains on the nearside track in a speed range of 77-100 km/h. The 95% confidence intervals are displayed as shaded regions and are of the order of 1-3 dB over the entire frequency range, which is notably narrow. The free field vibration level attenuates with increasing distance to the track due to a combined effect of geometrical spreading and material damping in the soil (figure 38a). There is no clear trend of vibration attenuation with floor height (figure 38b) . This corresponds with the findings of Xia et al. [206], but runs counter to the FRA recommendation of an adjustment factor of 1-2 dB attenuation per floor. The vibration levels within the building are, on the whole, smaller than those measured directly outside the building. This again concurs with the trend observed by Xia et al. [206].

The building coupling loss values can be estimated using the vibration velocity levels measured in the free field and the building during train passages using equation (83). Figure 39 shows the coupling loss at locations XX-125-z and XX-309-z, where XX refers to any of the four floor levels. The location of $\mathbf{x}_1$ is 1 m from the building on measurement line A. The 95% confidence intervals are shown as shaded regions and are remarkably narrow across the entire frequency range. For receivers located near a structural column (figure 39a), the trend of increasing floor vibration with increasing floor elevation is observed. For receivers located at mid-span (figure 39a), at less than 10 Hz there is a large response on the second floor, and, to a lesser extent, on the first floor. This is due to a dominant, fundamental building mode that involves some coupling between the first and second floors [110]. The greatest variation between the coupling loss values at various floors occurs at frequencies greater than 25 Hz.

(a)
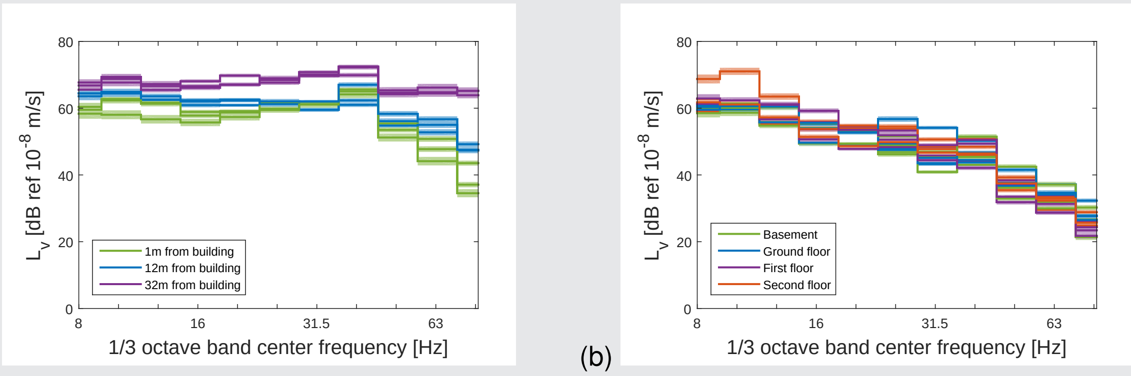

Figure 38: Average vertical vibration velocity levels determined using 117 passenger train passages (77-100 km/h) measured (a) in the free field along three measurement lines; and (b) in Blok D at four measurement locations within each storey. Shaded areas indicate the 95% confidence intervals.

(a)
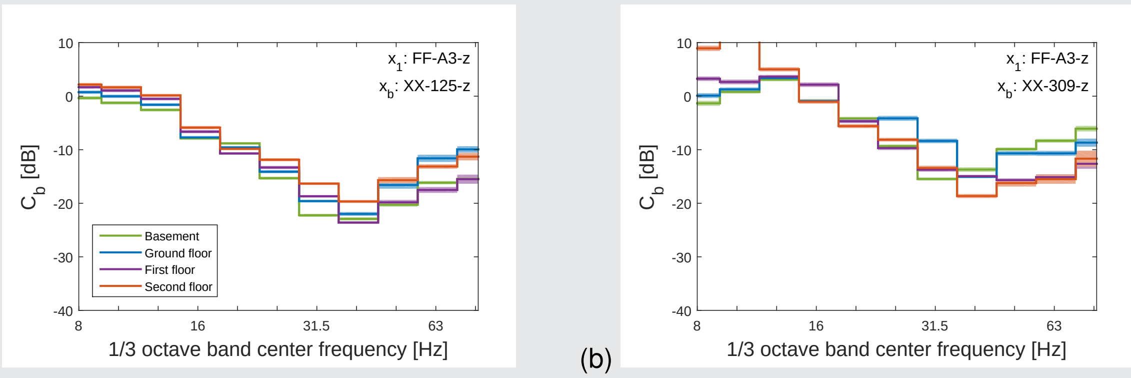

Figure 39: Coupling loss values calculated with receivers $\mathbf{x}_b$ at various floors with locations (a) XX-125-z and (b) XX-309-z, using 117 passenger train passages (77-100 km/h). Free field receiver $\mathbf{x}_1$ is located 1 m from the building on measurement line A. Shaded areas indicate the 95% confidence intervals.

Figure 40 shows the line source transfer mobilities for receivers in the free field and in the building, determined as the summation of the seventeen point source transfer mobilities.

Figure 41 shows the force density terms calculated using the average vibration velocities shown in figure 38 and the line source transfer mobilities shown in figure 40. The magnitude and the frequency dependence of the force density is similar regardless of which receiver points are used. The observed scatter, particularly at frequencies greater than 31.5 Hz, does not strongly depend on distance from the building nor floor elevation. The assumption of equivalent force terms therefore appears to be reasonable for this site.

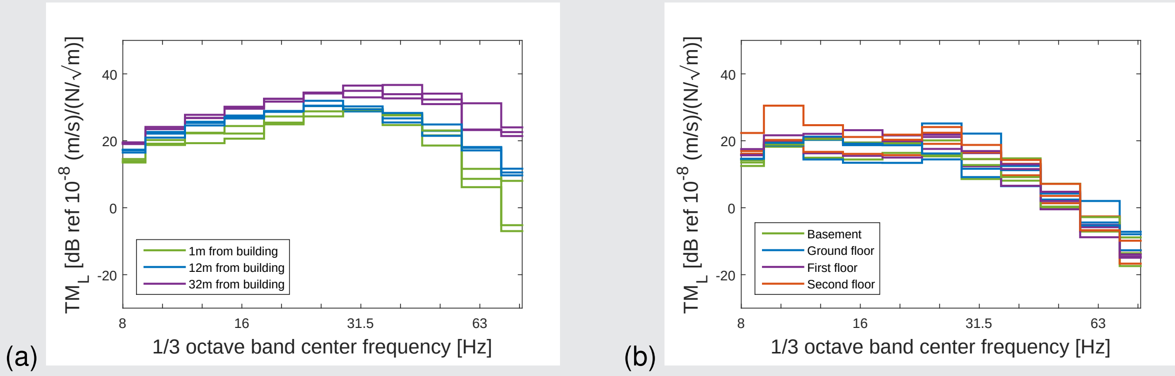

Figure 40: Line source transfer mobilities determined using more than 100 hammer excitations on the sleeper at each of seventeen source locations and measured (a) in the free field along three measurement lines; and (b) in Blok D at four measurement locations within each storey.

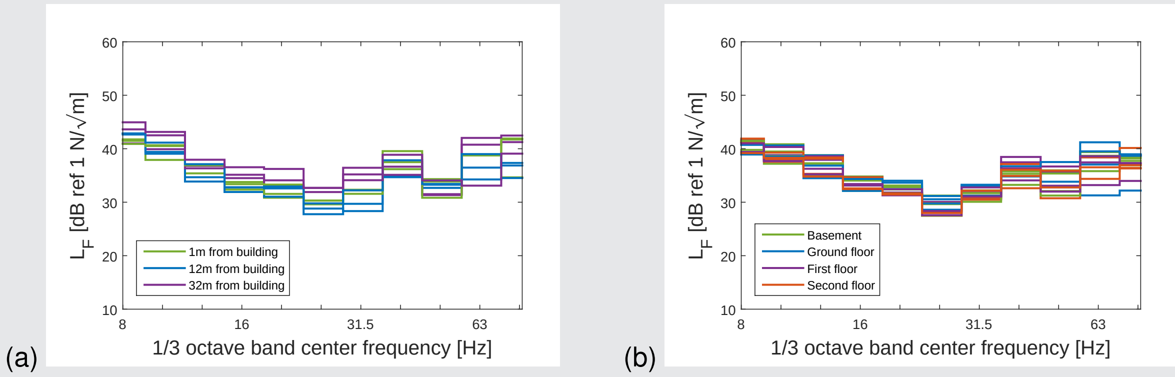

Figure 41: Force density calculated using average vibration velocities resulting from 117 passenger train passages (77-100 km/h) and line source transfer mobilities determined using more than 100 hammer excitations on the sleeper at each of seventeen source locations. Sensors are located (a) in the free field along three measurement lines; and (b) in Blok D at four measurement locations within each storey.

Approximate coupling loss values can be calculated as per equation (86) using the line source transfer mobilities and are shown in figure 42. As is expected having demonstrated the equivalence of force density terms, these approximate coupling loss values show a strong likeness to the values shown in figure 39, both in terms of magnitude and variation with frequency. There is especially good agreement at frequencies below 25 Hz for all sensor locations. The greatest deviations occur at above 31.5 Hz, where the approximate values generally show greater scatter in the floor-to-floor attenuation.

The closeness of the approximate coupling loss values to the coupling losses calculated using train passages has important practical implications:

- A building's coupling loss can be estimated with reasonable accuracy without the existence of train passages, which means in the case of a new railway the track does not yet have to be operational.

- Using hammer impacts, which produce a much smaller magnitude of vibration than train passages, nevertheless enables the coupling loss to be quantified with reasonable accuracy.
- Although more than one hundred hammer impacts were applied at each source location for this study, it has previously been shown that using twenty impacts is sufficient for determining the point source transfer mobilities [109]. Furthermore, it has also been shown that using a source length of 200 m with source point spacing of 10 m does not produce a significantly different line source transfer mobility to a source length of 100 m with a source point spacing of 20 m [187]. This may result in a more practical implementation, limiting the number of sensors, impact points and impacts [110].

(a) (b)

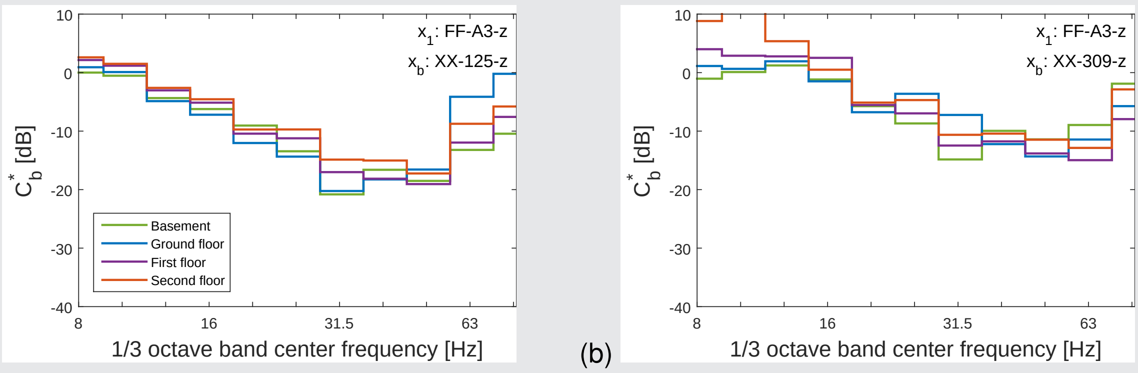

Figure 42: Approximate coupling loss values calculated with receivers $\mathbf{x}_\mathrm{b}$ at various floors with locations (a) XX-125-z and (b) XX-309-z, using hammer impacts on the track. Free field receiver $\mathbf{x}_1$ is located 1 m from the building on measurement line A.

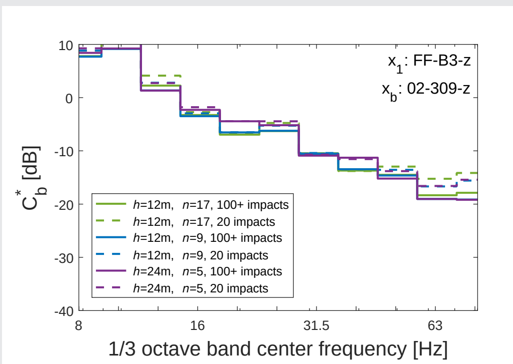

Figure 43: Approximate coupling loss values calculated with receiver $\mathbf{x}_\mathrm{b}$ at mid-span on the top floor (02-309-z) and free field receiver $\mathbf{x}_1$ at 1 m from the building on measurement line B, using various source configurations and numbers of hammer impacts for determining the line source transfer mobilities.

Figure 43 compares the coupling loss value calculated using line source transfer mobilities determined with $n = 17$ sources with spacing $h = 12$ m and a total length of 192 m to that calculated using $n = 9$ sources with spacing $h = 12$ m, giving a length of 96 m, and $n = 5$ sources with spacing $h = 24$ m, also with length 96 m. The dotted lines illustrate the effect of using only 20 impacts at every source position.

The variation due to the reduced number of sources and hammer impacts is less than 5 dB over the entire frequency range, which illustrates that this practical implementation may provide a suitably accurate means of determining the coupling loss at this location.

5.4 Prediction for new-build situations

5.4.1 New railway infrastructure

According to the FRA procedure, several steps are required to predict and assess the free field vibration level.

In the case where a prediction is required for a site where new railway infrastructure is to be built, the following two-step approach is followed [192]:

- First, a reference site is selected (site 1) where a track is present and where the characteristics of the track, soil, and rolling stock, as well as the environment (urban, green field) are similar to those at the site where the new track will be built (site 2). Depending on the requirements of a specific project, sites with different type of track (ballast track, slab track, floating slab track) can be selected. On site 1, the vibration velocity level $\mathrm{L_{v1}}(\mathbf{x}_1)$ due to a train passage is recorded and the line source transfer mobility $\mathrm{TM_{L1}}(\mathbf{X}, \mathbf{x}_1)$ is measured, so that equation (82) can be used to estimate the force density $\mathrm{L_{F1}}(\mathbf{X}, \mathbf{x}_1)$ as:

$$\mathrm{L_{F1}}(\mathbf{X}, \mathbf{x}_1) \quad = \quad \mathrm{L_{v1}}(\mathbf{x}_1) - \mathrm{TM_{L1}}(\mathbf{X}, \mathbf{x}_1) \tag{87}$$

- Second, the line source transfer mobility $\mathrm{TM_{L2}}(\mathbf{X}, \mathbf{x}_1)$ is measured on site 2 where the new track will be built. Equation (81) is subsequently applied to predict the vibration velocity level $\mathrm{L_{v2}}(\mathbf{x}_1)$ due to the new railway infrastructure on site 2, using the estimated force density $\mathrm{L_{F1}}(\mathbf{X}, \mathbf{x}_1)$ (from site 1) and the measured line source transfer mobility $\mathrm{TM_{L2}}(\mathbf{X}, \mathbf{x}_1)$ (from site 2):

$$\mathrm{L_{v2}}(\mathbf{x}_1) \quad = \quad \mathrm{L_{F1}}(\mathbf{X}, \mathbf{x}_1) + \mathrm{TM_{L2}}(\mathbf{X}, \mathbf{x}_1) \tag{88}$$

  Alternatively, inserting equation (87) into equation (88) results in:

$$\mathrm{L_{v2}}(\mathbf{x}_1) \quad = \quad \mathrm{L_{v1}}(\mathbf{x}_1) + \underline{\mathrm{TM_{L2}}(\mathbf{X}, \mathbf{x}_1) - \mathrm{TM_{L1}}(\mathbf{X}, \mathbf{x}_1)} \tag{89}$$

  where the underlined term denotes the difference in line source transfer mobilities at both sites that can be used as a correction term on the vibration level $\mathrm{L_{v1}}(\mathbf{x}_1)$ at the reference site 1 to obtain a prediction of the vibration level $\mathrm{L_{v2}}(\mathbf{x}_1)$ at the site where the new track is to be built.

The vibration velocity level $\mathrm{L_v}(\mathbf{x}_1)$ due to a train passage, and therefore also the force density, can only be determined at a site where the track is already present. As no track is present yet on site 2, the line source transfer mobility $\mathrm{TM_{L2}}(\mathbf{X}_1, \mathbf{x}_1)$ can only be determined by means of impacts at locations $\mathbf{X}_1$ at the soil's surface. The line source transfer mobility $\mathrm{TM_{L1}}(\mathbf{X}_1, \mathbf{x}_1)$ at site 1 should therefore be determined in a similar way with impacts at locations $\mathbf{X}_1$ at the soil's surface adjacent to the track. In order to account for the distance to the centre of the track, the impact points at site 2 should be located at the same distance from the track centre line. When the force density $\mathrm{L_{F1}}(\mathbf{X}_1, \mathbf{x}_1)$ is determined in this way, it no longer represents the actual force transmitted by the wheel/track system, but an equivalent force that has to be applied adjacent to the track in order to obtain the same vibration velocity as the one recorded during the train passage.

The above procedure was focusing on free field vibration, but can be extended (within the framework of the FRA/FTA procedure) to predict vibration levels in (existing) buildings by adding the receiver term $\mathrm{C_b}(\mathbf{x}_1, \mathbf{x}_\mathrm{b})$.

In the FRA procedure, the local transmission of vibration through the soil is correctly accounted for due to the experimental determination of the transfer mobility $\mathrm{TM_L}(\mathbf{X}, \mathbf{x}_1)$. This is an advantage compared to numerical prediction models where the model parameters need to be determined for an accurate prediction. The accuracy of the empirical prediction is largely dependent, however, on the availability of an appropriate force density $\mathrm{L_F}(\mathbf{X}, \mathbf{x}_1)$.

5.4.2 New rolling stock

In the case where a prediction is required (within the framework of the FRA/FTA procedure) for new rolling stock on an existing track, a similar procedure can be followed, on the condition that a reference site is available where this new rolling stock is already running, and this on a similar track and soil as on the site where the new rolling stock will be used in the future.

The previous procedure can again be extended to predict vibration levels in (existing) buildings by adding the receiver term $\mathrm{C_b}(\mathbf{x}_1, \mathbf{x}_\mathrm{b})$.

5.4.3 New building constructed close to an existing track

In the case where a prediction is required for a new building that is planned but not yet built on a site close to an existing railway line, the vibration level $\mathrm{L_v}(\mathbf{x}_1)$ in the free field can be measured for a representative number of train passages, covering different rolling stock (freight and passenger trains) and train speeds. These vibration levels need to be corrected with a receiver term $\mathrm{C_b}(\mathbf{x}_1, \mathbf{x}_\mathrm{b})$ as specified in the FRA/FTA procedure. There is no need in this situation to determine force densities.

Alternatively, the measured vibration levels characterizing the incoming wave field can be used for dynamic analysis of the building due to imposed base motion, taking dynamic soil-structure interaction into account, or not. This, however, would already be a hybrid approach as will be explained in section 6.

5.5 Source characterization by means of a reference ground vibration level

According to ISO 14837-1:2005, the source $S(f)$ could also be a vibration response (velocity or acceleration) at a defined location (e.g. tunnel invert, tunnel wall or in the ground to the side of the tunnel, or to the side of the track at grade), as an alternative to a forcing function. In Germany and the Netherlands, for example, it is common practice to use a vibration velocity level $\mathrm{L_v}(\mathbf{x}_\mathrm{ref})$ at a reference distance $\mathbf{x}_\mathrm{ref}$ of respectively 8 m and 25 m from tracks at grade [173].

Although within SILVARSTAR, the use of a force density level is highly preferred, we will discuss in the following subsections how, alternatively, vibration velocity level $\mathrm{L_v}(\mathbf{x}_\mathrm{ref})$ at a reference distance $\mathbf{x}_\mathrm{ref}$ can be used to predict the vibration velocity level $\mathrm{L_v}(\mathbf{x}_1)$ at a receiver $\mathbf{x}_1$ in the free field. A similar procedure can be followed for the vibration velocity level $\mathrm{L_v}(\mathbf{x}_\mathrm{b})$ at a receiver $\mathbf{x}_\mathrm{b}$ in the building.

5.5.1 Formulation within the framework of the FRA/FTA procedure

The vibration velocity level $\mathrm{L_v}(\mathbf{x}_1)$ is first written according to equation (81), which is repeated here for convenience:

$$\mathrm{L_v}(\mathbf{x}_1) = \mathrm{L_F}(\mathbf{X}, \mathbf{x}_1) + \mathrm{TM_L}(\mathbf{X}, \mathbf{x}_1) \tag{90}$$

A similar equation holds for the vibration velocity level $\mathrm{L_v}(\mathbf{x}_\mathrm{ref})$ at a reference distance $\mathbf{x}_\mathrm{ref}$:

$$\mathrm{L_v}(\mathbf{x}_\mathrm{ref}) = \mathrm{L_F}(\mathbf{X}, \mathbf{x}_\mathrm{ref}) + \mathrm{TM_L}(\mathbf{X}, \mathbf{x}_\mathrm{ref}) \tag{91}$$

Subtracting equations (90) and (91) and rearranging terms results in the following equation for the vibration velocity level $\mathrm{L_v}(\mathbf{x}_1)$:

$$\mathrm{L_v}(\mathbf{x}_1) = \mathrm{L_v}(\mathbf{x}_\mathrm{ref}) + \mathrm{L_F}(\mathbf{X}, \mathbf{x}_1) - \mathrm{L_F}(\mathbf{X}, \mathbf{x}_\mathrm{ref}) + \mathrm{TM_L}(\mathbf{X}, \mathbf{x}_1) - \mathrm{TM_L}(\mathbf{X}, \mathbf{x}_\mathrm{ref}) \tag{92}$$

If it can be assumed that the force density $\mathrm{L_F}(\mathbf{X}, \mathbf{x}_\mathrm{ref})$ determined at the reference point $\mathbf{x}_\mathrm{ref}$ is equal to the force density $\mathrm{L_F}(\mathbf{X}, \mathbf{x}_1)$ determined at the output receiver $\mathbf{x}_1$, then equation (92) can be simplified to:

$$\mathrm{L_v}(\mathbf{x}_1) \simeq \mathrm{L_v}(\mathbf{x}_\mathrm{ref}) + \underline{\mathrm{TM_L}(\mathbf{X}, \mathbf{x}_1) - \mathrm{TM_L}(\mathbf{X}, \mathbf{x}_\mathrm{ref})} \tag{93}$$

It should be noted, however, that vibration measurements and numerical computations demonstrate that the force density depends on the location of the output point [192, 111]. Therefore, in a practical case, the validity of the assumption needs to be verified. Otherwise, equation (92) must be used.

The underlined term in equation (93) represents the difference in line source transfer mobilities at the output receiver $\mathbf{x}_1$ and the reference point $\mathbf{x}_\mathrm{ref}$, identified for excitation at source locations $\mathbf{X}$ on (or beside) the track. Note that, intentionally, we do not call this term a transfer function, since this nomenclature is generally reserved to denote the ratio between a response quantity and an input force.

5.5.2 Prediction for new railway infrastructure

When the source is characterized by means of a reference ground vibration level $\mathrm{L_v}(\mathbf{x}_\mathrm{ref})$, the following procedure can be applied to predict vibration levels for new railway infrastructure:

- At site 1 (the reference site), the vibration velocity level $\mathrm{L_{v1}}(\mathbf{x}_\mathrm{ref})$ is measured at a reference distance $\mathbf{x}_\mathrm{ref}$ from the track.
- At site 2 (the prediction site), the difference between line source transfer mobilities at the receiver $\mathbf{x}_1$ and the reference location $\mathbf{x}_\mathrm{ref}$ is measured by means of impacts at source locations $\mathbf{X}$ on the track (for an existing track that will be operated by new rolling stock) or at source locations $\mathbf{X}_1$ at the soil surface besides the track (for a new track to be built):

$$\Delta\mathrm{TM_{L2}}(\mathbf{X}_1) = \mathrm{TM_{L2}}(\mathbf{X}_1, \mathbf{x}_1) - \mathrm{TM_{L2}}(\mathbf{X}_1, \mathbf{x}_\mathrm{ref}) \tag{94}$$

The reference distance $\mathbf{x}_{\mathrm{ref}}$ is identical to the one used at site 1 to characterize the source. The vibration velocity level $\mathrm{L}_{\mathrm{v2}}(\mathbf{x}_1)$ is subsequently obtained as follows:

$$\mathrm{L}_{\mathrm{v2}}(\mathbf{x}_1) = \mathrm{L}_{\mathrm{v1}}(\mathbf{x}_{\mathrm{ref}}) + \mathrm{TM}_{\mathrm{L2}}(\mathbf{X}_1, \mathbf{x}_1) - \mathrm{TM}_{\mathrm{L2}}(\mathbf{X}_1, \mathbf{x}_{\mathrm{ref}}) \tag{95}$$

This so-called velocity coupling method was tested numerically by Nélain et al. [134] for the case where identical conditions (train, track, and soil properties) hold at sites 1 and 2. When sites 1 and 2 are different, a transposition is required on the reference vibration level $\mathrm{L}_{\mathrm{v1}}(\mathbf{x}_{\mathrm{ref}})$ before applying equation (95). Such a transposition method will be developed in WP2 of SILVARSTAR.

5.6 Conclusion

In this section, we have reviewed the empirical procedure for Detailed Vibration Assessment as proposed in the FRA/FTA guidelines, and illustrated its application by means of two in situ measurement campaigns. We also discussed how this procedure can be applied for prediction in new-build situations.

In the following section, we will discuss how this procedure can serve as a basis for hybrid predictions, combining experimental results and numerical predictions.

6. HYBRID MODELS

6.1 Introduction

Hybrid models combine numerical and empirical methods, offering greater flexibility and robustness than a single modelling method. By integrating field measurements with state-of-the-art modelling techniques, the need for simplifying modelling assumptions and detailed parameter identification can be partially avoided. This is expected to result in a reduction of prediction uncertainty at a reduced cost. Hybrid models can also be employed in situations where there is insufficient experimental data to characterise the source strength and vibration transmission fully, such as when the vibration behaviour of new tracks, new trains, or the installation of vibration mitigation measures is to be evaluated.

For each term in equations (77) or (78), use can be made of either measured data or a numerical model, e.g. a train-track-soil interaction model for dynamic axle loads or force densities, a track-soil interaction model for transfer functions or line source transfer mobilities, and a building-soil interaction model for the receiver term.

Verbraken et al. [192] derived analytical expressions for the force density and the line source transfer mobility, assuming fixed, incoherent, and equal point loads at the axle locations. Kuo et al. used a hybrid model to predict railway induced vibration in the free field [111] and determined experimentally building correction factors for a three-storey building [110]. Vibratec's hybrid GroundVIB model [134] combines several of the aforementioned numerical models with an experimental database.

The following presentation of hybrid models follows the lines of the paper by Kuo et al. [111].

6.2 General framework

The ISO 14387-1:2005 framework involving division of the vibration response into separate source and propagation terms forms an ideal basis for hybrid models, as each of the terms can be determined using field measurements, or calculated using numerical procedures. Thus two generic hybrid models are defined: model 1, which involves numerical prediction of the source term and a propagation term determined using field measurements:

$$A^{\mathrm{HYB}}(f) \quad = \quad S^{\mathrm{NUM}}(f)P^{\mathrm{EXP}}(f) \tag{96}$$

and model 2, which involves determination of the source term using field measurements and numerical prediction of the propagation term:

$$A^{\mathrm{HYB}}(f) \quad = \quad S^{\mathrm{EXP}}(f)P^{\mathrm{NUM}}(f) \tag{97}$$

where the superscripts HYB, NUM and EXP represent hybrid, numerical, and experimental (measured) means of determining the vibration terms.

The use of a numerical prediction of the source term in model 1 is particularly suited to situations where a railway does not yet exist at the site of interest, or has only been partially constructed. This model also provides a means of easily assessing the effect of alterations to the track, such as the installation of track-based mitigation measures like resilient fasteners, rail pads and floating slab track, and alterations to the train, such as reduced wheel/rail roughness and increased train speed. The use of a measured propagation term offers resilience in the case of a site with complex soil stratification, avoiding both the expense of extensive soil characterisation tests and the modelling effort required to implement multiple soil layers. However, in situ measurements are still required to obtain transfer functions that characterise the propagation path.

Model 2 employs a measured source term that is particularly useful in situations where the track conditions and/or geometry are not well-suited to numerical modelling procedures. For example, it may not be possible to conduct in situ measurements of the track unevenness to determine the dynamic axle loads, or transition zones may be present with changing track support stiffness, which currently cannot be incorporated into 2.5D formulations. The use of a numerical prediction of the propagation term provides a means of assessing the effect of installing mitigation measures such as trenches, wave barriers and wave impeding blocks. This type of hybrid model can also significantly reduce the numerical model complexity by avoiding the need for characterisation of the track parameters and inclusion of the train and track elements.

6.3 Model implementation: definition of terms

The generic hybrid models can be implemented using any prescribed method of determining the source and propagation terms. In the following implementation, these terms are defined as per the FRA procedure described in subsection 5.3. The determination of the line source transfer mobilities and force density terms using in situ measurements has already been described; here a summary of the derivation of analytical expressions for these terms is presented. The full derivation is found in Verbraken et al. [192].

Starting with equation (9), the assumptions of fixed, incoherent and equal point loads at the axles are systematically introduced. The narrow band transfer function is replaced by its averaged value in one-third octave bands and the mean square value of the stationary part of the vibration velocity v^2_{RMS} is determined in one-third octave bands. The vibration velocity level $\mathrm{L_v}(\mathbf{x}')$ is defined as 10 times the logarithm to base 10 of v^2_{RMS}. Separation of the source and propagation terms results in an analytical expression for the force density $\mathrm{L_F}(\mathbf{X})$:

$$\mathrm{L_F}(\mathbf{X}) \quad = \quad 10\log_{10}\left[\frac{n_{\mathrm{a}}}{L_{\mathrm{t}}} g^2_{\mathrm{dRMS}} \frac{1}{F^2_{\mathrm{ref}}}\right] \tag{98}$$

where $F^2_{\mathrm{ref}} = 1\ \mathrm{N^2/m}$ is the reference value used for the force density, and an analytical expression for the line source transfer mobility $\mathrm{TM_L}(\mathbf{X}, \mathbf{x}_1)$:

$$\mathrm{TM_L}(\mathbf{X}, \mathbf{x}_1) \quad = \quad 10\log_{10}\left[\frac{L_{\mathrm{t}}}{n_{\mathrm{a}}} \sum_{k=1}^{n_{\mathrm{a}}} \frac{\int_{\omega_1}^{\omega_2} |\hat{h}_{zz}(\mathbf{X}_k, \mathbf{x}_1, \omega)|^2 \,\mathrm{d}\omega}{\Delta\omega} \frac{1}{v^2_{\mathrm{ref}}}\right] \tag{99}$$

where v_{ref} is the reference value used for the line source transfer mobility level. Equation (98) represents the mean-square force per unit length applied by the axles at the wheel/rail contact at a fixed position. It is calculated based on the spectrum g_{dRMS} of a single dynamic axle load of the train, using equation (57), and expressed in one-third octave bands, and the ratio of the number of axles n_{a} to the train length L_{t}. It should be noted that the term g_{dRMS} contains only the dynamic component of the axle load. The static component of the axle loads manifests itself in the free field response as a quasi-static contribution that cannot be written in the form of equation (77). This quasi-static contribution is only significant at low frequencies when close to the track and can thus be neglected. The expression for the force density level is independent of the separation distance of the source and receiver, as a result of the approximations introduced at the start of this derivation. This expression will be referred to as the "direct" method of calculating the force density level, cf. the "indirect" method given in equation (82). It is only indirectly influenced by the speed of the train via the dynamic axle load term.

Equation (99) represents the average value of the vibration energy transfer for all axles multiplied by the train length. The term $\hat{h}_{zz}(\mathbf{X}_k, \mathbf{x}_1, \omega)$ is the transfer function relating the vibration at receiver point $\mathbf{x}'$ in the direction $\mathbf{e}_z$ due to a point load at source point $\mathbf{x}_k$ in direction $\mathbf{e}_z$, and is first averaged over the frequency band $[\omega_1, \omega_2]$ with bandwidth $\Delta\omega$, then summed over the total number of axles. This expression for the line source transfer mobility is dependent on, yet relatively insensitive to, the exact position of the axles and the number of source points considered [187]. It should be noted the fact that the transfer function $\hat{h}_{zz}(\mathbf{X}_k, \mathbf{x}_1, \omega)$ here is assumed to represent a velocity rather than a displacement, so multiplication with a factor $\mathrm{i}\omega$ is already incorporated in this notation.

The line source transfer mobility can also be written as the superposition of point source transfer mobilities:

$$\mathrm{TM}_{\mathrm{L}}(\mathbf{X}, \mathbf{x}_1) = 10 \log_{10} \left[L_{\mathrm{a}} \sum_{k=1}^{n_{\mathrm{a}}} 10^{\frac{\mathrm{TM}_{\mathrm{P}}(\mathbf{X}_k, \mathbf{x}_1)}{10}} \right] \tag{100}$$

where the point source transfer mobility $\mathrm{TM}_{\mathrm{P}}(\mathbf{X}_k, \mathbf{x}_1)$ is defined as:

$$\mathrm{TM}_{\mathrm{P}}(\mathbf{X}_k, \mathbf{x}_1) = 10 \log_{10} \left[\frac{\int_{\omega_1}^{\omega_2} |\hat{h}_{zz}(\mathbf{X}_k, \mathbf{x}_1, \omega)|^2 \, \mathrm{d}\omega}{\Delta\omega} \frac{1}{v_{\mathrm{ref}}^2} \right] \tag{101}$$

Each of these point loads are located by Verbraken et al. [192] at the position of the corresponding axle. However, the FRA procedure uses point loads that are distributed equidistantly along the train. Coupled FE-BE analysis shows that the use of equidistant loads is valid for the case of predicting the approximately stationary part of the vibrations due to railway traffic [192]. It is estimated that this results in differences of the order of 4 to 6 dB in the one-third octave band predictions [187].

6.4 Predicted force density combined with measured line source transfer mobility

The first hybrid model presented herein combines a numerical prediction of the force density with a line source transfer mobility determined using field measurements. There are two possible methods for obtaining the numerical prediction of the force density.

6.4.1 Hybrid model 1a: direct numerical prediction of the force density

Direct prediction uses an analytical expression for the force density, derived in subsection 6.3, which uses source points $\mathbf{X}$ located at both rail heads and is independent of the receiver location. The resulting hybrid model is described using the equation:

$$\mathrm{L_v^{HYB}}(\mathbf{x}_1) \quad = \quad \mathrm{L_F^{NUM}}(\mathbf{X}) + \mathrm{TM_L^{EXP}}(\mathbf{X}, \mathbf{x}_1) \tag{102}$$

As this model does not fully account for the movement of the train, it is expected that more accurate predictions will be obtained using an indirect numerical prediction of the force density.

6.4.2 Hybrid model 1b: indirect numerical prediction of the force density

The second method for obtaining the numerical prediction of the force density is the indirect prediction method that utilises the difference between the numerical prediction of the vibration velocity level and the numerical line source transfer line mobility:

$$\mathrm{L_F^{NUM}}(\mathbf{X}, \mathbf{x}_1) \quad = \quad \mathrm{L_v^{NUM}}(\mathbf{x}_1) - \mathrm{TM_L^{NUM}}(\mathbf{X}, \mathbf{x}_1) \tag{103}$$

This results in a force density level $\mathrm{L_F^{NUM}}(\mathbf{X}, \mathbf{x}_1)$ that depends on both the source $\mathbf{X}$ and receiver $\mathbf{x}_1$ locations. The hybrid model expression is therefore:

$$\mathrm{L_v^{HYB}}(\mathbf{x}_1) \quad = \quad \mathrm{L_F^{NUM}}(\mathbf{X}, \mathbf{x}_1) + \mathrm{TM_L^{EXP}}(\mathbf{X}, \mathbf{x}_1) \tag{104}$$

and substitution of equation (103) yields:

$$\mathrm{L_v^{HYB}}(\mathbf{x}_1) \quad = \quad \mathrm{L_v^{NUM}}(\mathbf{x}_1) \underline{- \mathrm{TM_L^{NUM}}(\mathbf{X}, \mathbf{x}_1) + \mathrm{TM_L^{EXP}}(\mathbf{X}, \mathbf{x}_1)} \tag{105}$$

This expression represents a numerical prediction of the vibration velocity at the receiver location $\mathbf{x}_1$, with the underlined correction term $\mathrm{TM_L^{EXP}}(\mathbf{X}, \mathbf{x}_1) - \mathrm{TM_L^{NUM}}(\mathbf{X}, \mathbf{x}_1)$ to account for the vibration propagation measurements. This correction term is expected to reduce the prediction error in the numerical model due to simplifying assumptions and parameter uncertainty in the underground environment, which is particularly pertinent when complex soil stratification is present.

Equation (105) implies that numerical calculations are required for each location $\mathbf{x}_1$ where hybrid predictions are to be obtained. As an approximation, equation (104) could be used with the force density evaluated based on single receiver location. The appropriateness of such an approximation needs to be investigated further.

The numerical predictions for the force density level have, up to now, been determined with source points $\mathbf{X}$ located at the rail heads, and have been combined in hybrid models with measured line source transfer mobility levels that are also determined with source points $\mathbf{X}$ at the rail heads. In the event that alternative source locations are required, where a track is not present at the site of interest, source point locations $\mathbf{X}_1$ away from the rail head can be used for both the force density level and the line source transfer mobility:

$$\mathrm{L_v^{HYB}}(\mathbf{x}_1) \quad = \quad \mathrm{L_F^{NUM}}(\mathbf{X}_1, \mathbf{x}_1) + \mathrm{TM_L^{EXP}}(\mathbf{X}_1, \mathbf{x}_1) \tag{106}$$

This expression uses an indirect prediction of the numerical force density $\mathrm{L_F^{NUM}}(\mathbf{X}_1, \mathbf{x}_1)$ with source points at $\mathbf{X}_1$, which is given by:

$$\mathrm{L_F^{NUM}}(\mathbf{X}_1, \mathbf{x}_1) \quad = \quad \mathrm{L_v^{NUM}}(\mathbf{x}_1) - \mathrm{TM_L^{NUM}}(\mathbf{X}_1, \mathbf{x}_1) \tag{107}$$

Substituting this into equation (106) results in:

$$\mathrm{L}_{\mathrm{v}}^{\mathrm{HYB}}(\mathbf{x}_1) \quad = \quad \mathrm{L}_{\mathrm{v}}^{\mathrm{NUM}}(\mathbf{x}_1)\underline{-\mathrm{TM}_{\mathrm{L}}^{\mathrm{NUM}}(\mathbf{X}_1,\mathbf{x}_1) + \mathrm{TM}_{\mathrm{L}}^{\mathrm{EXP}}(\mathbf{X}_1,\mathbf{x}_1)} \tag{108}$$

This expression is the alternative to equation (105), and is suitable for indirect numerical prediction of the force density with sources located away from the rail heads, for example on the sleeper's edge or next to the track. It can be regarded as a numerical prediction of the vibration velocity level at receiver location $\mathbf{x}_1$ together with the underlined correction term $\mathrm{TM}_{\mathrm{L}}^{\mathrm{EXP}}(\mathbf{X}_1,\mathbf{x}_1) - \mathrm{TM}_{\mathrm{L}}^{\mathrm{NUM}}(\mathbf{X}_1,\mathbf{x}_1)$ that makes use of the alternative source location $\mathbf{X}_1$ to account for the propagation path measurements.

The numerical vibration velocity $\mathrm{L}_{\mathrm{v}}^{\mathrm{NUM}}(\mathbf{x}_1)$ can be obtained using the direct expression for the force density:

$$\mathrm{L}_{\mathrm{v}}^{\mathrm{NUM}}(\mathbf{x}_1) \quad = \quad \mathrm{L}_{\mathrm{F}}^{\mathrm{NUM}}(\mathbf{X}) + \mathrm{TM}_{\mathrm{L}}^{\mathrm{NUM}}(\mathbf{X},\mathbf{x}_1) \tag{109}$$

resulting in:

$$\mathrm{L}_{\mathrm{v}}^{\mathrm{HYB}}(\mathbf{x}_1) \quad = \quad \mathrm{L}_{\mathrm{F}}^{\mathrm{NUM}}(\mathbf{X}) + \underline{\mathrm{TM}_{\mathrm{L}}^{\mathrm{NUM}}(\mathbf{X},\mathbf{x}_1) - \mathrm{TM}_{\mathrm{L}}^{\mathrm{NUM}}(\mathbf{X}_1,\mathbf{x}_1)} + \mathrm{TM}_{\mathrm{L}}^{\mathrm{EXP}}(\mathbf{X}_1,\mathbf{x}_1) \tag{110}$$

This expression is the alternative to equation (102), and is suitable for direct numerical prediction of the force density with sources located away from the rail heads. It combines the analytical expression for the force density with a measured line source transfer mobility using source location $\mathbf{X}_1$. The difference in source point locations is accounted for in the underlined numerical correction term $\mathrm{TM}_{\mathrm{L}}^{\mathrm{NUM}}(\mathbf{X},\mathbf{x}_1) - \mathrm{TM}_{\mathrm{L}}^{\mathrm{NUM}}(\mathbf{X}_1,\mathbf{x}_1)$.

6.5 Measured force density combined with predicted line source transfer mobility

The second hybrid model combines field measurements of the force density with a numerical prediction of the line source transfer mobility. The resulting hybrid model is described using the equation:

$$\mathrm{L}_{\mathrm{v}}^{\mathrm{HYB}}(\mathbf{x}_1) \quad = \quad \mathrm{L}_{\mathrm{F}}^{\mathrm{EXP}}(\mathbf{X},\mathbf{x}_1) + \mathrm{TM}_{\mathrm{L}}^{\mathrm{NUM}}(\mathbf{X},\mathbf{x}_1) \tag{111}$$

which involves source locations $\mathbf{X}$ at the rail heads for determining both the force density and the line source transfer mobility.

As per the FRA procedure, the measured force density is determined as the difference between the measured vibration velocity level and the line source transfer mobility:

$$\mathrm{L}_{\mathrm{F}}^{\mathrm{EXP}}(\mathbf{X},\mathbf{x}_1) \quad = \quad \mathrm{L}_{\mathrm{v}}^{\mathrm{EXP}}(\mathbf{x}_1) - \mathrm{TM}_{\mathrm{L}}^{\mathrm{EXP}}(\mathbf{X},\mathbf{x}_1) \tag{112}$$

The hybrid model expression is therefore:

$$\mathrm{L}_{\mathrm{v}}^{\mathrm{HYB}}(\mathbf{x}_1) \quad = \quad \mathrm{L}_{\mathrm{v}}^{\mathrm{EXP}}(\mathbf{x}_1)\underline{-\mathrm{TM}_{\mathrm{L}}^{\mathrm{EXP}}(\mathbf{X},\mathbf{x}_1) + \mathrm{TM}_{\mathrm{L}}^{\mathrm{NUM}}(\mathbf{X},\mathbf{x}_1)} \tag{113}$$

This expression represents a measured vibration velocity at the receiver location $\mathbf{x}_1$, with a numerical adjustment of the propagation path term $\mathrm{TM}_{\mathrm{L}}^{\mathrm{NUM}}(\mathbf{X},\mathbf{x}_1) - \mathrm{TM}_{\mathrm{L}}^{\mathrm{EXP}}(\mathbf{X},\mathbf{x}_1)$.

This model would be relevant when the effect of a modification to the vibration propagation path of an existing railway is to be evaluated. Examples of such modifications include open trenches [203], soft or stiff wave barriers [126, 98], and heavy masses next to the track [174], all of which have been shown to impede the transmission of waves through the soil.

As per model 1, a hybrid model expression can be formulated for situations where the source point locations $\mathbf{X}_1$ are located away from the rail heads:

$$\mathrm{L}_{\mathrm{v}}^{\mathrm{HYB}}(\mathbf{x}_1) \quad = \quad \mathrm{L}_{\mathrm{F}}^{\mathrm{EXP}}(\mathbf{X}_1, \mathbf{x}_1) + \mathrm{TM}_{\mathrm{L}}^{\mathrm{NUM}}(\mathbf{X}_1, \mathbf{x}_1) \tag{114}$$

If the source point locations are on the soil surface, sufficiently far from the track, the presence of the track could be disregarded in the calculation of the line source transfer mobility. This will result in significant computational savings, as the need for characterisation of the excitation mechanism and the track can be avoided when formulating the numerical model.

Using equation (112) to determine the measured force density results in:

$$\mathrm{L}_{\mathrm{v}}^{\mathrm{HYB}}(\mathbf{x}_1) \quad = \quad \mathrm{L}_{\mathrm{v}}^{\mathrm{EXP}}(\mathbf{x}_1) \underline{- \mathrm{TM}_{\mathrm{L}}^{\mathrm{EXP}}(\mathbf{X}_1, \mathbf{x}_1) + \mathrm{TM}_{\mathrm{L}}^{\mathrm{NUM}}(\mathbf{X}_1, \mathbf{x}_1)} \tag{115}$$

This expression is the alternative to equation (113) and is suitable for numerical prediction of the line source transfer mobility with sources located away from the rail heads. It combines a measured vibration velocity level at receiver location $\mathbf{x}_1$ with an adjustment term $\mathrm{TM}_{\mathrm{L}}^{\mathrm{NUM}}(\mathbf{X}_1, \mathbf{x}_1) - \mathrm{TM}_{\mathrm{L}}^{\mathrm{EXP}}(\mathbf{X}_1, \mathbf{x}_1)$ that makes use of the alternative source location $\mathbf{X}_1$ to account for modification to the vibration propagation path.

6.6 Case history

In examples 5.1 and 5.2, we have illustrated how the line source transfer mobility and force density were determined by means of in situ vibration measurements next to HST line L2 Brussels-Köln in Lincent [187]. These results have been used by Kuo et al. [111] to make hybrid vibration predictions using the different formulations outlined in subsections 6.4 and 6.5. The vibration predicted with the hybrid models was compared with the experimental results and numerical predictions with a 2.5D FE-BE model. The reader is referred to the paper by Kuo et al. [111] for full details.

6.7 GroundVIB, an example of a hybrid vibration prediction tool

GroundVIB is a software package that was initially developed by Vibratec to solve the train-track interaction problem in the context of ground-borne vibration problems (TrackVIB module). This module was validated within the EU funded Brite-Euram project CONVURT (2002), including the train and track receptances and vibration levels of rails and sleepers. The TrackVIB module can deal with a prescribed track unevenness spectrum, as well as parametric excitation and singularities (wheel flats or rail joints). The roughness excitation module was validated by comparison with other software, such as TRAFFIC (KU Leuven), while predictions for parametric excitation and singularities were compared with other dedicated approaches.

Modules were added by Vibratec to compute soil vibration and validated by comparison with in situ measurements. These modules include the coupling of TrackVIB (roughness excitation) with empirical data (soil decay rate or soil transfer function), or with pre-computed slab-soil transfer functions that were computed with external 2.5D and 3D models.

Vibration and noise levels in buildings are obtained using building correction terms from an empirical database (from the FP7 project RIVAS and other references), or directly from in situ measurements in specific sensitive buildings.

The output of GroundVIB is compliant with ISO 2631-2:2003 [87] and can also be used to evaluate vibration criteria as defined in DIN 4150-2:1999 [38] ($\mathrm{KB_F}$) or BS 6472-1:2008 (eVDV) [15]. The GroundVIB modules are also compliant with the ISO 14837-1:2005 standard [88]. In particular, they follow a three-step prediction scheme, differentiating between the source, the propagation path and the building.

The train-track interaction model is decoupled from the computation of wave propagation in the soil and response of the building. The rails are modelled as Timoshenko beams which is adequate for the frequency range of interest. The vehicle models incorporate an assemblage of rigid components (wheelsets, bogies, coach) without accounting for their flexibility.

GroundVIB can be used to estimate vibration and noise level inside buildings (4-250 Hz) in a relative (e.g. insertion gain, mitigation efficiency) or absolute way. Prediction accuracy is limited by uncertainty on input parameters (track, soil, building,...). The formulation of the hybrid model in GroundVIB follows closely the hybrid model presented in subsection 6.4. Up to now, GroundVIB was used mainly for urban railway transport (tramway, metro, RER,...), and not for freight or high speed lines.

6.7.1 Train-track interaction module

The basic vehicle model has 4 vertical degrees of freedom, representing one quarter of a conventional coach (i.e. a single axle, half a bogie and a quarter of a car body), and can be used to simulate three types of bogie, as illustrated in figure 44.

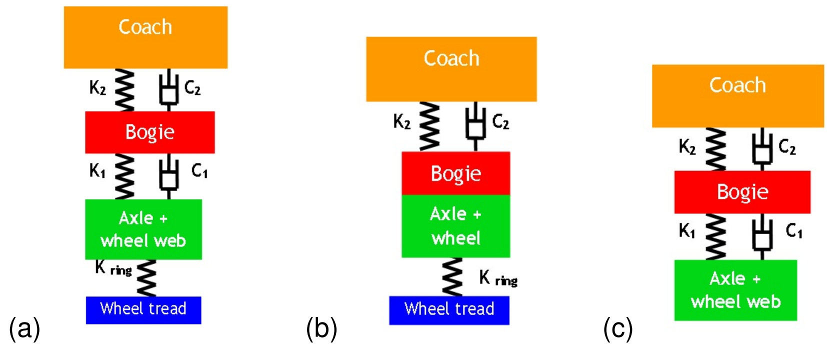

Figure 44: 4DOF vehicle models used in GroundVIB for (a) bogie with primary and secondary and resilient wheel, (b) bogie with secondary suspension and resilient wheel and (c) bogie with primary and secondary suspension and monobloc wheel.

Three track models are available to simulate ballasted track, slab track, and floating slab track (figure 45). The rail is modelled as a Timoshenko beam (including shear deformation and rotational inertia) and assumed to be continuously connected to sleepers by means of resilient rail pads. The sleepers (for ballasted track) are modelled as masses on springs, representing the ballast or under sleeper pad. The (floating) slab is modelled as an Euler beam, resting on a continuous resilient layer (slab mat).

The train-track interaction problem is solved in the frequency domain by first calculating the train, track and

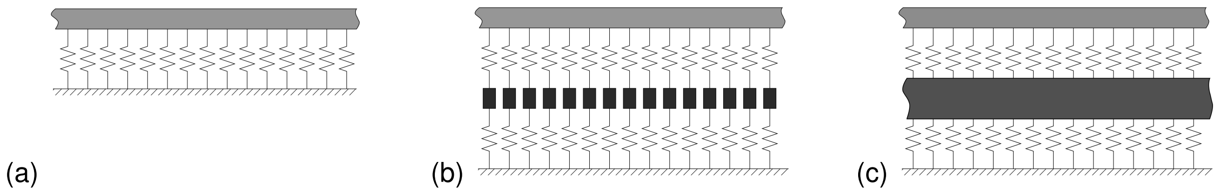

Figure 45: Track models used in GroundVIB for (a) rail on rail pads, (b) rail on sleepers, and (c) rail on (floating) slab.

contact receptance. The following equilibrium equation (which corresponds to a one-dimensional version of equation (57)) allows the dynamic axle load $\hat{g}_{\mathrm{d}k}(\omega)$ at axle k to be computed:

$$\hat{g}_{\mathrm{d}k}(\omega) = \frac{\hat{u}_{\mathrm{w/r}}(\omega)}{\hat{\alpha}_{\mathrm{c}}(\omega) + \hat{\alpha}_{\mathrm{t}}(\omega) + \hat{\alpha}_{\mathrm{v}}(\omega)} \tag{116}$$

with $\hat{u}_{\mathrm{w/r}}(\omega)$ the combined wheel-rail unevenness, $\hat{\alpha}_{\mathrm{c}}(\omega)$ the receptance at the wheel-rail contact, $\hat{\alpha}_{\mathrm{t}}(\omega)$ the track receptance, and $\hat{\alpha}_{\mathrm{v}}(\omega)$ the vehicle receptance.

For a single wheel/rail force, the force $\hat{F}_{\mathrm{ts}}(\omega)$ transmitted to the subgrade is computed as:

$$\hat{F}_{\mathrm{ts}}(\omega) = \int_{-\infty}^{+\infty} k\hat{u}(y,\omega)\,\mathrm{d}y \tag{117}$$

where k is the (complex) stiffness per unit length in the lowest resilient component of the track, and $\hat{u}_z(y,\omega)$ is the relative vertical displacement of this component with respect to the rigid subgrade, as a function of the coordinate y along the track. The integral in equation (117) is truncated to values $\pm L_{\mathrm{ts}}$ as the energy is usually contained within a limited distance from the point of load application. In practice, a value of ± 20 m gives sufficiently accurate results. The force $\hat{F}_{\mathrm{ts}}(\omega)$ transmitted to the subgrade is subsequently combined with the soil transfer function to calculate the free field response.

6.7.2 Subgrade-to-soil transfer function

Below the track superstructure, there is a subgrade which depends on the type of track: below a ballasted track, the soil is generally reinforced using gravel; below a (floating) slab track, a light concrete slab is mounted on the soil.

The transmitted force $\hat{F}_{\mathrm{ts}}(\omega)$ for a single axle load is multiplied with the subgrade-to-soil transfer function for a point source to obtain the vibration level at the soil surface. The response due to a train passage is obtained by summation of the contribution of each axle. Alternatively, the force density is computed according to equation (98), while the line source transfer mobility is obtained from equation (100).

GroundVIB offers the choice between two types of transfer functions: (1) a measured or an externally computed (using another software) transfer function, read from an Excel file, and (2) pre-computed transfer functions for a given slab width and homogeneous soil properties that are available within the software. The latter transfer functions were computed with external 2.5D and 3D models (figure 46) for a slab with variable thickness and fixed width and material properties, and a homogeneous soil with variable Young's modulus, while other material properties are fixed.

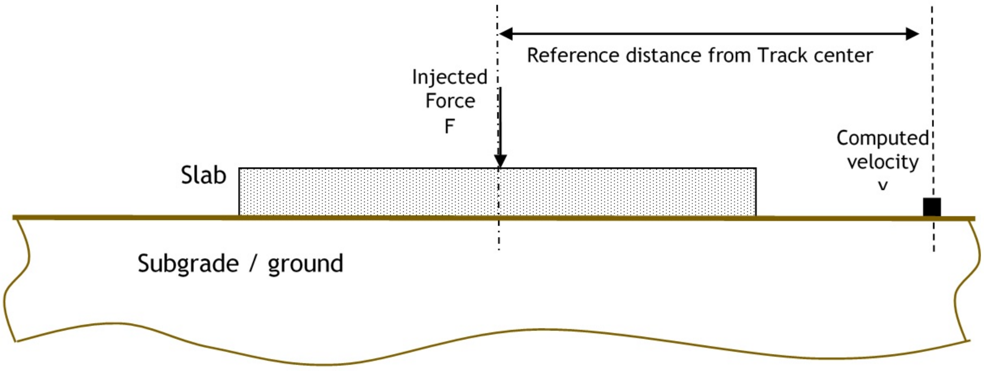

Figure 46: Subgrade-to-soil transfer function.

For a slab track (figure 47), the train-track interaction model includes the rail and its rail pads. The subgrade-to-soil transfer function includes the slab on which the rail pads are attached in order to reduce the approximation error due to the use of blocked force for the coupling [134]. For a floating slab track (figure 48), the train-track interaction model includes the rail, the rail pads, the slab and its supporting mat. The subgrade-to-soil transfer function includes the light concrete slab below the mat.

Figure 47: (a) Slab track and (b) coupling of sub-structures.

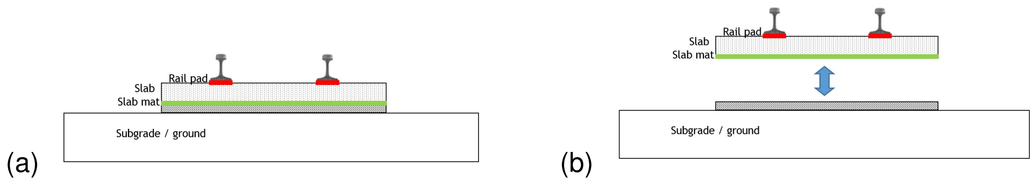

Figure 48: (a) Floating slab track and (b) coupling of sub-structures.

6.7.3 Wave propagation in the soil

The vibration velocity $\hat{v}(r, \omega)$ at a point at a distance r from a harmonic source at a frequency ω at the surface of a homogeneous halfspace with a shear wave velocity C_{s} and material damping ratio β_{s} can be approximated as follows [9]:

$$\frac{\hat{v}(r,\omega)}{\hat{v}(r_{\mathrm{ref}},\omega)} = \left(\frac{r}{r_{\mathrm{ref}}}\right)^{-n} \exp\frac{-\omega\beta_{\mathrm{s}}(r-r_{\mathrm{ref}})}{C_{\mathrm{s}}} \tag{118}$$

where the exponent n represents geometrical attenuation and equals 0.5 for a point source and 0.0 for a line load; r_{ref} is the distance between the source and a reference point in the soil where the vibration velocity equals $\hat{v}(r_{\mathrm{ref}},\omega)$.

Equation (118) can be reformulated as:

$$\mathrm{L_v}(r,\omega) = \mathrm{L_v}(r_{\mathrm{ref}},\omega) - 20n\log_{10}\left(\frac{r}{r_{\mathrm{ref}}}\right) - (r-r_{\mathrm{ref}})\mathrm{DR}(\omega) \tag{119}$$

where $\mathrm{L_v}(r,\omega)$ is the velocity level in dB with reference $v_0 = 5\times10^{-8}$ m/s:

$$\mathrm{L_v}(r,\omega) = 20\log_{10}\left(\frac{\hat{v}(r,\omega)}{v_0}\right) \tag{120}$$

and $\mathrm{DR}(\omega)$ is the decay rate:

$$\mathrm{DR}(\omega) = \frac{\omega\beta_{\mathrm{s}}}{C_{\mathrm{s}}}\frac{20}{\ln 10} \tag{121}$$

When a line load is assumed ($n=0$), the second term in equation (119) equals zero, resulting in the following formulation:

$$\mathrm{L_v}(r,\omega) = \mathrm{L_v}(r_{\mathrm{ref}},\omega) - (r-r_{\mathrm{ref}})\mathrm{DR}(\omega) \tag{122}$$

In practice, the soil is not homogeneous, as assumed in the previous derivations. However, it is possible to integrate heterogeneity in the above formulation by measuring the decay rate in one-third octave bands, as illustrated in figure 49a. The decay rate is subsequently used to compute the vibration level $\mathrm{L_v}(r,\omega)$ at different distances from the track. This is a convenient and fast way to interpolate or extrapolate measured transfer functions. GroundVIB incorporates a database of soil decay rates, as illustrated in figure 49b, where measured data are superimposed on theoretical decay curves for a homogeneous halfspace consisting of soft, medium, and stiff soil.

6.7.4 Building correction factors

In GroundVIB, the building response is computed with the same building correction factors as defined in Deliverable D1.6 of the FP7 project RIVAS [196].

In Deliverable D1.6 of RIVAS, the following so-called transfer functions are proposed: $\mathrm{TF}_2(\omega)$ is the transfer function from the ground to the foundation of the building (usually an attenuation); $\mathrm{TF}_3(\omega)$ is the transfer function from the foundation of the building to a floor in the building (usually an amplification); and $\mathrm{TF}_4(\omega)$ is the transfer function from the mid span floor vibration to a noise level in the room. However, these functions are not really transfer functions, but rather represent correction factors that are applied to a free field

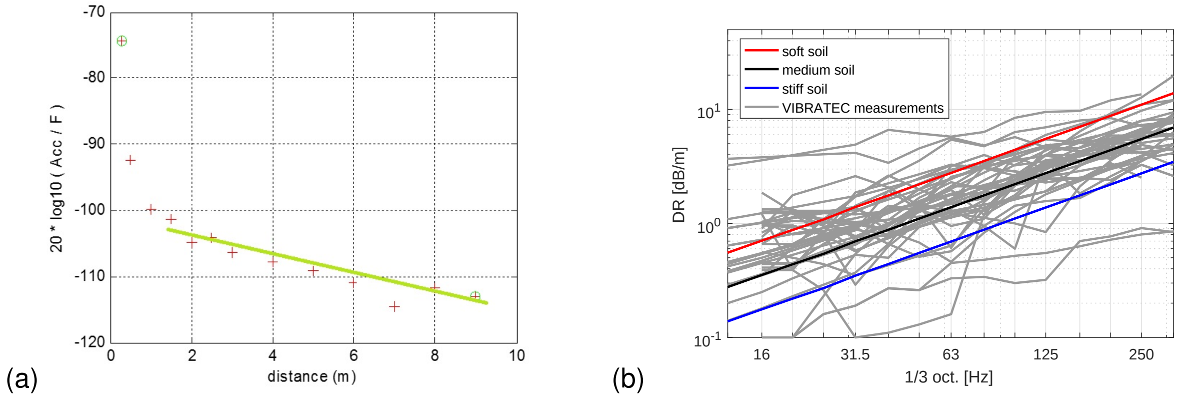

Figure 49: (a) Soil decay rate, measured as the slope of a vibration amplitude versus distance curve. (b) Examples of measured (grey lines) and computed soil decay rates for soft (red line), medium (black line) and stiff (blue line) soil.

vibration level in order to obtain a vibration level in the building, much along the same lines as the building correction factors $C_b(\mathbf{x}_1, \mathbf{x}_b)$ proposed in the FRA procedure. Therefore, we will prefer to denote these building correction factors by $C_{b2}(\omega)$, $C_{b3}(\omega)$, and $C_{b4}(\omega)$.

In the RIVAS project, the building correction factors $C_{b2}(\omega)$ and $C_{b3}(\omega)$ were extracted from a database of SBB that is based on experimental data collected in single family dwellings and small buildings with wooden and concrete floors. These data sets were selected based on a validation by means of building correction factors published in the literature or available in databases of RIVAS partners. These correction factors are plotted in one-third octave bands in figures 50 and 51, respectively.

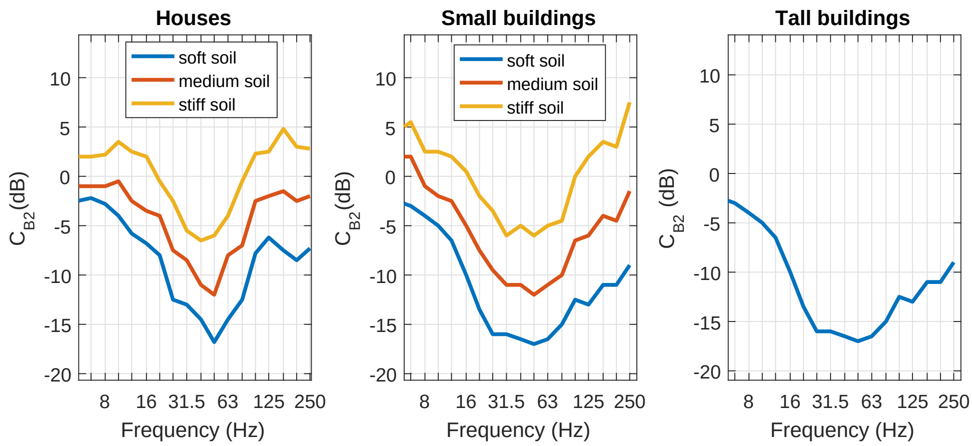

Figure 50: Building correction factors $C_{b2}(\omega)$ from the soil to the building foundation for single family dwellings, medium size buildings (less than 4 storeys), and tall buildings (more than 4 storeys). In the first two cases, these factors are shown for soft, medium, and stiff soil.

1. The building correction factor $C_{b2}(\omega)$ from the ground to the building foundation depends on the type of building and the soil stiffness. Figure 50 presents building correction factors for single family

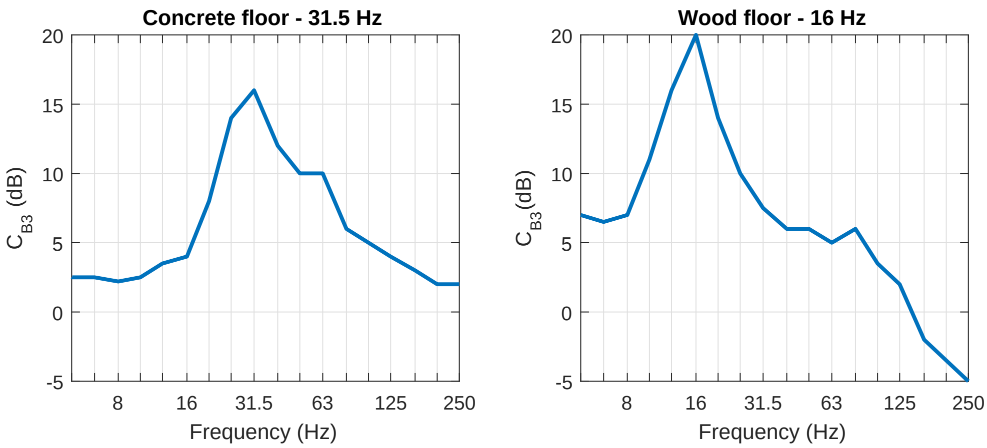

Figure 51: Building correction factors $\mathrm{C_{b3}}(\omega)$ for concrete and wooden floors.

dwellings, medium size buildings (less than 4 storeys), and tall buildings (more than 4 storeys). In most cases, attenuation can be observed when vibration is transmitted from the ground to a building foundation. For small and medium size buildings, building correction factors are shown for soft, medium and stiff soil, revealing that soil-structure interaction effects are more important when soft soil conditions prevail. Reference [196] does not define very clearly the different soil categories, but the following values of the corresponding shear wave velocity C_{s} can reasonably be assumed, following the soil classification in Eurocode 8 [49]:

(a) soft soil: $C_{\mathrm{s}} \leq 180$ m/s;
(b) medium soil: 180 m/s $\leq C_{\mathrm{s}} \leq 360$ m/s;
(c) stiff soil: $C_{\mathrm{s}} \geq 360$ m/s.

2. The correction factor $\mathrm{C_{b3}}(\omega)$ from the building foundation to a floor is shown in figure 51.
   (a) For concrete floors, an average floor resonance frequency of 31.5 Hz with an amplification factor of the order of 15 dB is observed.
   (b) For wooden floors, an average floor resonance frequency of 16 Hz with an amplification factor of 20 dB is noted.
3. The building correction factor $\mathrm{C_{b4}}(\omega)$ from the mid span floor vibration level to a noise level in a room is defined as follows:
   (a) For concrete floors, the A-weighted sound pressure level $\mathrm{L_p}(\omega)$ in a room can be related as follows to the mid-span floor vibration level $\mathrm{L_v}(\omega)$ in dB with reference value $v_0 = 5 \times 10^{-8}$ m/s:

$$\mathrm{L_p}(\omega) \quad \simeq \quad \mathrm{L_v}(\omega) + W_A(\omega) + 7\,\mathrm{dB} \tag{123}$$

   where $W_A(\omega)$ is the A-weighting curve in one-third octave bands. This approximation takes into account that both floor and ceiling radiate noise. It follows immediately that the building correction factor $\mathrm{C_{b4}}(\omega)$ in this case equals $W_A(\omega) + 7\,\mathrm{dB}$. Heavier (loaded) older wooden floors most likely behave as concrete floors.

(b) For light-weight floors, the approximation of the A-weighted sound pressure level $\mathrm{L_p}(\omega)$ in a room becomes:

$$\mathrm{L_p}(\omega) \quad = \quad \mathrm{L_v}(\omega) + W_A(\omega) - 3\,\mathrm{dB} \tag{124}$$

so that the building correction factor $\mathrm{C_{b4}}(\omega)$ equals $W_A(\omega) - 3\,\mathrm{dB}$.

6.7.5 Graphical User Interface

Figure 52 illustrates GroundVIB's main Graphical User Interface. The main menu refers to project management and analysis. The input parameters are related to the properties of the train, the track, the roughness and the soil. Separate spectra for wheel and rail unevenness, or combined wheel-rail unevenness spectrum, can be specified as excitation. Computations can be performed for several train speeds and at different distances from the track.

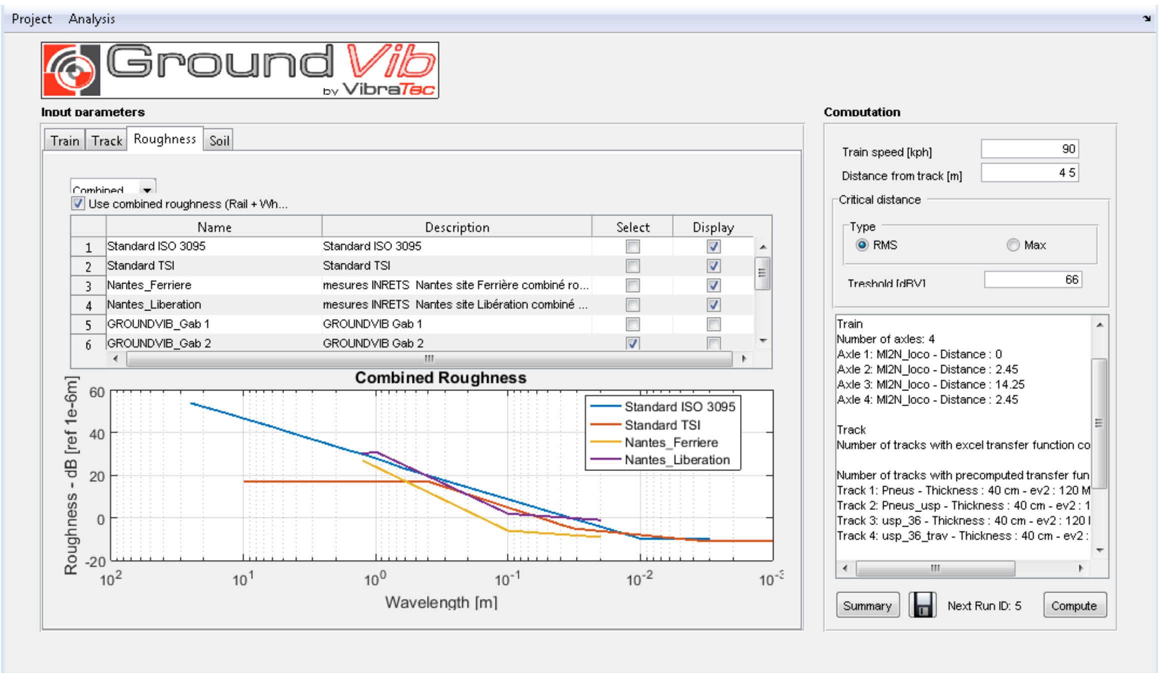

Figure 52: GroundVIB's Graphical User Interface.

Part II

CONCEPT OF THE VIBRATION PREDICTION TOOL

7. PROPOSED METHODOLOGY IN SILVARSTAR

7.1 Hybrid formulation

Based on the review of the state-of-the-art presented in the preceding sections, the most appropriate procedure, compliant with the ISO 14837-1:2005 standard, will be chosen as a framework for a hybrid vibration prediction tool operating in the frequency domain. The method for coupling the source and propagation term will be studied in detail.

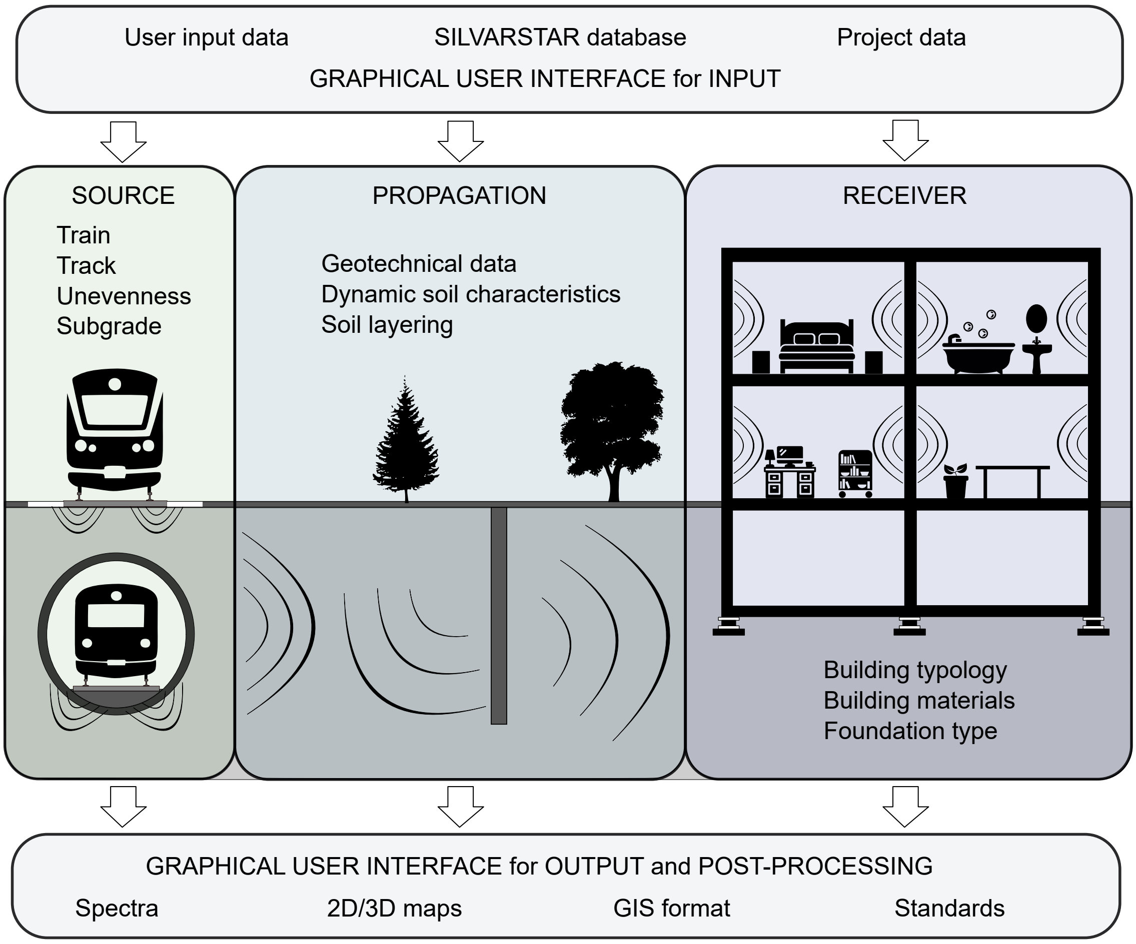

Figure 53: Ground vibration prediction process and integration of GUIs.

The basic concept for ground vibration in SILVARSTAR is to develop a frequency-based hybrid prediction tool, following the procedure for Detailed Vibration Assessment proposed by the Federal Railroad Administration (FRA) and Federal Transit Administration (FTA) of the U.S. Department of Transportation

[71, 72, 70, 152], but allowing for a numerical or experimental representation for each of the terms involved in the prediction. Such an approach conforms to the general framework recommended in ISO 14837-1:2005 [88].

Even the simpler semi-analytical approaches are computationally intensive and hence impractical for dealing with large-scale assessment in railway projects. The proposed approach (figure 53) is therefore built around a computationally highly-efficient source model for train-track-ground interaction. The vehicle and track properties can be selected by the user, either from a database or as numerical values. However, to reduce computation times, the user will have the possibility to use pre-computed impedance functions of the soil; the same will apply for the transfer functions between the track and the free field. These impedance and transfer functions will be computed for a range of configurations with state-of-the-art models MOTIV (ISVR) and TRAFFIC (KU Leuven), and collected in a numerical database in WP2. This will considerably speed up calculations and allow the user to assess in real-time the effect of changes in train, track, and soil parameters on dynamic axle loads, on free field and building vibration, as well as the efficiency of vibration mitigation measures.

The response of the building will be estimated by means of building correction factors, as specified for example in the FTA procedure [70, 152] and in Deliverable D1.6 of the FP7 project RIVAS [196]. These correction factors will also be selected from a database established in WP2.

The framework will also be oriented to compatibility with railway projects considering both input and output. The user will be able to import data from existing project databases dedicated to railway line development. In particular, geographical and geotechnical data will be made importable through an interface with a Geographical Information System (WP3). The user will also be able to add to the database where data are not already available.

WP1 will result in the implementation of a prototype vibration prediction tool, provided with a simple GUI to visualise results on 2D maps; GUI and visualisation capabilities will be further enhanced in WP3. Well-documented numerical and experimental case histories collected in WP2 will be used for approval testing and validation.

This framework should also allow for the transposition from one situation into another, based on corrections that can be derived either numerically or experimentally. This transposition method will be elaborated in Task T2.4.

7.2 Database with numerical results

Numerical predictions in the hybrid vibration prediction tool that will be developed in SILVARSTAR will be made following the state-of-the-art methodology outlined in section 4, that is implemented in the MOTIV (ISVR) and TRAFFIC (KU Leuven) software.

Vibration studies where a change in a parameter (e.g. track unevenness, rolling stock properties, train speed,. . .) does not require long additional computations, can be performed in real-time. A change in other parameters, such as the dynamic soil characteristics, however, necessitates the track-soil impedance and transfer functions to be recomputed, which requires much longer computation times. This mainly depends on soil layering, frequency range of interest, discretization of the track-soil interface, as well as required sampling in the frequency and wavenumber domains. To reduce computation times, the user will therefore have the possibility to use pre-computed impedance functions of the soil and transfer functions between the track and the free field, that will be collected in a numerical database in WP2. This database will considerably speed up calculations and allow the user to assess in real-time the effect of changes in train, track, and soil parameters on dynamic axle loads, on free field and building vibration, as well as the efficiency of a selection of vibration mitigation measures.

Ground impedance functions will be pre-computed for tracks at grade with different widths, e.g. 4 m and 6 m for a single track. Ground impedance functions will also be pre-computed for tunnels with different diameter (e.g. 4 m, 6 m and 8 m and possibly also larger diameter for twin-track tunnels) and embedment depth (e.g. 10 m, 15 m and 20 m). Transfer functions will be computed for a wide range of lateral distances to the track (e.g. every 4 m up to 64 m). Predictions at larger distances (e.g. 96 m and 128 m) will also be made, but this number will be limited as the wavenumber spacing needs to be (substantially) reduced as the source-receiver distance increases in order to ensure an accurate evaluation of the inverse wavenumber integrals.

It will be assumed that the soil can be represented as a homogeneous halfspace; the dynamic soil properties (wave velocities, density, material damping ratio) will be varied in order to accommodate soft, medium, and stiff soil conditions. For surface tracks, seven layered soil cases which are typical for different European countries (Sweden, Belgium, Germany, Spain, The Netherlands, United Kingdom) and were identified in the FP7 project RIVAS will also be considered. Computations will be performed by ISVR with the MOTIV software and by KU Leuven with the TRAFFIC software, which will also allow for cross-validation for a number of selected cases.

All calculations will be made in the frequency range between 1 Hz and 80 Hz as a minimum requirement. This frequency range will possibly be extended to 250 Hz (if feasible up to 315 Hz) for trains running in tunnels when ground-borne noise is a concern.

Impedance functions and transfer functions between the track and the free field are computed in the MOTIV and TRAFFIC software in the wavenumber-frequency domain, as explained in sections 3 and 4 and detailed in equation (74). When the speed of the train is low with respect to the dominant surface wave velocities in the soil, it is possible to separate the dynamic axle loads from the transfer functions, as demonstrated in equation (75). This approximation would allow pre-computed impedance and transfer functions to be stored in the spatial-frequency domain instead of the wavenumber-frequency domain, resulting in considerable savings in disk storage as well as a substantial reduction of computation time when different configurations need to be compared. The error made by this approximation will be quantified in the relevant one-third octave bands and compared with other modelling errors.

Tracks on embankments or in cuttings can conveniently be modelled with 2.5D FE-BE or 2.5D FE-PML models; these formulations remain expensive, however, in terms of computation time and will therefore not be used within SILVARSTAR. The software MOTIV, however, permits an embankment to be modelled as an equivalent beam, but the accuracy of this approximation must be verified.

In order to compute vibration levels on floors and re-radiated noise in buildings, use will be made of building correction factors, as specified for example in the FTA procedure [70, 152] and in Deliverable D1.6 of the FP7 project RIVAS [196]; building correction factors have also been reported by Xia et al. [207] and Kuo et al. [110]. The user will be able to select these correction factors from a database that will be established in WP2. Depending on the needs of a specific project, a user can of course opt to perform a more detailed finite element analysis of a building excited by base motion.

This work will be performed in Task T2.2 "Numerical database for the tool" as part of WP2 "Supporting data and modelling for the vibration prediction tool". Results will be reported in Deliverable D2.1 "Database for vibration emission, ground transmission and building transfer functions".

7.3 Database with experimental results

Apart from the numerical calculations, an experimental database of force densities, transfer functions (e.g. point transfer mobilities and/or line source transfer mobilities), free field vibration and input parameters (rolling stock, track, track unevenness, subgrade, soil,. . .) will be provided that can be integrated into the new hybrid vibration prediction tool.

Experimental data from well-documented measurement campaigns collected by the partners will be stored in the database that will be linked to the software. Priority will be given to test campaigns where considerable attention was paid to the collection of input data and where, apart from vibration of track, free field, and buildings during train passages, also transfer functions and mobilities were measured.

The following case histories are identified:

- **Lincent (Belgium).** This site is located next to the high speed line (HSL) L2 Brussels-Köln, consisting of two classical ballasted tracks with UIC 60 rails supported by resilient studded rubber rail pads on pre-stressed mono-block concrete sleepers. The track is located in a cutting with a depth of about 1 m and supported by a porphyry ballast layer and a limestone sub-ballast layer.

  Borings performed before the construction of the HSL L2 reveal the presence of a shallow quaternary top layer of silt with a thickness of 1.2 m, followed by a layer of fine sand up to a depth of 3.2 m. Between 3.2 and 7.5 m is a sequence of stiff layers of arenite (a sediment of a sandstone residue) embedded in clay. Below the arenite layers is a layer of clay (from 7.5 to 8.5 m depth), followed by fine sand (from 8.5 to 10.0 m), below which thin layers of fine sand and clay are found.

  Extensive in situ and laboratory testing was performed to determine the thickness and dynamic characteristics of the different soil layers. These tests include geophysical prospection tests (MASW, seismic refraction, SCPT) [149, 35, 160, 156, 10, 158], laboratory tests (void ratio, water content, density), and bender element tests on undisturbed samples (wave velocities and material damping ratios) [68, 95, 96]. As a result, the site in Lincent is very well documented; the identified soil stratigraphy was therefore used as one of seven reference cases in the FP7 project RIVAS to study the efficiency of vibration mitigation measures [190].

  Elaborate in situ testing was performed to measure track receptance [104], track unevenness [119], transfer functions from track to free field (both point source mobilities and line source transfer mobility) [105, 159, 5, 189, 187] and vibration due to train passages (InterCity, ICE, and Thalys) [103, 188]. This resulted in an extensive database that was used to validate numerical models [119, 115, 62], to verify the empirical FRA procedure [193, 187] and to support hybrid prediction of free field vibration [111].

- **Heverlee (Belgium).** Vibration measurements were performed in a three-storey reinforced concrete building, located at about 40 m from the railway line L1390 Leuven-Ottignies [110, 146]. This line has two classical ballasted tracks with continuously welded UIC 60 rails that are supported every 0.60 m by resilient studded rubber pads on pre-stressed mono-block concrete sleepers.

  This site is located in the alluvial plain of the Dijle river consisting of an approximately 6 m thick quaternary layer of loose to dense sand (locally clayey) on top of a tertiary formation consisting of medium to dense sand with sand stone concretions. The ground water table is located at a depth of about 8 m. Dynamic soil characteristics were identified by means of geophysical prospection (SASW and seismic refraction along 2 measurement lines, SCPT at 2 locations) [185, 186]; data from these tests were combined in a probabilistic Bayesian inversion framework to identify a set of possible soil profiles [184].

The dynamic properties of the ballast layer, embankment and upper soil layer were identified from track receptance tests and transfer functions from sleeper to near free field locations [61]. Rail unevenness was measured by Infrabel one week before the measurement campaign, revealing a track of moderate to poor quality.

Modal properties (eigenfrequencies, eigenmodes, modal damping ratios) of the building were determined by means of dynamic system identification using ambient and forced vibration measurements on different floors of the building [145].

Accelerometers were mounted on 10 consecutive sleepers. Six shock accelerometers were placed on both sides of the rail foot of the left rail above two sleepers and at mid-span between two sleepers. Four strain gauges were glued to the rail web to determine axle loads. Free field accelerations were recorded at 9 positions along three parallel lines perpendicular to the track, using 18 uniaxial seismic accelerometers and two wireless sensors. The dynamic response of the building was measured at four locations on each floor of the building using 18 tri-axial wireless sensors. This enabled synchronous measurements in 84 directions.

Transfer functions were measured between track, free field and building, applying multiple impacts with an instrumented hammer on 17 sleepers at 12 m spacing over a total distance of 192 m along the track. These were used to determine the line source mobility to free field and building.

Freight and passenger trains operate on the line. Continuous monitoring during one week resulted in a database of over 500 train passages, including track, free field and building response.

These vibration measurements are documented in internal reports [125, 107] and are invaluable in validating models and providing insights into the physical process of vibration generation and propagation.

- **Steventon and Grazely Green (United Kingdom).** These are two sites with soft clay soil adjacent to railway lines in Southern England. At Steventon the track is raised on a shallow embankment, approximately 0.7 m high, whereas at Grazeley Green the embankment is approximately 3.5 m high. Measurements included MASW soil investigations along a line perpendicular to the railway up to a distance of 42 m from the forcing point. The properties of the soil, including its layered structure, were identified from comparisons with results of a layered ground model. Train passages were also measured at a number of positions and vibration was also measured on the track. However, no transfer function measurements were made on or from the track. The maximum frequency was 250 Hz in each case. Rail unevenness was also measured at both sites. The main results have been reported by Triepaischajonsak et al. [182]. The soil properties from Steventon were also reported in RIVAS Deliverable D4.1 [26]. The data are useful for validation of models and as part of a database of soil properties. However, they cannot be used to derive force densities as no transfer functions were measured from the track.

- **Fishbourne (United Kingdom).** This is a site with soft clay soil adjacent to a secondary railway line on the South coast of Southern England. MASW tests were performed in the field adjacent to the track for distances up to 42 m and the properties of the soil, including its layered structure, were identified from comparisons with results of a layered ground model. Additionally, soil samples were recovered and tested in the laboratory using triaxial testing and resonant column testing. Train pass-by measurements were made at several positions perpendicular to the track but no measurements were possible on the track itself. The results have been written up in an undergraduate thesis and a PhD thesis [44] but have not yet been published further. The site could be interesting because of the possibility to compare onsite measurement with laboratory studies but further analysis is needed to complete the study. The data are useful for validation of models and as part of a database of soil properties. However, they cannot be used to derive force densities as no transfer functions were measured from the track.

- **Bakerloo Line, Regent's Park, London (United Kingdom).** Within the frame of the CONVURT project, vibration measurements were performed at a site in Regent's Park on the Bakerloo line of London Underground during 35 passages of a test train at a speed between 20 and 50 km/h [36]. Vibration was measured on the axle boxes of the test train [30], on the rails, the tunnel invert and tunnel wall [199], and on two parallel lines in the free field, both at the surface and in a seismic cone at a depth of 15 m [17, 75]. Measurements were also performed on floors and columns of two Regency buildings on York Terrace West at a distance of 70 m from the tunnel [17].

  The tunnel on the Bakerloo line is a deep-bored tunnel with a cast-iron lining and a single track, embedded in London clay at a depth of about 28 m below the surface. The track in the tunnel is of the conventional London Underground type. It is a non-ballasted concrete slab track with 95lb Bull head rail supported on hard Jarrah wooden sleepers nominally spaced at 0.95 m with cast-iron chairs. The ends of a sleeper are embedded in the concrete invert, which runs along the sides of the floor of the tunnels. The space between the sleepers is filled with shingle which does not support the sleepers but provides drainage and a flat surface for evacuation in emergencies. The rails are not supported by rail pads and the resilience is mainly provided by the local resilience of the timber sleeper.

  Historical borings and geological maps of London show that the average thickness of the (saturated) London clay layer at the site is 40 m. This was confirmed by cone penetration tests up to a depth of 21 m, which also revealed the presence of a shallow top layer with a thickness of 4 to 6 m and inclusions of sand and gravel and varying cone resistance. The deep layer is very homogeneous with a gradually increasing cone resistance. The dynamic soil characteristics were determined by in situ tests (MASW and SCPT) and laboratory tests on undisturbed samples (bender element test, free torsion pendulum test) [75, 150]. Rail and wheel roughness was measured [30] and track properties were determined by rail receptance and wave decay measurements [199]. No transfer functions from track to free field were measured on this site.

No additional in situ vibration measurements will be performed within the frame of the SILVARSTAR project. Additional well-documented data sets, with a similar degree of available information as specified for the aforementioned case histories, will be welcomed. Users will also have the possibility to upload their own experimental data.

This work will be performed in Task T2.1 "Collection of experimental database" as part of WP2 "Supporting data and modelling for the vibration prediction tool". Results will be reported in Deliverable D2.1 "Database for vibration emission, ground transmission and building transfer functions".

7.4 Computational workflow

7.4.1 Introduction

The user will perform vibration analysis following a step-wise methodology. First, the geometry of the line will be imported in the main IMMI interface, along with the geometrical definition of the buildings. The user hence starts with a 2D map including the railway line and buildings (figure 54). The line is subsequently divided into sections; for each section, the user selects source, propagation and receiver terms from predefined lists, that are included in the integrated database or available as imported data. In the next step, the prediction tool computes in each section the vibration level on the ground adjacent to the buildings and the vibration and noise levels inside the buildings. In the last step, the user will post-process and analyse the results.

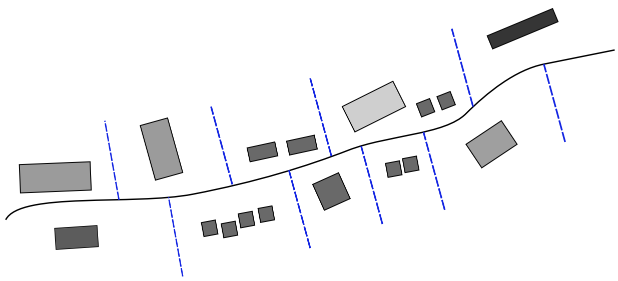

Figure 54: Definition of sections along a railway line. In each section, the user selects the source, propagation and receiver terms.

For preliminary vibration assessment, the user will benefit from the integrated databases (train, track, soil and building) to perform a fast assessment of the affected corridor. For detailed vibration assessment, the user will be able to import external results (measured or computed) to assess noise and vibration level with higher precision.

Three schemes are provided for the prediction for ground-borne noise and vibration: fully numerical, fully empirical, and hybrid. In the hybrid prediction scheme, there are two options: a numerical source model combined with an empirical propagation term and an empirical source model combined with a numerical propagation term. In all prediction schemes, the receiver is represented by building correction factors $\mathrm{C_b}(\mathbf{x}_1, \mathbf{x}_\mathrm{b})$, that can be selected depending on building characteristics (construction type, number of storeys, floor type,...). Comparative studies according to a standards or guidelines (e.g. DB Ril 820.2050 [31]), where a set of building correction factors for different floor types is prescribed, will also be facilitated; in this case, the vibration prediction tool will give results for the complete set of building correction factors. Alternatively, the user will also be able to import measured or computed building correction factors associated with specific building characteristics.

The vibration prediction tool will automatically adapt the computation scheme to the chosen input data. The details of each prediction scheme are described in the next subsections and summarized in table 4.

Table 4: Overview of prediction schemes.

	Fully numerical	Fully empirical	Hybrid model 1	Hybrid model 2
Source	**Train-track interaction model** Train, track, subgrade and soil parameters Track unevenness Pre-computed impedance functions Dynamic axle loads	**Empirical source model** Equivalent force density rail heads Equivalent force density next to track Vibration level next to track	**Train-track interaction model** Appropriate source term is computed to be combined with empirical propagation term	**Empirical source model** Selection "fully empirical"
Propagation	**Track-soil interaction model** Track and soil parameters (Pre-)computed transfer functions	**Empirical propagation model** Line source transfer mobility rail heads Line source transfer mobility next to track Difference in line source transfer mobility	**Empirical propagation model** Selection "fully empirical"	**Track-soil interaction model** Appropriate propagation term is computed to be combined with empirical source model
Receiver	*No integrated building models* Building correction factors (external computation) Dynamic (SSI) analysis	Building correction factors (database or imported)	Building correction factors (database or imported)	Building correction factors (database or imported)

7.4.2 Fully numerical prediction scheme

The fully numerical scheme will be based on the formulations described in section 4. This workflow can be used, for instance, to evaluate the affected corridor along a railway line at an early design phase, when results of in situ measurements are not yet available.

Numerical source models. The prediction model will be used to compute the dynamic axle loads, as described in section 4.

Similarly to the current acoustic version of IMMI, a specific interface will be opened from the main IMMI interface to define the model input parameters, related to the rolling stock, the track, the subgrade and the soil. The following lists are not meant to be exhaustive, but give examples of important parameters that are needed to set up the train-track interaction model and to compute the dynamic axle loads.

1. Rolling stock:

   - General information: axle positions, operating conditions (e.g. train speed).
   - Wheelsets, bogies, coaches: position, mass and mass moment of inertia.
   - Primary and secondary suspensions, ring of resilient wheel: stiffness and damping.
   - Wheel unevenness.

   As a minimum requirement, the user will need to define the axle positions, the operating conditions, and the unsprung masses. In the case of a bogie with resilient wheels but without primary suspension (specific architecture of some tramway vehicles), the user will have to define the wheel tread mass (i.e. unsprung mass), the stiffness and damping of the ring, and the suspended mass on the ring (axle and bogie frame). For a full model, the user will have to add the suspensions' stiffness and damping, as well as the suspended masses.

   The database (cf. subsection 7.2) will include established models for tramways, intercity, high-speed, and freight trains.

   The model will also allow a vehicle receptance computed with external software to be uploaded.

2. Track:

   - Rail: cross-section, moment of inertia, density, Young's modulus.
   - Rail pad: dynamic stiffness and damping.
   - Sleeper: dimensions, density, sleeper distance.
   - Under-sleeper pad: dynamic stiffness and damping.
   - Ballast: dimensions, density, stiffness, damping.
   - Under-ballast mat: dynamic stiffness and damping.
   - Slab: dimensions, density, Young's modulus, Poisson's ratio.
   - Floating slab mat: dynamic stiffness and damping.
   - Rail/track unevenness.

   The database (cf. subsection 7.2) will include established models for common track types such as ballasted tracks, slab tracks, and floating slab tracks.

3. Subgrade and soil:

   - Subgrade: dimensions, density, shear and dilatational wave velocity, material damping ratios.
   - Soil: layer thicknesses, density, shear and dilatational wave velocity, material damping ratios.

   The database (cf. subsection 7.2) will include pre-computed soil impedance functions and transfer functions for typical cases. Interpolations will allow the user to modify several parameters. The subgrade and soil parameters mentioned above will be needed if additional computation is needed, for example with the purpose of transposition.

Numerical propagation model. The user will have two options for the propagation term in the numerical prediction scheme.

The first option is to choose the transfer functions from the integrated numerical database (including tunnel situations), as described in subsection 7.2.

The second option is to import transfer functions from external computations. This option can be used, for example, to evaluate the effect of mitigation measures in the propagation path. The type and format of imported data will be the same as for the empirical prediction scheme, described in subsection 7.4.3.

The source and the propagation terms will be combined to compute the free field vibration levels at several distances from the track.

Receiver models. No numerical model will be integrated in the tool for the buildings. Hence, the user will have to compute the building correction factors $\mathrm{C_b}(\mathbf{x}_1, \mathbf{x}_\mathrm{b})$ externally and import these results into the software, using the same format as for the empirical data.

7.4.3 Fully empirical prediction scheme

The fully empirical scheme will follow the FRA/FTA procedure as described in section 5. This workflow can be used when data sets are available or collected in conditions that are sufficiently close to the situation under consideration. In the main IMMI interface, the user will choose the source, propagation and receiver terms.

Empirical source model. The user has several possibilities to define the source:

- The equivalent force density $\mathrm{L_F}(\mathbf{X}, \mathbf{x}_1)$ with excitation on the track (rail head).
- The equivalent force density $\mathrm{L_F}(\mathbf{X}_1, \mathbf{x}_1)$ with excitation at positions $\mathbf{X}_1$ under or next to the track.
- The vibration velocity level $\mathrm{L_v}(\mathbf{x}_\mathrm{ref})$ at a reference distance $\mathbf{x}_\mathrm{ref}$ from the track.

Further parameters (metadata) are also necessary for a full definition of the excitation (train dimensions, train type, train speed, track type, operating conditions).

In the case where the source is characterized by an equivalent force density or a reference vibration level that was measured on a site with different characteristics than the site for which predictions must be made, a transposition procedure will be needed. This transposition procedure may be related to the characteristics of the rolling stock, the track, the subgrade and the soil, and will be further developed in WP2.

Empirical propagation model. Several possibilities are offered to the user to define the propagation term in terms of a line source transfer mobility (or a difference of mobility levels). The particular choice must be compatible with the definition of the force term:

- For a source defined by an equivalent force density $\mathrm{L_F}(\mathbf{X}, \mathbf{x}_1)$ with excitation on the rail heads $\mathbf{X}$, the line source transfer mobility $\mathrm{TM_L}(\mathbf{X}, \mathbf{x}_1)$ also needs to be measured with excitation on the rail head positions $\mathbf{X}$, as described in subsection 5.3.1.
- For a source defined by an equivalent force density $\mathrm{L_F}(\mathbf{X}_1, \mathbf{x}_1)$ with excitation at positions $\mathbf{X}_1$ under or next to the track, the line source transfer mobility $\mathrm{TM_L}(\mathbf{X}_1, \mathbf{x}_1)$ also needs to be measured with excitation at corresponding positions $\mathbf{X}_1$, as described in subsection 5.3.1.
- For a source defined by a vibration level $\mathrm{L_v}(\mathbf{x}_{\mathrm{ref}})$ at a reference distance $\mathbf{x}_{\mathrm{ref}}$ from the track, the propagation term is defined as the level difference in line source transfer mobilities $\mathrm{TM_L}(\mathbf{X}, \mathbf{x}_1) - \mathrm{TM_L}(\mathbf{X}, \mathbf{x}_{\mathrm{ref}})$ with impact positions $\mathbf{X}$ on the rail heads, as described in subsection 5.5.1. For the case of a new track that has yet to be built, impact positions $\mathbf{X}_1$ below or next to the future track can be chosen.

In view of the required compatibility, the user should be careful when using the propagation terms. In order to avoid mistakes, the software will select propagation terms depending on the chosen source.

For preliminary vibration assessment of a new railway line, the propagation term can be selected from the integrated experimental database or from previous in situ measurements. For a detailed vibration assessment, the propagation term will be measured at the site where the impact study is performed.

Empirical receiver model. Several possibilities are offered to the user to define the receiver term. The user will be able to select building correction factors from the main IMMI interface. The data will come either from the integrated database of building correction factors for a range of typical buildings, or from on-site measurements, as described in subsection 5.3.3.

7.4.4 Hybrid prediction with numerical source model and empirical propagation model

The hybrid formulations follow the same terminology as introduced in sections 5 and 6. In this subsection, we consider the case where the source is represented by a numerical model and the propagation term is based on in situ measurements.

The user will first define the train, track and soil parameters using a dedicated interface (cf. the description of the numerical source model in subsection 7.4.3), so that the model can compute the dynamic axle loads.

Next, the user will choose the empirical propagation term from the integrated database or from imported experimental data. This could be (a) a line source transfer mobility $\mathrm{TM_L}(\mathbf{X}, \mathbf{x}_1)$ with excitation on rail head positions $\mathbf{X}$; (b) a line source transfer mobility $\mathrm{TM_L}(\mathbf{X}_1, \mathbf{x}_1)$ with excitation at positions $\mathbf{X}_1$ below or next to the track; or (c) a level difference in line source transfer mobilities $\mathrm{TM_L}(\mathbf{X}, \mathbf{x}_1) - \mathrm{TM_L}(\mathbf{X}, \mathbf{x}_{\mathrm{ref}})$, as described in subsection 7.4.3.

Next, the program will automatically compute the appropriate secondary source term that can correctly be combined with this empirical propagation term: this could be (a) an equivalent force density $\mathrm{L_F}(\mathbf{X}, \mathbf{x}_1)$ with excitation on the rail heads $\mathbf{X}$, (b) an equivalent force density $\mathrm{L_F}(\mathbf{X}_1, \mathbf{x}_1)$ with excitation at positions $\mathbf{X}_1$ below or adjacent to the track; or (c) a vibration level $\mathrm{L_v}(\mathbf{x}_{\mathrm{ref}})$ at a reference distance $\mathbf{x}_{\mathrm{ref}}$ from the track.

Example 7.1: Computation scheme for hybrid prediction with coupling next to the track

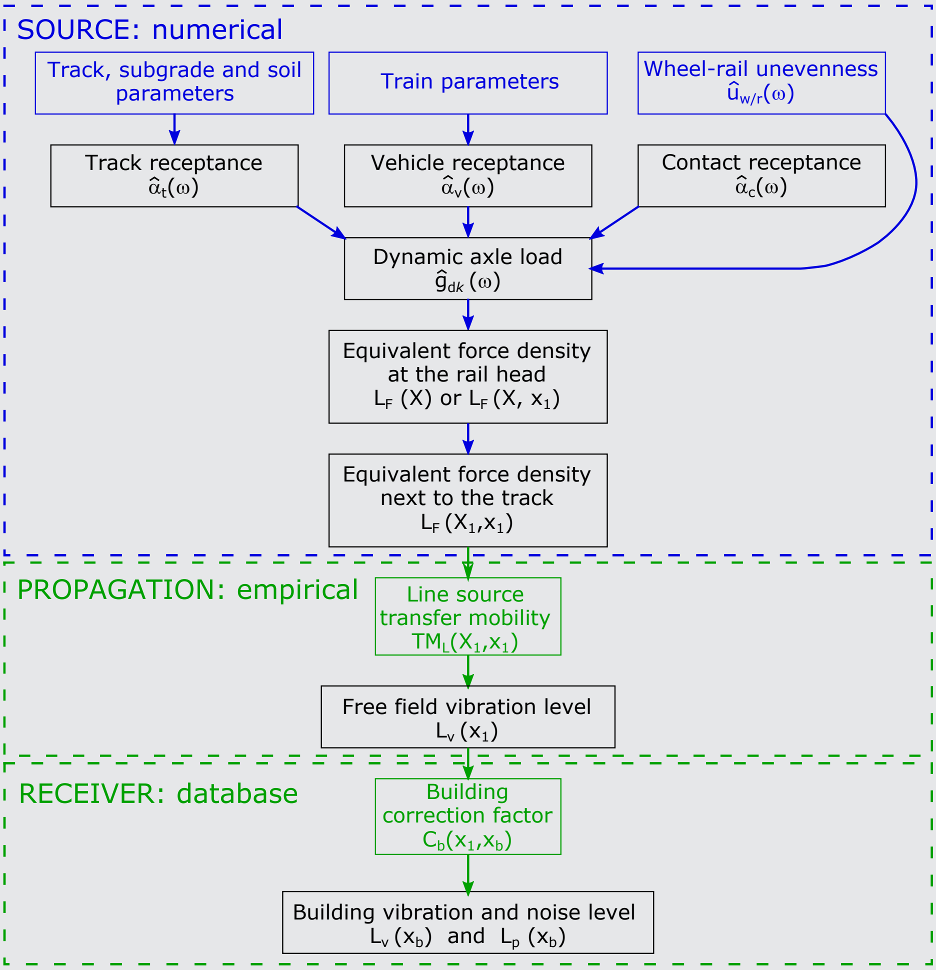

Figure 55: Hybrid prediction scheme combining a predicted source with experimental transfer functions.

This example illustrates the main hybrid prediction scheme proposed in SILVARSTAR for the assessment of the vibration impact of a new railway line (figure 55). The user combines results obtained with a numerical model of the source and in situ measurements of transfer functions, obtained with impact at positions next to the (future) track. The building correction term is selected from the integrated database.

The line source transfer mobility $\mathrm{TM_L}(\mathbf{X}_1, \mathbf{x}_1)$ is measured with impact forces applied at positions $\mathbf{X}_1$ next to the future track. The excitation will hence be characterized by a force density $\mathrm{L_F}(\mathbf{X}_1, \mathbf{x}_1)$ with excitation at the same positions. To do so, the user will set-up the parameters of the train, track, subgrade, and soil and select the track unevenness. The program will then compute the receptance at the wheel-rail contact $\hat{\alpha}_{\mathrm{c}}(\omega)$, the track receptance $\hat{\alpha}_{\mathrm{t}}(\omega)$, the vehicle receptance $\hat{\alpha}_{\mathrm{v}}(\omega)$, as well as the wheel-rail contact forces $\hat{g}_{\mathrm{d}k}(\omega)$. The latter are subsequently transformed into a force density $\mathrm{L_F}(\mathbf{X})$ (cf. equation (98)) or $\mathrm{L_F}(\mathbf{X}, \mathbf{x}_1)$ with excitation on the rail head, which in turn is transformed into a force density $\mathrm{L_F}(\mathbf{X}_1, \mathbf{x}_1)$ with excitation at positions $\mathbf{X}_1$ next to the track. The computed force density $\mathrm{L_F}(\mathbf{X}_1, \mathbf{x}_1)$ is added to the measured line source transfer mobility $\mathrm{TM_L}(\mathbf{X}_1, \mathbf{x}_1)$ to obtain the vibration level $\mathrm{L_v}(\mathbf{x}_1)$. The vibration level in a building $\mathrm{L_v}(\mathbf{x}_\mathrm{b})$ is finally obtained by adding a building correction term $\mathrm{C_b}(\mathbf{x}_1, \mathbf{x}_\mathrm{b})$. Additional correction terms are applied to predict noise levels in rooms.

Example 7.2: Computation scheme for hybrid prediction with coupling at the rail head

This example illustrates the main hybrid prediction scheme proposed in SILVARSTAR for the assessment of the vibration impact due to a modification of an existing railway line, for instance the introduction of a new rolling stock. The user combines results obtained with a numerical model of the source and in situ measurements of transfer functions, obtained with impact at the rail head. The building correction term is selected from the integrated database.

This example is very similar to the previous one. The only difference is that the source and propagation terms are now coupled at the rail head. Hence, the computation scheme is similar as the one shown in figure 55, except that the force density $\mathrm{L_F}(\mathbf{X}, \mathbf{x}_1)$ is computed at the rail head and not next the track. This source term is subsequently added to the measured line source transfer mobility $\mathrm{TM_L}(\mathbf{X}, \mathbf{x}_1)$ to obtain the vibration level $\mathrm{L_v}(\mathbf{x}_1)$. This different procedure will be transparent to the user, as the program will automatically adapt the computation scheme for the source to the type of experimental line source transfer mobility.

7.4.5 Hybrid prediction with empirical source model and numerical propagation model

In this subsection, we consider the case where the source is represented by means of measured data and wave propagation in the soil is computed with a numerical model.

The user will first choose an excitation from the database or import measured data, as described in subsection 7.4.3. This could be (a) an equivalent force density $\mathrm{L_F}(\mathbf{X}, \mathbf{x}_1)$ with excitation on the rail heads $\mathbf{X}$, (b) an equivalent force density $\mathrm{L_F}(\mathbf{X}_1, \mathbf{x}_1)$ with excitation at positions $\mathbf{X}_1$ below or adjacent to the track; or (c) a vibration level $\mathrm{L_v}(\mathbf{x}_\mathrm{ref})$ at a reference distance $\mathbf{x}_\mathrm{ref}$ from the track. In addition, the user may need to provide train, track and soil parameters in case a transposition is required.

Next, the user will select the soil model from the integrated database. The program will automatically compute the propagation terms for coupling with the empirical soil model. Depending on the source model chosen, this could again be a line source transfer mobility $\mathrm{TM_L}(\mathbf{X}, \mathbf{x}_1)$ or $\mathrm{TM_L}(\mathbf{X}_1, \mathbf{x}_1)$, or a level difference in line source transfer mobilities $\mathrm{TM_L}(\mathbf{X}, \mathbf{x}_1) - \mathrm{TM_L}(\mathbf{X}, \mathbf{x}_\mathrm{ref})$, as described in subsection 7.4.3.

Example 7.3: Computation scheme for hybrid prediction with coupling next to the track

This example could be used to assess the efficiency of a vibration mitigation measure in the propagation path. The user starts from measured source data, which is a vibration level next to the track, and imports transfer functions from external computations (figure 56).

The vibration level $\mathrm{L_v}(\mathbf{x}_{\mathrm{ref}})$ at a reference distance $\mathbf{x}_{\mathrm{ref}}$ is measured during train passages. The user computes externally the line source transfer mobility $\mathrm{TM_L}(\mathbf{X}, \mathbf{x}_1)$. The program subsequently combines the vibration level $\mathrm{L_v}(\mathbf{x}_{\mathrm{ref}})$ with a computed level difference in line source transfer mobilities $\mathrm{TM_L}(\mathbf{X}, \mathbf{x}_1) - \mathrm{TM_L}(\mathbf{X}, \mathbf{x}_{\mathrm{ref}})$, to obtain the vibration level $\mathrm{L_v}(\mathbf{x}_1)$, as described in subsection 5.5.

The user can import the line source transfer mobilities for the propagation without and with mitigation measure, so that the vibration isolation efficiency can be calculated and plotted in the IMMI interface.

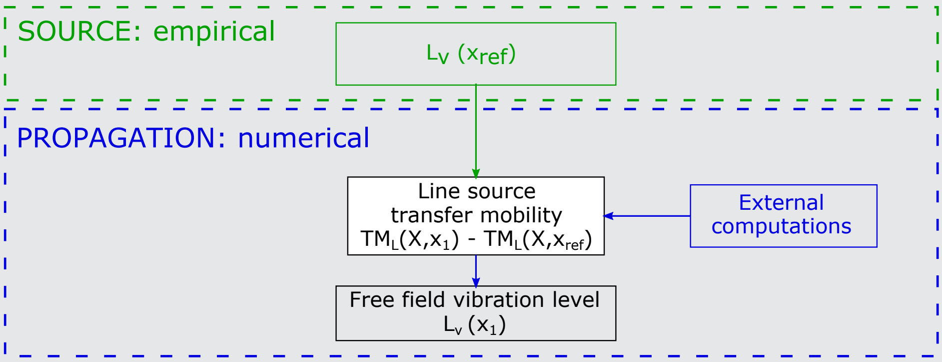

Figure 56: Hybrid prediction scheme combining a measured source with predicted transfer functions.

7.5 Assessment of vibration mitigation measures

Vibration mitigation measures can be implemented at the source (train-track-soil interaction), in the transmission path, or at the receiver. In this subsection, we briefly review some of these vibration mitigation measures [117] and discuss how the hybrid vibration prediction will allow the user to evaluate the efficiency of these measures. A more detailed account of different vibration mitigation measures can be found in the review paper by Lombaert et al. [117] and several deliverables of the FP7 project RIVAS.

7.5.1 Mitigation measures at the source

At the source, train-track-soil interaction generated by combined wheel and track unevenness as well as parametric excitation determine the dynamic vehicle loads transferred to the track. In order to reduce dynamic vehicle loads, one could therefore try to reduce the excitation, i.e. geometric unevenness and parametric excitation, or modify the dynamic characteristics of the rolling stock and the track.

Wheel and track unevenness. Reduction of combined wheel and track unevenness will only lead to vibration mitigation when it is in the relevant range of wavelengths (table 1). The following measures can be taken: wheel reprofiling or truing [201, 135], rail grinding or reprofiling [63], and ballast tamping

[176]. Each of these measures has an impact on dynamic axle loads in a specific range of wavelengths or frequencies, as summarized by Lombaert et al. [117].

The hybrid vibration prediction tool will allow to take into account the effect of the combined wheel and track unevenness on the dynamic axle loads or the force density, as revealed by equations (57) and (98).

Rolling stock. Dynamic axle loads can also be reduced through modification of rolling stock characteristics [201], such as the stiffness of the primary suspension and the unsprung mass, which are reported as most influential [129, 201, 135]. Geometrical parameters (e.g. bogie and axle distance) mainly affect the axle and bogie passage frequencies. Resilient wheels were found to effectively reduce ground vibration arising from rail defects [106]. Opportunities for reduction of ground-borne vibration by modification of rolling stock characteristics may be limited for conventional trains, however. Considerable room for improvement may exist for freight trains which generally lack a primary or secondary suspension.

The hybrid vibration prediction tool will allow to take into account the effect of rolling stock properties on the dynamic axle loads through the vehicle receptance, as is clear from equation (57).

Track structure. Dynamic isolation of the track structure can be accomplished by introduction of resilient elements at different levels. Examples of resilient track elements include resilient fasteners [135], under-sleeper pads [91, 66, 161, 12], under-ballast mats [23, 72, 135, 200], and slab mats in floating slab tracks [201, 135]. Measures providing resilience at a lower level in the track dynamically isolate a larger part of the track mass and work in a lower frequency range. Under-ballast mats and floating slab tracks therefore seem best suited for treatment of ground-borne vibration whereas other measures are, at least at first sight, mostly of benefit for reduction of ground-borne noise. The introduction of resilient elements in the track affects the dynamic axle loads, as well as the transfer function from the track to the soil [117], hence determining the overall effect on ground vibration during a train passage. Adding resilience in the track system may also lead to a reduction of parametric excitation due to differences in support stiffness [91, 78]. The efficiency of several vibration mitigation measures in the track was studied in WP3 of the FP7 project RIVAS [13].

In the hybrid vibration prediction tool, the user will be able to add or modify the properties of track components in order to evaluate and compare their vibration mitigation efficiency. A database of typical track properties for ballast and slab track will be provided with the software (direct fasteners, under sleeper pads, under ballast mats, slab mats in floating slab track,. . .) in order to facilitate computations and comparative studies. The user will also be able to import measured force densities for tracks without and with vibration mitigation measures; this may require transposition from one site to another.

Track subgrade. Stiffening of the subgrade under the track is essentially performed for improving the bearing capacity of soft soils and avoiding excessive track settlements, but has also been shown to be effective in reducing ground vibration [1], in particular when quasi-static excitation is important [147]. Various techniques for soil stiffening have been developed, some of which also allow for the treatment of soil under existing tracks. Subgrade stiffening is not considered as a practical option for vibration mitigation by railway operators because the works generally require interruption of railway operation.

Subgrade stiffening can conveniently be modelled with 2.5D FE-BE or 2.5D FE-PML models [177, 62]; these formulations remain expensive, though, in terms of computation time and will therefore not be used within SILVARSTAR. In the hybrid vibration prediction tool, the user will be able to import force densities and transfer functions that are measured or computed with external software.

7.5.2 Mitigation measures in the transmission path

Mitigation measures in the transmission path aim at impeding the propagation of elastic waves travelling in the soil from the railway track to nearby buildings. Examples include open and in-filled trenches, buried wall barriers, subgrade stiffening next to the track, wave impeding blocks, and placement of heavy masses or wave reflectors next to the track [117, 26]. The efficiency of these mitigation measures was studied in detail in the FP7 project RIVAS, by means of numerical computation [43] as well as large scale in situ tests involving the installation of a sheet pile wall in Furet (Sweden) [42] and a jet grouting wall in El Realengo (Spain) [25], as described in Deliverable D4.5 of RIVAS [40].

The efficiency of vibration mitigation measures in the transmission path can conveniently be studied using 2.5D FE-BE or 2.5D FE-PML models (with or without spatial windowing) [28, 27, 41, 178]. These models remain expensive in terms of computation time and will therefore not be integrated in the hybrid vibration prediction tool in SILVARSTAR. Instead, the user will have the opportunity to upload transfer functions that account for the installation of a mitigation measure in the transmission path that was measured in situ (on a similar site) or computed with external software.

7.5.3 Mitigation measures at the receiver

Mitigation measures at the receiver include base isolation of the building [175] or box-in-box arrangements of rooms [52]. These solutions are most often applied when vibration sensitive buildings are to be constructed near an existing railway; this is the case, for example, for laboratories, micro-electronic production units and hospitals with very sensitive equipment, as well as recording studios and concert halls, that are constructed near existing railways. When constructing new railways or upgrading existing railways, mitigation measures at source are often considered to be more effective and economical [74] as a larger number of buildings can be simultaneously protected.

In the hybrid vibration prediction tool, the user will have the opportunity to upload transfer functions that were obtained externally by numerical computation or experiments. Alternatively, the user may also opt to use vibration levels in the free field, predicted with the tool, as an input to a more detailed (finite element) analysis of a building subjected to base excitation.

7.6 Compatibility with international standards and guidelines

The new vibration prediction tool has to meet the requirements of existing standards and guidelines. The general approach for the prediction of ground-borne noise and vibration arising from rail systems is described in ISO 14837-1:2005 [88] and VDI 3837 [194]. Both guidelines involve separating the problem into three subproblems: emission (source), transmission (propagation) and immission (receiver). The new vibration prediction tool follows this approach. According to the ISO 14837-1:2005 and VDI 3837 standards, all components of the prediction can be determined by measurements or calculations. This requirement is also met by the hybrid approach followed in the new vibration prediction tool.

The outputs of the hybrid vibration prediction tool have to be compatible with international standards, as well as country-specific guidelines that are used for vibration assessment. In Europe, many standards are used to evaluate ground-borne vibration from railways, such as ISO 2631-2:2003 [87], BS 6472-1:2008 [15], DIN 4150-2:1999 [38], UNI 9614:1990, NS 8176:2017, Real Decreto 1307/2007, and SS 460 48 61. They are based on frequency domain or time domain indicators, derived from acceleration or velocity, with various weighting functions.

There is a general need for harmonization of vibration standards in Europe, resulting in a European Standard that can be applied in combination with National Application Documents, in which country specific limits and conditions are defined. One can take example from the Eurocode 8 that defines guidelines for design of structures for earthquake resistance [49]. Such undertaking is beyond the scope of the SILVARSTAR project, however.

In Deliverable D1.4 of the FP7 project RIVAS, Elias and Villot [47] reviewed standards and country-specific guidelines, as well as laboratory and field studies relating to human exposure to vibration. Additionally, they proposed four exposure descriptors based on maximum and equivalent values of both Wm-weighted vibration and A-weighted ground-borne noise. An idealised exposure-response curve of the same form was proposed for all four descriptors and target values were identified from existing exposure-response curves. Waddington et al. [198] summarised the work on human response carried out in the FP7 project CARGOVIBES, which included laboratory trials to measure the effects of vibration on sleep and a meta-analysis to determine exposure-response relationships for railway vibration.

SILVARSTAR will ensure compatibility for assessment with some of the most commonly used international standards (e.g. ISO 2631-2:2003, BS 6472-1:2008, DIN 4150-2:1999), in so far as these are based on frequency domain indicators (both velocity and acceleration). As the proposed hybrid vibration prediction tool operates in the frequency domain and the output will be a vibration velocity level in one-third octave bands, this can easily be accomplished. Different frequency-based weighting functions given in the standards will be integrated in the tool. Furthermore, SILVARSTAR will incorporate the exposure descriptors proposed in RIVAS. An open interface will be provided so that other international standards and guidelines can be applied.

SILVARSTAR will also check compatibility with standards based on time domain indicators and provide relations for appropriate post-processing. As an example, a methodology for such post-processing given in the German guideline DB Ril 820.2050 [31] is explained here. The output of the spectral prediction method using the statistical transfer functions is primarily a one-third octave band spectrum of the vibration velocity level on the floor $\mathrm{L_v}(f)$ [dB]. The computation of the vibration velocity level $\mathrm{L_v}(f)$ as described in DB Ril 820.2050 [31] is based on a measured and averaged vibration velocity level $\mathrm{L_{eq}}(f)$ in the free field. This influences the post-processing and calculation of the required time domain indicators $\mathrm{KB_{Fmax}}$ and $\mathrm{KB_{FTr}}$, as described in the following.

In a first step, a one-third octave band spectrum of the vibration velocity is generated as follows:

$$\hat{v}(f) \quad = \quad v_{\mathrm{ref}}\, 10^{\frac{\mathrm{L_v}(f)}{20}} \qquad [\mathrm{mm/s}] \tag{125}$$

with $v_{\mathrm{ref}} = 5 \times 10^{-8}$ m/s the reference velocity level. Based on this one-third octave band spectrum, the $\mathrm{KB}(f)$-value is assessed according to DIN 4150-2:1999 [38] (a summary of procedures defined in DIN 4150-2:1999 is also given in Deliverable D1.4 of RIVAS [47]):

$$\mathrm{KB}(f) \quad = \quad \frac{\hat{v}(f)}{\sqrt{1+\left(\frac{f_0}{f}\right)^2}} \qquad [-] \tag{126}$$

with $f_0 = 5.6$ Hz the cut-on frequency of the high-pass filter. The basis of the description still is a one-third octave band spectrum.

For the usual assessment in the time domain, an effective value $\mathrm{KB}_{\mathrm{FTm}}$ is calculated based on maximum values $\mathrm{KB}_{\mathrm{FT}i}$ of the KB-weighted time signal in 30 s segments:

$$\mathrm{KB}_{\mathrm{FTm}} = \sqrt{\frac{1}{N}\sum_{i=1}^{N}\mathrm{KB}_{\mathrm{FT}i}^2} \quad [-] \tag{127}$$

The square of this effective value $\mathrm{KB}_{\mathrm{FTm}}$ quantifies the signal's energy. As vibration is predicted in the frequency domain in the hybrid prediction tool, equation (127) cannot be used. Based on Parseval's theorem, which states that the signal's energy in the time and frequency domain are equal, the DB Ril 820.2050 guideline defines the effective value $\mathrm{KB}_{\mathrm{FTm}}$ as the following sum of centre values in one-third octave bands:

$$\mathrm{KB}_{\mathrm{FTm}} = \sqrt{\sum_{f=4\,\mathrm{Hz}}^{80\,\mathrm{Hz}}\mathrm{KB}^2(f)} \quad [-] \tag{128}$$

Since the $\mathrm{KB}_{\mathrm{Fmax}}$-value required for the vibration assessment cannot be determined from the prediction in the frequency domain, VDI 3837 provides the following approximate formula [194]:

$$\mathrm{KB}_{\mathrm{Fmax}} = c_{\mathrm{m}}\,\mathrm{KB}_{\mathrm{FTm}} \quad [-] \tag{129}$$

where c_{m} is an empirical value that can be taken as 1.5 for concrete floors and 1.7 for wooden floors. The $\mathrm{KB}_{\mathrm{FTr}}$ value, which is also required for the assessment, can be calculated based on $\mathrm{KB}_{\mathrm{FTm}}$ [38].

A similar approach as used for $\mathrm{KB}_{\mathrm{FTm}}$ is proposed in Deliverable D8.1 of the FINE-2 project [173] for the maximum transient vibration value (MTVV) defined in the ISO 2631-1:1997 standard [86]. This document also points out that the estimated vibration level $\mathrm{L_v}(f)$ depends on the input considered. If this input is an averaged spectrum, then $\mathrm{L_v}(f)$ also is an average level; if, on the other hand, the input is a max-hold spectrum, then $\mathrm{L_v}(f)$ also represents a maximum level. Further post-processing and, hence, also the calculation of descriptors such as MTVV depend on these choices. SILVARSTAR will further investigate the appropriateness of the proposed relationships.

For the vibration dose value (VDV), ISO 2631-1:2003 (Annex C) [87] proposes the following approximation to calculate an estimated vibration dose value (eVDV) from the frequency weighted RMS acceleration a_{w}:

$$\mathrm{eVDV} = 1.4\,a_{\mathrm{w}}\,T^{1/4} \tag{130}$$

where T is the exposure duration in seconds.

Vibration assessment in BS 6472-1:2008 [15] is also based on vibration dose values, so that similar estimations will be suitable.

An overview of the aforementioned standards and guidelines for vibration assessment is given in table 5 (after Elias and Villot [47]).

Furthermore, the output of the new hybrid vibration prediction tool also has to meet the requirements of national standards and guidelines for ground-borne noise. The indoor ground-borne noise is calculated

Table 5: Standards and guidelines for vibration assessment [47].

	ISO 2631-1:1997-05 ISO 2631-2:1997-05	United Kingdom BS 6472:1-2008	Germany DIN 4150-2:1999-06 DB Ril 820.2050
Measured / predicted quantity	Acceleration [m/s^2]	Acceleration [m/s^2]	Velocity [mm/s]
Indicator	RMS weighted value Vibration dose value (VDV) Maximum transient vibration value (MTVV)	VDV	$\mathrm{KB}_{\mathrm{Fmax}}$ $\mathrm{KB}_{\mathrm{FTr}}$ (day/night)
Estimation of indicator from frequency domain	$\mathrm{eVDV} = 1.4 a_{\mathrm{w}} T^{1/4}$	$\mathrm{eVDV} = 1.4 a_{\mathrm{w}} T^{1/4}$	$\mathrm{KB}_{\mathrm{Fmax}} = c_{\mathrm{m}} \mathrm{KB}_{\mathrm{FTm}}$

Table 6: Standards and guidelines for ground-borne noise assessment [47].

	ISO 14837-1:2005-07	United Kingdom Contractual guidelines	Germany TA Lärm DB Ril 820.2050
Frequency weighting	A	A	A
Indicator	Maximum SPL $\mathrm{L}_{\mathrm{pASmax}}$ [dB] Equivalent SPL $\mathrm{L}_{\mathrm{Aeq}}$ (per event or longer duration)	Maximum SPL $\mathrm{L}_{\mathrm{pASmax}}$	$\mathrm{L}_{\mathrm{sek,max}}$ L_{m} (day/night) $\mathrm{L}_{\mathrm{Aeq}}$

from the predicted velocity level on building floors by using correlation functions. Standards and guidelines for the assessment of ground-borne noise were also reviewed by Elias and Villot [47] in Deliverable D1.4 of the FP7 project RIVAS. All reviewed guidelines use sound pressure level (SPL) as an indicator. ISO 14837-1:2005 uses the maximum A-weighted SPL $\mathrm{L}_{\mathrm{pASmax}}$ and an equivalent SPL $\mathrm{L}_{\mathrm{Aeq}}$, while other guidelines use only one of the aforementioned indicators. Few guidelines use a C-weighting of the SPL.

An overview of some of the standards and guidelines for noise assessment is given in table 6.

7.7 Compatibility with external GIS software

The compatibility of output with respect to external GIS software will be ensured, so that the results can easily be exported to GIS formatted data and visualised in existing software. Within SILVARSTAR, the IMMI software developed by Wölfel will be used.

IMMI provides bidirectional integration of shape files, i.e. any shape file can be imported and used to generate objects in IMMI, and data sets (mainly calculation results, but also object geometries if required) can be exported as shapes. This means that data sets from all common GIS programmes can be imported into IMMI and model data and results can be exported from IMMI to shape data sets. The assignment of GIS data to IMMI model data is done via a flexible filter. It is only necessary to ensure that the corresponding attributes are available in IMMI for the assignment. The attributes required for SILVARSTAR (e.g. soil, buildings) to compute vibration levels must be defined and implemented in IMMI at a suitable location. Shape files basically consist of three individual files with different properties as summarized in table 7.

Table 7: Shape files used in IMMI.

Extension	Format	Description
.shp	Shape	Feature geometry
.shx	Shape index	Positional index of the feature geometry to allow for quick forward and backward searching
.dbf	Attribute	columnar attributes for each shape, in dBase IV format

7.8 Compatibility with requirements formulated by FINE-2 partners

SILVARSTAR will ensure that the developed methodology and vibration prediction tool are compatible with the requirements formulated in Deliverable D8.1 by the partners in the complementary project FINE-2 [173].

These requirements concern several aspects of the development:

1. The planning of the model development, in relation to the planning of the FINE-2 project.
2. The content and organisation of the numerical and experimental databases.
3. The input and output data (type, formats, frequency content, compatibility,. . .).
4. The step-wise methodology for ground vibration impact studies:
   (a) Rapid identification of the affected corridor along the railway line.
   (b) Detailed vibration assessment for buildings inside the affected corridor.
   (c) Evaluation of vibration mitigation measures.
5. The Graphical User Interface.
6. The interface with Geographical Information Systems.

Table 11 in appendix A.2 presents a detailed summary of all requirements for the vibration prediction tool as formulated by FINE-2 [173], together with an indication on how SILVARSTAR will meet these requirements. From this overview, it is clear that the modular and hybrid approach of SILVARSTAR and its integration into the IMMI software meet most of the detailed requirements as formulated by FINE-2.

The development of the hybrid vibration prediction tool in SILVARSTAR will commence from numerical models of the train-track-soil interaction problem to ensure the scientific validity of the prediction results. This constitutes the main deviation from the FINE-2 requirements, which expect a development based on empirical approaches. The final hybrid vibration prediction tool, however, will allow the user to use empirical data, numerical results, or a mixture of both. This is in line with the requirements formulated by FINE-2.

8. USE OF THE PREDICTION TOOL IN PRACTICAL VIBRATION STUDIES

8.1 Overview of vibration impact studies

As summarized by Garburg [59] during the UIC Railway Noise Days (February 2021), one can differentiate between the following practical situations when infrastructure managers, permanent way owners and vibration consultants are confronted with noise and vibration problems:

1. New railway infrastructure to be built:
    - Absolute values are to be predicted and evaluated according to given standards or guidelines.
    - Many buildings along the line must be assessed.
    - Experimental data are limited, as the line does not yet exist. Most input parameters are determined from databases or simulations, in particular the excitation.
2. Structural modification or extension of an existing railway line (change of excitation):
    - The relative increase (or decrease) with respect to the current situation is to be predicted.
    - Field measurements are performed to determine the source, propagation and receiver terms.
3. New buildings to be constructed next to an existing railway line:
    - On site measurements are performed to determine the source and propagation terms.
    - The building must be modelled to obtain the receiver term.

8.2 Current practices for prognosis and assessment

The three aforementioned situations are regularly handled by Vibratec and Wölfel in vibration consultancy projects. The following subsections describe the current processes and approaches taken, and how the SILVARSTAR vibration prediction tool is expected to support these.

The SILVARSTAR hybrid vibration prediction tool will allow users to perform the three types of studies, with great flexibility to define input data. The integrated experimental and numerical databases will allow users to perform fast assessment along the railway line, with assumed train, track and soil types. The Graphical User Interface will facilitate the inclusion of measured (or computed) data to describe the source, the propagation and the receiver.

8.2.1 Prediction for a new railway infrastructure

This type of project is frequently handled by Vibratec.

For the construction of new tracks or a new network, the vibration prediction procedure can take several forms, depending on the input data, but also on the type of traffic. Two cases are described here: a tramway and an underground subway line. In both situations, the first step is to identify sensitive buildings along the railway line. This is currently done by means of simple rules (based on distance between track and building) or by fast estimations (e.g FRA guidelines).

This first step will be made easier and more complete in the SILVARSTAR vibration prediction tool, thanks to the integrated databases of source, propagation and receiver terms (cf. subsections 7.2 and 7.3). The user will be able to import the railway line trajectory and building positions (GIS data) and to perform fast predictions of vibration levels in the buildings, with a minimum amount of input data (train and track types, broad soil description, generic building descriptions).

The second step is to predict vibration and noise levels inside the selected buildings, with more accurate data for the source, the propagation and the receivers. Currently, this is done separately from the first step. With the new tool, it will be possible to perform this assessment subsequently to the previous step, with the same railway line trajectory and building positions. Each component of the vibration transmission path (source, propagation, reception) will be updated by measurements or numerical results, depending on the situation.

When dealing with a tramway (or any other track at grade), it is generally easiest to go on site and to directly measure the transfer functions. Alternatively, geophysical prospection (MASW, seismic refraction, cross-hole, down-hole,. . .) can be performed to determine the dynamic soil characteristics [77], so that transfer functions can be computed, but such a procedure can be difficult in an urban environment. For the case of an underground line, the dynamic soil characteristics may need to be determined up to a larger depth.

For a tramway or surface railway, the vibration prediction procedure with the SILVARSTAR tool will be as follows:

1. Source (experimental): if a similar track and rolling stock are available on another site, measurements are performed to obtain ground vibration levels due to train pass-bys. On this site, the line source transfer mobilities are also measured, so that the equivalent force density can be determined and imported in the SILVARSTAR tool.

2. Source (numerical): a train-track-soil numerical model is set up, using the integrated databases and numerical models. If results of previous in situ measurements on sites with similar conditions sites are available, these can be used for validation or model updating.

3. Propagation (experimental): on-site measurements are performed to obtain the transfer functions on the sites where the predictions must be made; the results are imported in the SILVARSTAR tool. As mentioned before, determining dynamic soil characteristics by means of geophysical prospection methods could be difficult in an urban environment, so that computation of transfer functions is only rarely pursued in this case.

4. Source and propagation (hybrid): the vibration level outside the building is predicted with the SILVARSTAR tool, using the source model and the measured transfer functions. The model is used to modify track parameters such as the rail pad stiffness or the floating slab mat stiffness. The choice of the track type and characteristics is the most crucial for the control of ground borne noise and vibration for new tramway lines.

5. Building: compute the vibration level and noise level inside the building, from all the previous steps combined with building correction factors.

For an underground railway, the vibration prediction procedure with the SILVARSTAR tool will be as follows:

1. Source (experimental): in situ measurements are performed in and near a tunnel to obtain the equivalent force density for a given track and for different speeds [195] (based on vibration levels during train passages and line source transfer mobilities). These results are imported in the SILVARSTAR tool.
2. Source (numerical): if no measurements are possible, coupled train-track-tunnel models are used to compute the equivalent force density. The models can be used to obtain the equivalent force density for different types of track.
3. Propagation (experimental): in situ measurements in various sections to obtain the transfer functions in the soil are seldom performed due to their practical complexity.
4. Propagation (numerical): tunnel-to-soil surface transfer functions are computed, using a model based on dynamic soil characteristics that are obtained by means of in situ geophysical prospection.
5. Building: compute the vibration level and noise level inside the building, from all the previous steps (source and propagation) combined with building correction factors.

In some cases, vibration consultants are not requested or allowed to perform vibration measurements inside houses or residences. In the case of a surface railway or tramway, the prediction will hence be made at the ground in front of the building; the usual vibration limit in France is 66 dBv (reference 5×10^8 m/s). For sensitive situations, margin can be added, or specific models can be set-up. In the case of underground lines, and for specific buildings in the proximity of surface lines, vibration and noise levels are computed using empirical transfer functions. The limit vibration levels are defined, for example, by the ISO 2631-2:1997 standard, while the limit noise levels are defined, for example, by the World Health Organisation (WHO) [204] or in local guidelines.

The results obtained within the vibration prediction tool will be easily convertible from one standard to another.

8.2.2 Prediction for change in emission

This type of project is also frequently handled by Vibratec. The main difference compared to the construction of a new railway line is that the line already exists and in situ measurements can be performed more extensively. In practice, the study is currently divided in several steps:

1. In situ measurements, analysis and diagnostics: this can involve pass-by measurements (initial noise and vibration state), track and soil characterization (propagation), visual inspection of the state and structural integrity of tracks and components, etc.
2. Modelling of the change in vibration emission: this step involves the use of numerical models with different degree of complexity, post-processing of measured data from reference sites (transpositions), etc.
3. Predictions, generally involving the coupling of numerical predictions and measured data. Predicted vibration levels are presented as relative values allowing a comparison of the new state with the initial state.

Similar steps will be performed within the SILVARSTAR tool. The initial source will be measured and transposed to the final situation (e.g. change of track components, increase of traffic volume). The measured propagation and receiver terms will subsequently be used to compute noise and vibration levels inside a building. The main enhancement will be the validated transposition method that will be developed in WP2. The integrated databases will also help to generate source terms for modified situations, based on measurements or numerical models.

In recent projects, consultants were asked to determine if part of an existing track base could be kept instead of being destroyed completely for renewal. This is not only done for economic, but also for ecological reasons, hence minimizing environmental impact as much as possible. Typical examples are the renewal of old resilient layers of floating slab tracks, or a replacement of rails, fasteners and pavements. Although not specifically designed to study such cases, the vibration prediction tool may be applied for these situations, if done carefully.

8.2.3 Prediction for new buildings

This type of project is frequently handled by Wölfel. The following description primarily refers to German vibration norms and guidelines, but is also applicable in combination with other guidelines.

According to DB Ril 820.2050 [31], the emission and transmission of vibration due to existing railway lines must be measured according to DIN 45672-1:2018 [39]. Therefore, railway induced vibration is measured at a reference distance of 8 m from the track centre and in the area of the planned building (usually in free field conditions). At least two parallel measurement lines perpendicular to the track are set up. If it is not possible to measure all train passages during a longer period (day and night), a representative number of train passages for each type of train can alternatively be measured (minimum 5 passages per class according to DIN 4150-2:1999). Every type of train running on each track then forms one class. If the variance of vibration levels for a particular class is too large (e.g. due to varying train speed, train composition, number of carriages, or the appearance of wheel flats), this class can be further subdivided in separate classes. A radar is used to measure the length and speed of the trains. Several classes per train type can be formed based on this information. This procedure also allows for different future scenarios of traffic volume and composition to be accounted for.

In the DIN 4150-2:1999 standard, vibration assessment is primarily based on measured velocity time histories. For vibration prediction in new buildings, however, a spectral analysis following the DB Ril 820.2050 guideline is usually performed, as it provides statistically determined building correction factors from the free field to building floors. These correction factors are defined for wooden and concrete floors, with a resonance frequency at one-third octave bands between 8 and 80 Hz; for each of these cases, they are tabulated at one-third octave band centre frequencies between 4 and 250 Hz. At every output point, the values $\mathrm{KB_{Fmax}}$ and $\mathrm{KB_{FTm}}$ are calculated using the building correction factors of a particular floor, defined by its material and estimated resonance frequency. The $\mathrm{KB_{FTm}}$-value is evaluated according to equation (128), which limits the frequency range of interest between 4 and 80 Hz. Depending on the traffic scenario considered (number and type of trains per class), the vibration dose values $\mathrm{KB_{FTr}}$ for day and night periods are also calculated. The vibration assessment is finally performed according to the DIN 4150-2:1999 standard by comparing the $\mathrm{KB_{Fmax}}$ values with the limits $\mathrm{A_u}$ and $\mathrm{A_o}$ or the $\mathrm{KB_{FTr}}$ values with the limit $\mathrm{A_r}$. These limit values depend on the classification of the area where the building is located. The prediction of vibration for different floor resonance frequencies makes it possible to give advice on the construction type and dimensions of the future building.

In addition, ground-borne noise is usually predicted based on additional correction factors between floor vibration levels and noise levels in rooms. Using the correction factors of the DB Ril 820.2050 guideline, the maximum and average ground-borne noise levels $\mathrm{L}_{\mathrm{sek,max}}$ and $\mathrm{L}_{\mathrm{sek,av}}$ are calculated for each output point, floor resonance frequency (distinguishing between wooden and concrete floors) and train class. Taking into consideration the number of trains, the assessment level L_{am} is determined for day and night periods. Limit values are provided in the German TA Lärm [16].

This process will be implemented in a similar form in the new vibration prediction tool, incorporating all steps. The vibration levels measured at free field locations can be imported directly in the tool. The assignment of measurement data to different train types as well as the definition of number of trains per type can also be done. The tool will further provide a variety of empirical building correction factors for the prediction of vibration levels on building floors as well as ground-borne noise in rooms. The classification of buildings or urban areas depending on use will also be possible. Finally, a variety of international standards and guidelines will be available for assessment of vibration and ground-borne noise.

REFERENCES

[1] D. Adam, A. Vogel, and A. Zimmermann. Ground improvement techniques beneath existing rail tracks. *Ground Improvement*, 11(4):229–235, 2007.

[2] K. Adolfsson, B. Andréasson, P.-E. Bengtson, A. Bodare, C. Madshus, R. Massarch, G. Wallmark, and P. Zackrisson. High speed lines on soft ground. Evaluation and analyses of measurements from the West Coast Line. Technical report, Banverket, Sweden, 1999.

[3] L. Andersen. Influence of dynamic soil-structure interaction on building response due to ground vibration. In *Proceedings of the 8th European Conference on Numerical Methods in Geotechnical Engineering*, Delft, The Netherlands, June 2014.

[4] L. Andersen and C.J.C. Jones. Coupled boundary and finite element analysis of vibration from railway tunnels – a comparison of two- and three-dimensional models. *Journal of Sound and Vibration*, 293(3-5):611–625, 2006.

[5] M. Arnst, Q.A. Ta, R. Taherzadeh, R. Cottereau, M. Schevenels, G. Lombaert, D. Clouteau, M. Bonnet, and G. Degrande. Measurements at a site in Lincent: transfer functions, dispersion curves and seismograms. Technical report, Laboratoire de Mécanique des Sols, Structures et Matériaux, Ecole Centrale de Paris, 2006.

[6] D. Aubry, D. Clouteau, and G. Bonnet. Modelling of wave propagation due to fixed or mobile dynamic sources. In N. Chouw and G. Schmid, editors, *Workshop Wave '94, Wave propagation and Reduction of Vibrations*, pages 109–121, Ruhr Universität Bochum, Germany, December 1994.

[7] L. Auersch. The excitation of ground vibration by rail traffic: theory of vehicle-track-soil interaction and measurements on high-speed lines. *Journal of Sound and Vibration*, 284(1-2):103–132, 2005.

[8] L. Auersch. Ground vibration due to railway traffic – The calculation of the effects of moving static loads and their experimental verification. *Journal of Sound and Vibration*, 293:599–610, 2006.

[9] L. Auersch. Theoretical and experimental excitation force spectra for railway-induced ground vibration: vehicle–track–soil interaction, irregularities and soil measurements. *Vehicle Systems Dynamics*, 48(2):235–261, 2010.

[10] S.A. Badsar, M. Schevenels, W. Haegeman, and G. Degrande. Determination of the damping ratio in the soil from SASW tests using the half-power bandwidth method. *Geophysical Journal International*, 182(3):1493–1508, 2010.

[11] E.G. Berggren. *Railway Track Stiffness. Dynamic measurements and evaluation for efficient maintenance*. PhD thesis, Royal Institute of Technology (KTH), Stockholm, Sweden, 2009.

[12] E. Bongini, G. Lombaert, S. François, and G. Degrande. A parametric study of the impact of mitigation measures on ground borne vibration due to railway traffic. In G. De Roeck, G. Degrande, G. Lombaert, and G. Müller, editors, *Proceedings of the 8th International Conference on Structural Dynamics, EURODYN 2011*, pages 663–670, Leuven, Belgium, July 2011. CD-ROM.

[13] E. Bongini, R. Müller, R. Garburg, and A. Pieringer. Design guide and technology assessment of the track mitigation measures. RIVAS project SCP0-GA-2010-265754, Deliverable D3.13, Report to the EC, December 2013.

[14] E.C. Bovey. Development of an impact method to determine the vibration transfer characteristics of railway installations. *Journal of Sound and Vibration*, 87(2):357–370, 1983.

[15] British Standards Institution. *BS 6472:2008: Guide to evaluation of human exposure to vibration in buildings. Part 1: Vibration sources other than blasting*, 2008.

[16] Bundesministerium für Umwelt. *Naturschutz und Reaktorsicherheit, Sechste Allgemeine Verwaltungsvorschrift zum Bundesimmissionsschutzgesetz (Technische Anleitung zum Schutz gegen Lärm - TA Lärm)*, 1998.

[17] P. Chatterjee, G. Degrande, and S. Jacobs. Free field and building vibrations due to the passage of test trains at the site of Regent's Park in London. Report BWM-2003-20, Department of Civil Engineering, KU Leuven, December 2003. CONVURT EC-Growth Project G3RD-CT-2000-00381.

[18] H. Chebli, R. Othman, D. Clouteau, M. Arnst, and G. Degrande. 3D periodic BE-FE model for various transportation structures interacting with soil. *Computers and Geotechnics*, 35:22–32, 2008.

[19] A.K. Chopra. *Dynamics of structures. Theory and applications to earthquake engineering*. Pearson Prentice-Hall, Upper Saddle River, NJ, fourth edition, 2012.

[20] D. Clouteau, M. Arnst, T.M. Al-Hussaini, and G. Degrande. Freefield vibrations due to dynamic loading on a tunnel embedded in a stratified medium. *Journal of Sound and Vibration*, 283(1–2):173–199, 2005.

[21] D. Clouteau, G. Degrande, and G. Lombaert. Numerical modelling of traffic induced vibrations. *Meccanica*, 36(4):401–420, 2001.

[22] D.P. Connolly, G.P. Marecki, G. Kouroussis, I. Thalassinakis, and P.K. Woodward. The growth of railway ground vibration problems - a review. *Science of the Total Environment*, 568:1276–1282, 2016.

[23] P.A. Costa, R. Calçada, and A.S. Cardoso. Ballast mats for the reduction of railway traffic vibrations. Numerical study. *Soil Dynamics and Earthquake Engineering*, 42:137–150, 2012.

[24] P.A. Costa, R. Calçada, A.S. Cardoso, and A. Bodare. Influence of soil non-linearity on the dynamic response of high-speed railway tracks. *Soil Dynamics and Earthquake Engineering*, 30(4):221–235, 2010.

[25] P. Coulier, V. Cuéllar, G. Degrande, and G. Lombaert. Experimental and numerical evaluation of the effectiveness of a stiff wave barrier in the soil. *Soil Dynamics and Earthquake Engineering*, 77:238–253, 2015.

[26] P. Coulier, G. Degrande, A. Dijckmans, J. Houbrechts, G. Lombaert, W. Rücker, L. Auersch, M.R. Plaza, V. Cuéllar, D. Thompson, A. Ekblad, and A. Smekal. Scope of the parametric study on mitigation measures on the transmission path. RIVAS project SCP0-GA-2010-265754, Deliverable D4.1, Report to the EC, October 2011.

[27] P. Coulier, A. Dijckmans, S. François, G. Degrande, and G. Lombaert. A spatial windowing technique to account for finite dimensions in 2.5D dynamic soil–structure interaction problems. *Soil Dynamics and Earthquake Engineering*, 59:51–67, 2014.

[28] P. Coulier, S. François, G. Degrande, and G. Lombaert. Subgrade stiffening next to the track as a wave impeding barrier for railway induced vibrations. *Soil Dynamics and Earthquake Engineering*, 48:119–131, 2013.

[29] P. Coulier, G. Lombaert, and G. Degrande. The influence of source–receiver interaction on the numerical prediction of railway induced vibrations. *Journal of Sound and Vibration*, 333(12):2520–2538, 2014.

[30] N. Dadkah. Axle box acceleration measurements in London, Regent's Park - Baker Street. Report R1064, MRCL, July 2003. CONVURT EC-Growth Project G3RD-CT-2000-00381.

[31] DB Netz AG. *DB Ril 820.2050 Erschütterungen und sekundärer Luftschall*, 2017.

[32] F.C.P. de Barros and J.E. Luco. Moving Green's functions for a layered visco-elastic halfspace. Technical report, Department of Applied Mechanics and Engineering Sciences, University of California, San Diego, La Jolla, California, May 1992.

[33] G. Degrande, D. Clouteau, R. Othman, M. Arnst, H. Chebli, R. Klein, P. Chatterjee, and B. Janssens. A numerical model for ground-borne vibrations from underground railway traffic based on a periodic finite element - boundary element formulation. *Journal of Sound and Vibration*, 293(3-5):645–666, 2006.

[34] G. Degrande and G. Lombaert. An efficient formulation of Krylov's prediction model for train induced vibrations based on the dynamic reciprocity theorem. *Journal of the Acoustical Society of America*, 110(3):1379–1390, 2001.

[35] G. Degrande, G. Lombaert, G. De Roeck, W. Haegeman, S.A. Badsar, and M. Schevenels. In situ determination of material damping in the soil at small deformation ratios. Report BWM-2008-19, Department of Civil Engineering, KU Leuven, December 2008. FWO Project G.0595.06.

[36] G. Degrande, M. Schevenels, P. Chatterjee, W. Van de Velde, P. Hölscher, V. Hopman, A. Wang, and N. Dadkah. Vibrations due to a test train at variable speeds in a deep bored tunnel embedded in London clay. *Journal of Sound and Vibration*, 293(3-5):626–644, 2006.

[37] Deutsches Institut für Normung. *DIN 45672 Teil 2: Schwingungsmessungen in der Umgebung von Schienenverkehrswegen: Auswerteverfahren*, 1995.

[38] Deutsches Institut für Normung. *DIN 4150 Teil 2: Erschütterungen im Bauwesen, Einwirkungen auf Menschen in Gebäuden*, 1999.

[39] Deutsches Institut für Normung. *DIN 45672 Teil 1: Schwingungsmessungen in der Umgebung von Schienenverkehrswegen: Meßverfahren für Schwingungen*, 2018.

[40] A. Dijckmans, P. Coulier, G. Degrande, G. Lombaert, A. Ekblad, A. Smekal, M. Rodríguez Plaza, Á. Andrés-Alguacil, V. Cuéllar, J. Keil, and G. Vukotic. Mitigation measures on the transmission path: results of field tests. RIVAS project SCP0-GA-2010-265754, Deliverable D4.5, Report to the EC, December 2013.

[41] A. Dijckmans, P. Coulier, J. Jiang, M.G.R. Toward, D.J. Thompson, G. Degrande, and G. Lombaert. Mitigation of railway induced ground vibration by heavy masses next to the track. *Soil Dynamics and Earthquake Engineering*, 75:158–170, 2015.

[42] A. Dijckmans, A. Ekblad, A. Smekal, G. Degrande, and G. Lombaert. Efficacy of a sheet pile wall as a wave barrier for railway induced ground vibration. *Soil Dynamics and Earthquake Engineering*, 84:55–69, 2016.

[43] A. Dijckmans, J. Jiang, M.G.R. Toward, G. Lombaert, G. Degrande, and D.J. Thompson. Numerical study of vibration mitigation measures in the transmission path. RIVAS project SCP0-GA-2010-265754, Deliverable D4.4, Report to the EC, December 2013.

[44] A. Duley. *Critical velocity effects on high speed railways*. PhD thesis, University of Southampton, 2019.

[45] T. Ekevid, H. Lane, and N.-E. Wiberg. Adaptive solid wave propagation – influences of boundary conditions in high-speed train applications. *Computer Methods in Applied Mechanics and Engineering*, 195:236–250, 2006.

[46] T. Ekevid and N.-E. Wiberg. Wave propagation related to high-speed train. A scaled boundary FE-approach for unbounded domains. *Computer Methods in Applied Mechanics and Engineering*, 191:3947–3964, 2002.

[47] P. Elias and M. Villot. Review of existing standards, regulations and guidelines as well as laboratory and field studies concerning human exposure to vibration. RIVAS project SCP0-GA-2010-265754, Deliverable D1.4, Report to the EC, 2011.

[48] C. Esveld. *Modern railway track. Second Edition.* MRT-Productions, Zaltbommel, 2001.

[49] European Commitee for Standardization. *Eurocode 8: Design provisions for earthquake resistance of structures - Part 1: General rules, seismic actions and rules for buildings*, 2004.

[50] P. Fiala, G. Degrande, and F. Augusztinovicz. Numerical modelling of ground borne noise and vibration in buildings due to surface rail traffic. *Journal of Sound and Vibration*, 301(3-5):718–738, 2007.

[51] P. Fiala, S. Gupta, G. Degrande, and F. Augusztinovicz. A numerical model for re-radiated noise in buildings from underground railways. In B. Schulte-Werning, D. Thompson, P.-E. Gautier, C. Hanson, B. Hemsworth, J. Nelson, T. Maeda, and P. de Vos, editors, *Proceedings of the 9th International Workshop on Railway Noise*, volume 99 of *Notes on Numerical Fluid Mechanics and Multidisciplinary Design*, pages 115–121, Munich, Germany, September 2007. Springer-Verlag, Berlin, Heidelberg.

[52] P. Fiala, S. Gupta, G. Degrande, and F. Augusztinovicz. A parametric study on countermeasures to mitigate subway traffic induced vibration and noise in buildings. In P. Sas and B. Bergen, editors, *Proceedings of ISMA2008 International Conference on Noise and Vibration Engineering*, pages 2751–2764, Leuven, September 2008.

[53] J.A. Forrest and H.E.M. Hunt. Ground vibration generated by trains in underground tunnels. *Journal of Sound and Vibration*, 294(4):706–736, 2006.

[54] J.A. Forrest and H.E.M. Hunt. A three-dimensional tunnel model for calculation of train-induced ground vibration. *Journal of Sound and Vibration*, 294(4):678–705, 2006.

[55] S. François, L. Pyl, H.R. Masoumi, and G. Degrande. The influence of dynamic soil-structure interaction on traffic induced vibrations in buildings. *Soil Dynamics and Earthquake Engineering*, 27(7):655–674, 2007.

[56] S. François, M. Schevenels, G. Lombaert, and G. Degrande. A 2.5D displacement based PML for elastodynamic wave propagation. *International Journal for Numerical Methods in Engineering*, 90(7):819–837, 2012.

[57] S. François, M. Schevenels, G. Lombaert, P. Galvín, and G. Degrande. A 2.5D coupled FE-BE methodology for the dynamic interaction between longitudinally invariant structures and a layered halfspace. *Computer Methods in Applied Mechanics and Engineering*, 199(23-24):1536–1548, 2010.

[58] P. Galvín, A. Romero, and J. Domínguez. Fully three-dimensional analysis of high-speed train–track–soil–structure dynamic interaction. *Journal of Sound and Vibration*, 329:5147–5163, 2010.

[59] R. Garburg. Ground vibration, and the need and requirements for developments of prediction tool from the railways perspective. UIC Railway Noise Days, February 2021.

[60] V.K. Garg and R.V. Dukkipati. *Dynamics of railway vehicle systems.* Academic Press, Canada, 1984.

[61] M. Germonpré. *The effect of parametric excitation on the prediction of railway induced vibration in the built environment*. PhD thesis, Department of Civil Engineering, KU Leuven, 2018.

[62] M. Germonpré, G. Degrande, and G. Lombaert. A study of modelling simplifications in ground vibration predictions for railway traffic at grade. *Journal of Sound and Vibration*, 406:208–223, 2017.

[63] S.G. Grassie. Rail irregularities, corrugation and acoustic roughness: characteristics, significance and effects of reprofiling. *Proceedings of the Institution of Mechanical Engineers, Part F: Journal of Rail and Rapid Transit*, 226(5):542–557, 2012.

[64] H. Grundmann and S. Lenz. Nonlinear interaction between a moving SDOF system and a Timoshenko beam/halfspace support. *Archive of Applied Mechanics*, 72:830–842, 2003.

[65] H. Grundmann, M. Lieb, and E. Trommer. The response of a layered half-space to traffic loads moving along its surface. *Archive of Applied Mechanics*, 69:55–67, 1999.

[66] C. Guigou-Carter, M. Villot, B. Guillerme, and C. Petit. Analytical and experimental study of sleeper SAT S312 in slab track SATEBA system. *Journal of Sound and Vibration*, 293(3-5):878–887, 2006. Proceedings of the 8th International Workshop on Railway Noise.

[67] S. Gupta, M.F.M. Hussein, G. Degrande, H.E.M. Hunt, and D. Clouteau. A comparison of two numerical models for the prediction of vibrations from underground railway traffic. *Soil Dynamics and Earthquake Engineering*, 27(7):608–624, 2007.

[68] W. Haegeman. In situ tests Retie-Waremme-Lincent. Report RUG IV.1.16.3, Soil Mechanics Laboratory, Ghent University, September 2001. STWW Programme Technology and Economy, Project IWT-000152.

[69] A. Hamid and T.L. Yang. Analytical description of track-geometry vibrations. *Transportation Research Record 838*, pages 19–26, 1981.

[70] C.E. Hanson, J.C. Ross, and D.A. Towers. High-Speed Ground Transportation Noise and Vibration Impact Assessment. Technical Report DOT/FRA/ORD-12/15, U.S. Department of Transportation, Federal Railroad Administration, Office of Railroad Policy and Development, September 2012.

[71] C.E. Hanson, D.A. Towers, and L.D. Meister. High-Speed Ground Transportation Noise and Vibration Impact Assessment. HMMH Report 293630-4, U.S. Department of Transportation, Federal Railroad Administration, Office of Railroad Development, October 2005.

[72] C.E. Hanson, D.A. Towers, and L.D. Meister. Transit Noise and Vibration Impact Assessment. Report FTA-VA-90-1003-06, U.S. Department of Transportation, Federal Transit Administration, Office of Planning and Environment, May 2006.

[73] M. Heckl, G. Hauck, and R. Wettschureck. Structure-borne sound and vibration from rail traffic. *Journal of Sound and Vibration*, 193(1):175–184, 1996.

[74] B. Hemsworth. Reducing groundborne vibrations: state of the art study. *Journal of Sound and Vibration*, 231(3):703–709, 2000.

[75] P. Hölscher and V. Hopman. Test site Regent's Park London. Soil description. Report 381540-104, Version 2, GeoDelft, December 2003. CONVURT EC-Growth Project G3RD-CT-2000-00381.

[76] R.A. Hood, R.J. Greer, M. Breslin, and P.R. Williams. The calculation and assessment of ground-borne noise and perceptible vibration from trains in tunnels. *Journal of Sound and Vibration*, 193(1):215–225, 1996.

[77] J. Houbrechts, M. Schevenels, G. Lombaert, G. Degrande, W. Rücker, V. Cuellar, and A. Smekal. Test procedures for the determination of the dynamic soil characteristics. RIVAS project SCP0-GA-2010-265754, Deliverable D1.1, Report to the EC, December 2011.

[78] H.E.M. Hunt. Modelling of rail roughness for the evaluation of vibration-isolation measures. In *12th International Congress on Sound and Vibration*, Lisbon, Portugal, July 2005.

[79] H.E.M. Hunt. Types of rail roughness and the selection of vibration isolation measures. In B. Schulte-Werning, D. Thompson, P.-E. Gautier, C. Hanson, B. Hemsworth, J. Nelson, T. Maeda, and P. de Vos, editors, *Noise and Vibration Mitigation for Rail Transportation Systems*, volume 99 of *Notes on Numerical Fluid Mechanics and Multidisciplinary Design*, pages 341–347. Springer Berlin/Heidelberg, 2008.

[80] H.E.M. Hunt and M.F.M. Hussein. Vibration from railways: can we achieve better than +/-10 dB prediction accuracy? In *14th International Congress on Sound and Vibration*, Cairns, Australia, July 2007.

[81] M.F.M. Hussein, S. François, M. Schevenels, H.E.M. Hunt, J.P. Talbot, and G. Degrande. The fictitious force method for efficient calculation of vibration from a tunnel embedded in a multi-layered half-space. *Journal of Sound and Vibration*, 333:6996–7018, 2014.

[82] M.F.M. Hussein and H.E.M. Hunt. Modelling of floating-slab tracks with continuous slabs under oscillating moving loads. *Journal of Sound and Vibration*, 297(1):37–54, 2006.

[83] M.F.M. Hussein and H.E.M. Hunt. A numerical model for calculating vibration from a railway tunnel embedded in a full-space. *Journal of Sound and Vibration*, 305(3):401–431, 2007.

[84] M.F.M. Hussein and H.E.M. Hunt. A numerical model for calculating vibration due to a harmonic moving load on a floating-slab track with discontinuous slabs in an underground railway tunnel. *Journal of Sound and Vibration*, 321(1-2):363–374, 2009.

[85] M.F.M. Hussein, H.E.M. Hunt, K. Kuo, P.A. Costa, and J. Barbosa. The use of sub-modelling technique to calculate vibration in buildings from underground railways. *Proceedings of the Institution of Mechanical Engineers, Part F: Journal of Rail and Rapid Transit*, 229(3):303–314, 2015.

[86] International Organization for Standardization. *ISO 2631-1:1997: Mechanical vibration and shock - Evaluation of human exposure to whole-body vibration - Part 1: General requirements. Second Edition*, 1997.

[87] International Organization for Standardization. *ISO 2631-2:2003: Mechanical vibration and shock - Evaluation of human exposure to whole-body vibration - Part 2: Vibration in buildings (1 to 80 Hz)*, 2003.

[88] International Organization for Standardization. *ISO 14837-1:2005 Mechanical vibration - Ground-borne noise and vibration arising from rail systems - Part 1: General guidance*, 2005.

[89] International Organization for Standardization. *ISO 3095:2013: Railway applications - Acoustics - Measurement of noise emitted by railbound vehicles*, 2013.

[90] Q. Jin, D. Thompson, D. Lurcock, M. Toward, and E. Ntotsios. A 2.5D finite element and boundary element model for the ground vibration from trains in tunnels and validation using measurement data. *Journal of Sound and Vibration*, 422:373–389, 2018.

[91] A. Johansson, J.C.O. Nielsen, R. Bolmsvik, A. Karlstrom, and R. Lunden. Under sleeper pads - Influence on dynamic train-track interaction. *Wear*, 265:1479–1487, 2008.

[92] C.J.C. Jones and J.R. Block. Prediction of ground vibration from freight trains. *Journal of Sound and Vibration*, 193(1):205–213, 1996.

[93] S. Jones and H.E.M. Hunt. The effect of inclined soil layers on surface vibration from underground railways using the thin layer method. *ASCE Journal of Engineering Mechanics*, 137(12):887–900, 2011.

[94] S. Jones and H.E.M. Hunt. Voids at the tunnel–soil interface for calculation of ground vibration from underground railways. *Journal of Sound and Vibration*, 330(2):245–270, 2011.

[95] L. Karl and W. Haegeman. Summary of the soil tests at the testing sites: Retie, Lincent, Waremme, Sint-Katelijne-Waver and Ghent. Report, Laboratory of Soil Mechanics, Ghent University, September 2004.

[96] L. Karl, W. Haegeman, and G. Degrande. Determination of the material damping ratio and the shear wave velocity with the Seismic Cone Penetration Test. *Soil Dynamics and Earthquake Engineering*, 26(12):1111–1126, 2006.

[97] A. Karlström and A. Boström. An analytical model for train induced ground vibrations from railways. *Journal of Sound and Vibration*, 292:221–241, 2006.

[98] S.E. Kattis, D. Polyzos, and D.E. Beskos. Vibration isolation by a row of piles using a 3-D frequency domain BEM. *International Journal for Numerical Methods in Engineering*, 46:713–728, 1999.

[99] E. Kausel. *Fundamental solutions in elastodynamics: a compendium*. Cambridge University Press, New York, 2006.

[100] E. Kausel and J.M. Roësset. Stiffness matrices for layered soils. *Bulletin of the Seismological Society of America*, 71(6):1743–1761, 1981.

[101] K. Knothe and S.L. Grassie. Modelling of railway track and vehicle/track interaction at high frequencies. *Vehicle Systems Dynamics*, 22: 209–262, 1993.

[102] K. Knothe and Y. Wu. Receptance behaviour of railway track and subgrade. *Archive of Applied Mechanics*, 68: 457–470, 1998.

[103] J. Kogut and G. Degrande. Free field vibrations due to the passage of an IC train and a Thalys high speed train on the L2 track Brussels-Köln. Report BWM-2002-10, Department of Civil Engineering, KU Leuven, November 2002. STWW Programme Technology and Economy, Project IWT-000152.

[104] J. Kogut and G. Degrande. Assessment of the dynamic parameters of the HST track L2 Brussels - Köln in Lincent using rail receptance measurements. Report BWM-2003-05, Department of Civil Engineering, KU Leuven, March 2003. STWW Programme Technology and Economy, Project IWT-000152.

[105] J. Kogut and G. Degrande. Transfer functions between the HST track and the free field on the line L2 Brussels-Köln in Lincent. Report BWM-2003-03, Department of Civil Engineering, KU Leuven, January 2003. STWW Programme Technology and Economy, Project IWT-000152.

[106] G. Kouroussis, O. Verlinden, and C. Conti. On the interest of integrating vehicle dynamics for the ground propagation of vibrations: the case of urban railway traffic. *Vehicle Systems Dynamics*, 48(12):1553–1571, 2010.

[107] K.A. Kuo, M. Germonpré, K. Maes, G. Degrande, and G. Lombaert. Processing of vibration measurements at the Blok D building of the administrative complex of KU Leuven. Report BWM-2017-20, Department of Civil Engineering, KU Leuven, November 2017. Project OT/13/59.

[108] K.A. Kuo, H.E.M. Hunt, and M.F.M. Hussein. The effect of a twin tunnel on the propagation of ground-borne vibration from an underground railway. *Journal of Sound and Vibration*, 330(25):6203–6222, 2011.

[109] K.A. Kuo, G. Lombaert, and G. Degrande. Quantifying uncertainties in measurements of railway vibration. In D. Anderson, editor, *Proceedings of the 12th International Workshop on Railway Noise*, pages 62–69, Terrigal, Australia, September 2016.

[110] K.A. Kuo, M. Papadopoulos, G. Lombaert, and G. Degrande. The coupling loss of a building subjected to railway induced vibrations: Numerical modelling and experimental measurements. *Journal of Sound and Vibration*, 442:459–481, 2019.

[111] K.A. Kuo, H. Verbraken, Degrande. G., and G. Lombaert. Hybrid predictions of railway induced ground vibration using a combination of experimental measurements and numerical modelling. *Journal of Sound and Vibration*, 373:263–284, 2016.

[112] H. Kuppelwieser and A. Ziegler. A tool for predicting vibration and structure-borne noise immissions caused by railways. *Journal of Sound and Vibration*, 193:261–267, 1996.

[113] M. Lieb. *Adaptive numerische Fouriertransformation in der Bodendynamik unter Verwendung einer Waveletzerlegung*. PhD thesis, Technische Universität München, München, Germany, 1996.

[114] G. Lombaert and G. Degrande. The isolation of railway induced vibrations by means of resilient track elements. In C. Soize, editor, *Proceedings of the 6th European Conference on Structural Dynamics, EURODYN 2005*, Paris, France, September 2005.

[115] G. Lombaert and G. Degrande. Ground-borne vibration due to static and dynamic axle loads of InterCity and high speed trains. *Journal of Sound and Vibration*, 319(3-5):1036–1066, 2009.

[116] G. Lombaert, G. Degrande, and D. Clouteau. Numerical modelling of free field traffic induced vibrations. *Soil Dynamics and Earthquake Engineering*, 19(7):473–488, 2000.

[117] G. Lombaert, G. Degrande, S. François, and D.J. Thompson. Ground-borne vibration due to railway traffic. In J.C.O. Nielsen, D. Anderson, P.-E. Gautier, M. Iida, J.T. Nelson, D. Thompson, T. Tielkes, D.A. Towers, and P. de Vos, editors, *Proceedings of the 11th International Workshop on Railway Noise*, volume 126 of *Notes on Numerical Fluid Mechanics and Multidisciplinary Design*, pages 253–287, Uddevalla, Sweden, September 2013. Springer, Heidelberg, New York, Dordrecht, London. Invited state of the art paper.

[118] G. Lombaert, G. Degrande, P. Galvín, E. Bongini, and F. Poisson. A comparison of predicted and measured ground vibrations due to high speed, passenger, and freight trains. In T. Maeda, P.-E. Gautier, C.E. Hanson, B. Hemsworth, J.T. Nelson, B. Schulte-Werning, D. Thompson, and P. de Vos, editors, *Proceedings of the 10th International Workshop on Railway Noise*, volume 118 of *Notes on Numerical Fluid Mechanics and Multidisciplinary Design*, pages 231–238, Nagahama, Japan, October 2010. Springer.

[119] G. Lombaert, G. Degrande, J. Kogut, and S. François. The experimental validation of a numerical model for the prediction of railway induced vibrations. *Journal of Sound and Vibration*, 297(3-5):512–535, 2006.

[120] G. Lombaert, G. Degrande, B. Vanhauwere, B. Vandeborght, and S. François. The control of ground borne vibrations from railway traffic by means of continuous floating slabs. *Journal of Sound and Vibration*, 297(3-5):946–961, 2006.

[121] G. Lombaert, S. François, and G. Degrande. TRAFFIC Matlab toolbox for traffic induced vibrations. Report BWM-2012-10, Department of Civil Engineering, KU Leuven, November 2012. User's Guide Traffic 5.2.

[122] J.E. Luco and R.J. Apsel. On the Green's functions for a layered half-space. Part I. *Bulletin of the Seismological Society of America*, 4:909–929, 1983.

[123] C. Madshus, B. Bessason, and L. Hårvik. Prediction model for low frequency vibration from high speed railways on soft ground. *Journal of Sound and Vibration*, 193(1):195–203, 1996.

[124] C. Madshus and A.M. Kaynia. High-speed railway lines on soft ground: dynamic behaviour at critical train speed. *Journal of Sound and Vibration*, 231(3):689–701, 2000.

[125] K. Maes, M. Germonpré, J. Zhang, M. Papadopoulos, A. Mukherjee, G. De Roeck, G. Degrande, and G. Lombaert. Vibration measurements at the Blok D building of the administrative complex building of KU Leuven. Report BWM-2017-11, Department of Civil Engineering, KU Leuven, August 2017. Project OT/13/59.

[126] K.R. Massarsch. Vibration isolation using gas-filled cushions. In *Proceedings of the Geo-Frontiers 2005 Congress*, Austin, Texas, January 2005. American Society of Civil Engineers.

[127] A.V. Metrikine and K. Popp. Steady-state vibrations of an elastic beam on a visco-elastic layer under moving load. *Archive of Applied Mechanics*, 70:399–408, 2000.

[128] A.V. Metrikine, S.N. Verichev, and J. Blauwendraad. Stability of a two-mass oscillator moving on a beam supported by a visco-elastic half-space. *International Journal of Solids and Structures*, 42:1187–1207, 2005.

[129] A.A. Mirza, A. Frid, J.C.O. Nielsen, and C.J.C. Jones. Ground vibrations induced by railway traffic - the influence of vehicle parameters. In B. Schulte-Werning, D. Thompson, P.-E. Gautier, C. Hanson, B. Hemsworth, J. Nelson, T. Maeda, and P. de Vos, editors, *Proceedings of the 10th International Workshop on Railway Noise IWRN10*, volume 118 of *Notes on Numerical Fluid Mechanics and Multidisciplinary Design*, pages 259–266. Springer, Nagahama, Japan, October 2012.

[130] G. Müller and H. Huber. Dynamische Bodeansprachungen infolgte bewegter Lasten. *Bauingenieur*, 66:375–380, 1991.

[131] K. Müller, H. Grundmann, and S. Lenz. Nonlinear interaction between a moving vehicle and a plate elastically mounted on a tunnel. *Journal of Sound and Vibration*, 310:558–586, 2008.

[132] B. Nélain, P. Huber, A. Mirza, M. Oppel, and R. Müller. Field test measurement report - the influence from vehicle design on the generation of ground-borne vibration. RIVAS project SCP0-GA-2010-265754, Deliverable D5.6, Report to the EC, December 2013.

[133] B. Nélain and N. Vincent. The effect of parametric excitation on ground borne vibration in railway applications. In A. Cunha, E. Caetano, P. Ribeiro, and G. Müller, editors, *Proceedings of 9th International Conference on Structural Dynamics (EURODYN 2014)*, pages 847–853, Porto, Portugal, 2014.

[134] B. Nélain, N. Vincent, and E. Reynaud. Towards hybrid models for the prediction of railway induced vibration: numerical verification of two methodologies. In G. Degrande and G. Lombaert, editors, *Proceedings of the 13th International Workshop on Railway Noise, IWRN13*, pages 1–8, Ghent, Belgium, September 2019.

[135] J.T. Nelson. Recent developments in ground-borne noise and vibration control. *Journal of Sound and Vibration*, 193(1):367–376, 1996.

[136] J.T. Nelson and H.J. Saurenman. A prediction procedure for rail transportation groundborne noise and vibration. *Transportation Research Record*, 1143:26–35, 1987.

[137] J.C.O. Nielsen and A. Igeland. Vertical dynamic interaction between train and track-influence of wheel and rail imperfections. *Journal of Sound and Vibration*, 187(5):825–839, 1995.

[138] J.C.O. Nielsen, B. Nélain, R. Müller, A. Frid, and A. Mirza. Train induced ground vibration - characterization of vehicle parameters from test data and simulations. RIVAS project SCP0-GA-2010-265754, Deliverable D5.2, Report to the EC, August 2012.

[139] J.C.O. Nielsen and J. Oscarsson. Simulation of dynamic train-track interaction with state-dependent track properties. *Journal of Sound and Vibration*, 275:515–532, 2004.

[140] E. Ntotsios, D.J. Thompson, and M.F.M. Hussein. The effect of track load correlation on ground-borne vibration from railways. *Journal of Sound and Vibration*, 402:142–163, 2017.

[141] E. Ntotsios, D.J. Thompson, and M.F.M. Hussein. A comparison of ground vibration due to ballasted and slab tracks. *Transportation Geotechnics*, 21(100256), 2019.

[142] J. O'Brien and D.C. Rizos. A 3D FEM-BEM methodology for simulation of high speed train induced vibrations. *Soil Dynamics and Earthquake Engineering*, 25:289–301, 2005.

[143] ORE. Question C116: Wechselwirkung zwischen Fahrzeugen und gleis, Bericht Nr. 1: Spektrale Dichte der Unregelmässigkeiten in der Gleislage. Technical report, Office for Research and Experiments of the International Union of Railways, Utrecht, NL, 1971.

[144] J. Oscarsson. Simulation of train-track interaction with stochastic track properties. *Vehicle Systems Dynamics*, 37(6):449–469, 2002.

[145] M. Papadopoulos. *Influence of dynamic SSI on the building response to ground vibration*. PhD thesis, Department of Civil Engineering, KU Leuven, 2018.

[146] M. Papadopoulos, K. Kuo, M. Germonpré, R. Verachtert, J. Zhang, K. Maes, G. Lombaert, and G. Degrande. Numerical prediction and experimental validation of railway induced vibration in a multi-storey office building. In G. Degrande, G. Lombaert, D. Anderson, P. de Vos, P.-E. Gautier, M. Iida, J.T. Nelson, J.C.O. Nielsen, D.J. Thompson, T. Tielkes, and D.A. Towers, editors, *Proceedings of the 13th International Workshop on Railway Noise, 16-19 September 2019, Ghent, Belgium*, volume 150 of *Notes on Numerical Fluid Mechanics and Multidisciplinary Design*, pages 529–537. Springer Nature Switzerland AG, 2021.

[147] A.T. Peplow and A.M. Kaynia. Prediction and validation of traffic vibration reduction due to cement column stabilization. *Soil Dynamics and Earthquake Engineering*, 27:793–802, 2007.

[148] J.E. Phillips and J.T. Nelson. Analysis and design of new floating slab track for special trackwork using finite element analysis (FEA). In B. Schulte-Werning, D. Thompson, P.-E. Gautier, C. Hanson, B. Hemsworth, J. Nelson, T. Maeda, and P. de Vos, editors, *Proceedings of the 10th International Workshop on Railway Noise IWRN10*, volume 118 of *Notes on Numerical Fluid Mechanics and Multidisciplinary Design*, pages 275–282. Springer, Nagahama, Japan, October 2012.

[149] L. Pyl and G. Degrande. Determination of the dynamic soil characteristics with the SASW method at a site in Lincent. Report BWM-2001-02, Department of Civil Engineering, KU Leuven, August 2001. STWW Programme Technology and Economy, Project IWT-000152.

[150] L. Pyl and G. Degrande. Determination of the dynamic soil characteristics with the SASW method at Regent's Park in London. Report BWM-2003-17, Department of Civil Engineering, KU Leuven, December 2003. CONVURT EC-Growth Project G3RD-CT-2000-00381.

[151] L. Pyl, G. Degrande, and D. Clouteau. Validation of a source-receiver model for road traffic induced vibrations in buildings. II: Receiver model. *ASCE Journal of Engineering Mechanics*, 130(12):1394–1406, 2004.

[152] A. Quagliata, M. Ahearn, E. Boeker, C. Roof, L. Meister, and H. Singleton. Transit Noise and Vibration Impact Assessment Manual. FTA 0123, U.S. Department of Transportation, Federal Transit Administration, John A. Volpe National Transportation Systems Center, September 2018.

[153] P. Reumers and G. Degrande. Vibration impact study for the Jokeri Light Rail Line in Helsinki. Report BWM-2020-02, Department of Civil Engineering, KU Leuven, March 2020.

[154] N. Rhayma, P. Bressolette, P. Breul, M. Fogli, and G. Saussine. A probabilistic approach for estimating the behavior of railway tracks. *Engineering Structures*, 33:2120–2133, 2011.

[155] P. Ropars. *Modélisation des vibrations d'origine ferroviaire transmises aux bâtiments par le sol*. PhD thesis, Université Paris-EST, 2011.

[156] M. Schevenels, G. Degrande, G. Lombaert, G. De Roeck, W. Haegeman, and S.A. Badsar. In situ determination of material damping in the soil at small deformation ratios. Report BWM-2010-04, Department of Civil Engineering, KU Leuven, February 2010. FWO Project G.0595.06.

[157] M. Schevenels, S. François, and G. Degrande. EDT: An ElastoDynamics Toolbox for MATLAB. *Computers & Geosciences*, 35(8):1752–1754, 2009.

[158] M. Schevenels, G. Lombaert, and G. Degrande. Determination of the dynamic soil properties by refracted P-wave and surface wave characterization at a site in Lincent (Belgium). Report BWM-2011-17, Department of Civil Engineering, KU Leuven, September 2011.

[159] M. Schevenels, G. Lombaert, G. Degrande, and M. Arnst. Measurement and prediction of the soil's transfer function at a site in Lincent. Technical Report BWM-2006-03, Department of Civil Engineering, KU Leuven, February 2006.

[160] M. Schevenels, G. Lombaert, G. Degrande, and S. François. A probabilistic assessment of resolution in the SASW test and its impact on the prediction of ground vibrations. *Geophysical Journal International*, 172(1):262–275, 2008.

[161] B. Schulte-Werning, B. Asmussen, W. Wehr, K.G. Degen, and R. Garburg. Advancements in noise and vibration abatement to support the noise reduction policy strategy of deutsche bahn. In B. Schulte-Werning, D. Thompson, P.-E. Gautier, C. Hanson, B. Hemsworth, J. Nelson, T. Maeda, and P. de Vos, editors, *Proceedings of the 10th International Workshop on Railway Noise IWRN10*, volume 118 of *Notes on Numerical Fluid Mechanics and Multidisciplinary Design*, pages 9–16. Springer, Nagahama, Japan, October 2012.

[162] J.-F. Semblat and A. Pecker. *Waves and vibrations in soils: earthquakes, traffic, shocks, construction works*. IUSS Press, Pavia, 2009.

[163] X. Sheng, C.J.C. Jones, and M. Petyt. Ground vibration generated by a harmonic load acting on a railway track. *Journal of Sound and Vibration*, 225(1):3–28, 1999.

[164] X. Sheng, C.J.C. Jones, and M. Petyt. Ground vibration generated by a load moving along a railway track. *Journal of Sound and Vibration*, 228(1):129–156, 1999.

[165] X. Sheng, C.J.C. Jones, and D.J. Thompson. A comparison of a theoretical model for quasi-statically and dynamically induced environmental vibration from trains with measurements. *Journal of Sound and Vibration*, 267(3):621–635, 2003.

[166] X. Sheng, C.J.C. Jones, and D.J. Thompson. A theoretical model for ground vibration from trains generated by vertical track irregularities. *Journal of Sound and Vibration*, 272(3):937–965, 2004.

[167] X. Sheng, C.J.C. Jones, and D.J. Thompson. Modelling ground vibrations from railways using wavenumber finite- and boundary-element methods. *Proceedings of the Royal Society A - Mathematical, Physical and Engineering Sciences*, 461:2043–2070, 2005.

[168] X. Sheng, C.J.C. Jones, and D.J. Thompson. Responses of infinite periodic structures to moving or stationary harmonic loads. *Journal of Sound and Vibration*, 282:125–149, 2005.

[169] X. Sheng, C.J.C. Jones, and D.J. Thompson. Prediction of ground vibration from trains using the wavenumber finite and boundary element methods. *Journal of Sound and Vibration*, 293:575–586, 2006.

[170] M. Shinozuka and G. Deodatis. Simulation of stochastic processes by spectral representation. *Applied Mechanics Reviews*, 44(4):191–204, 1991.

[171] M. Shinozuka and C. Jan. Digital simulation of random processes and its application. *Journal of Sound and Vibration*, 25(1):111–128, 1972.

[172] M.J.M.M. Steenbergen and A.V. Metrikine. The effect of the interface conditions on the dynamic response of a beam on a half-space to a moving load. *European Journal of Mechanics, A/Solids*, 26:33–54, 2007.

[173] D. Stiebel, H. Brick, R. Garburg, G. Schleinzer, H. Zandberg, B. Faure, A. Pfeil, S. Thomas, A. Guiral, and M. Oregui. Specification of model requirements including descriptors for vibration evaluation. FINE2 project GA-881791, Deliverable D8.1, Report to the EC, 2020.

[174] H. Takemiya and A. Fujiwara. Wave propagation/impediment in a stratum and wave impeding block (WIB) measured for SSI response reduction. *Soil Dynamics and Earthquake Engineering*, 13:49–61, 1994.

[175] J.P. Talbot. Base-isolated buildings: towards performance-based design. *Proceedings of the Institution of Civil Engineers - Structures and Buildings*, 169(8):574–582, 2016.

[176] D.J. Thompson. *Railway noise and vibration: mechanisms, modelling, and means of control*. Elsevier, Oxford, 2009.

[177] D.J. Thompson, J. Jiang, M.G.R. Toward, M.F.M. Hussein, A. Dijckmans, P. Coulier, G. Degrande, and G. Lombaert. Mitigation of railway-induced vibration by using subgrade stiffening. *Soil Dynamics and Earthquake Engineering*, 79, Part A:89–103, 2015.

[178] D.J. Thompson, J. Jiang, M.G.R. Toward, M.F.M. Hussein, E. Ntotsios, A. Dijckmans, P. Coulier, G. Lombaert, and G. Degrande. Reducing railway–induced ground–borne vibration by using open trenches and soft–filled barriers. *Soil Dynamics and Earthquake Engineering*, 88:45–59, 2016.

[179] D.J. Thompson, G. Kouroussis, and E. Ntotsios. Modelling, simulation and evaluation of ground vibration caused by rail vehicles. *Vehicle Systems Dynamics*, 57:936–983, 2019.

[180] N. Triepaischajonsak. *The influence of various excitation mechanisms on ground vibration from trains*. PhD thesis, University of Southampton, 2011.

[181] N. Triepaischajonsak, D.J. Thompson, C.J.C. Jones, and J. Ryue. Track-based control measures for ground vibration. The influence of Quasi-static Loads and Dynamic Excitation. In B. Schulte-Werning, D. Thompson, P.-E. Gautier, C. Hanson, B. Hemsworth, J. Nelson, T. Maeda, and P. de Vos, editors, *Proceedings of the 10th International Workshop on Railway Noise IWRN10*, volume 118 of *Notes on Numerical Fluid Mechanics and Multidisciplinary Design*, pages 249–257. Springer, Nagahama, Japan, October 2012.

[182] N. Triepaischajonsak, D.J. Thompson, C.J.C. Jones, J. Ryue, and J.A. Priest. Ground vibration from trains: experimental parameter characterization and validation of a numerical model. *Proceedings of the Institution of Mechanical Engineers, Part F: Journal of Rail and Rapid Transit*, 225:140–153, 2011.

[183] J.N. Varandas, P. Hölscher, and M.A.G. Silva. Dynamic behaviour of railway tracks on transitions zones. *Computers and Structures*, 89:1468–1479, 2011.

[184] R. Verachtert. *Deterministic and probabilistic determination of dynamic soil characteristcs*. PhD thesis, Department of Civil Engineering, KU Leuven, 2018.

[185] R. Verachtert and G. Degrande. Determination of the dynamic soil characteristics at site 1 next to the Blok D building of the administrative complex of KU Leuven. Report BWM-2017-03, Department of Civil Engineering, KU Leuven, October 2017. Project OT/13/59.

[186] R. Verachtert and G. Degrande. Determination of the dynamic soil characteristics at site 2 next to the Blok D building of the administrative complex of KU Leuven. Report BWM-2017-18, Department of Civil Engineering, KU Leuven, October 2017. Project OT/13/59.

[187] H. Verbraken. *Prediction of railway induced vibration by means of numerical, empirical, and hybrid methods*. PhD thesis, Department of Civil Engineering, KU Leuven, 2013.

[188] H. Verbraken, P. Coulier, G. Lombaert, and G. Degrande. Measurement of train passages and transfer functions at a site in Lincent. Report BWM-2012-05, Department of Civil Engineering, KU Leuven, June 2012.

[189] H. Verbraken, P. Coulier, G. Lombaert, and G. Degrande. Measurement of transfer functions at a site in Lincent. Report BWM-2012-07, Department of Civil Engineering, KU Leuven, July 2012.

[190] H. Verbraken, G. Degrande, G. Lombaert, B. Stallaert, and V. Cuéllar. Benchmark tests for soil properties, including recommendations for standards and guidelines. RIVAS project SCP0-GA-2010-265754, Deliverable D1.11, Report to the EC, December 2013.

[191] H. Verbraken, H. Eysermans, E. Dechief, S. François, G. Lombaert, and G. Degrande. Verification of an empirical prediction method for railway induced vibration. In T. Maeda, P.-E. Gautier, C.E. Hanson, B. Hemsworth, J.T. Nelson, B. Schulte-Werning, D. Thompson, and P. de Vos, editors, *Proceedings of the 10th International Workshop on Railway Noise*, volume 118 of *Notes on Numerical Fluid Mechanics and Multidisciplinary Design*, pages 239–247, Nagahama, Japan, October 2010. Springer.

[192] H. Verbraken, G. Lombaert, and G. Degrande. Verification of an empirical prediction method for railway induced vibrations by means of numerical simulations. *Journal of Sound and Vibration*, 330(8):1692–1703, 2011.

[193] H. Verbraken, G. Lombaert, and G. Degrande. Experimental and numerical prediction of railway induced vibration. *Journal of Zhejiang University - Science A*, 13(11):802–813, 2012.

[194] Verein Deutscher Ingenieure. *VDI 3837 Ground-borne vibration in the vicinity of at-grade rail systems - Spectral prediction method*, 2013.

[195] M. Villot and E. Augis. Vibration emission from railway lines in tunnnel - characterization and prediction. *International Journal of Rail Transportation*, 4(4):208–228, 2016.

[196] M. Villot, C. Guigou, P. Jean, and N. Picard. Procedures to predict exposure in buildings and estimate annoyance. RIVAS project SCP0-GA-2010-265754, Deliverable D1.6, Report to the EC, 2012.

[197] M. Villot, P. Ropars, P. Jean, E. Bongini, and F. Poisson. Modeling the influence of structural modifications on the response of a building to railway vibration. *Noise Control Engineering Journal*, 59(6):641–651, 2011.

[198] D. Waddington, J. Woodcock, M.G. Smith, S. Janssen, and K. Persson Waye. CargoVibes: human response to vibration due to freight rail traffic. *International Journal of Rail Transportation*, 3(4):233–248, 2015.

[199] A. Wang. Track measurements on London Underground Bakerloo Line. Report 16487-2, Pandrol, May 2003. CONVURT EC-Growth Project G3RD-CT-2000-00381.

[200] R. Wettschureck and U.J. Kurze. Einfügungsdämmass von Unterschottermatten. *Acustica*, 58:177–182, 1985.

[201] G.P. Wilson, H.J. Saurenman, and J.T. Nelson. Control of ground-borne noise and vibration. *Journal of Sound and Vibration*, 87(2):339–350, 1983.

[202] C. With, A.V. Metrikine, and A. Bodare. Identification of effective properties of the railway substructure in the low-frequency range using a heavy oscillating unit on the track. *Archive of Applied Mechanics*, 80:959–968, 2010.

[203] R.D. Woods. Screening of surface waves in soils. *Journal of the Soil Mechanics and Foundation Division, Proceedings of the ASCE*, 94(SM4):951–979, 1968.

[204] World Health Organisation. *Environmental noise guidelines for the European Region*, 2018.

[205] T.X. Wu and D.J. Thompson. On the parametric excitation of the wheel/track system. *Journal of Sound and Vibration*, 278(4-5):725–747, 2004.

[206] H. Xia, J.G. Chen, P.B. Wei, C.Y. Xia, G. De Roeck, and G. Degrande. Experimental investigation of railway train-induced vibrations of surrounding ground and a nearby multi-story building. *Earthquake Engineering and Engineering Vibration*, 8(1):137–148, 2009.

[207] H. Xia and H. Takemiya, editors. *The Fourth International Symposium on Environmental vibrations: Prediction, Monitoring, Mitigation and Evaluation. ISEV 2009*, Beijing, China, October 2009. Science Press.

[208] Y.B. Yang and H.H. Hung. A 2.5D finite-infinite element approach for modelling visco-elastic bodies subjected to moving loads. *International Journal for Numerical Methods in Engineering*, 51:1317–1336, 2001.

[209] Y.B. Yang and H.H. Hung. Soil vibrations caused by underground moving trains. *Journal of Geotechnical and Geoenvironmental Engineering, Proceedings of the ASCE*, 134(11):1633–1644, 2008.

[210] Y.B. Yang and H.H. Hung. *Wave propagation for train-induced vibrations*. World Scientific, Taipei, 2009.

[211] X. Zhang, D. Thompson, H. Jeong, M. Toward, M. Toward, D. Herron, C. Jones, and N. Vincent. Measurements of the high frequency dynamic stiffness of railway ballast and subgrade. *Journal of Sound and Vibration*, 468(115081), 2020.

[212] X. Zhang, D. Thompson, and X. Sheng. Differences between euler-bernoulli and timoshenko beam formulations for calculating the effects of moving loads on a periodically supported beam. *Journal of Sound and Vibration*, 481(115432), 2020.

A. APPENDICES

A.1 Parameters for case history

In the case history, several calculations are performed with the models MOTIV and GroundVIB in order to illustrate different aspects of the numerical prediction of ground vibration due to passing trains.

The train consists of a single vehicle moving with a speed of 150 km/h (41.7 m/s). The vehicle parameters used for all computations are given in table 8 and correspond to a generic train vehicle.

Table 8: Vehicle parameters.

Car body	Mass	$m_\mathrm{c} = 32000$ kg
	Pitching moment of inertia	$J_\mathrm{c} = 1.2 \cdot 10^6$ kg$\cdot\mathrm{m}^2$
Bogie	Mass	$m_\mathrm{b} = 5000$ kg
	Pitching moment of inertia	$J_\mathrm{b} = 6000$ kg$\cdot\mathrm{m}^2$
	Half distance between bogie centres	$l_\mathrm{b} = 8.5$ m
Wheelset (unsprung mass)	Mass	$m_\mathrm{a} = 1200$ kg
	Static axle load	$g_{sk} = 114.8$ kN
	Contact stiffness (per wheel)	$k_\mathrm{H} = 1.26 \cdot 10^6$ kN/m
	Half distance between axles	$l_\mathrm{a} = 1.25$ m
Primary suspension	Vertical stiffness per axle	$k_\mathrm{p} = 2000$ kN/m
	Vertical viscous damping per axle	$c_\mathrm{p} = 40$ kN$\cdot\mathrm{s/m}$
	Spring lateral half distance	$l_\mathrm{p} = 0.9$ m
Secondary suspension	Vertical stiffness per axle	$k_\mathrm{s} = 500$ kN/m
	Vertical viscous damping per axle	$c_\mathrm{s} = 31.6$ kN$\cdot\mathrm{s/m}$

The track considered in the simulations is a typical ballasted track with UIC60 rails, fastened on the sleepers using standard grooved rail pads. A second case with softer rail pads is also considered in the simulations. The rail pad stiffness k_rp in this case is assumed equal to 30 MN/m, with a damping loss factor $\eta_\mathrm{rp} = 0.25$.

The ballast layer has a width of 3.0 m at the top and 3.6 m at the base, and a height of 0.3 m. The ballast mass and stiffness parameters are based on measurements presented by Zhang et al. [211]. These parameters are listed in table 9. The density of the ballast is equal to 1500 kg/m^3.

The rail unevenness spectrum used is the limit spectrum from ISO 3095:2013 which is typical of a low amplitude roughness spectrum. For wavelengths longer than 0.4 m the unevenness spectrum has been extrapolated. At 150 km/h and for frequencies from 1 Hz to 315 Hz, the range of wavelengths is 42 m to 0.13 m. The assumed unevenness spectrum is plotted in figure 57 in one-third octave bands.

The ballasted track is located on the surface of a homogeneous ground, represented as an elastic half-space. Three different types of ground are considered for the simulations, corresponding to soft, medium

Table 9: Parameters used for the ballasted track.

Rail UIC60	Mass per unit length	$\rho_r A_r = 60.21$ kg/m
	Bending stiffness	$E_r I_r = 6.22$ MN$\cdot$m^2
	Damping loss factor	$\eta_r = 0.02$
	Rail positions	$l_1 = l_2 = 0.75$ m
Rail fastener (pads)	Rail pad stiffness	$k_{rp} = 150$ MN/m
	Rail pad damping loss factor	$\eta_{rp} = 0.3$
Sleeper	Sleeper mass	$m_{sl} = 325$ kg
	Length	$2b = 2.6$ m
	Width	$b_{sl} = 0.25$ m
	Sleeper spacing	$d = 0.6$ m
Ballast	Ballast smeared mass	$\overline{m}_b = 1485$ kg/m
	Ballast smeared stiffness	$\overline{k}_b = 833$ MN/m^2
	Damping loss factor	$\eta_b = 0.15$

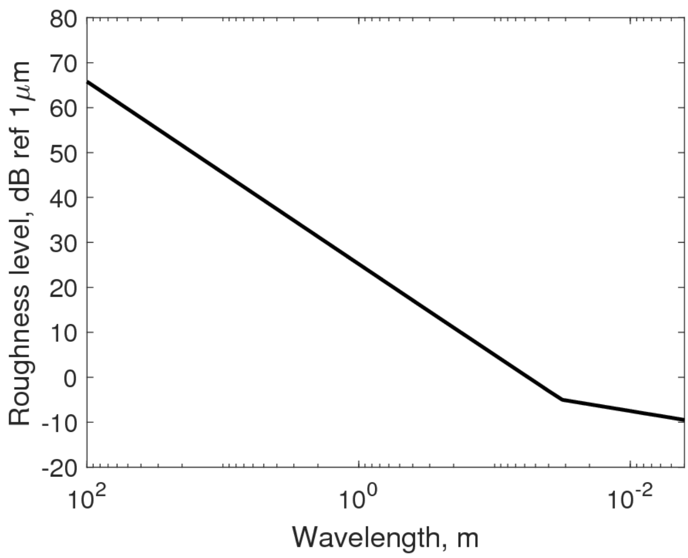

Figure 57: Assumed unevenness spectrum in one-third octave bands. At 150 km/h and for frequencies from 1 Hz to 315 Hz, the range of wavelengths is 42 m to 0.13 m.

and stiff soil. The dynamic soil characteristics are summarized in table 10 and are defined in terms of the dilatational and shear wave velocity, the density, and the material damping. Although not based on actual sites, these properties are chosen as typical values for soft, medium and stiff soil.

Both quasi-static and dynamic excitation due to rail unevenness are considered and comparisons are made of the following quantities of interest:

- The wheel and rail receptance, i.e. the displacement due to a unit load distributed over both wheels and rails.
- The dynamic axle loads due to the track unevenness.

Table 10: The parameters used for the different types of ground.

Ground type	P-wave velocity (m/s)	S-wave velocity (m/s)	Density (kg/m^3)	Material damping ratio
Soft	200	100	1800	0.025
Medium	400	200	1800	0.025
Stiff	800	400	1800	0.025

- One-third octave band RMS values for the vibration velocity in the free field at 4 m, 8 m, 15 m, and 20 m due to the passage of the train.

A.2 Requirements formulated by FINE-2 partners

Table 11: Requirements for the vibration prediction tool defined by the FINE-2 project and compatibility of the hybrid vibration prediction methodology proposed by SILVARSTAR.

Item	Requirement	SILVARSTAR tool	Comments from SILVARSTAR
2.1 General approach	Compliance with ISO 14837-1 or VDI 3837. $L_v = L_s + \Delta L_p + \Delta L_r$ At receiver position: inside building or on the ground. Force density or reference vibration level at 8 m from track.	yes	We prefer force density. We can also provide reference vibration level at 8 m from track, but only if we also have a line transfer mobility for this location.
	Base version: measurements only (at grade, including embankment and cutting), database and Graphical User Interface (GUI).	yes	The tool will be based on physical numerical models, which will gradually be expanded to allow for inclusion of measurement data.
	Empirical model version: re-calculated measured data (transposition from one site to another, change of train speed, point sources such as switches,...).	yes	
	Hybrid model version: numerical (or analytical) models and measured data.	yes	
2.2.1 Calculation domain	$1\ \text{Hz} \leq f \leq 315\ \text{Hz}$ $1\ \text{Hz} \leq f \leq 80\ \text{Hz}$ as a minimum requirement	yes	This depends on the user's input data.
	z-direction or x, y, z direction.	yes	
2.2.2 Physical dimensions	Reference velocity v_0 for vibration level in dB.	yes	We will preferably use 5e-8 m/s, but options for transferring will be available in the tool.
2.2.3 Vibration descriptors	MTVV and VDV according to ISO 2631-1:1997 and ISO 2631-2:2003.	yes	VDV requires time signals so cannot be obtained from a frequency domain calculation. The approximate value eVDV as defined in Annex C of ISO2631-1:1997 can be obtained. MTVV is the maximum transient vibration value, calculated at a one-second interval; this can also not be obtained from a frequency domain model.
	KB_Fmax and KB_FTr according to DIN 4150-2:1999.	yes	In the DIN standards, approximate formula are proposed to obtain the time domain descriptors KB_Fmax and KB_FTr from results in the frequency domain.
	L_vSmax according to ISO/TS 14837-31:2017.	yes	L_vSmax requires time signals so cannot be obtained from a frequency domain calculation. We can estimate it from the RMS spectrum with an empirical correction.
2.2.4 Calculation time	Base version: few minutes to less then 60 min. Very advanced module: less then 8 hours.	yes	Base version: typical number of receivers to be computed is ~50.
2.2.5 Interfaces	GUI	yes	Prototype version: simple GUI for testing purposes. Final version : IMMI interface.
	Interface to GIS based software.	yes	Prototype version: will not include a GIS interface. Final version: IMMI already includes this and will be adapted.
	Import of measurement data.	yes	The measurement data format will be defined (source spectra, transfer functions,...).
	Open interface allowing for future improvements.	?	Must be further discussed with FINE-2 partners.
	Tunnel ($1\ \text{Hz} \leq f \leq 315\ \text{Hz}$)	yes	Some pre-calculated tunnel situations will be included in the tool.
2.2.6 User group	Ground vibration expert with training.	yes	
	Support for the user to select appropriate data.	yes	A User's Guide will be written.
2.2.7 Software	At least Windows 10	yes	
	A stand-alone application is preferred.	yes	Final version included in IMMI and commercialised by Wölfel as an independent module from the noise and air pollution calculation modules.
	Maintenance and updates ensured by developpers.	yes	To a certain extent: interface maintained through IMMI
	Publicly available programming language for prototype software.	yes	Matlab will be used. However, the source code won't be made fully open source.
	Database (measured source spectra, transfer functions).	yes	The database will include few well-documented cases with in-depth measurement data. The user will be able to import measured data such as roughness spectra, ground vibration levels or transfer functions, as well as physical data such as train or track parameters for the numerical prediction model.
	Traceability of results (linked to input data).	yes	Project (data) and results will be saved.

2.2.8 Time schedule	GUI concept at early stage	yes	The GUI of the prototype prediction tool and the GUI of the final vibration prediction tool won't be the same. The prototype prediction tool will be available at an early stage.
	Development of the GUI: stepwise and in close cooperation with FINE-2.	yes	
	Working base version: January 2022.	yes	Prototype vibration prediction tool available at M12 (Oct 2021) and validated at M18. Final version available at M20.
	Calculation models for empirical model validated in January 2022.	?	Transposition method will allow the "empirical model" at M18 (April 2022).
2.3 Base version			See comments on Section 2.1 (general approach).
2.4 Extended versions			See comments on Section 2.1 (general approach).
2.5.1 General procedure	Step1: import 3D geodata; create new tracks and buildings (geometrical data); selection of vibration descriptors.	yes	IMMI already uses these steps for acoustics, and will be adapted for ground vibration.
	Step 2: definition of emission data for each track sections; definition of parameters for variations.	yes	
	Step 3: definition of soil propagation and type of buildings.	yes	
	Step 4: prediction of corridor of affected buildings (including variation of floor resonance frequencies). Based on maximum vibration descriptor value.	yes	
	Step 5: definition of individual building characteristics in the corridor; change of relevant parameters or components.	yes	
	Step 6: full calculation and output data (2D plot with colour indication and ordered list of calculated vibration values at receivers).	yes	
2.5.2 Refinement of the prediction	Use of building transfer functions for refinement.	yes	IMMI vibration module will be developped in this way.
2.5.3 Comparison of configurations	Possibility to compare two or more configurations.	yes	IMMI already includes this and will be adapted.
	Possibility to define reference data.	yes	
	2D color map.	yes	
2.6 Input	Geodata: tracks and buildings.	yes	IMMI already includes this
	Vibration descriptors.	yes	IMMI will be adapted
	Building description: type, number of floors, limit values for vibration.	yes	IMMI will be adapted
	Building classification (residential, workshop,…).	yes	IMMI already includes this
	Data for train emissions and vibration transfer: number of trains per day or night.	yes	IMMI already includes this, and will be adapted for vibration
	Vibration spectrum at 8 m from track.	yes	We would prefer force density. We can accept vibration data at 8 m but only if we also have a line transfer mobility for this location
	Spectrum of blocked or coupled force at wheel-rail contact (and track-to-soil transfer function).	yes	We expect to use a force density spectrum but this is to be defined further in the project
	Vibration spectrum at the tunnel invert.	yes	Potential problem with quasi-static component which will not propagate to the far fiel. We would prefer force density.
	ΔL_GE: transfer function from track to point of emission.	yes	The concept of the tools will integrate this subdivision of the vibration propagation path.
	ΔL_GP: transfer function from point of emission to building.	yes	
	ΔL_RStruct1: transfer function from ground to building foundation.	yes	
	ΔL_RStruct2: transfer function from building foundation to floors.	yes	
2.7 Output	2D map: corridor limits, green or red dots for buildings.	yes	IMMI already includes this and will be adapted for vibration.
	Comparison of initial and final configurations: visualised as differences betweent the indicators.	yes	IMMI already includes this and will be adapted for vibration.
	Ordered list of calculated vibration values at receivers and limit values (UFF or CSV files), including: -unweighted velocity spectra in one-third octave bands from 1 to 80 Hz at receiver positions; - extracted single number values = vibration descriptors at the receiver positions inside buildings.	yes	IMMI already includes this and will be adapted for vibration.
	Receiver positions: - minimum at the middle of ground floor and highest floor; - depending on local situation at other positions inside the building; - on the ground at specific distances from the track.	yes	IMMI will be adapted.
	Output linked to input data for traceability.	yes	IMMI will be adapted.

3 Database	Source data and metadata (associated information).	yes	based on CNOSSOS as far as possible
	Import function for spectra.	yes	must be discussed with FINE-2
	Status of data in progress, released or invalid).	yes	must be discussed with FINE-2
	Database structure avaliable at early stage of the project.	yes	See WP2, database available at M12 (Oct 2021).
3.1 Documentation	User's manual.	yes	IMMI
	Documentation of input and output interfaces.	yes	IMMI
	Documentation of calculation model and validation.	yes	Deliverables D1.1 and D1.2.